Technical Report No. 32-458

Mars Atmosphere Entry Parametric Study

J. M. Brayshaw

jpl
JET PROPULSION LABORATORY
CALIFORNIA INSTITUTE OF TECHNOLOGY
PASADENA, CALIFORNIA

September 15, 1963

Technical Report No. 32-458

Mars Atmosphere Entry Parametric Study

J. M. Brayshaw

M. G. Comuntzis

M. G. Comuntzis, *Acting Chief*
Spacecraft Design Section

JET PROPULSION LABORATORY
CALIFORNIA INSTITUTE OF TECHNOLOGY
PASADENA, CALIFORNIA

September 15, 1963

Prepared Under Contract No. NAS 7-100
National Aeronautics & Space Administration

CONTENTS

TABLES

FIGURES

ABSTRACT

In anticipation that the many technical disciplines involved in a Mars planetary entry program will require such information for design studies and preliminary design decisions, a fairly complete parametric study of the Mars atmospheric entry was performed. The expected extreme model atmospheres[1] as well as the anticipated extremes of initial entry velocity, entry angle and ballistic coefficient were included. As functions of these variables, the following parameters are plotted in graphical form:

1. Flight path acceleration vs altitude
2. Mach No. vs altitude
3. Dynamic pressure vs altitude
4. Heating rate vs altitude
5. Flight path angle vs altitude
6. Atmospheric velocity vs altitude
7. Altitude vs time
8. Altitude vs planet centered angle

In addition, summary plots of peak heating rate, peak acceleration, unretarded impact velocity, and altitude for parachute deployment are shown as a function of entry angle for the extremes of ballistic coefficient and model atmosphere.

The material is presented for reference use only, and no attempt is made to analyze the significance of the relationships depicted for a particular mission.

[1]New planet spectrographic observations now under evaluation at JPL tentatively indicate a considerably lower limit on the density-altitude profile band.

I. INTRODUCTION

In order to assess the vehicle design problems involved in entering the atmosphere of Mars, to weigh compromise solutions to these problems, and to provide the terminal extension of planet approach space trajectories, a parametric study varying initial trajectory conditions, planet atmosphere models, and vehicle ballistic coefficient was performed. The Jet Propulsion Laboratory powered flight entry program (Refs. 1 and 2) was used on the IBM 7090 computer. This is a point-mass trajectory solution, i.e., it considers only the translatory motion of the vehicle.

A. Constant conditions

1. Motion confined to equatorial plane, counter to planet rotation
2. Mars rotation velocity
3. Mars diameter
4. Mars gravity, surface
5. Initial altitude: 1,000,000 ft above surface
6. Vehicle drag coefficient (hypersonic): 0.7 with Mach No. variation
7. Atmosphere fixed to planet: no wind
8. Vehicle maximum diameter: 2.75 ft
9. Angle of attack: 0°

B. Variable conditions

1. Model atmosphere (Ref. 3): *A*, *B*, *C* and *F* as defined in Table 1 and Figs. 1 and 2
2. Initial velocity with respect to atmosphere: 15,200 to 37,000 ft/sec
3. Initial angle, flight path to local horizon: 20 to 90 deg
4. Ballistic coefficient or $\frac{m}{C_D A}$: 0.5 to 5.0, corresponding to gross weights of 67 to 670 lb

Table 1. Some properties of model atmospheres for Mars

Model designation	A	B	C	D	E	F
Composition (by volume)						
N_2	86.8	97.25	98.7	86.8	97.25	98.7
CO_2	7.2	1.9	0.7	7.2	1.9	0.7
A	6.0	0.85	0.6	6.0	0.85	0.6
Molecular weight	29.9	28.4	28.2	29.9	28.4	28.2
Surface pressure						
lb/ft^2	113	196	284	113	196	284
millibar	54	94	136	54	94	136
Ratio of specific heats	1.41	1.41	1.42	1.41	1.41	1.41
Temperature in stratosphere						
°R	410	320	230	230	410	410
°K	230	180	130	130	230	230
Temperature near surface						
°R	470	410	380	470	410	470
°K	260	230	210	260	230	260
Scale height*						
$ft \times 10^{-3}$	59	41	29	29	59	56
km	18	12.5	9	9	18	17
Reciprocal scale height*						
$ft^{-1} \times 10^5$	1.7	2.4	3.4	3.4	1.7	1.8
$km^{-1} \times 10^2$	5.6	8.0	11.0	11.0	5.6	5.9
Lapse rate						
$°R\ ft^{-1} \times 10^3$	−1.96	−2.04	−2.13	−1.96	0	−1.96
$°K\ km^{-1}$	−3.43	−3.75	−4.10	−3.43	0	−3.43
Surface density						
$slugs \times ft^{-3} \times 10^4$	1.4	2.7	4.3	1.4	2.7	3.4
$gm \times cm^{-3} \times 10^4$	0.75	1.4	2.2	0.75	1.4	1.8
Acceleration of gravity						
ft/sec^2	11.8	12.3	12.8	12.8	11.8	12.8
cm/sec^2	360	375	390	390	360	390

* stratosphere

C. Results

The results give atmospheric ballistic entry variations of certain design parameters versus altitude or time (see nomenclature). Terminal motion under the influence of an auxiliary decelerator may be approximated by the assumption of a vertical trajectory starting at the desired Mach number and corresponding altitude. Results presented here (except for heating rates) also apply to vehicles having the same ballistic coefficients, but different combinations of diameter, weight, and drag coefficient (except in the low velocity terminal portion).

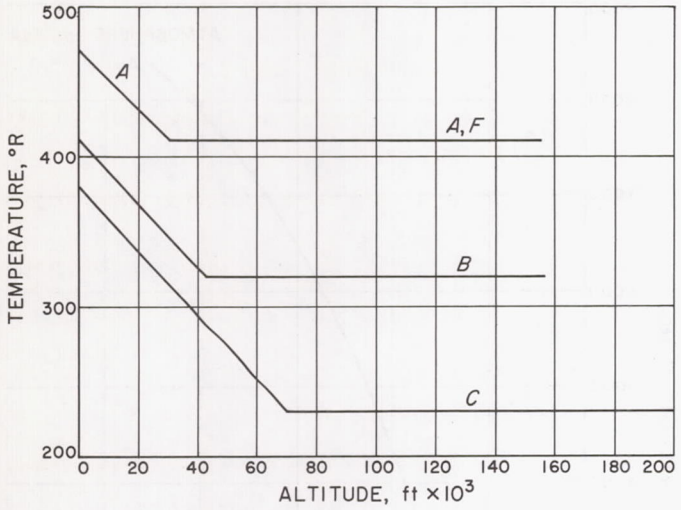

Fig. 1. Model atmospheres for Mars—temperature profile

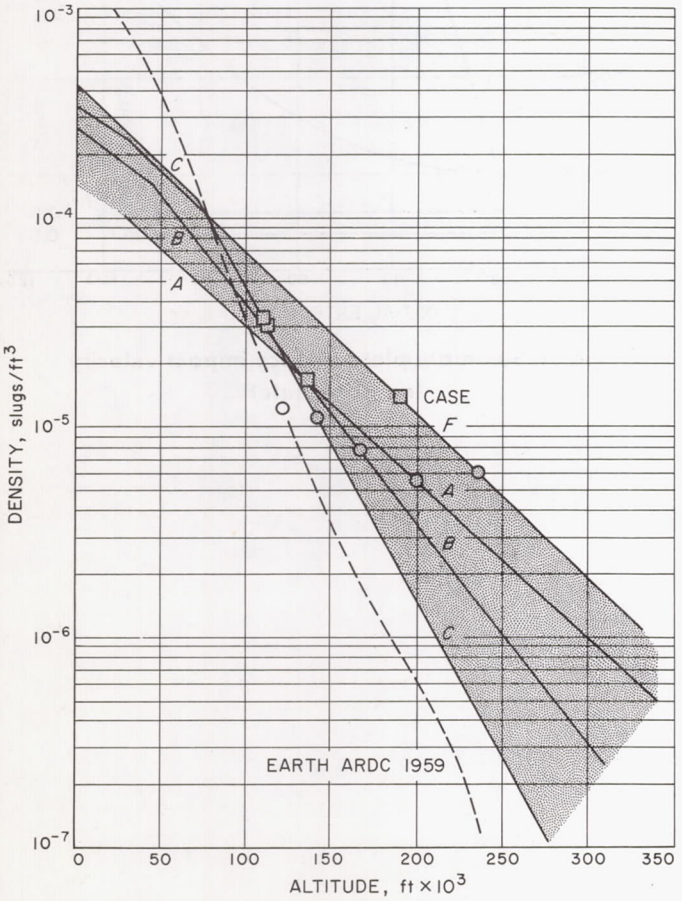

Fig. 2. Model atmospheres for Mars—density profile

The atmosphere models chosen for use in this program span the expected temperature and density bands (see Figs. 1 and 2).

The initial velocity range extends from slightly less than escape velocity to a high value typical of short flight-time, low-payload missions. The most practical initial *VE* will probably fall between the two middle values.

At the highest ballistic coefficient and initial velocity it can be noted that the initial flight path angle of 20 deg below horizon is a marginal or overshoot condition. Depending on the atmosphere assumption, the vehicle is correspondingly captured immediately, captured after a reversal in rate of altitude change, or it escapes the planet. This is most easily seen in the plot of altitude vs *ARC*, which may be interpreted as ground range expressed in multiples of planet radius. The *ALT* vs *ARC* plot is thus a physical picture (with mismatched scales) of the trajectory. Figure 3 graphically defines trajectory geometry.

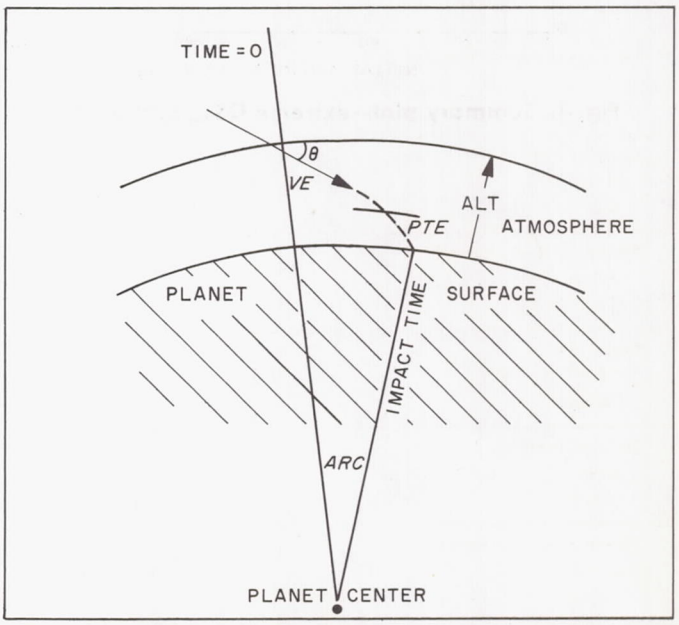

Fig. 3. Trajectory geometry

For purposes of comparison, all plot scales are the same. The percentage definition of small values suffers correspondingly. Printed output data and plotting tapes are available for fine-grained reexamination of any portion of this study. Some of the extreme conditions possible within these bands of parameters are presented in Figs. 4, 5, and 6.

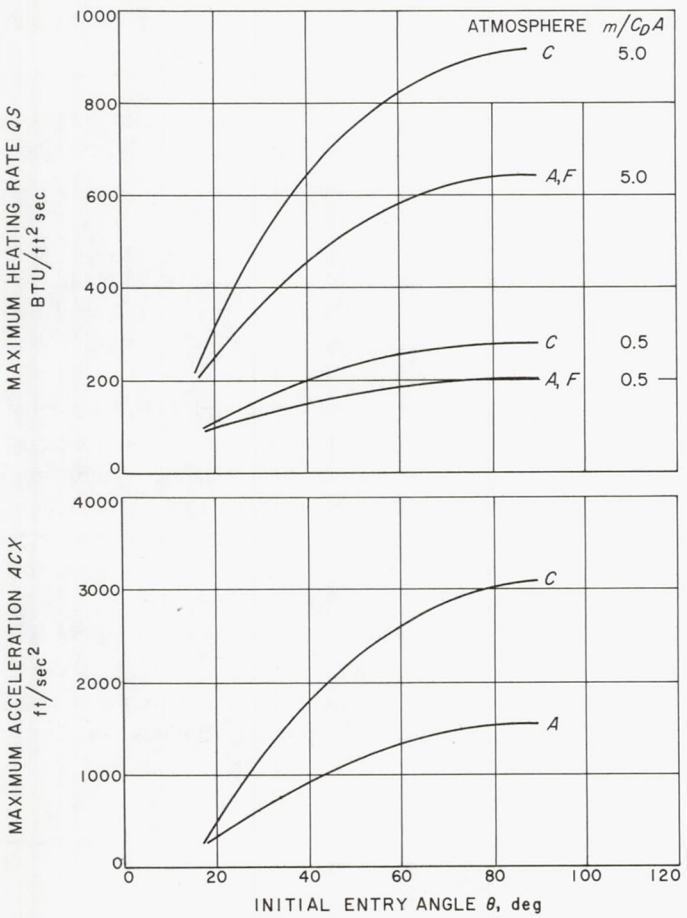

Fig. 4. Summary plot—extreme QS_{max} and ACX_{max}

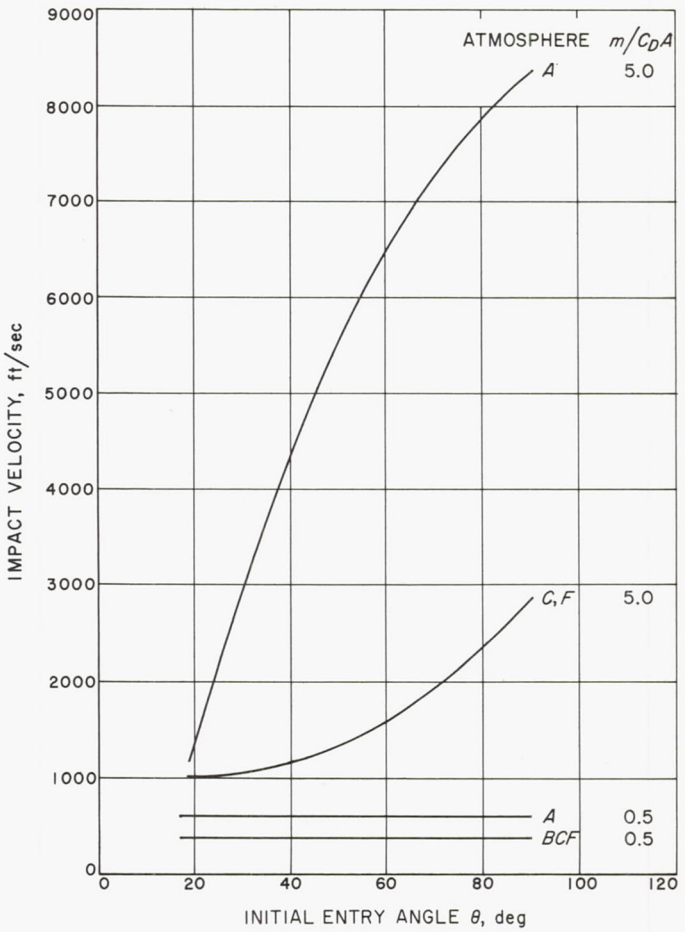

Fig. 5. Summary plot—surface impact velocity (no parachute)

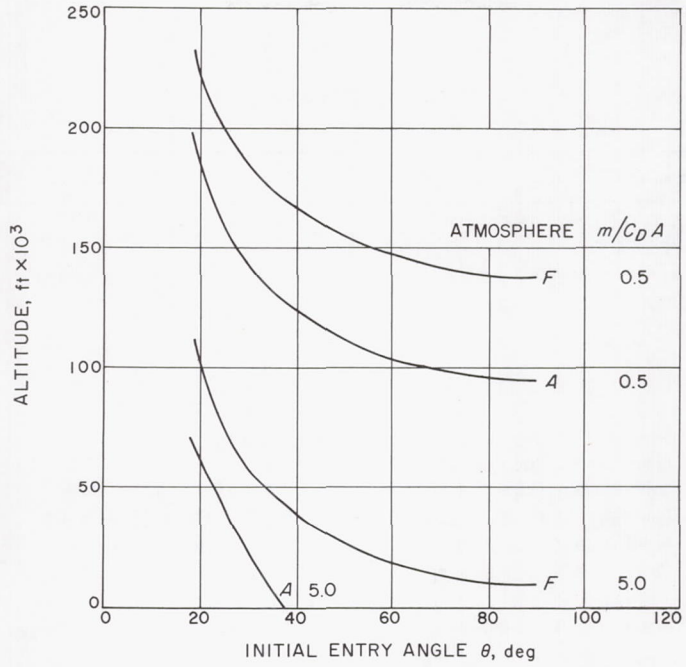

Fig. 6. Summary plot—altitude for possible parachute deployment (Mach No. = 3, extreme *VE* = 21,700 ft/sec)

II. DESCRIPTION OF PLOTS

Quantities Plotted (see Table 2)

ACX, Mach, *Q*, *QS*, *PTE*, *VE* vs *ALT*

ALT vs *TIM*

ALT vs *ARC*

Each of the four curves on a given plot (see Appendix) represents a different initial velocity (*VE*) of

15,200
21,700
29,300
or 37,000 ft/sec

The automatic plotting process does not allow machine labelling of curves. However, in most cases the identity of the curves is evident, i.e., highest peak *ACX*, *Q*, *QS*, lowest initial decay rate of *PTE* vs *ALT*, and highest initial decay rate of *ALT* vs *TIM* correspond to highest initial *VE*.

The WEIGHT, which is a constant for each plot, corresponds to the following ballistic coefficients (m/C_DA), and densities. The density range is roughly that between balsa wood and water.

WEIGHT, lb	m/C_DA	Gross Density, lb/ft³
67	0.5	5.7
200	1.5	17.1
400	3.0	34.2
667	5.0	57.0

The 200 lb, 21,700 ft/sec combination has received considerable attention at JPL in the past.

Table 2. Table of plots

Figure number	Ordinate	Abscissa	Weight	m/C_DA	ϕ	Atmosphere
A-1	*ALT*	*TIM*	67	0.5	20	A
A-2	*VE*	*ALT*	67	0.5	20	A
A-3	Mach	*ALT*	67	0.5	20	A
A-4	*QS*	*ALT*	67	0.5	20	A
A-5	*Q*	*ALT*	67	0.5	20	A
A-6	*ACX*	*ALT*	67	0.5	20	A
A-7	*PTE*	*ALT*	67	0.5	20	A
A-8	*ALT*	*ARC*	67	0.5	20	A
A-9 through A-16	Same as (A-1 through A-8)		200	1.5	20	A
A-17 through A-24	Same as (A-1 through A-8)		400	3.0	20	A
A-25 through A-32	Same as (A-1 through A-8)		667	5.0	20	A
A-33 through A-64	Same as (A-1 through A-8)		Same as (A-1 through A-32)		40	A
A-65 through A-96	Same as (A-1 through A-8)		Same as (A-1 through A-32)		90	A
A-97 through A-192	Same as (A-1 through A-8)		Same as (A-1 through A-32)		Same as (A-1 through A-96)	B
A-193 through A-288	Same as (A-1 through A-8)		Same as (A-1 through A-32)		Same as (A-1 through A-96)	C
A-289 through A-384	Same as (A-1 through A-8)		Same as (A-1 through A-32)		Same as (A-1 through A-96)	F

NOMENCLATURE

A	Vehicle projected frontal area, π (max. diam)^2 /4, ft/sec^2
ACX	Acceleration along flight path direction, ft/sec^2
ALT	Length of perpendicular from vehicle to planet surface, ft
ARC	Planet centered angle between initial and current vehicle positions, $\frac{\text{Surface range}}{\text{Mars radius}}$
ATMOS	Atmosphere models defined in Table 1 and Figs. 1 and 2
C_D	Drag coefficient drag force/QA
m	Gross vehicle mass, slugs
Mach	Mach number, ratio of VE to local ambient sonic velocity
PTE	Local angle between VE and local horizon, rad
Q	Dynamic pressure, $(VE)^2\rho/2$, lb/ft^2/10.76
QS	Stagnation point heating rate, 2.15×10^{-8} $R_n^{-0.5}$ $\rho^{0.5}$ $V^{3.0}$, BTU/ft^{2}sec
R_n	Vehicle nose radius (max. diam)/2, ft
THETA	Initial angle between VE and local horizon, deg
TIM	Time after initial time, sec
VE	Velocity of vehicle with respect to atmosphere, ft/sec
WEIGHT	Gross vehicle weight on Earth, lb
ρ	Atmosphere local density, slugs/ft^3

REFERENCES

1. Gianopulos, G. N., *Generalized Powered Flight Trajectory Program,* Technical Report No. 32-38, Jet Propulsion Laboratory, Pasadena, California, September 28, 1960.

2. Kohlhase, C. E., *Additions to JPL Powered Flight Trajectory Program to Permit Planet Entry Simulation,* Jet Propulsion Laboratory Interoffice Memorandum, September 18, 1961.

3. Schilling, G. F., "Extreme Model Atmospheres of Mars," Report RM-2782-JPL, Rand Corporation, June 22, 1961.

APPENDIX

Mars Atmosphere Entry Parameters

The values for varied initial trajectory conditions, planet atmosphere models, and vehicle ballistic coefficients are presented in Figs. A-1 through A-384.

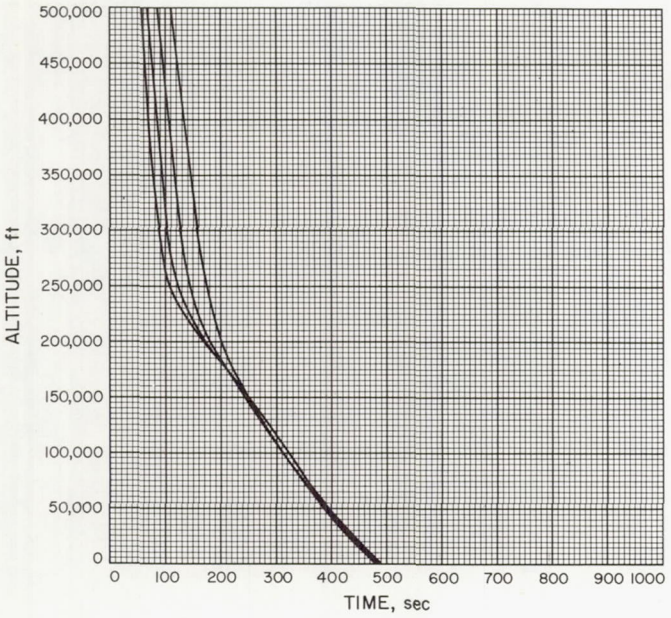

Fig. A-1

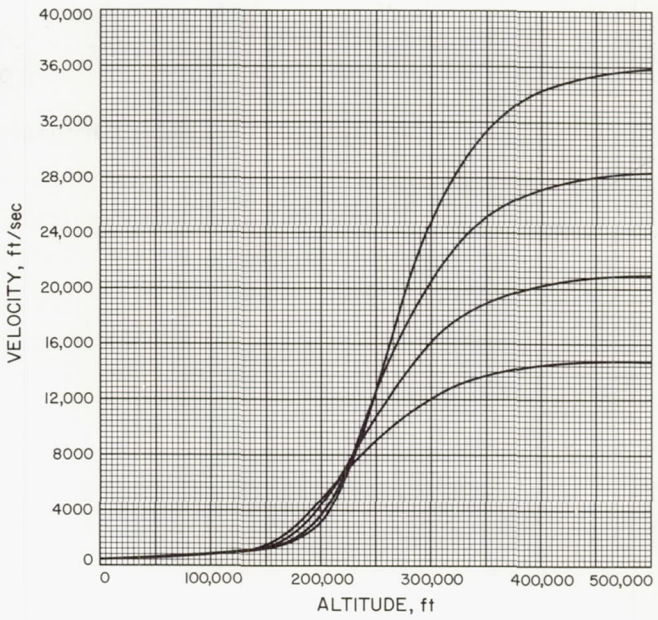

Fig. A-2

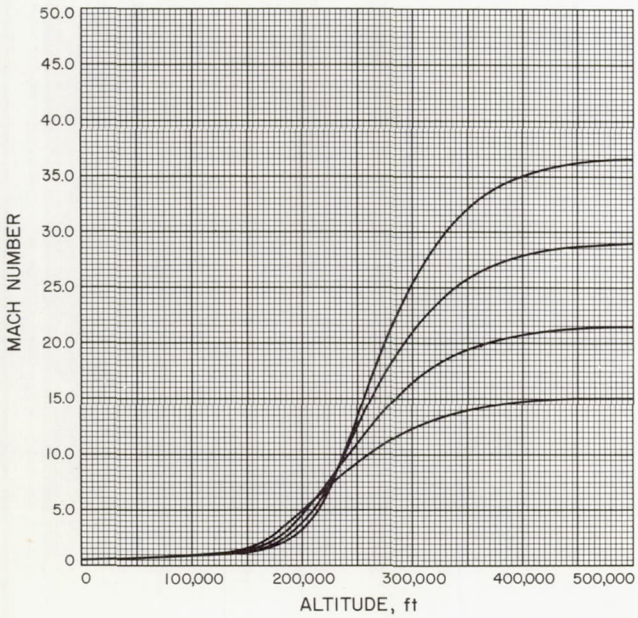

Fig. A-3

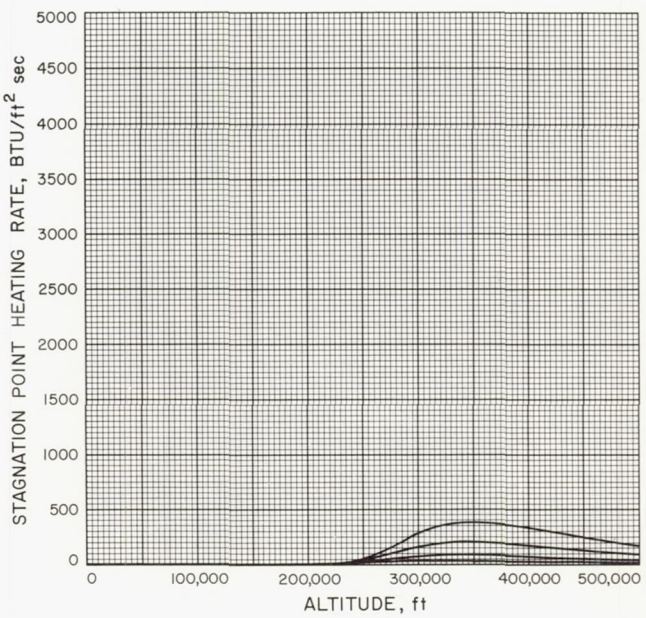

Fig. A-4

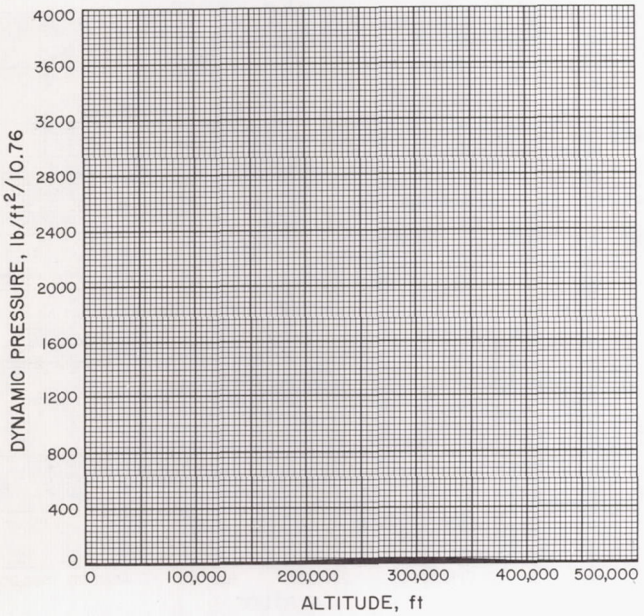

Fig. A-5

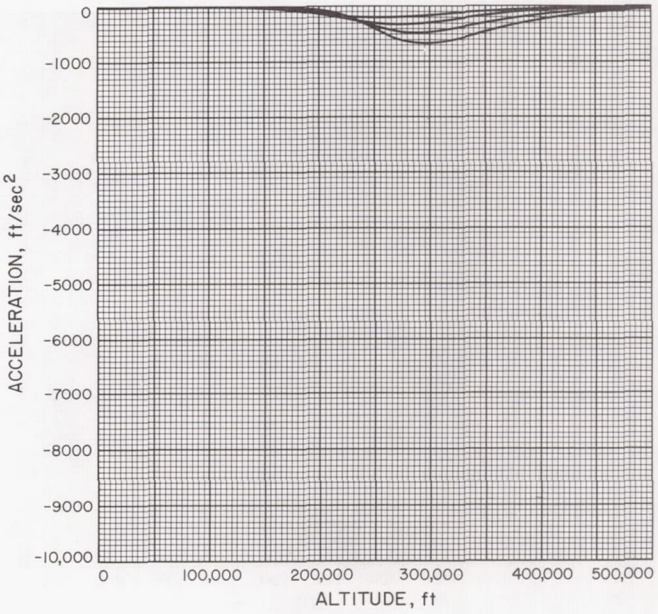

Fig. A-6

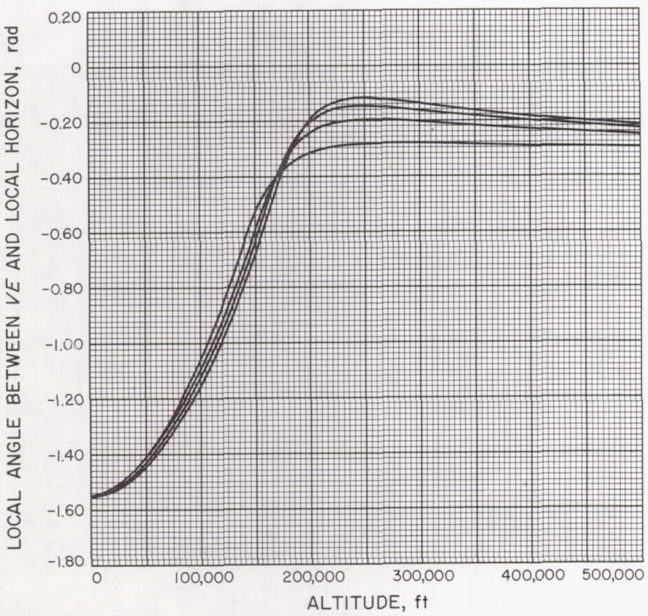

Fig. A-7

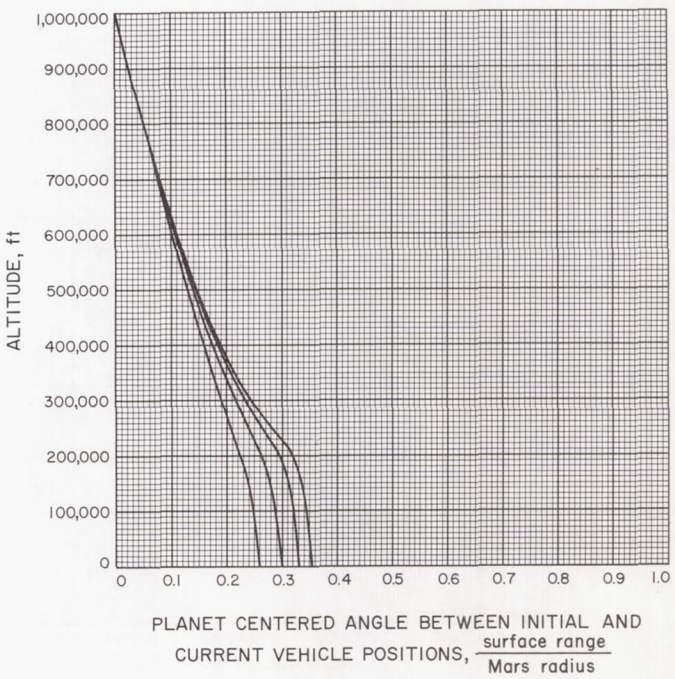

Fig. A-8

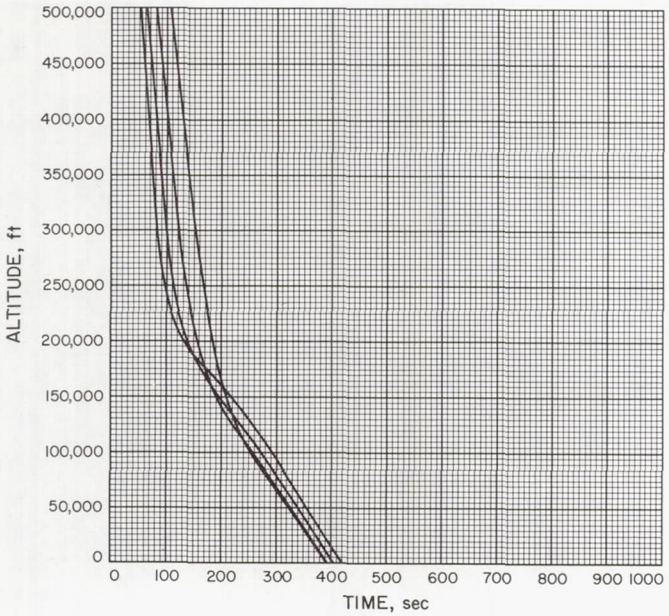

Fig. A-9

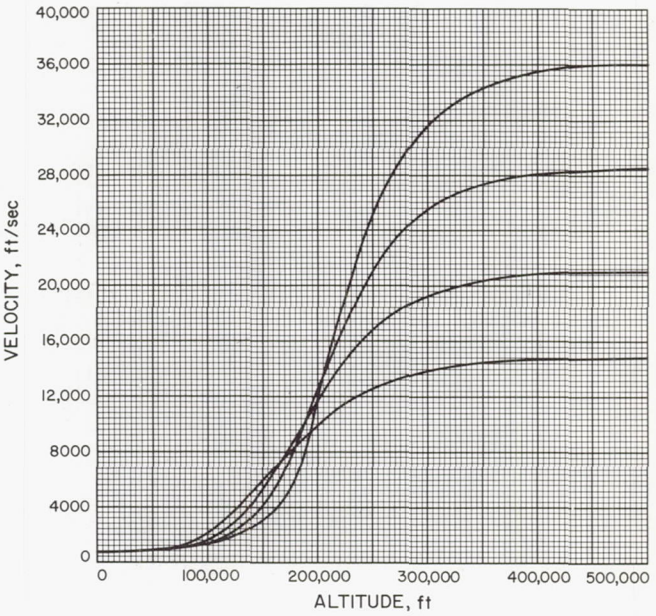

Fig. A-10

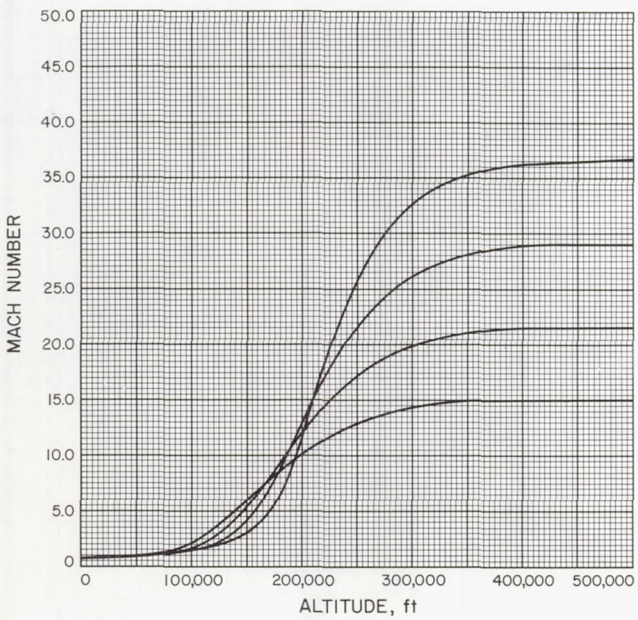

Fig. A-11

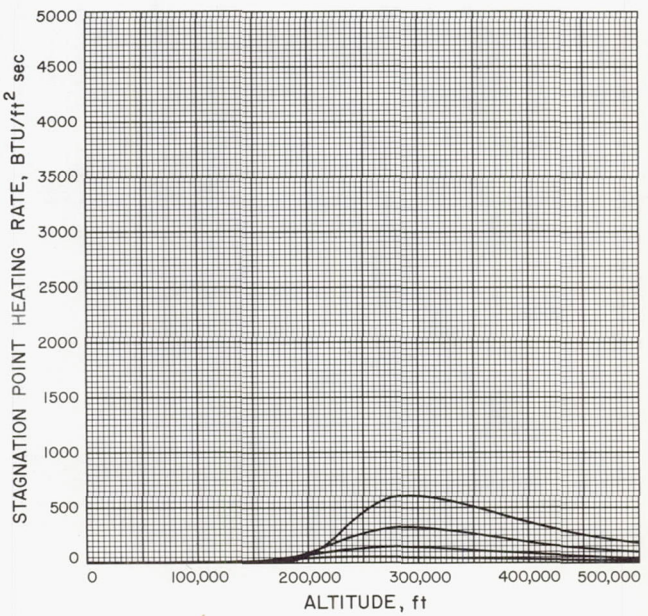

Fig. A-12

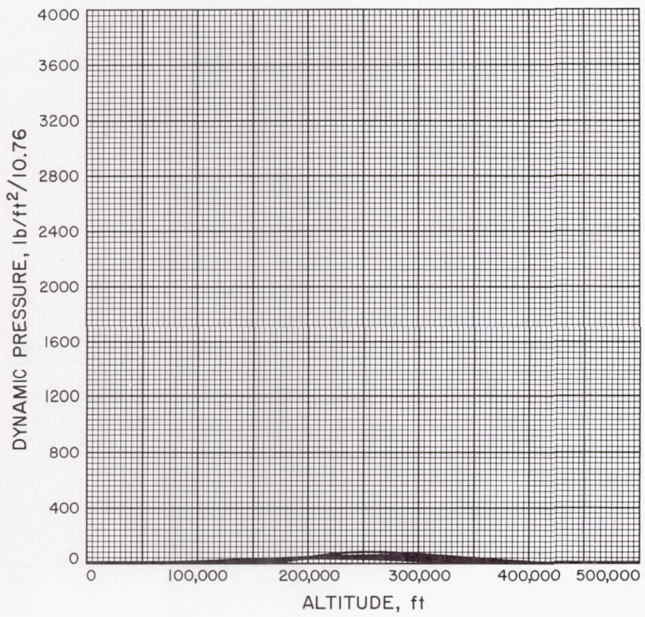

Fig. A-13

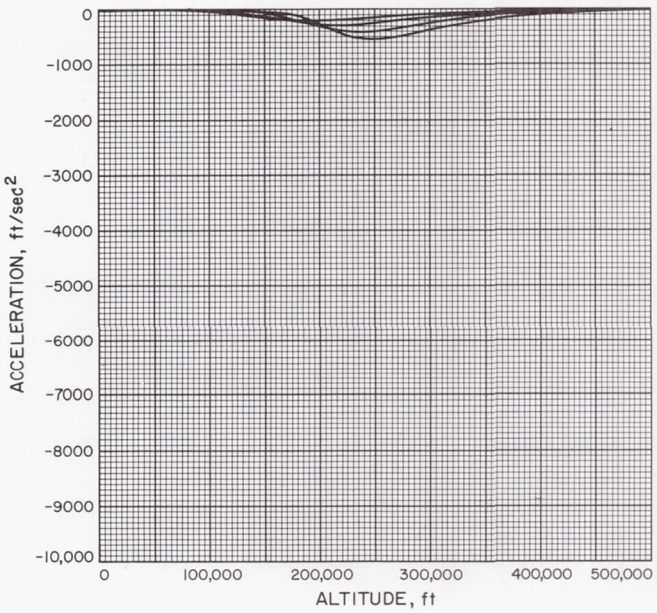

Fig. A-14

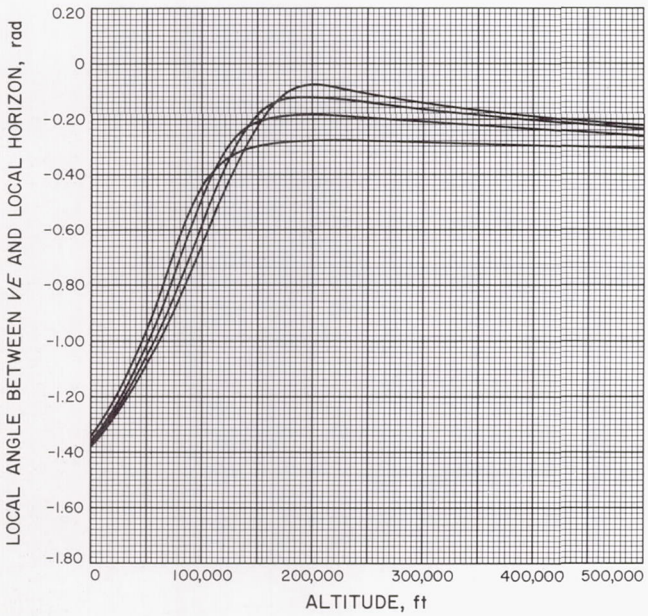

Fig. A-15

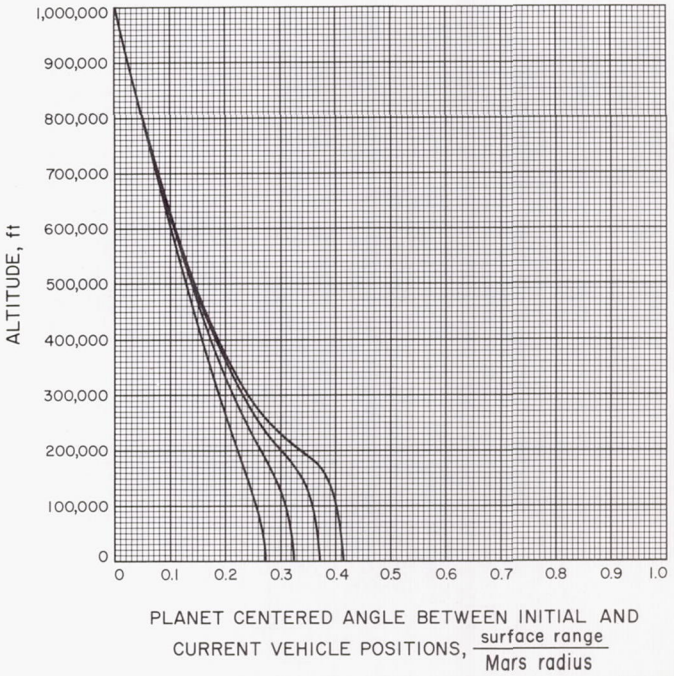

Fig. A-16

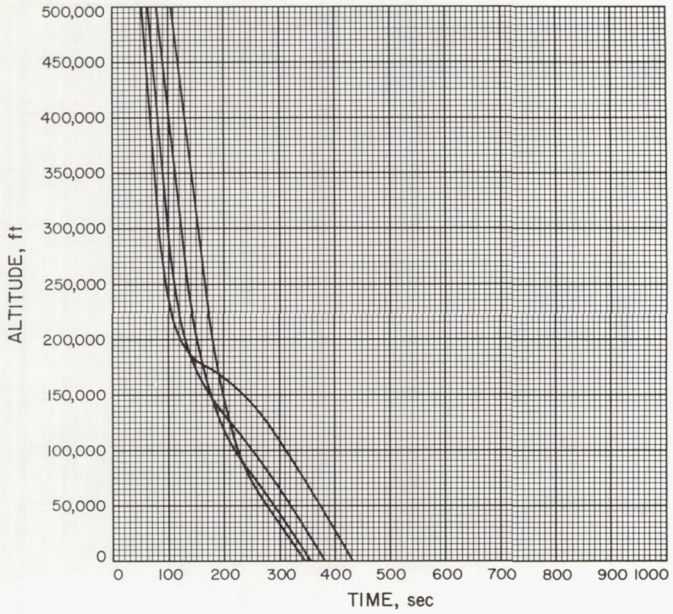

Fig. A-17

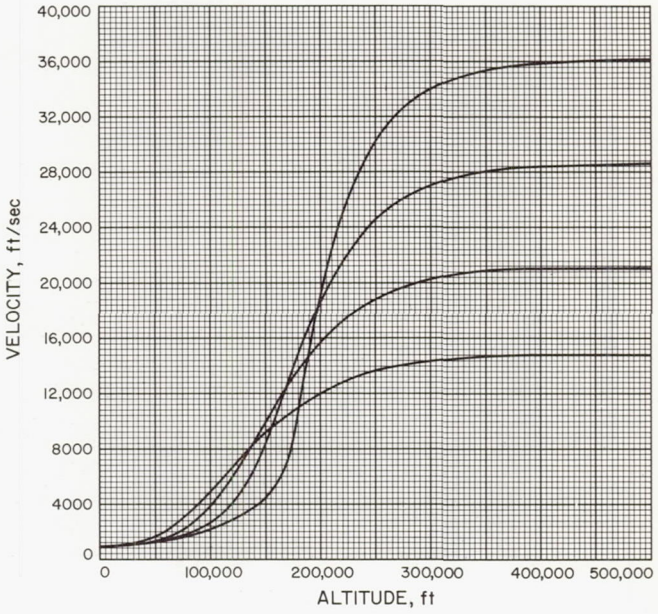

Fig. A-18

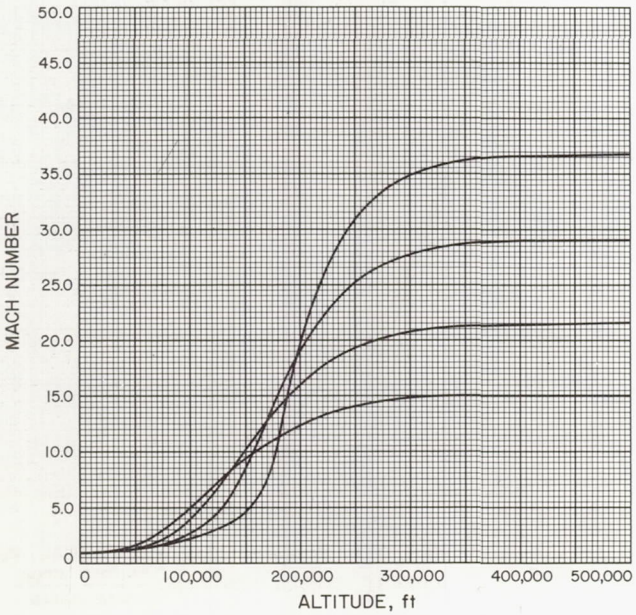

Fig. A-19

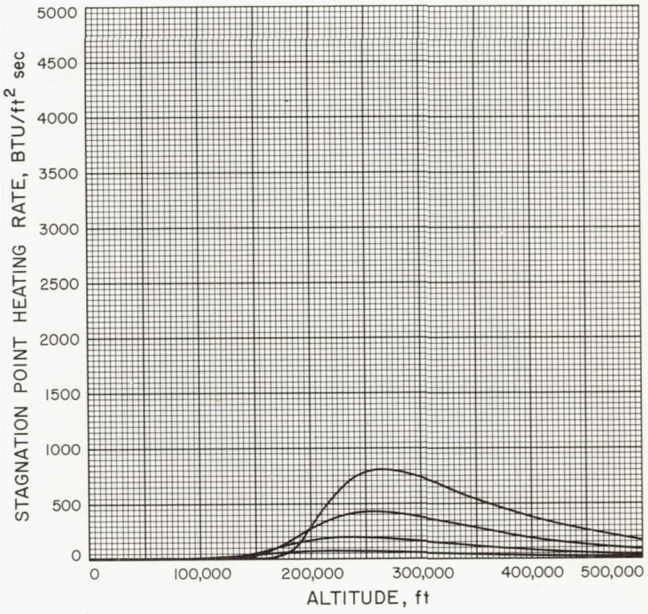

Fig. A-20

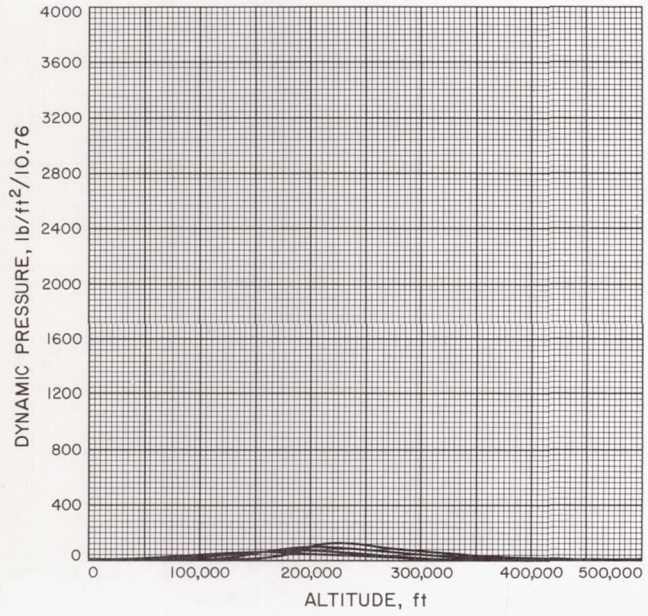

Fig. A-21

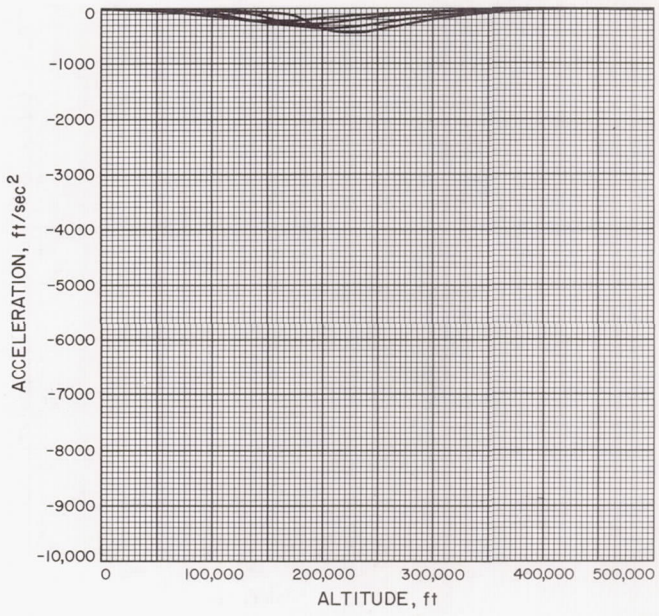

Fig. A-22

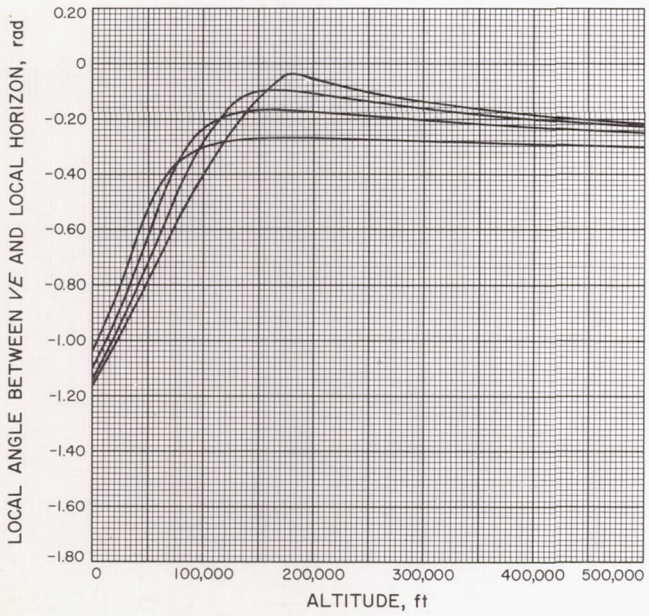

Fig. A-23

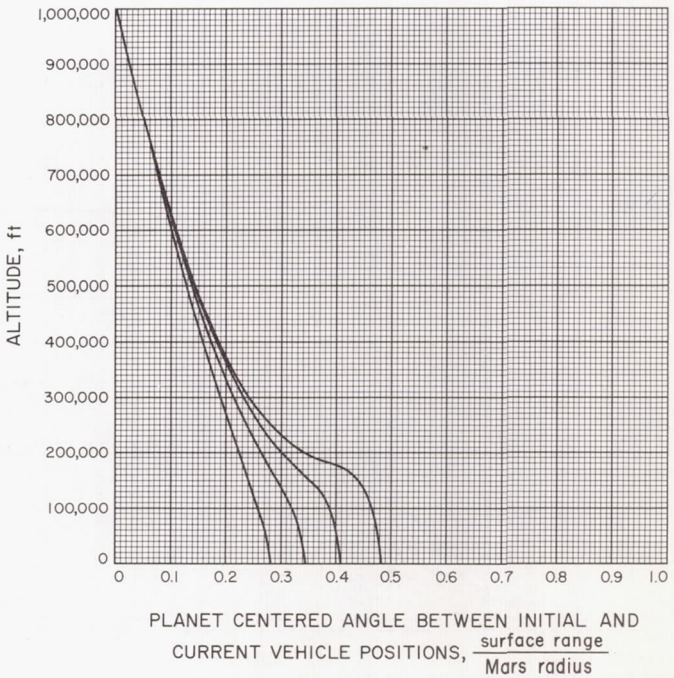

Fig. A-24

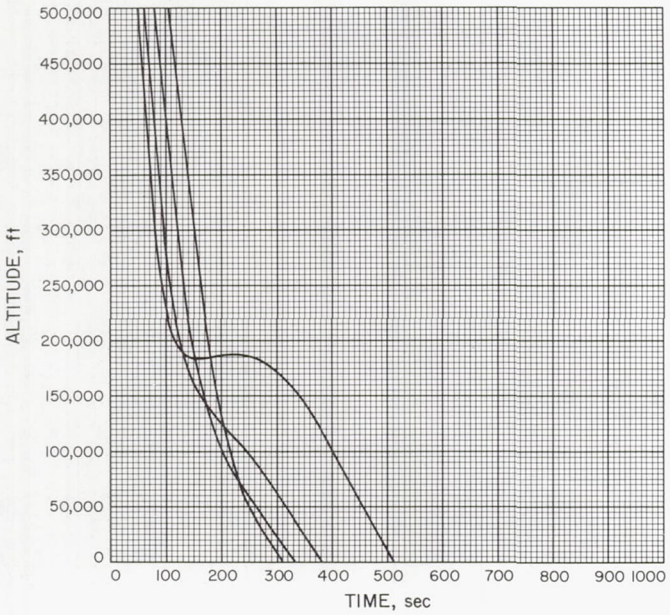

Fig. A-25

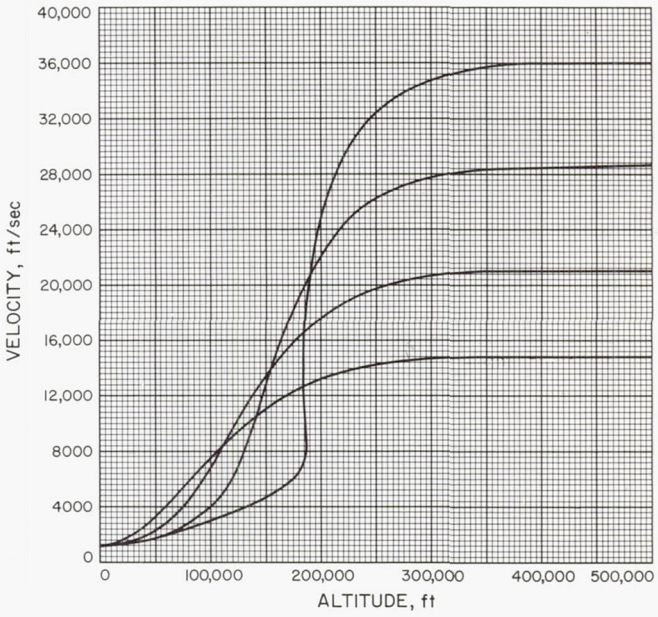

Fig. A-26

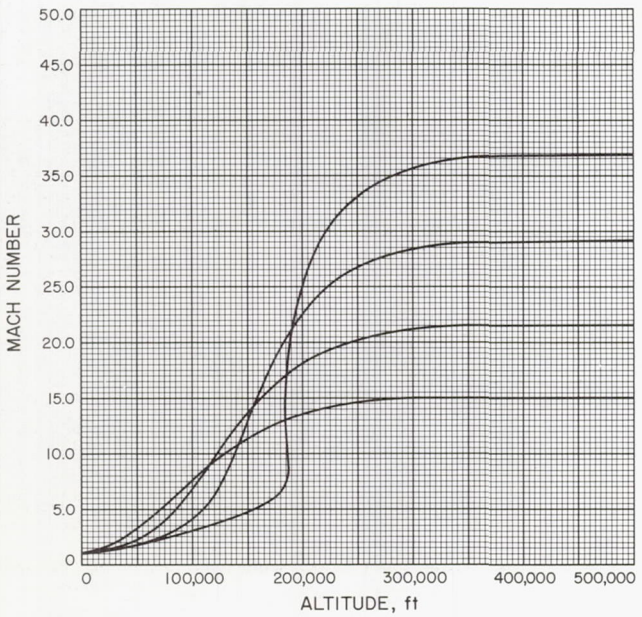

Fig. A-27

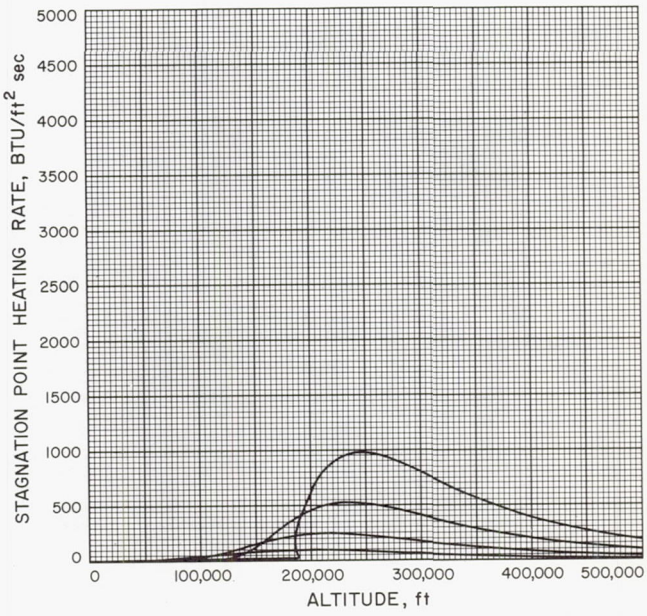

Fig. A-28

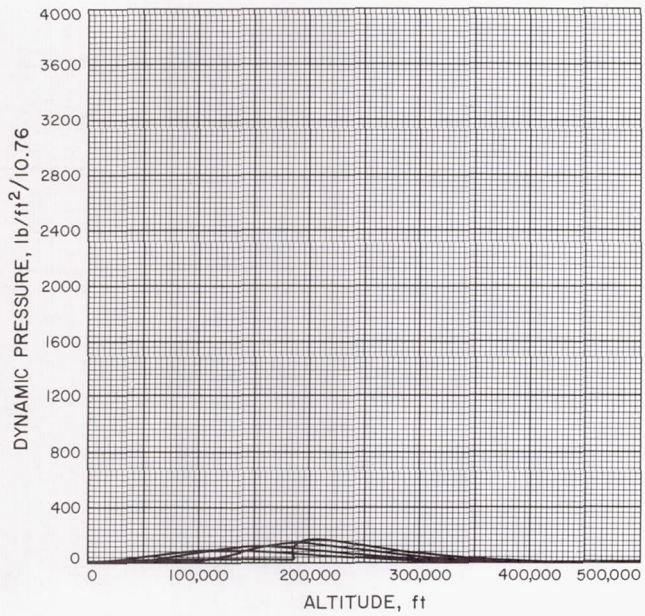

Fig. A-29

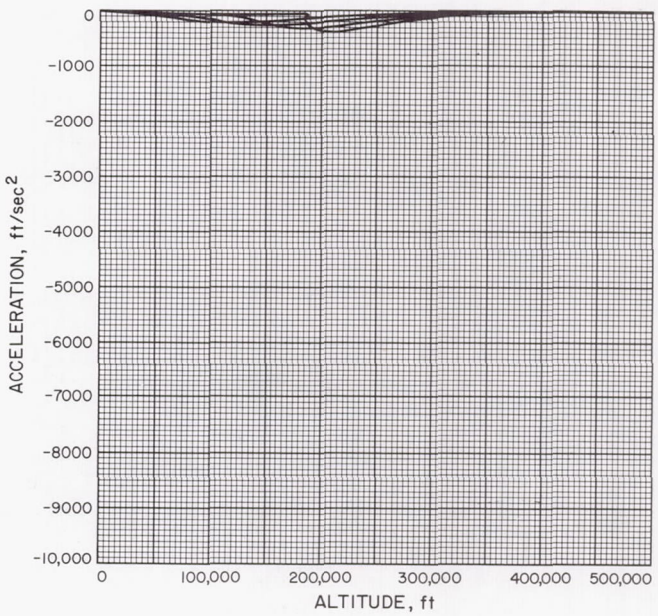

Fig. A-30

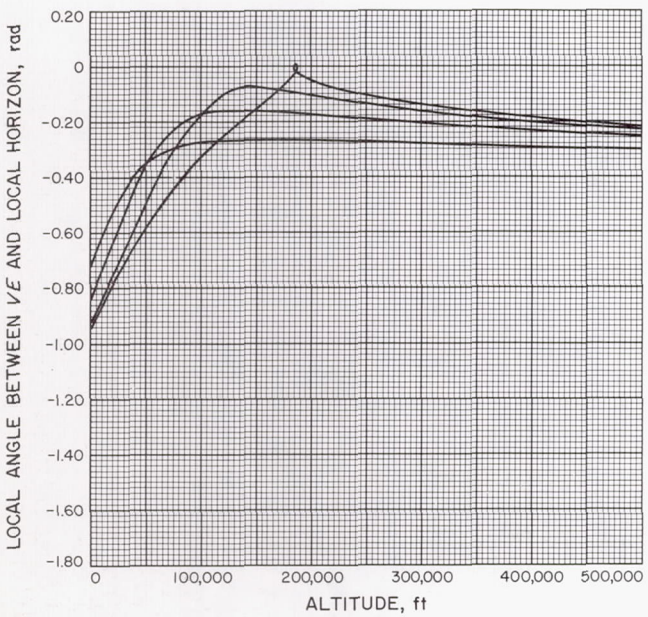

Fig. A-31

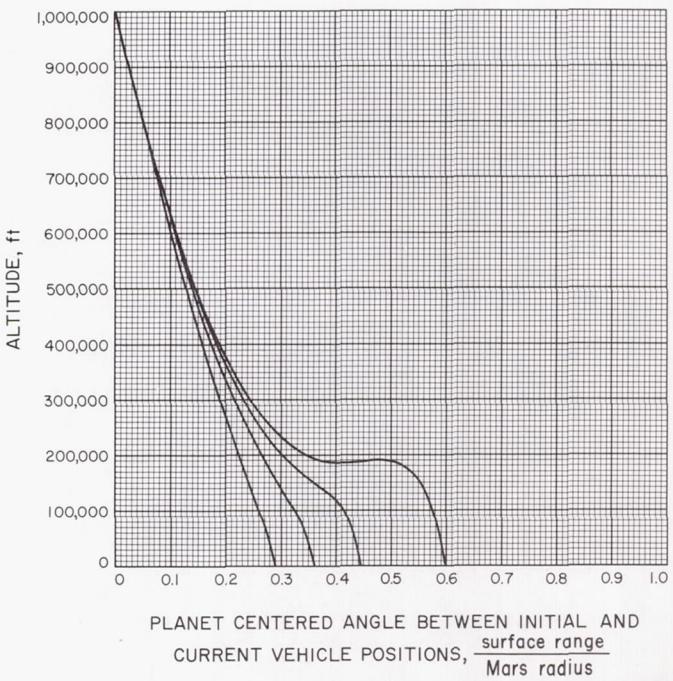

Fig. A-32

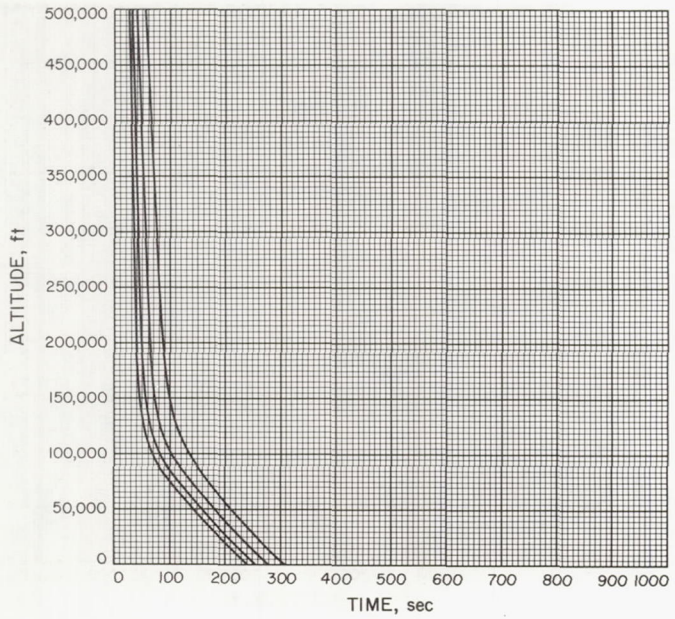

Fig. A-33

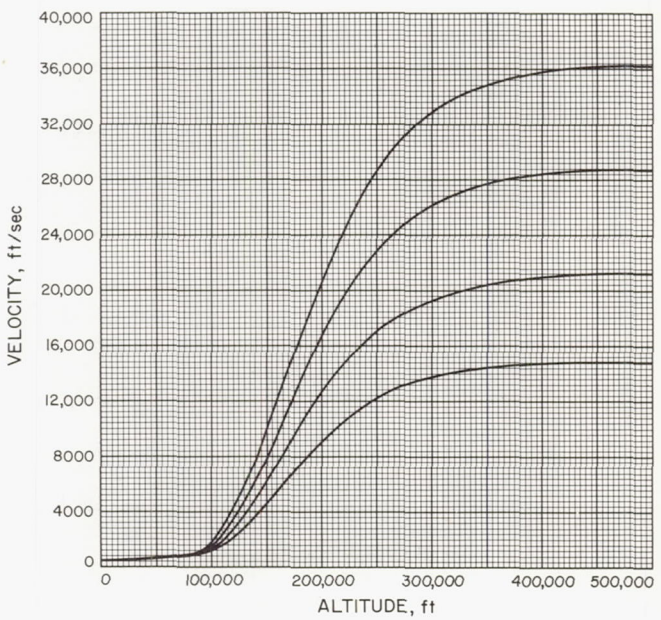

Fig. A-34

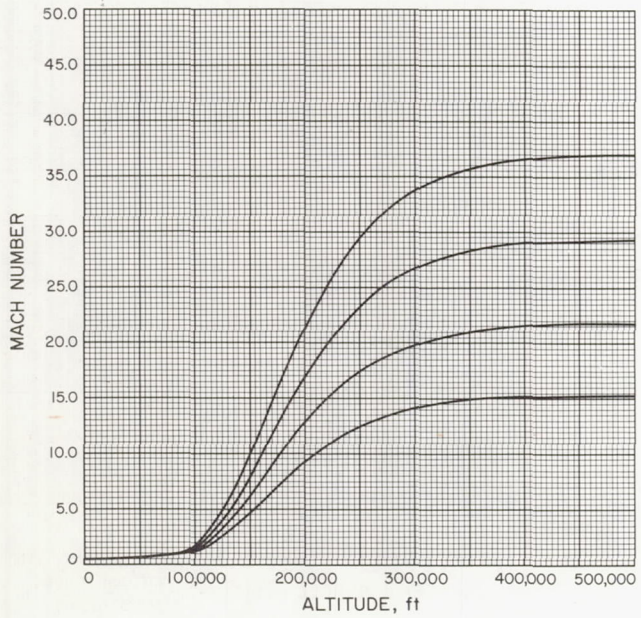

Fig. A-35

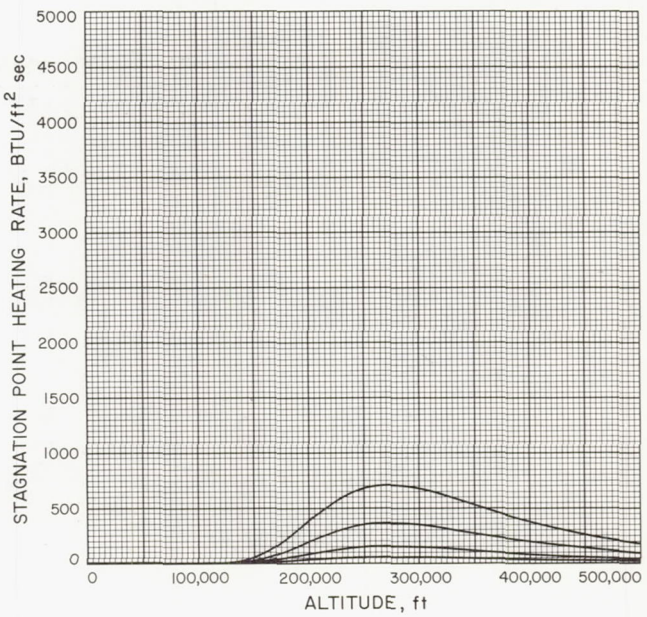

Fig. A-36

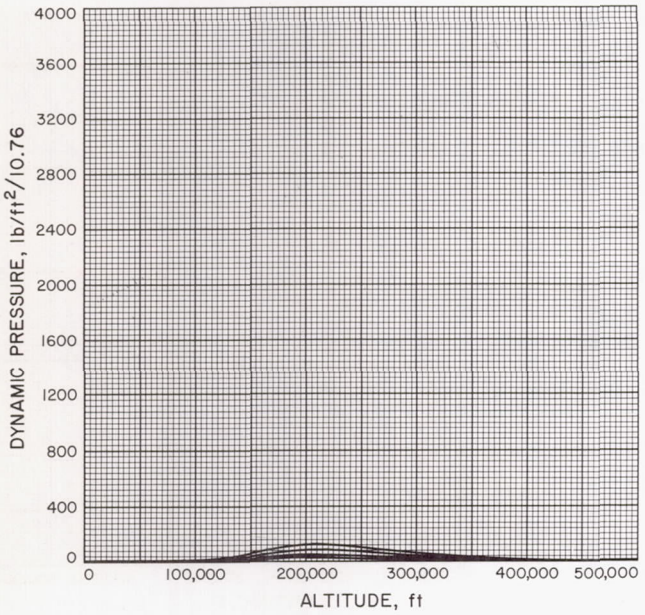

Fig. A-37

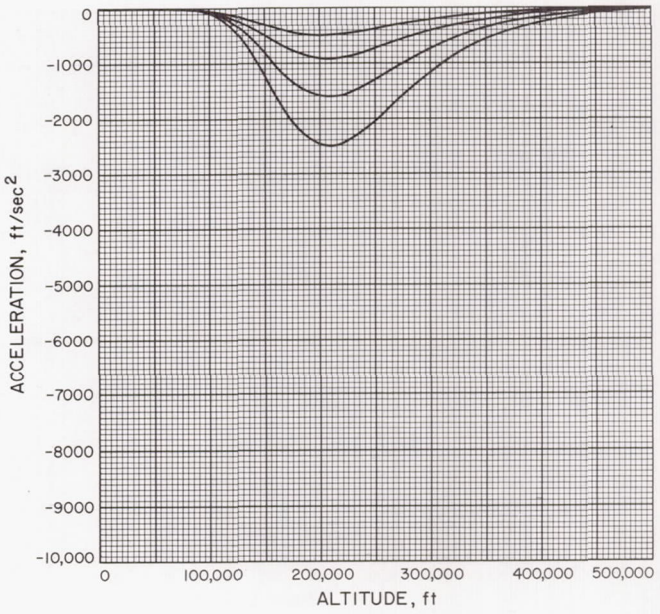

Fig. A-38

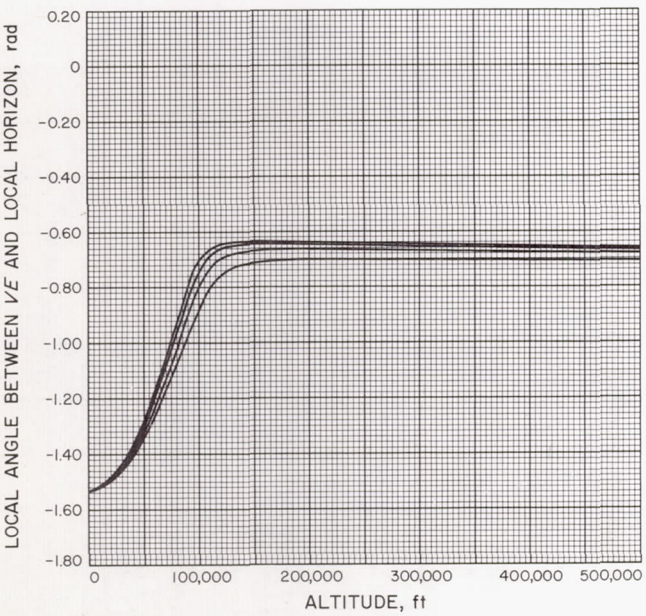

Fig. A-39

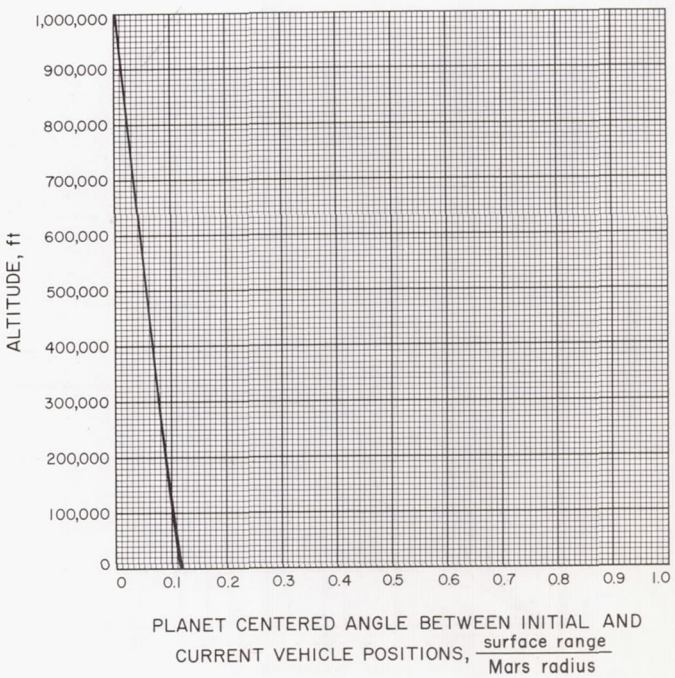

Fig. A-40

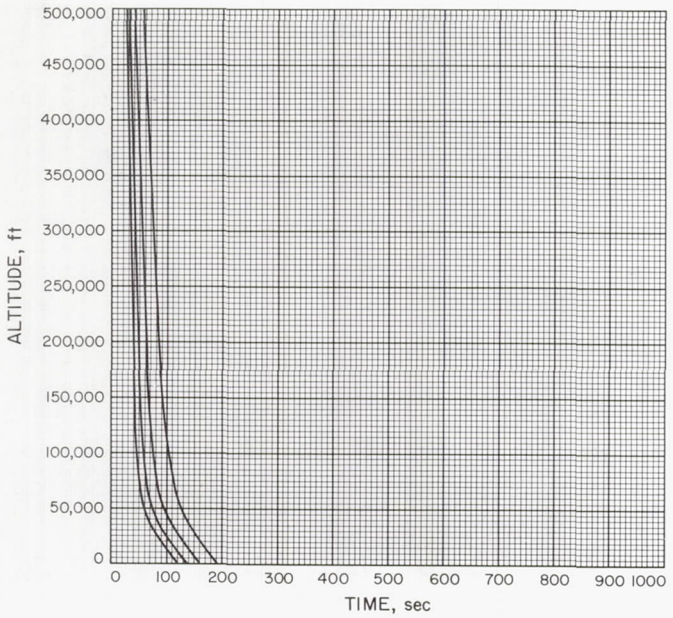

Fig. A-41

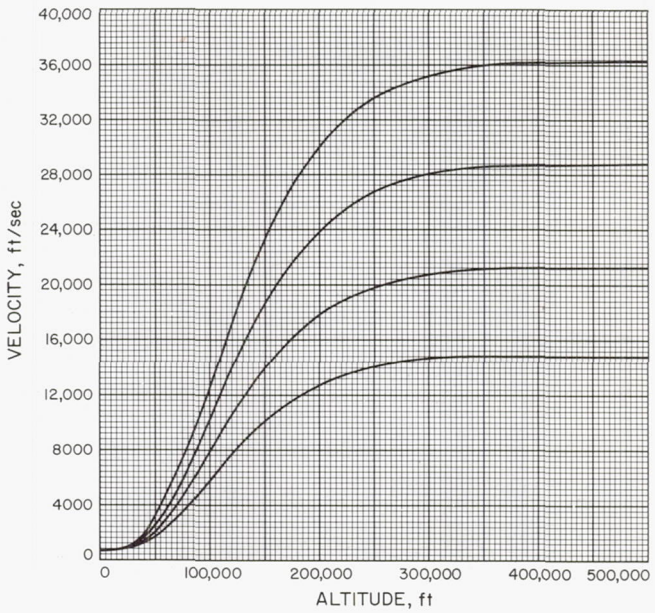

Fig. A-42

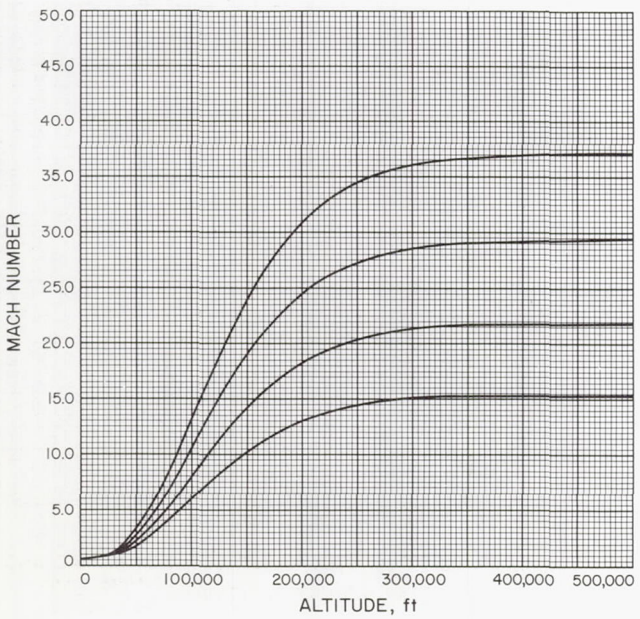

Fig. A-43

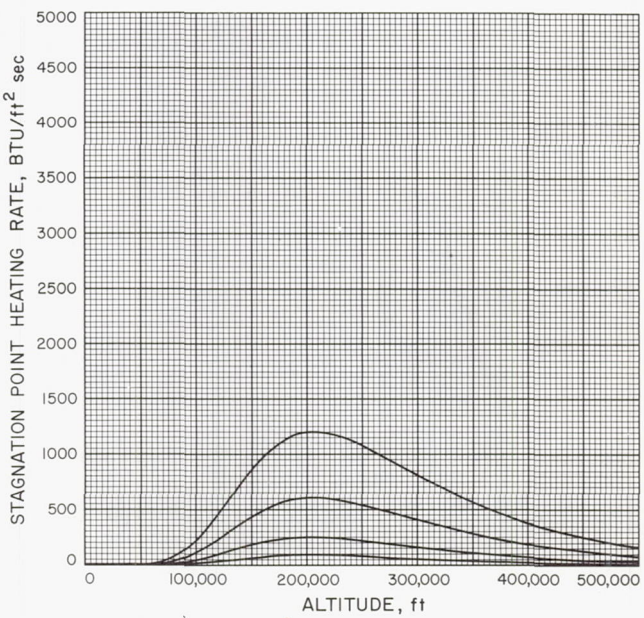

Fig. A-44

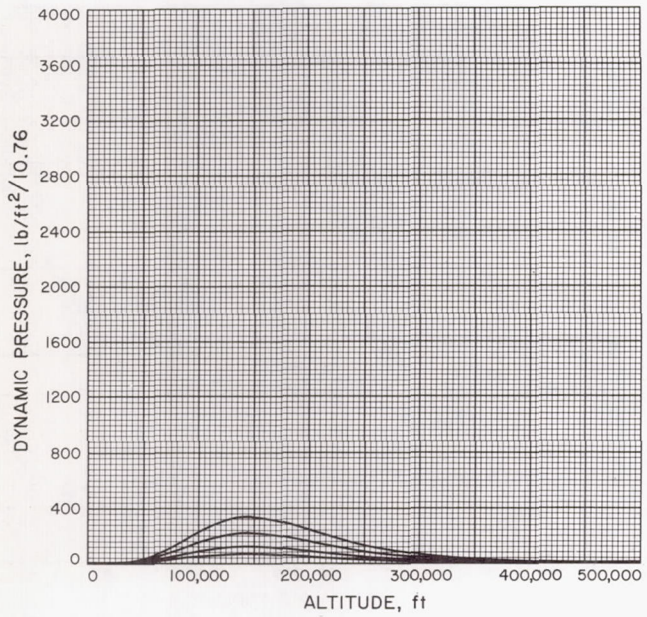

Fig. A-45

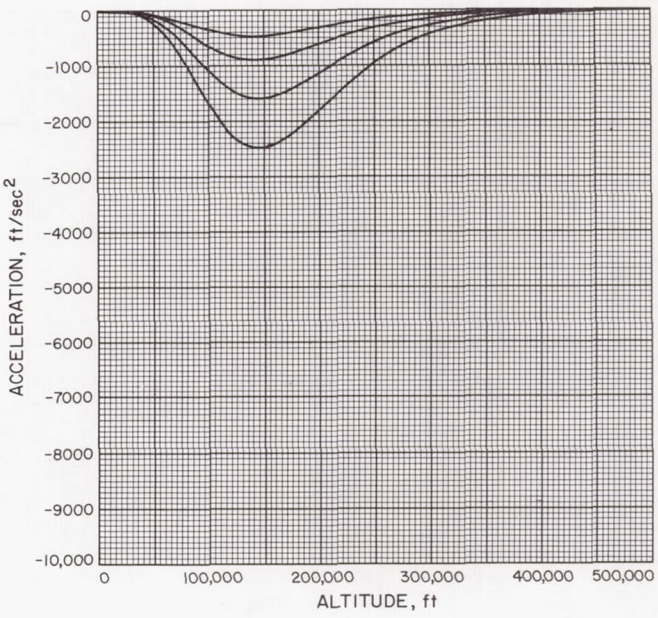

Fig. A-46

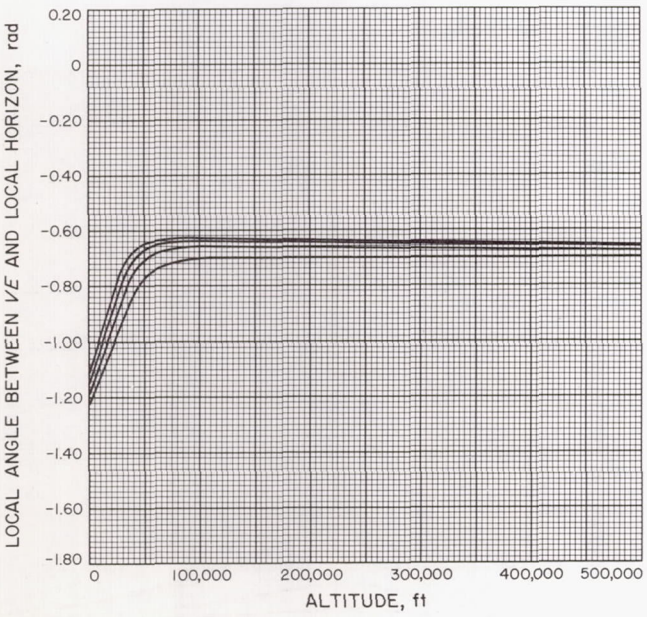

Fig. A-47

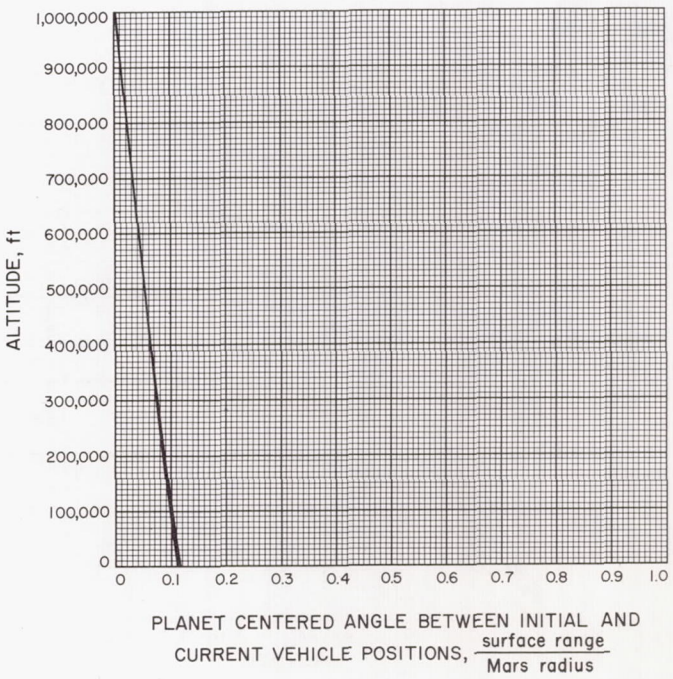

Fig. A-48

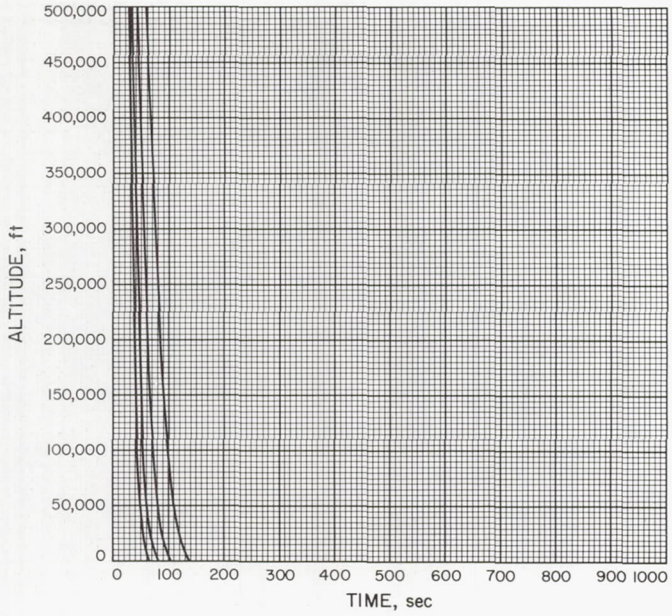

Fig. A-49

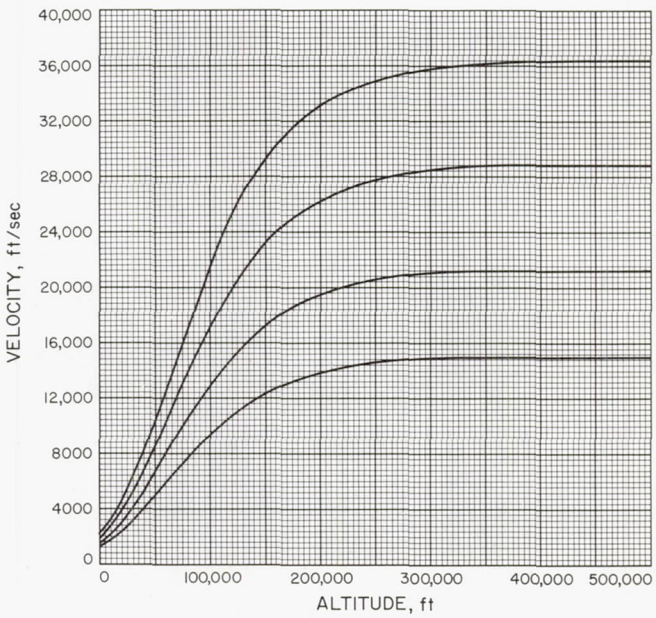

Fig. A-50

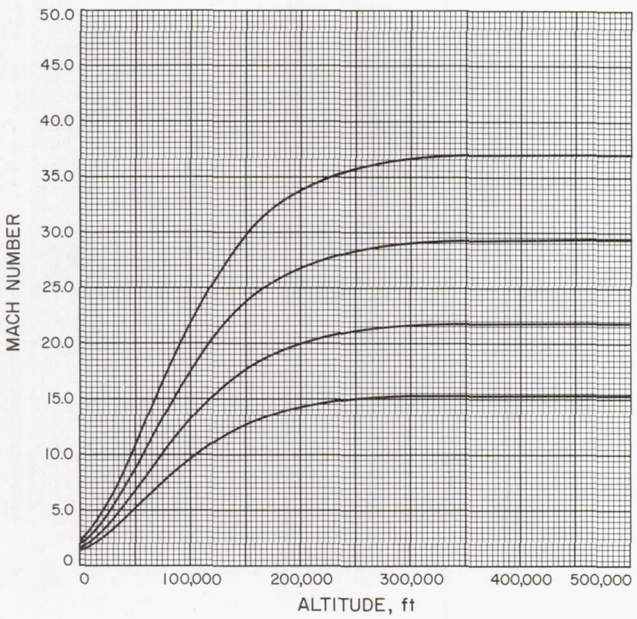

Fig. A-51

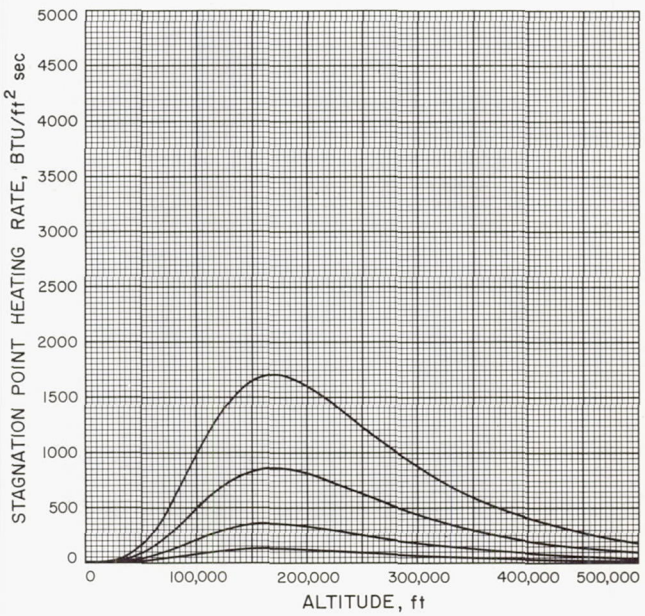

Fig. A-52

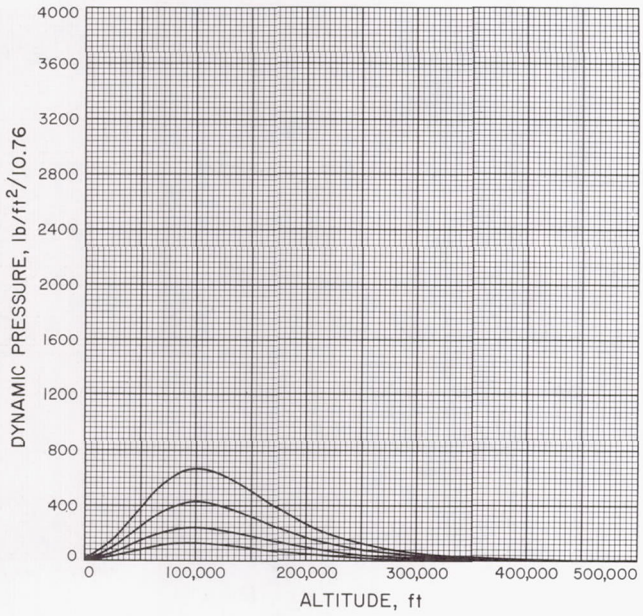

Fig. A-53

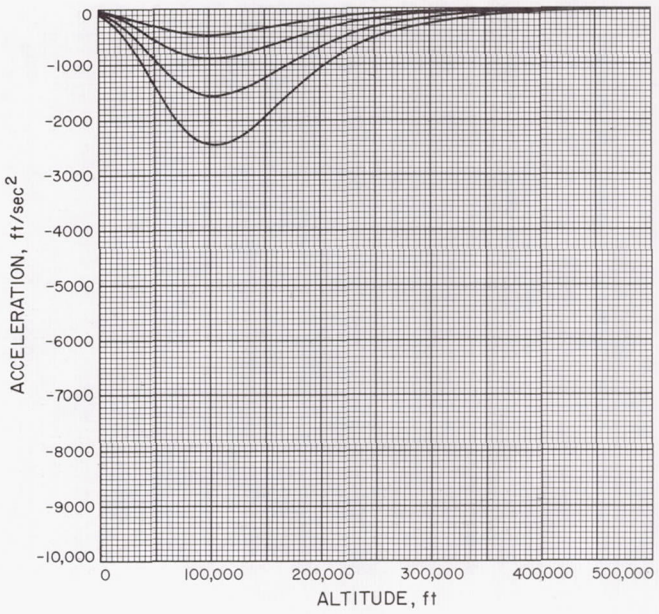

Fig. A-54

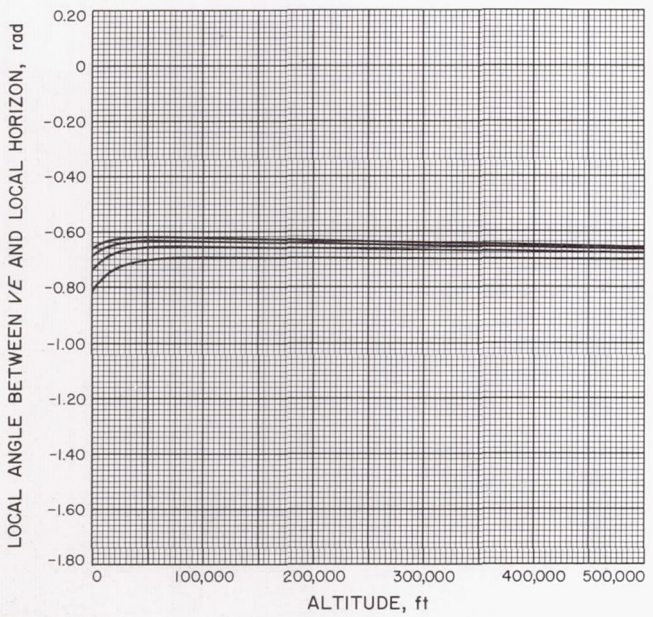

Fig. A-55

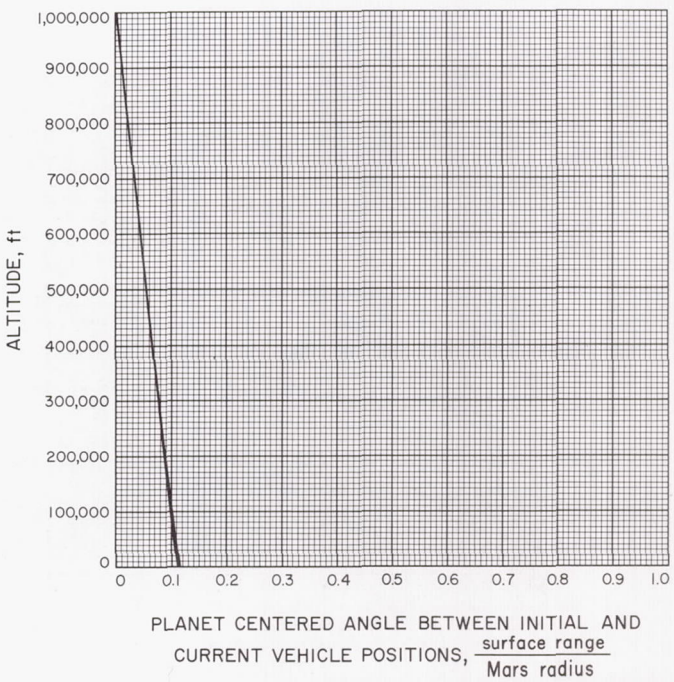

Fig. A-56

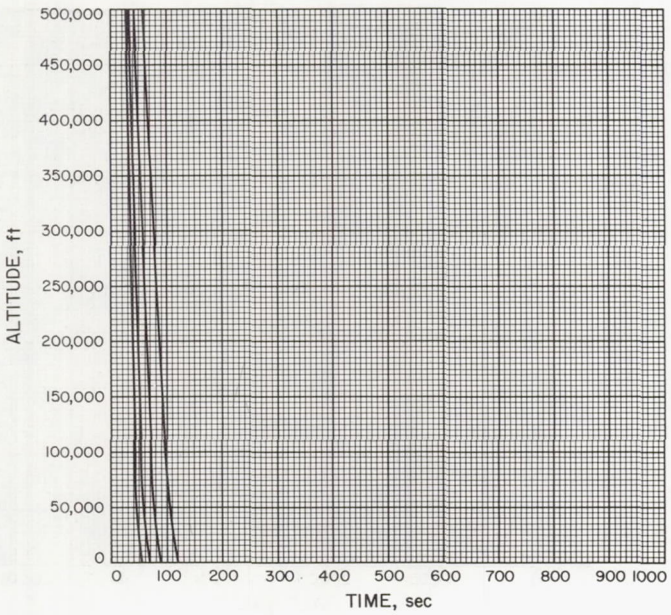

Fig. A-57

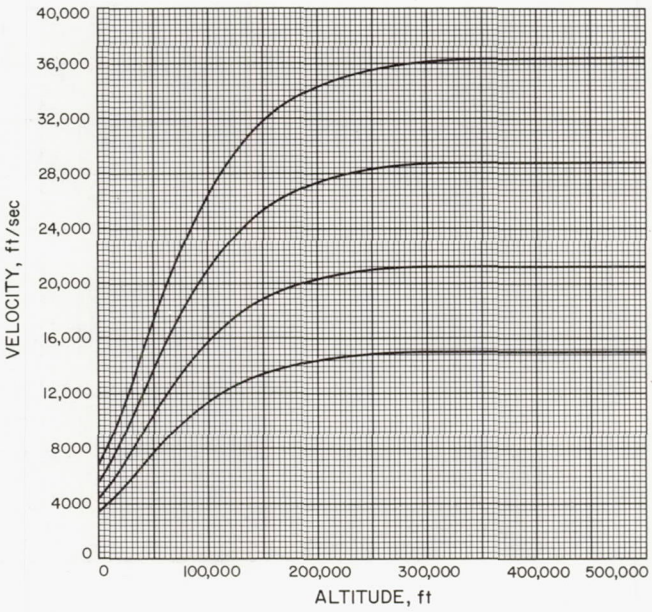

Fig. A-58

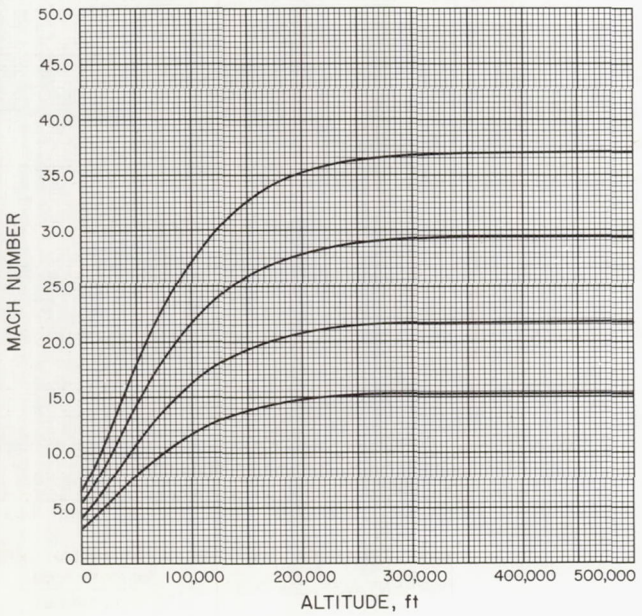

Fig. A-59

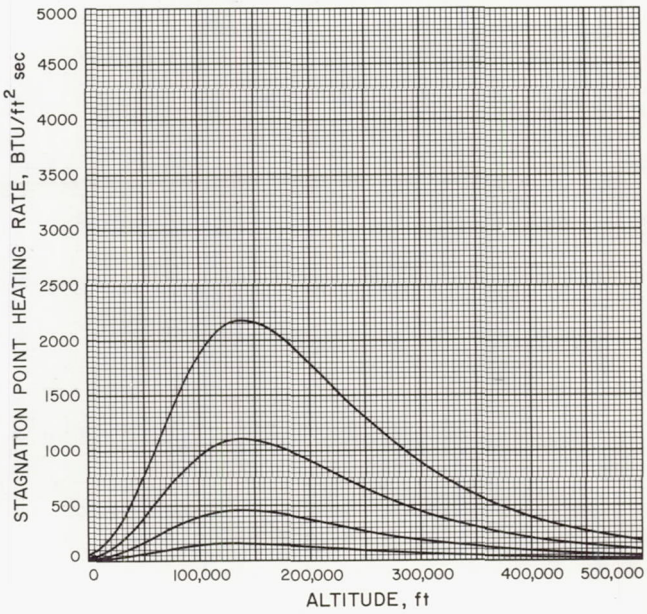

Fig. A-60

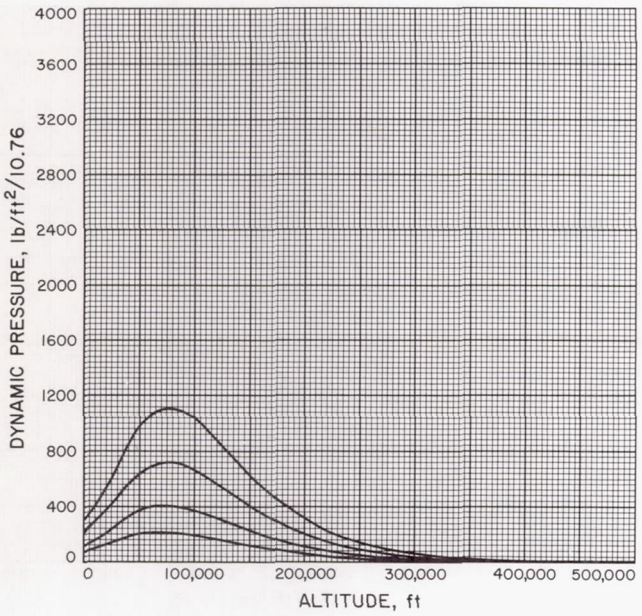

Fig. A-61

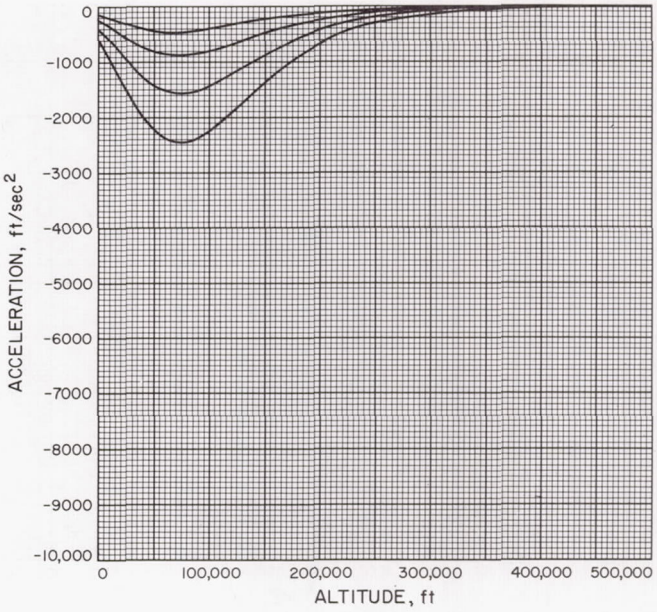

Fig. A-62

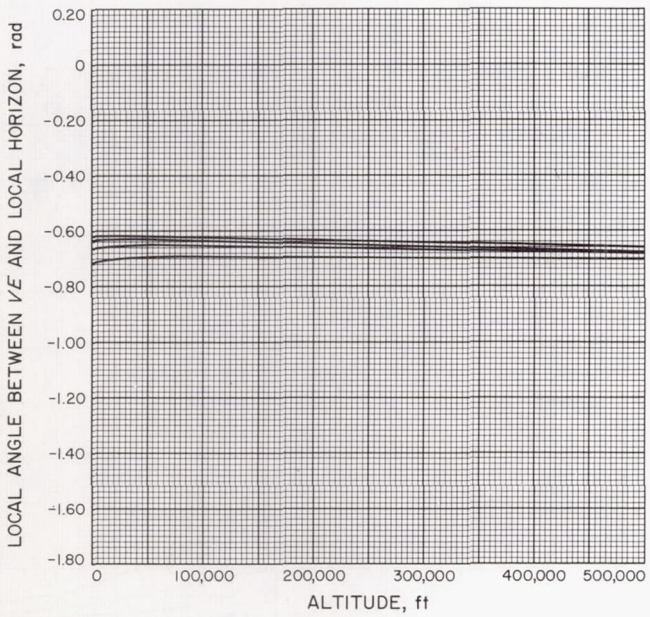

Fig. A-63

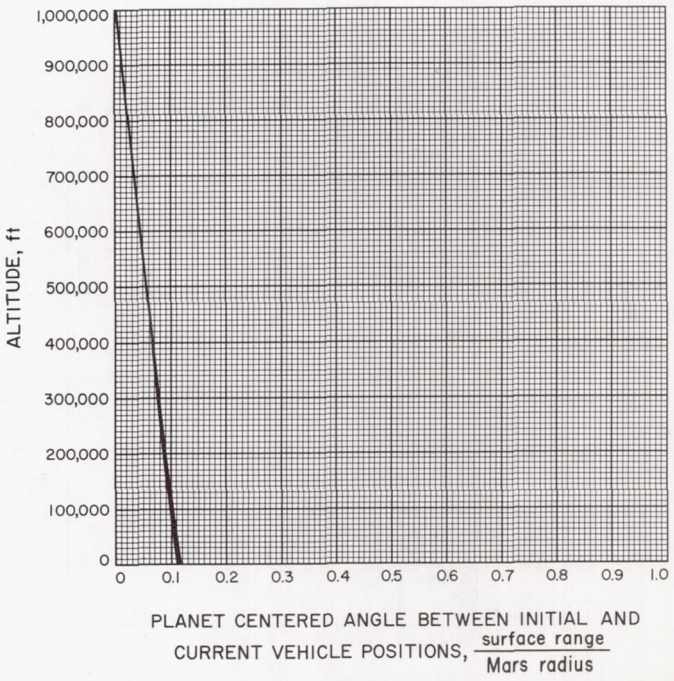

Fig. A-64

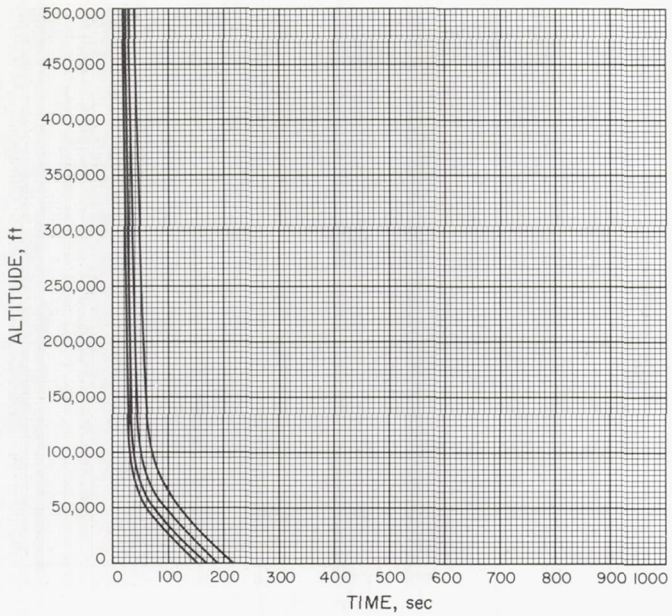

Fig. A-65

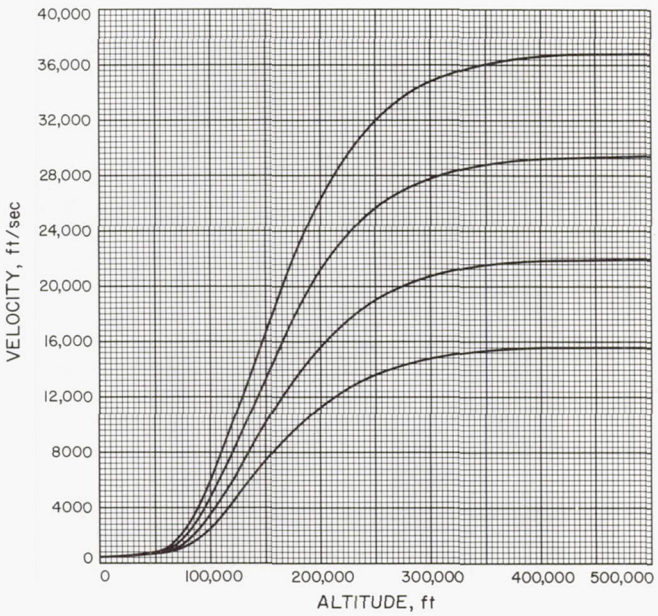

Fig. A-66

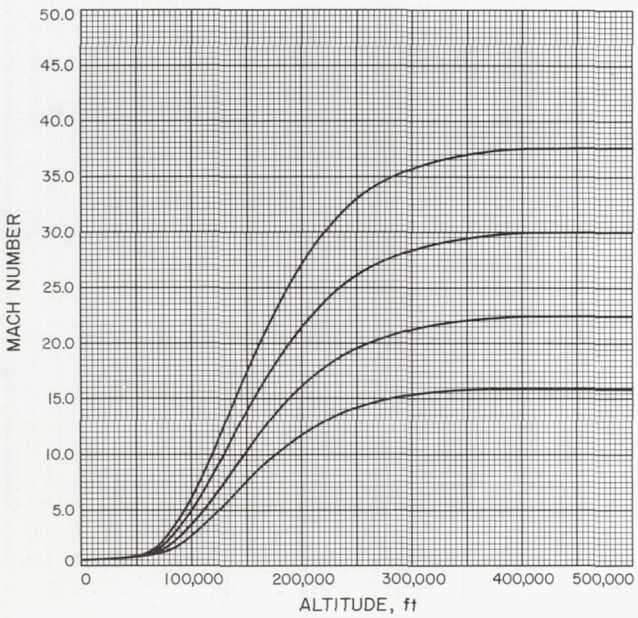

Fig. A-67

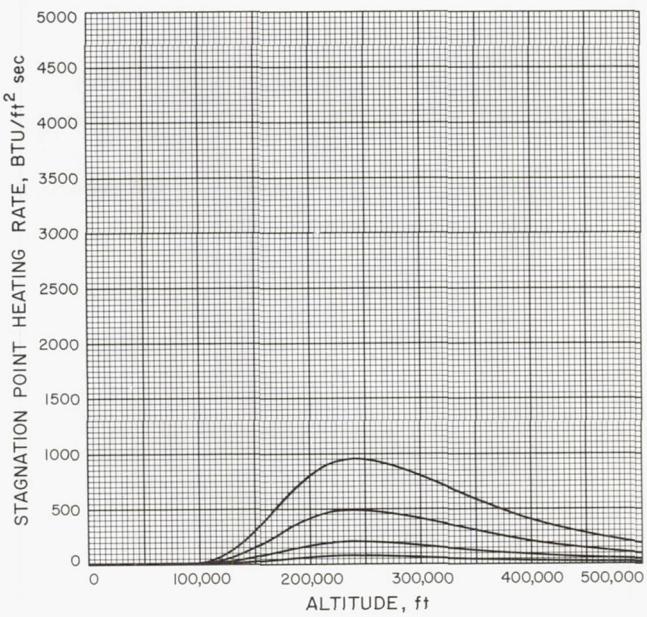

Fig. A-68

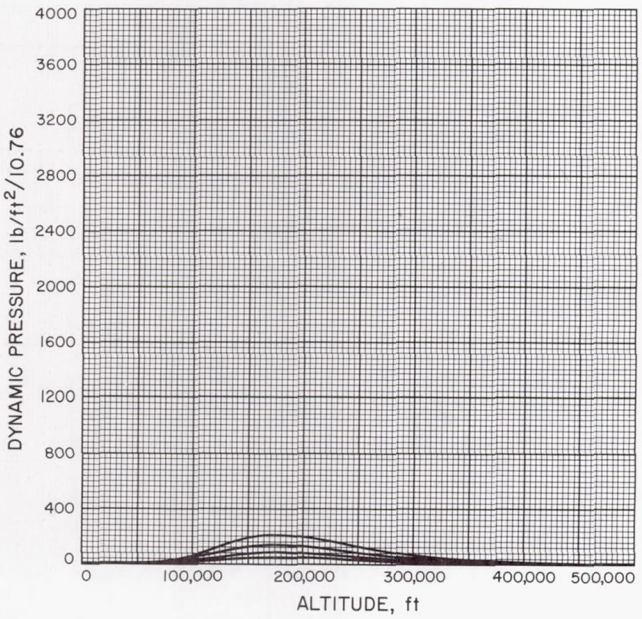

Fig. A-69

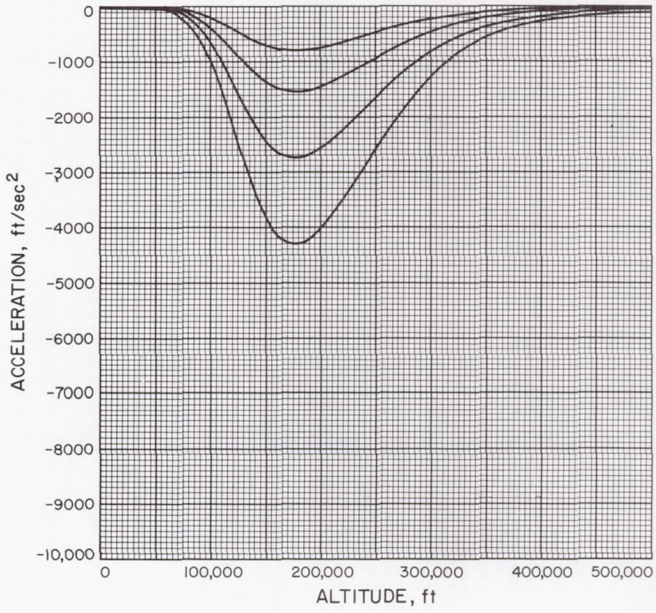

Fig. A-70

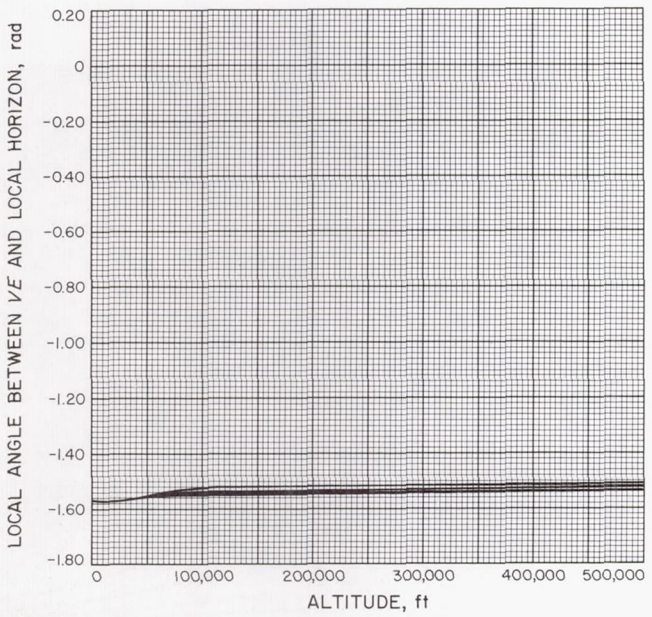

Fig. A-71

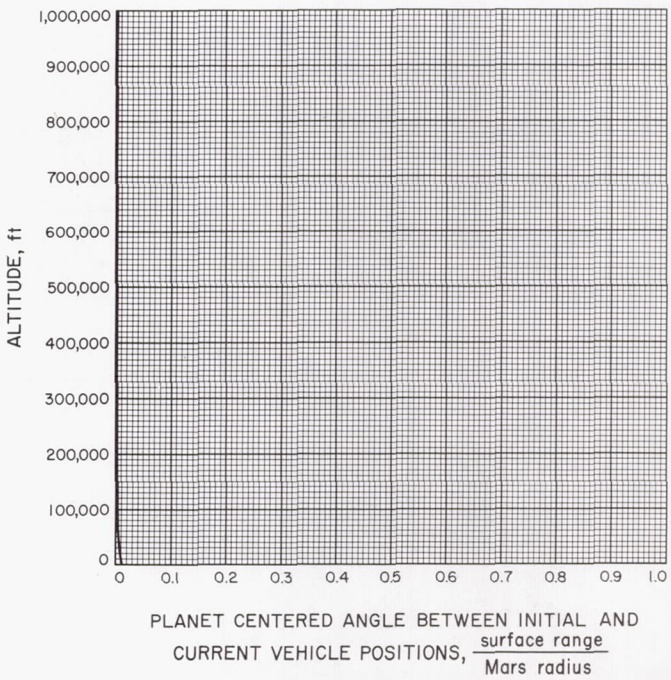

Fig. A-72

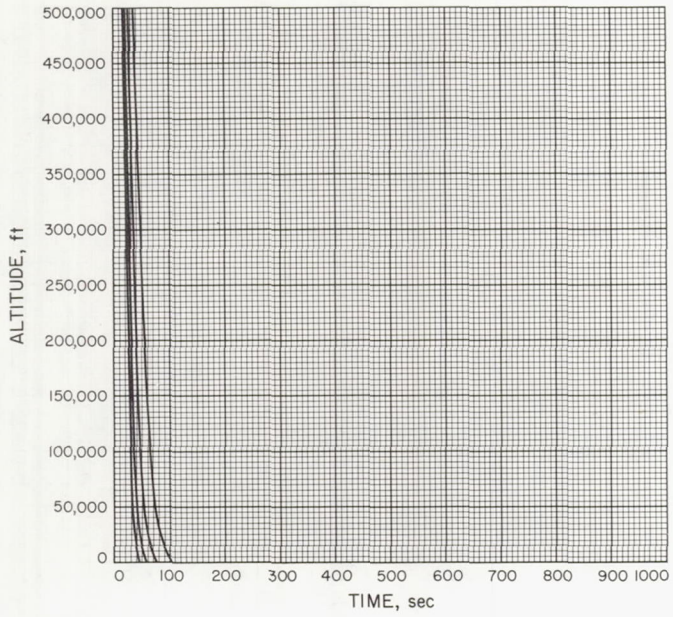

Fig. A-73

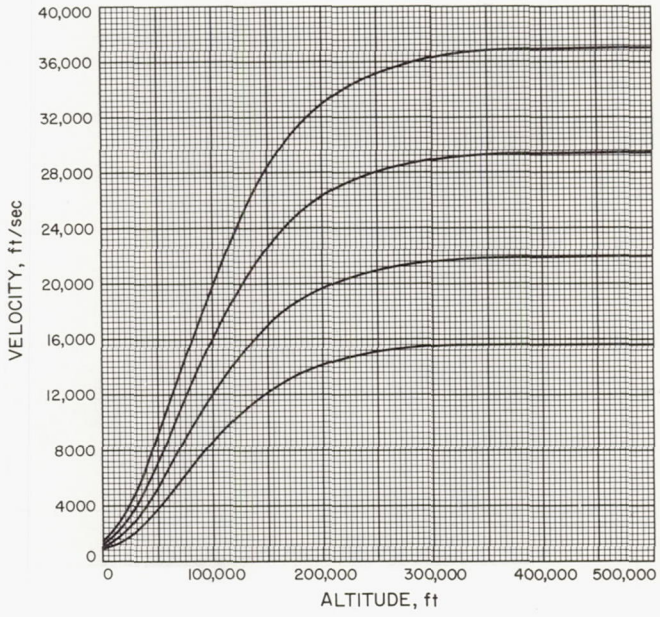

Fig. A-74

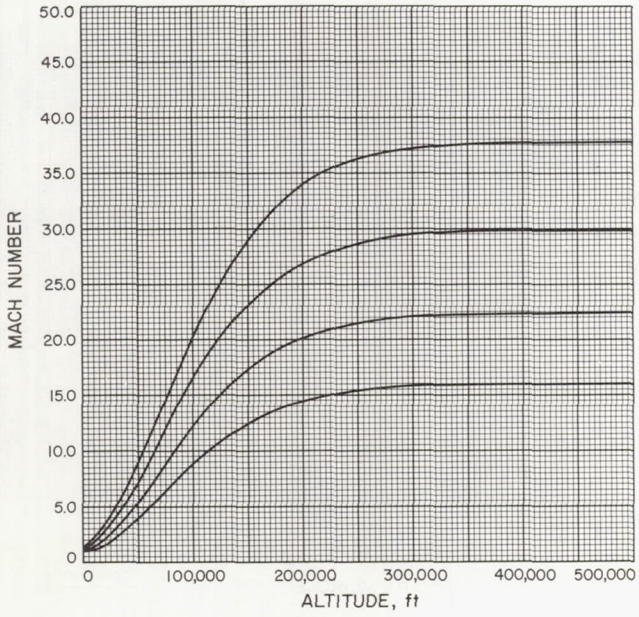

Fig. A-75

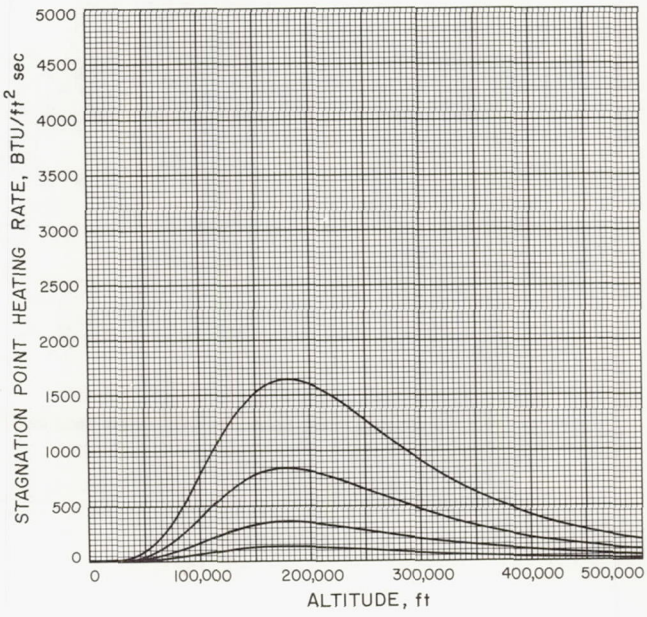

Fig. A-76

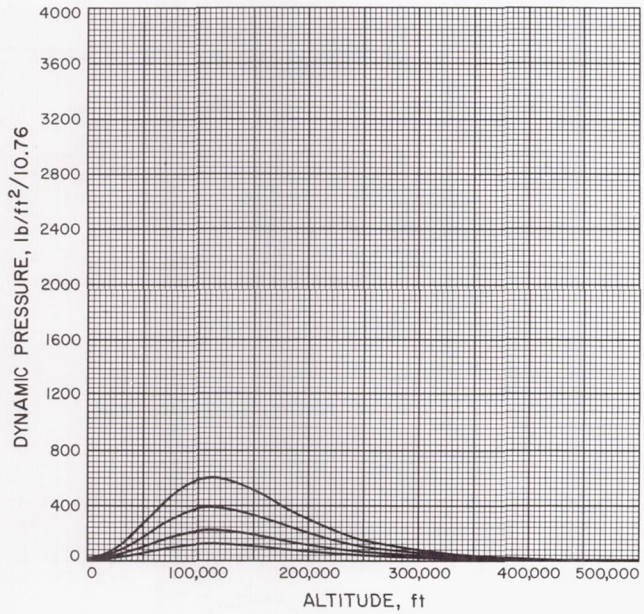

Fig. A-77

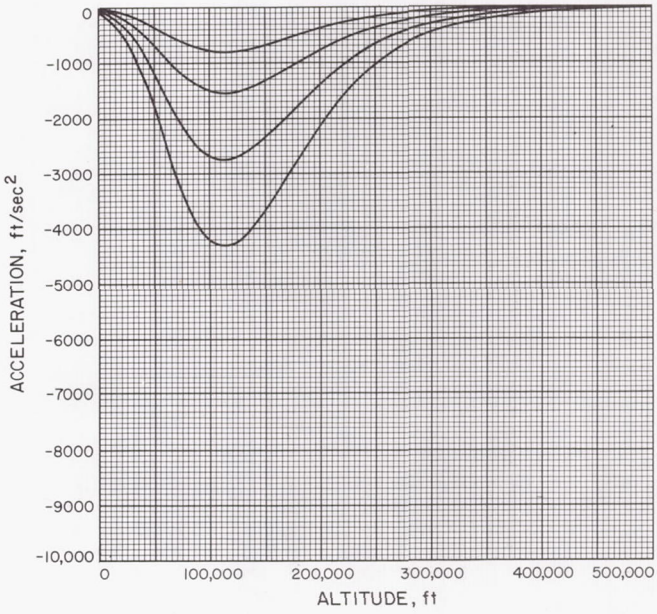

Fig. A-78

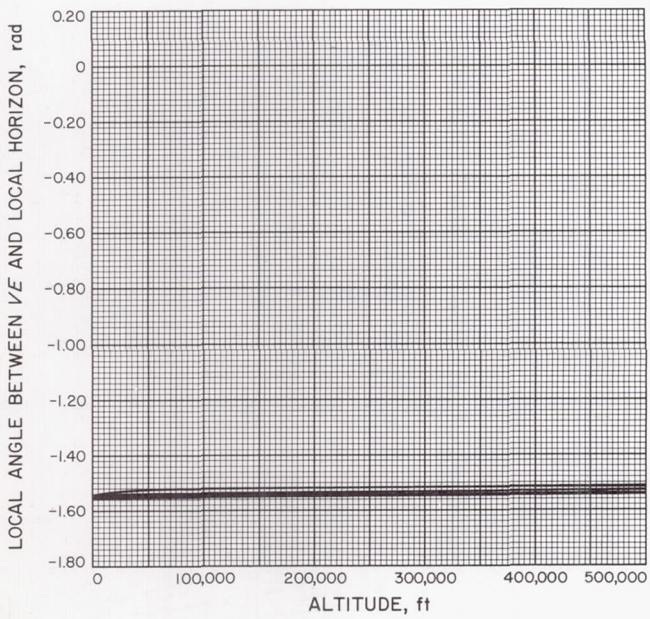

Fig. A-79

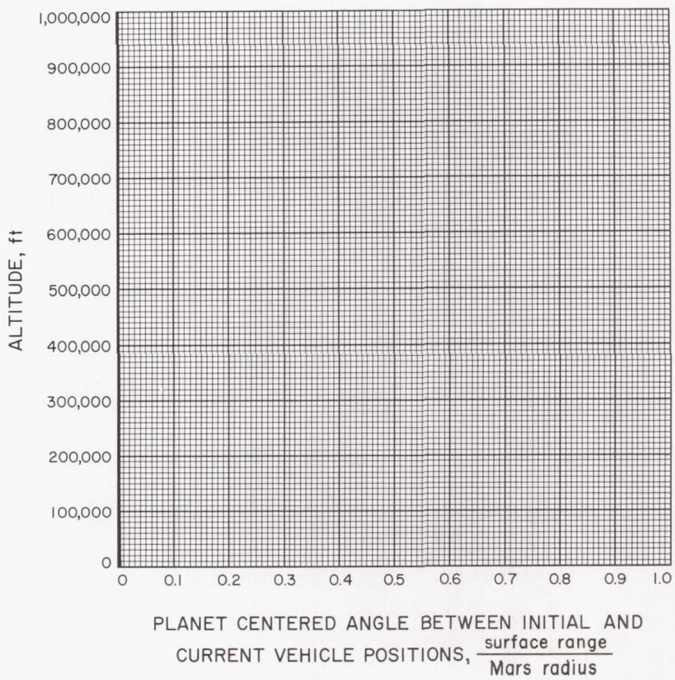

Fig. A-80

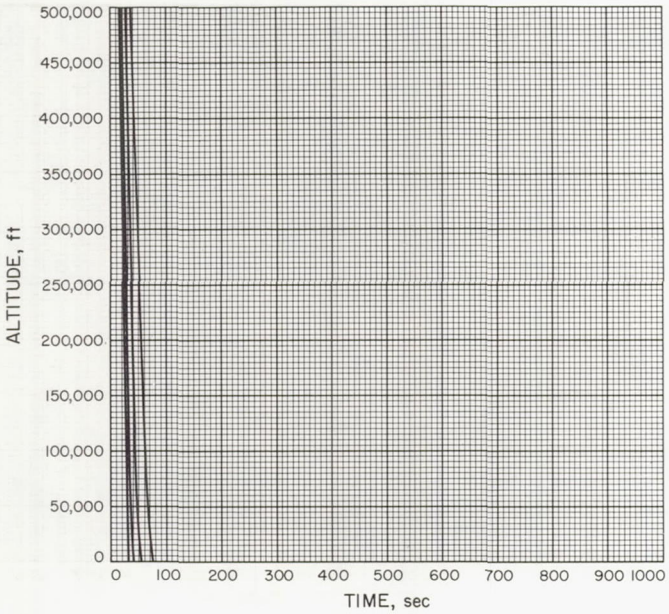

Fig. A-81

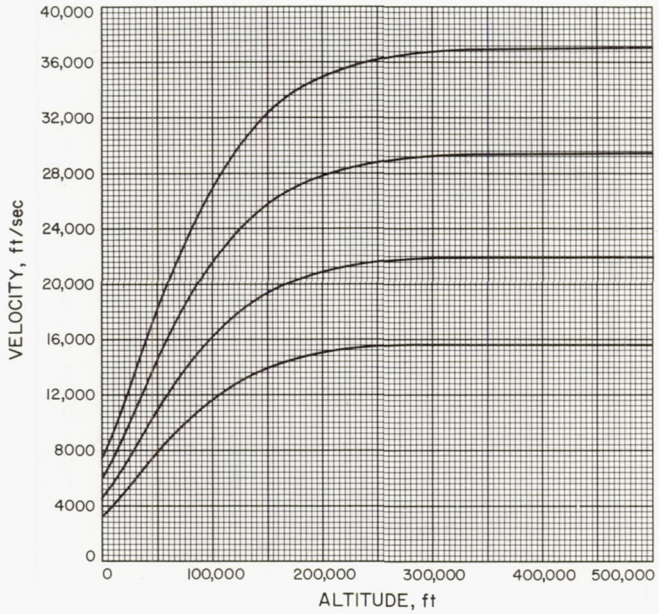

Fig. A-82

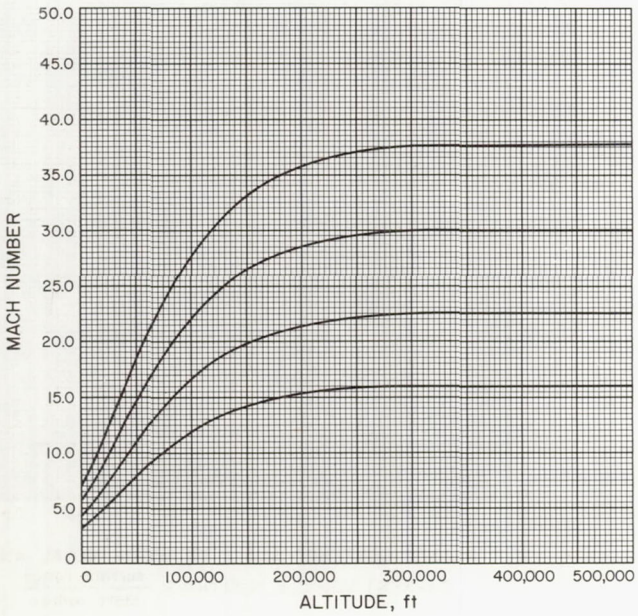

Fig. A-83

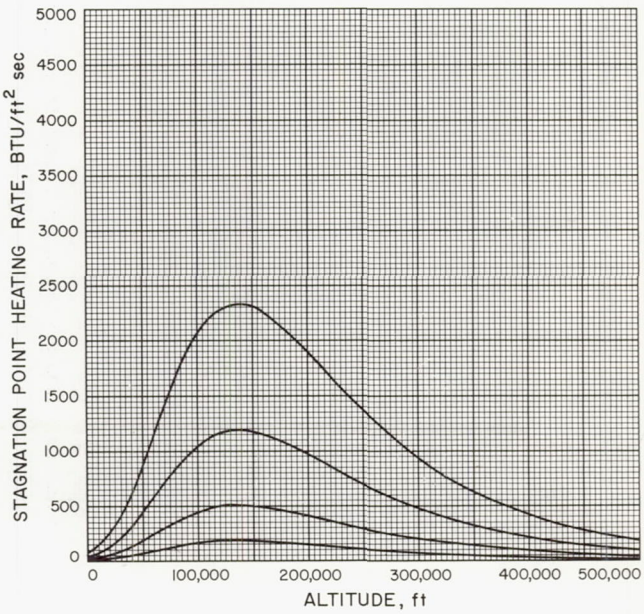

Fig. A-84

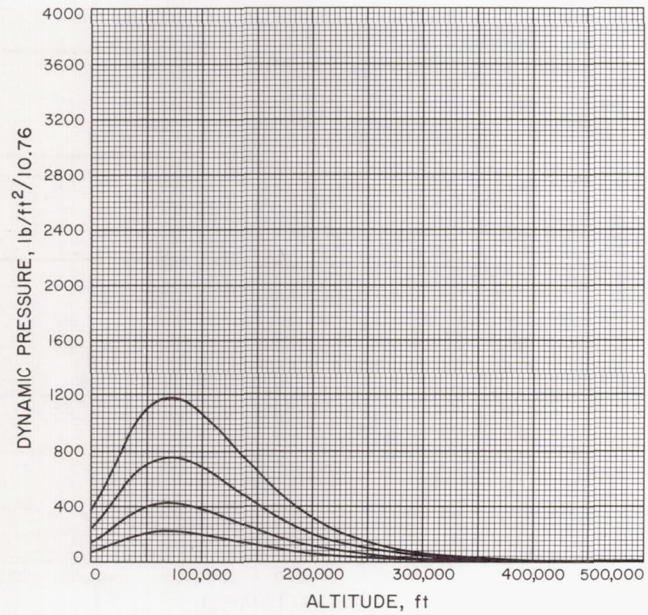

Fig. A-85

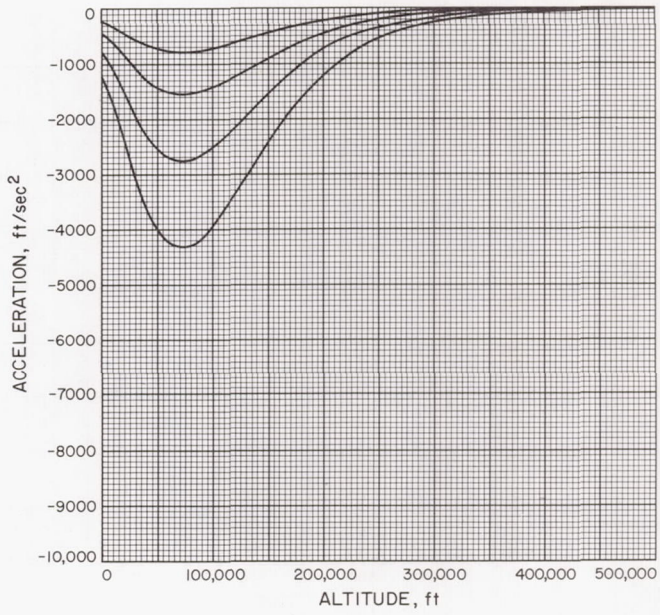

Fig. A-86

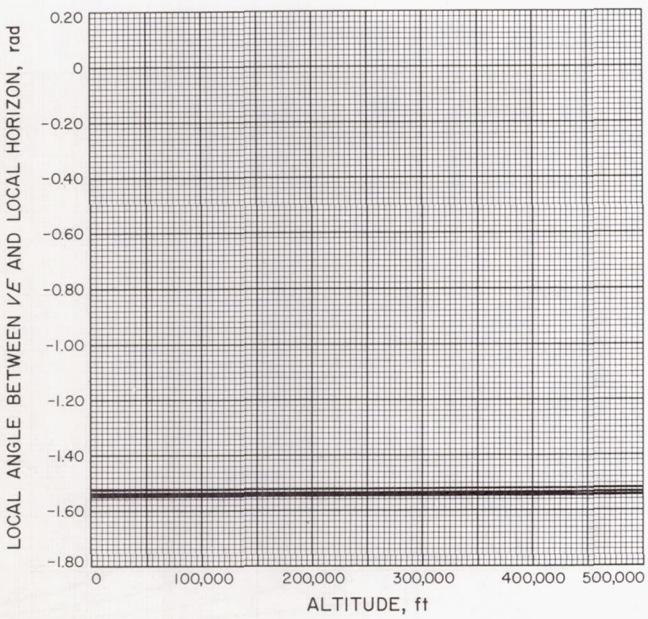

Fig. A-87

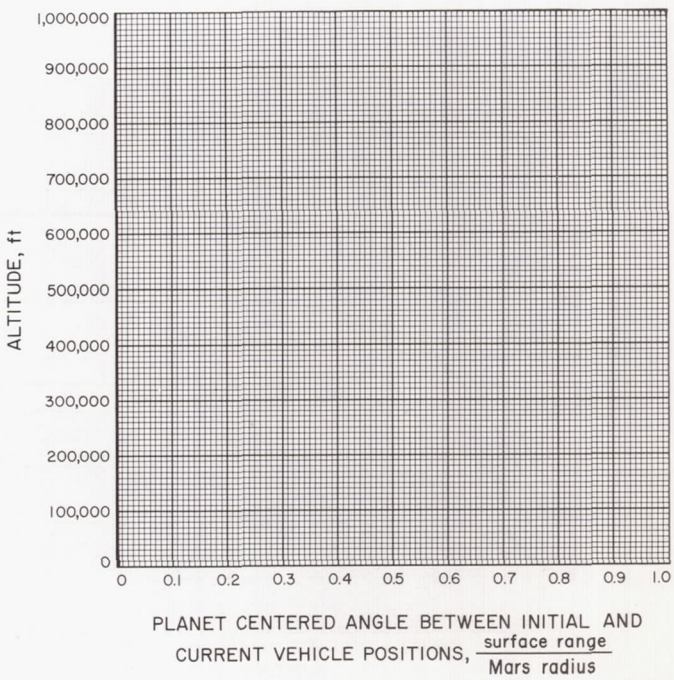

Fig. A-88

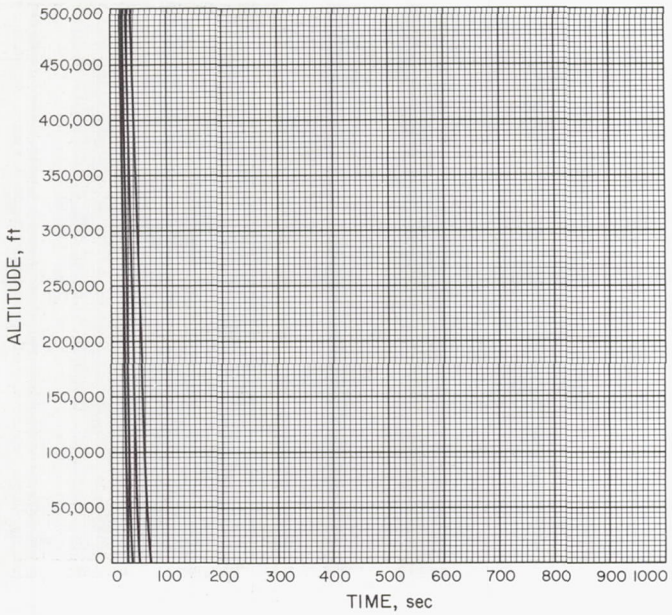

Fig. A-89

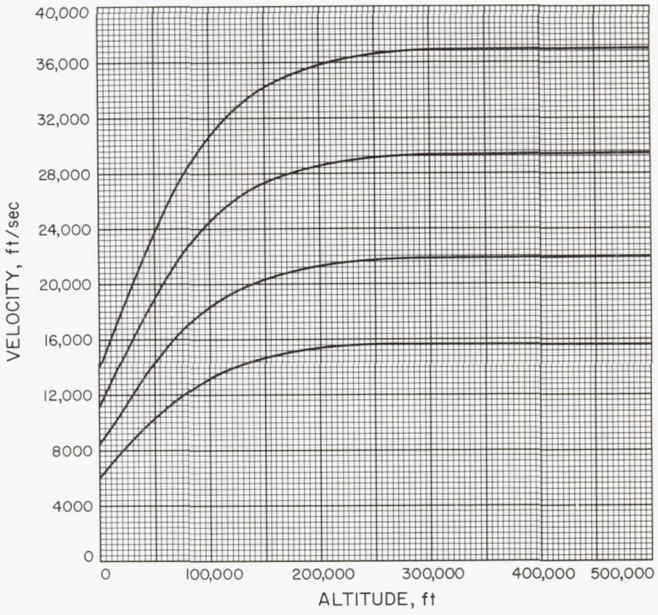

Fig. A-90

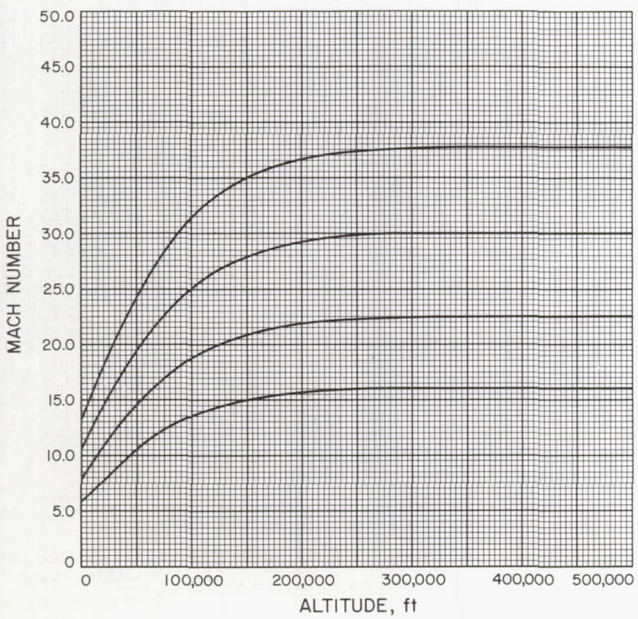

Fig. A-91

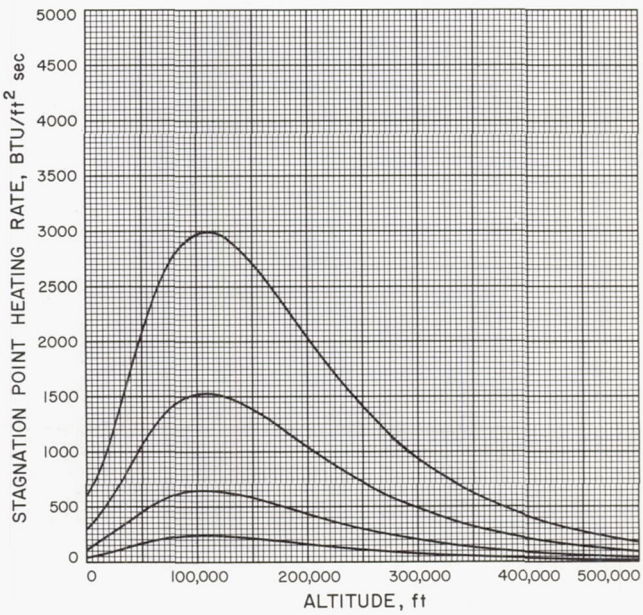

Fig. A-92

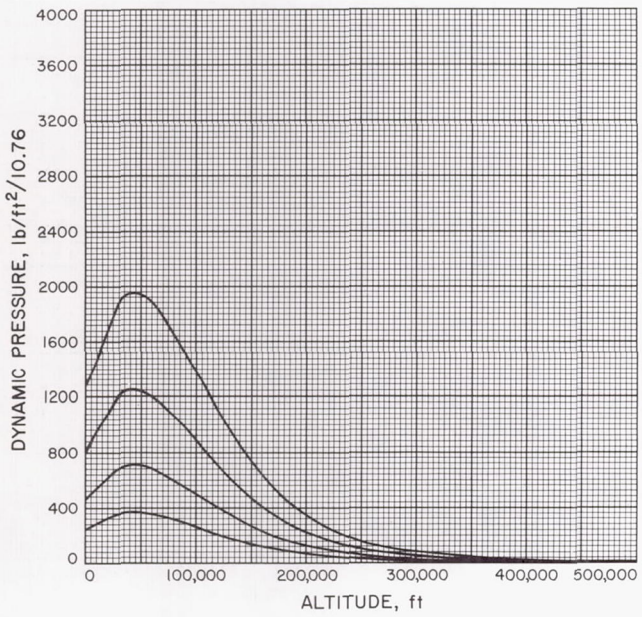

Fig. A-93

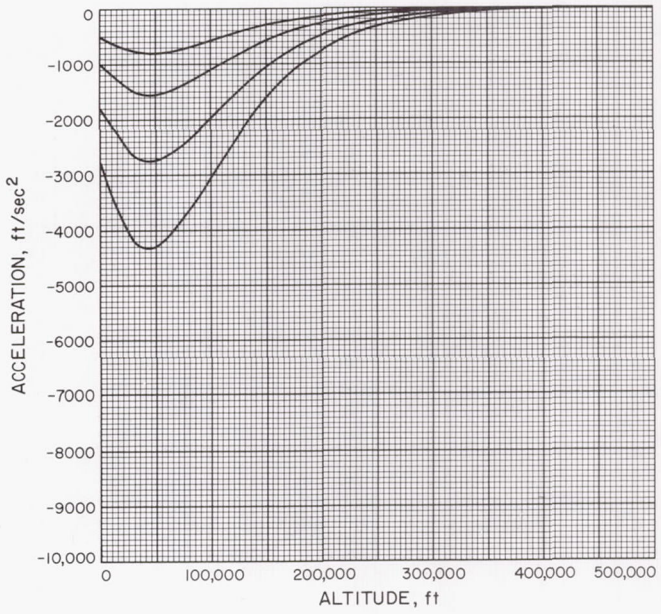

Fig. A-94

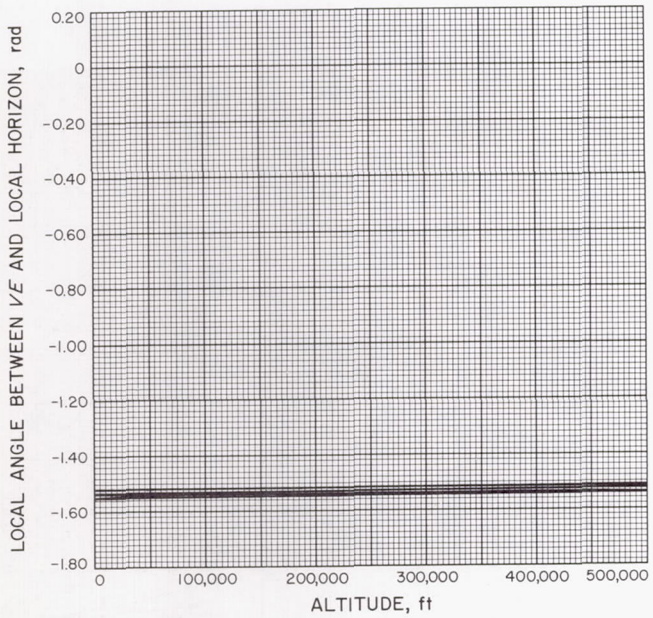

Fig. A-95

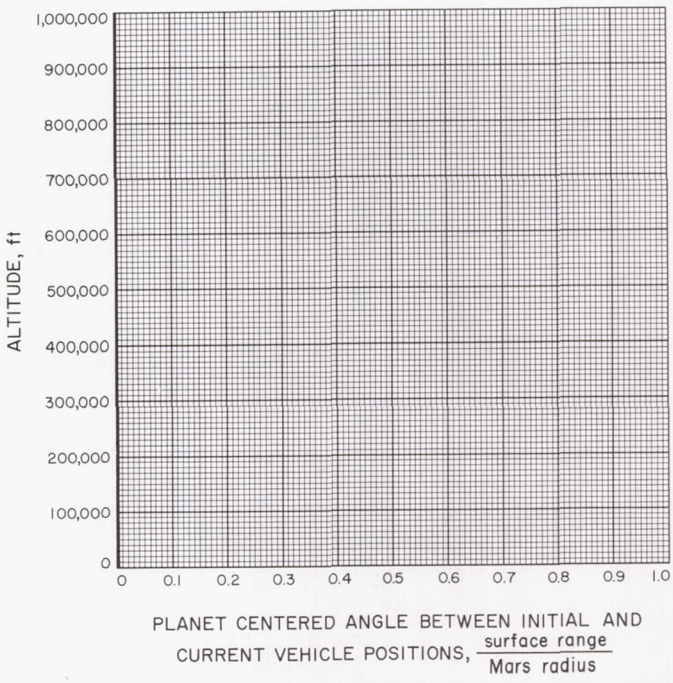

Fig. A-96

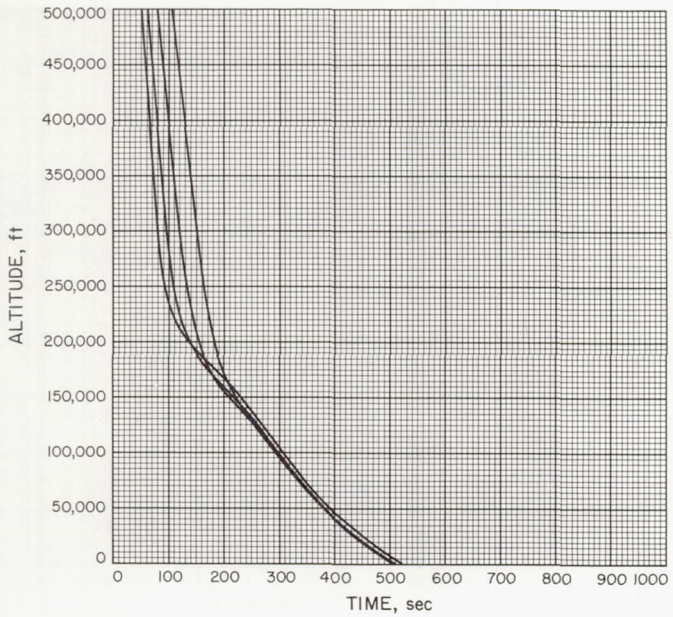

Fig. A-97

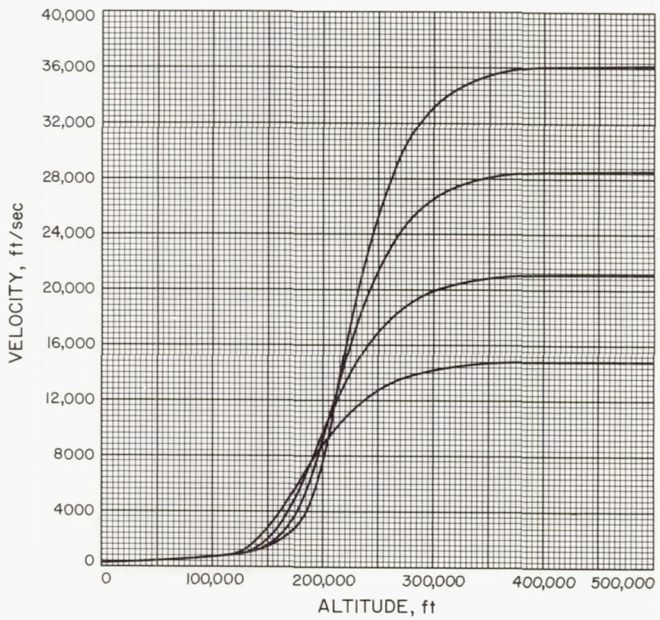

Fig. A-98

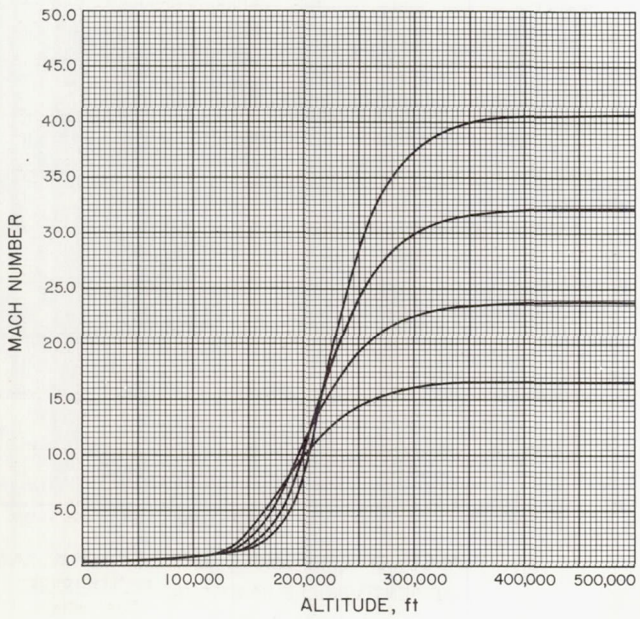

Fig. A-99

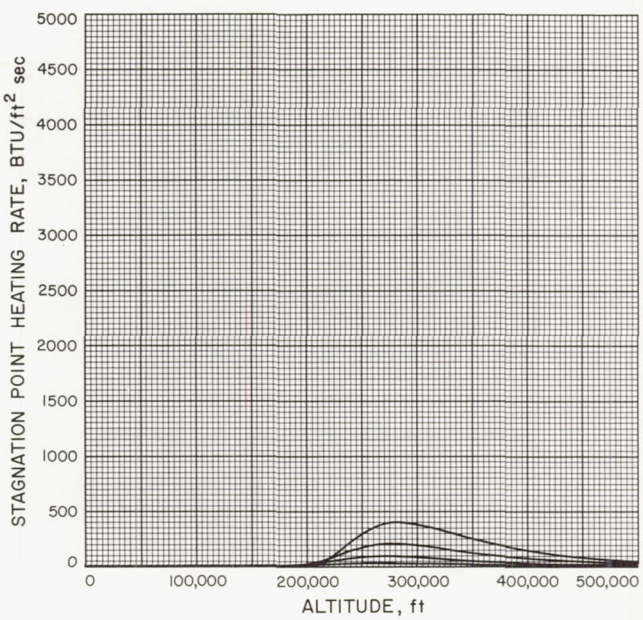

Fig. A-100

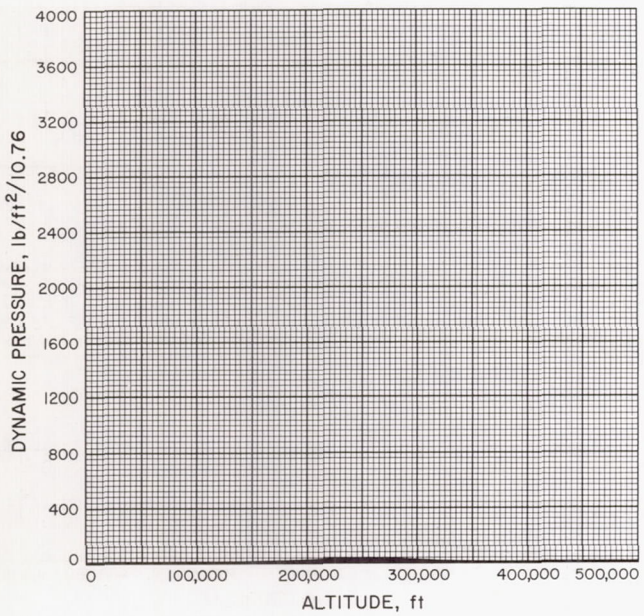

Fig. A-101

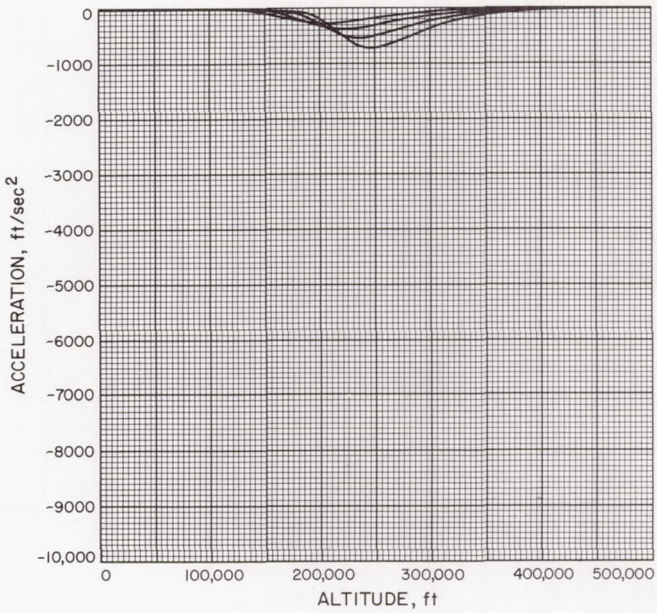

Fig. A-102

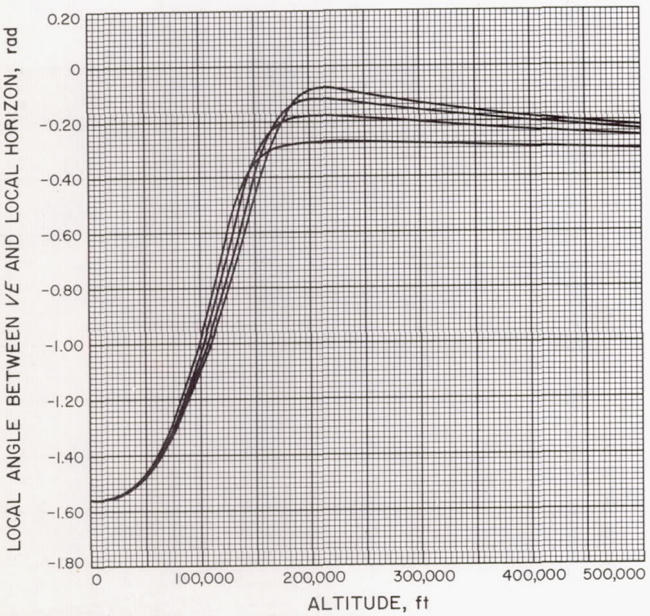

Fig. A-103

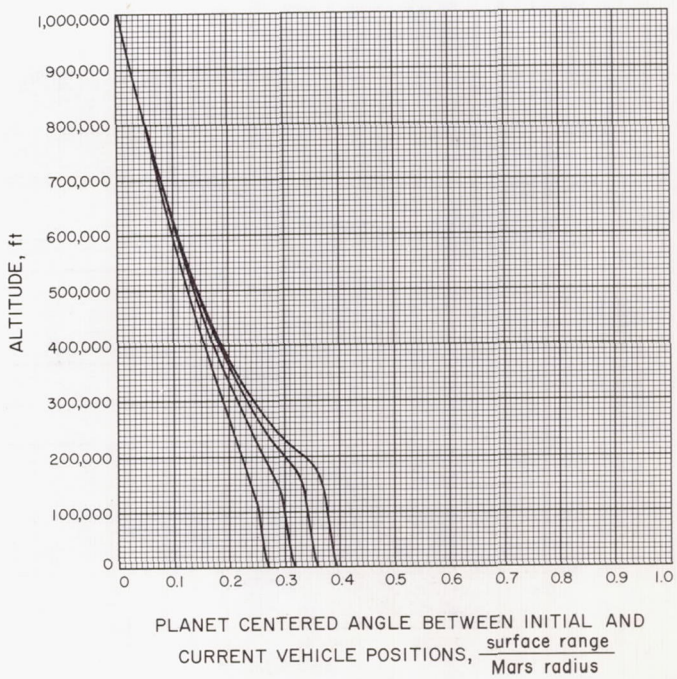

Fig. A-104

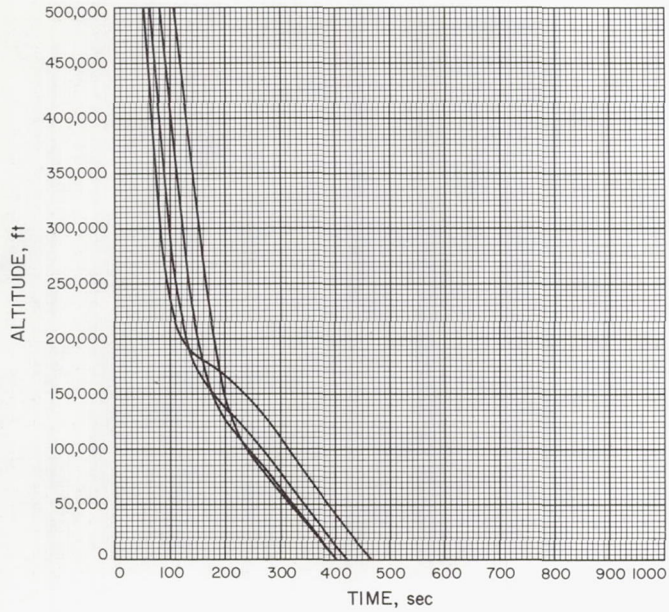

Fig. A-105

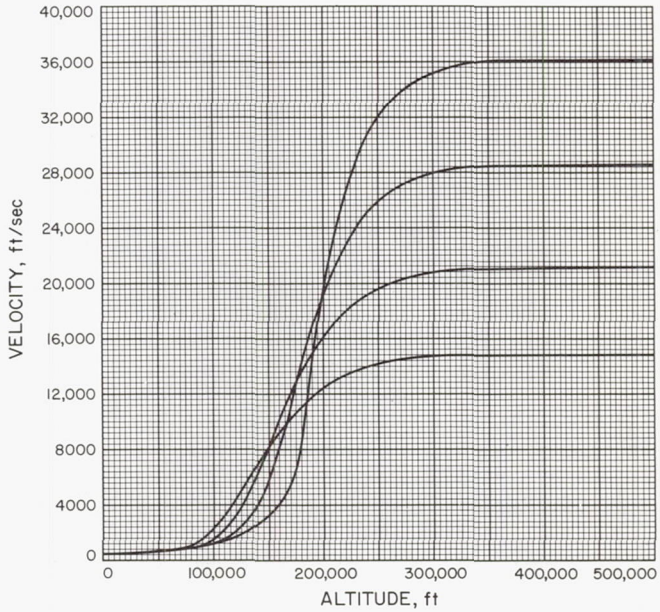

Fig. A-106

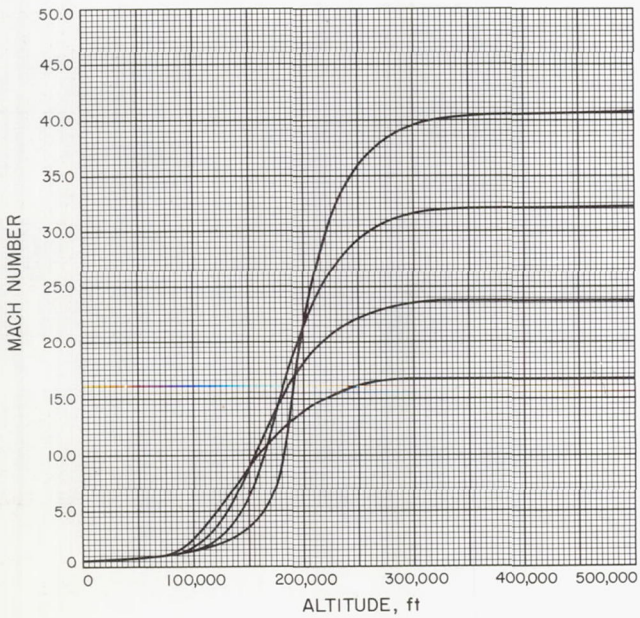

Fig. A-107

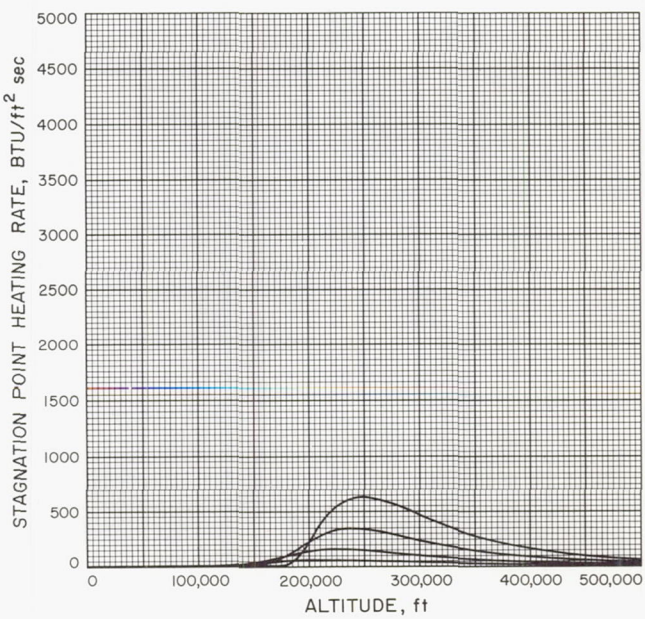

Fig. A-108

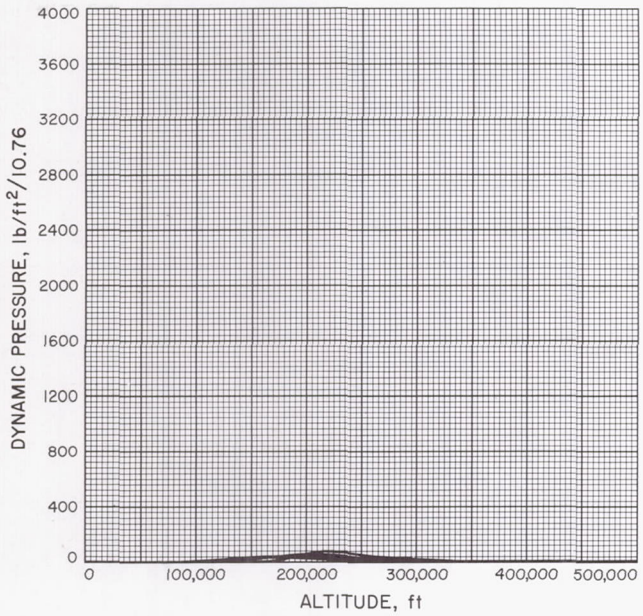

Fig. A-109

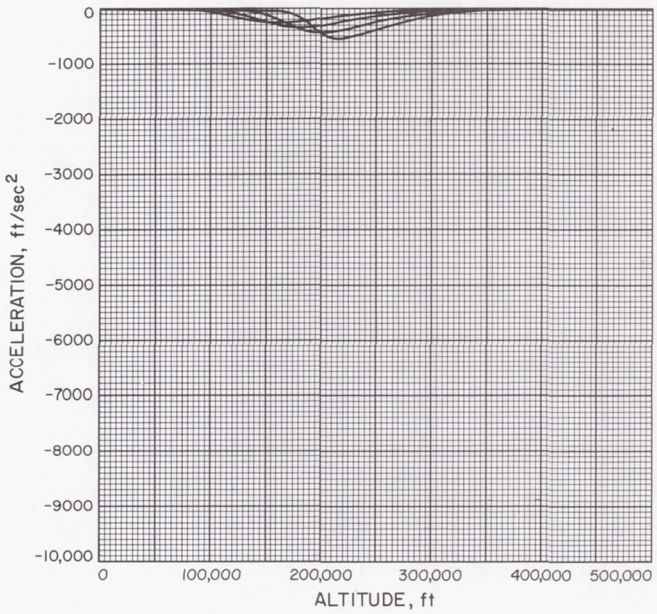

Fig. A-110

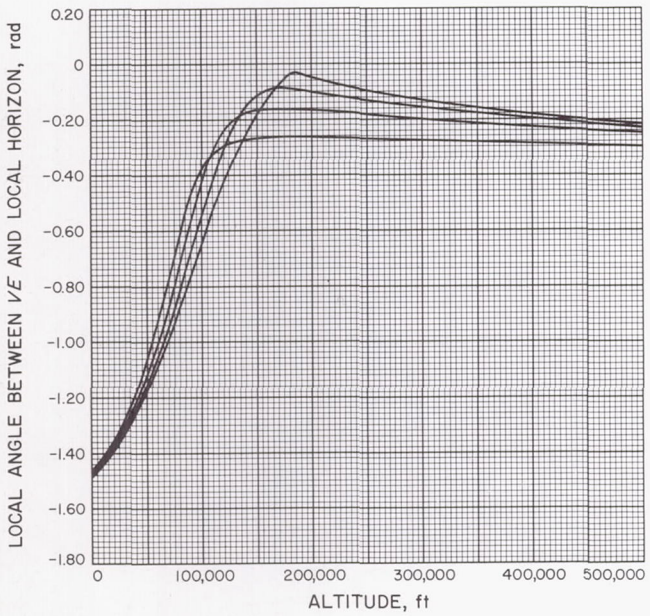

Fig. A-111

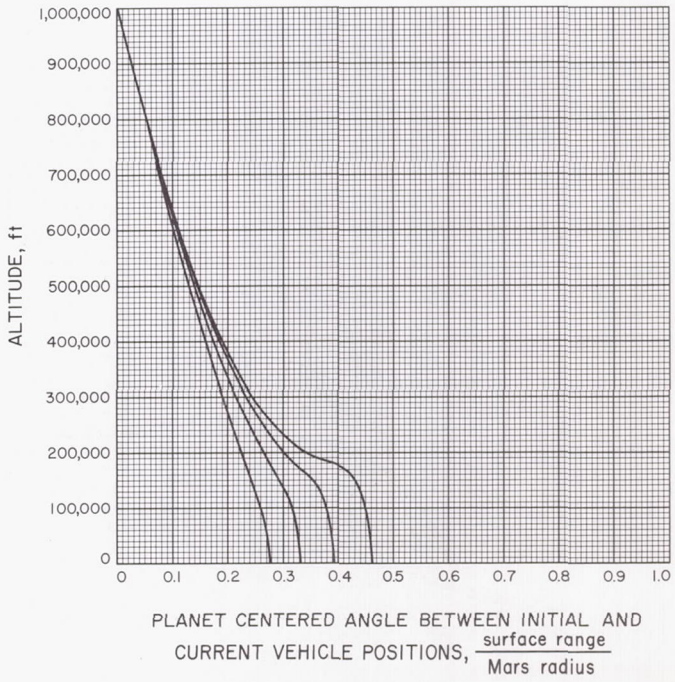

Fig. A-112

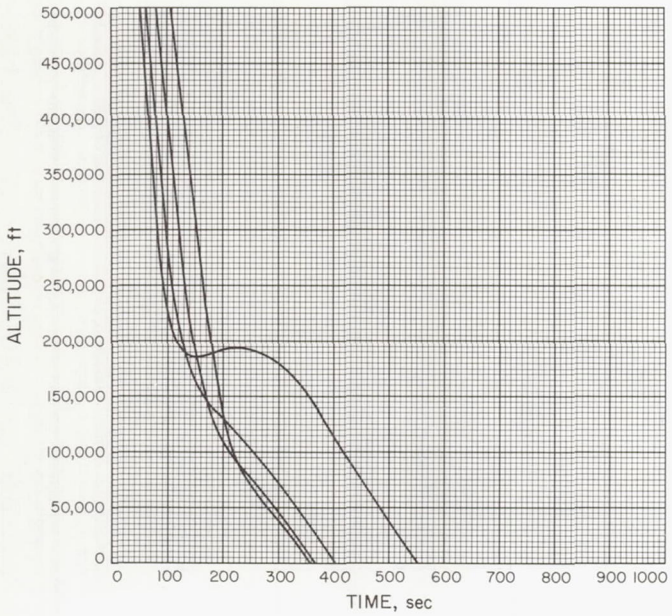

Fig. A-113

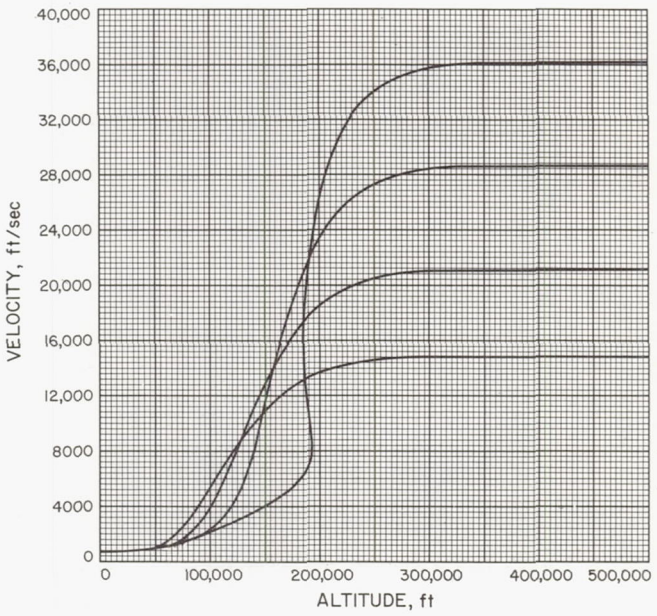

Fig. A-114

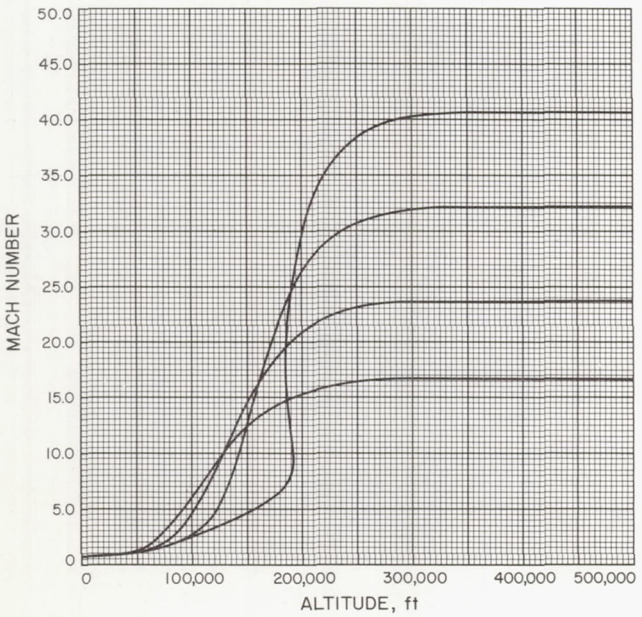

Fig. A-115

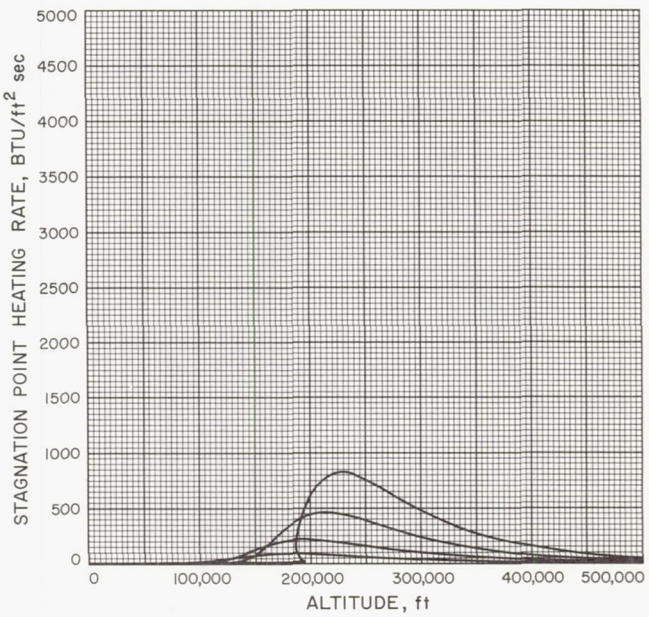

Fig. A-116

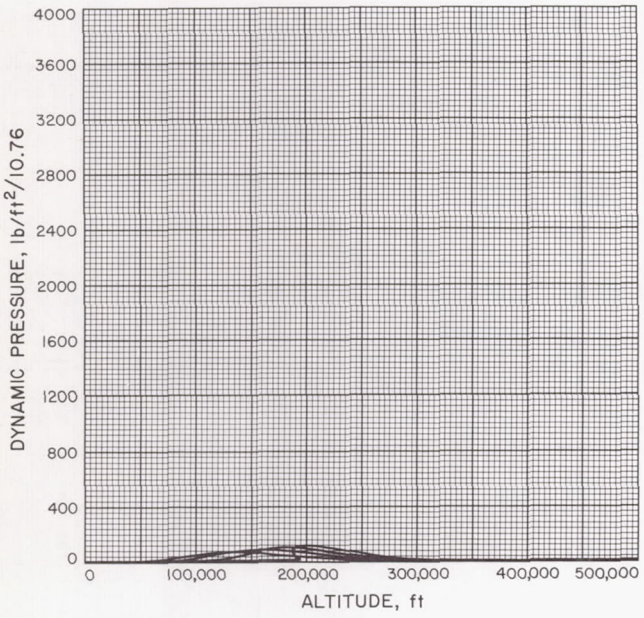

Fig. A-117

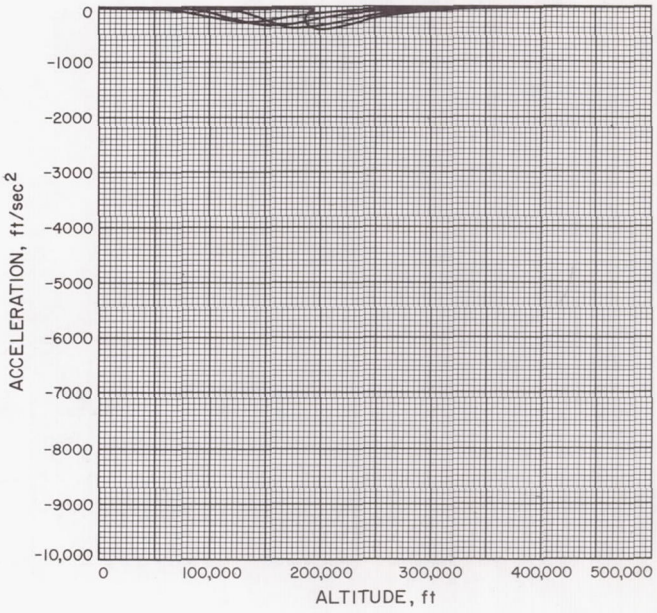

Fig. A-118

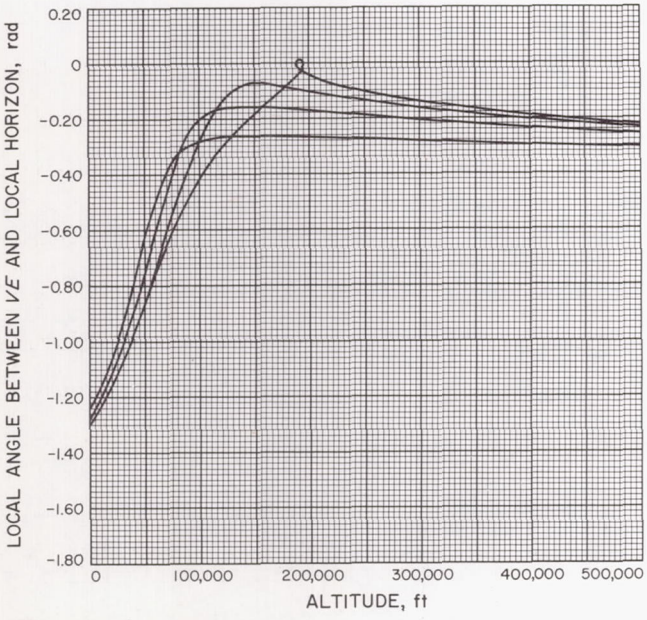

Fig. A-119

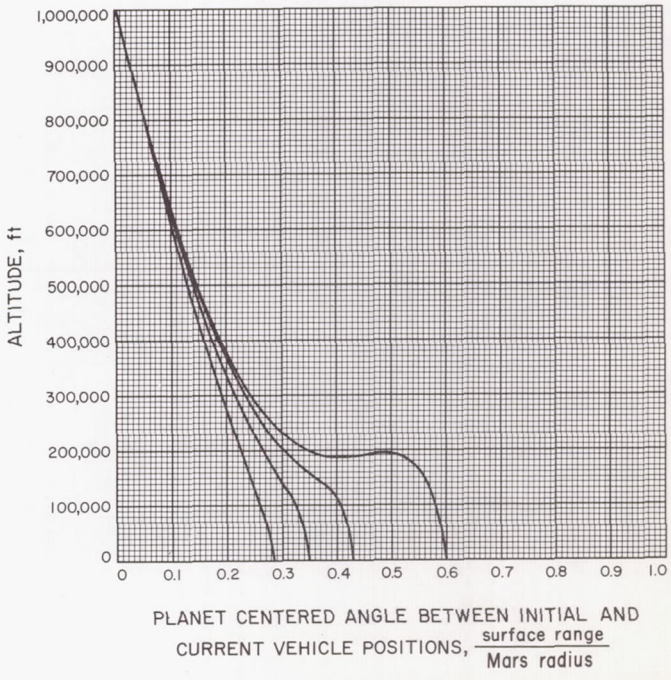

Fig. A-120

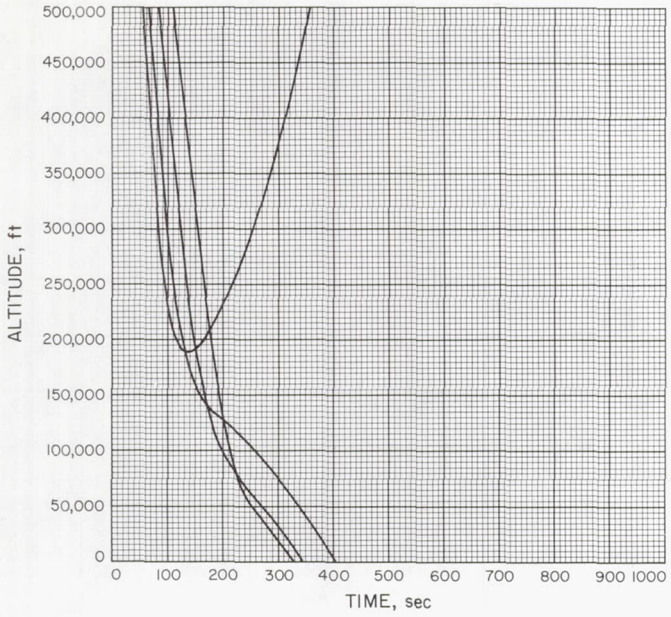

Fig. A-121

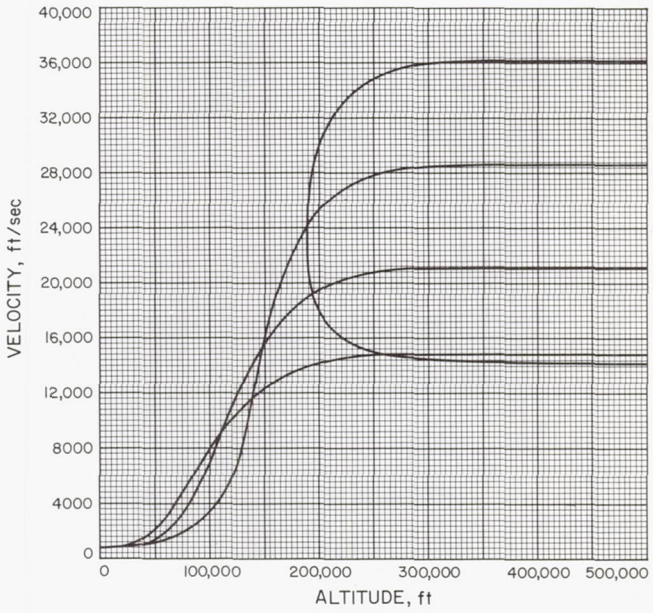

Fig. A-122

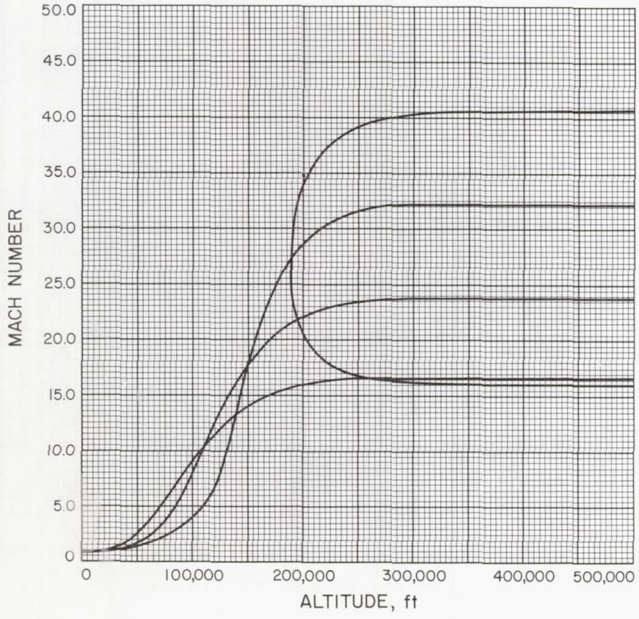

Fig. A-123

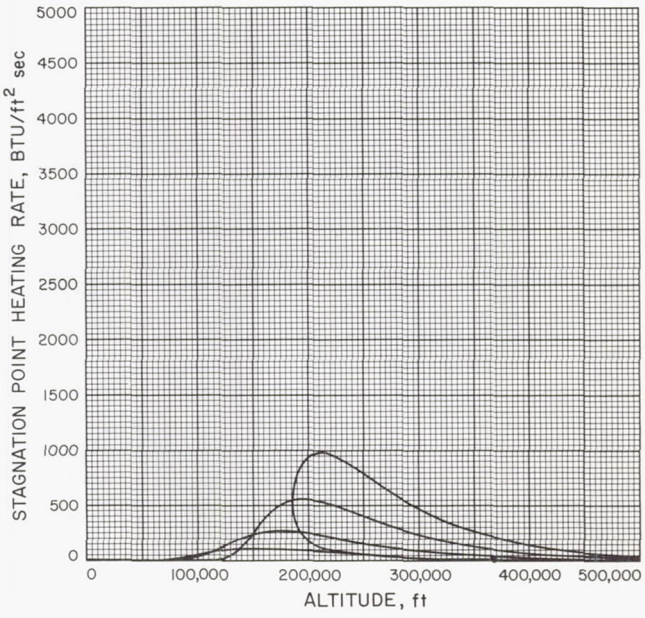

Fig. A-124

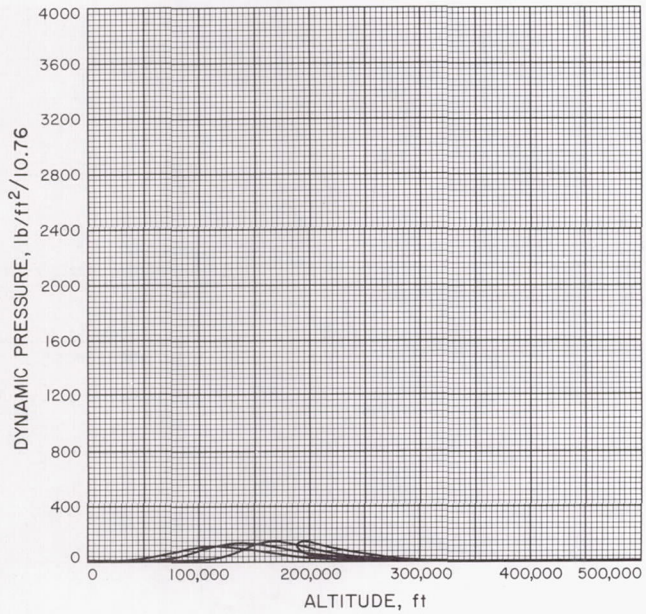

Fig. A-125

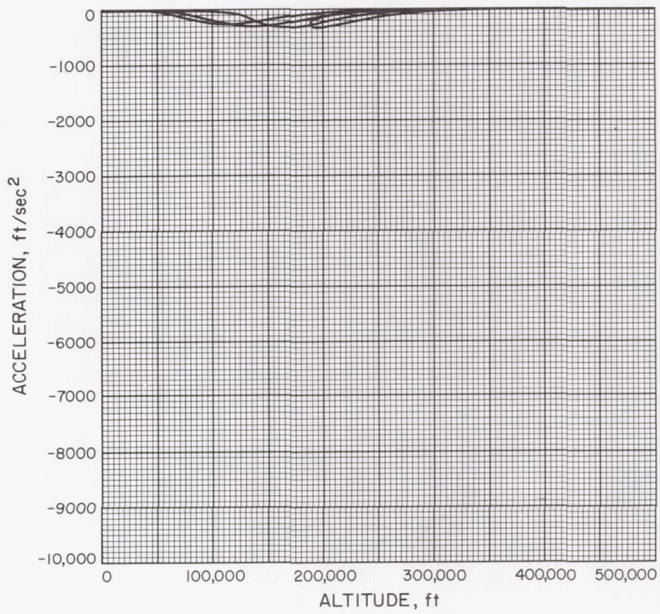

Fig. A-126

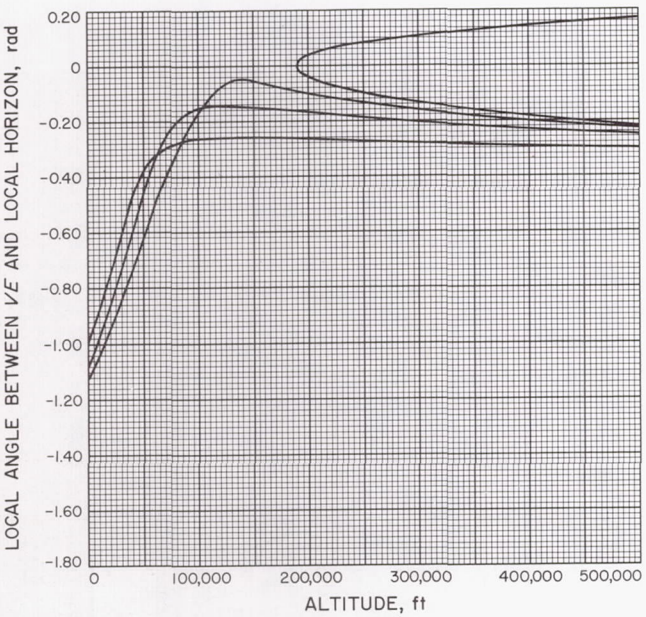

Fig. A-127

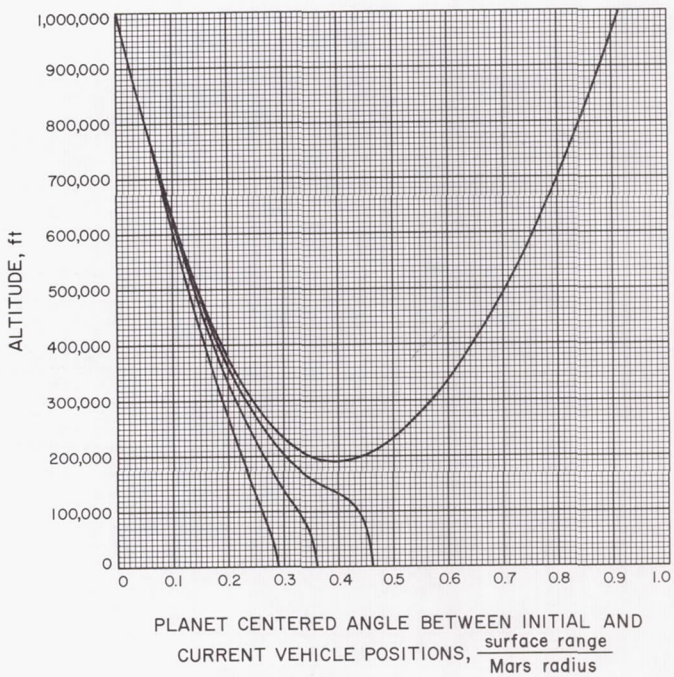

Fig. A-128

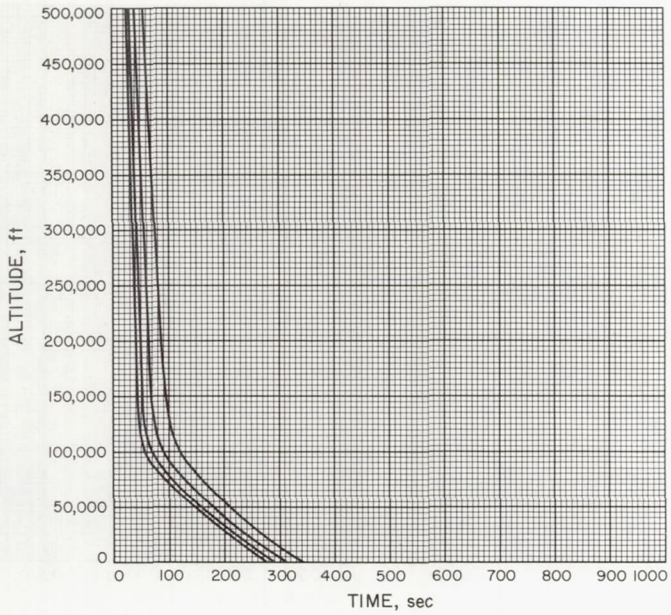

Fig. A-129

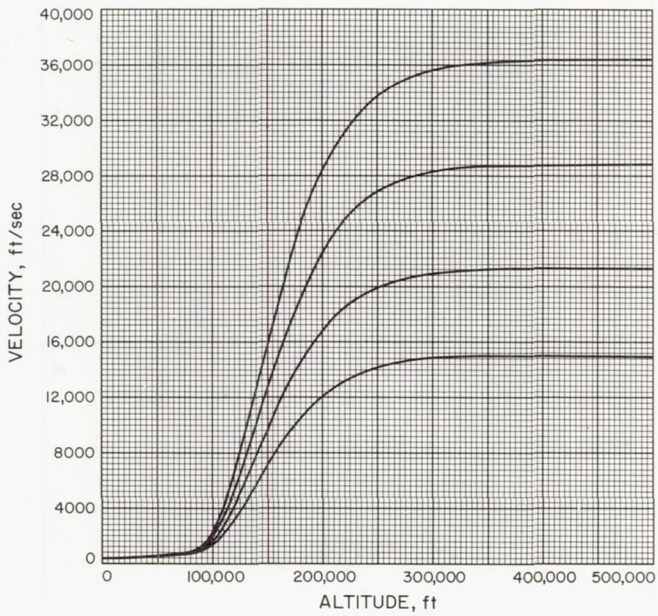

Fig. A-130

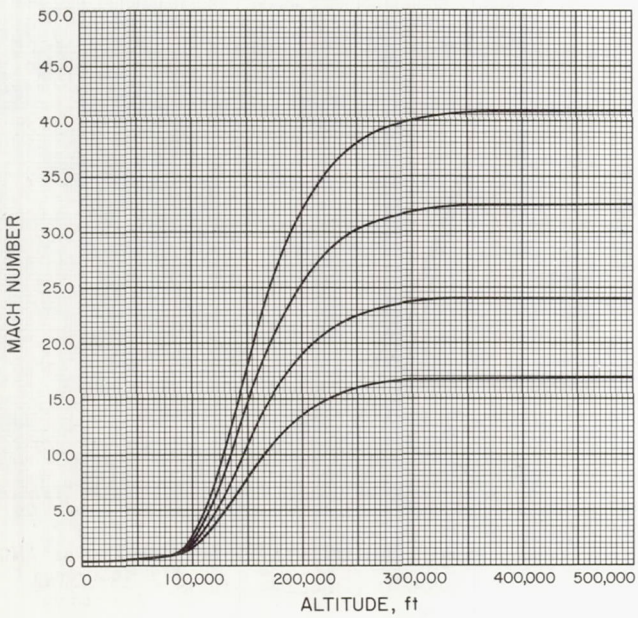

Fig. A-131

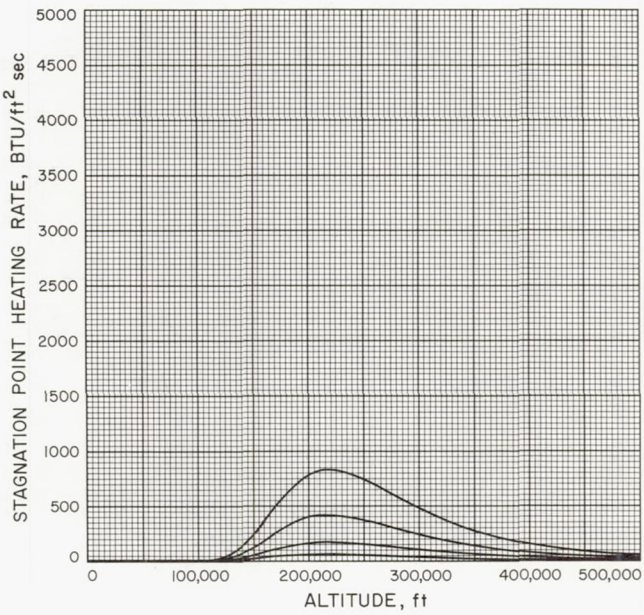

Fig. A-132

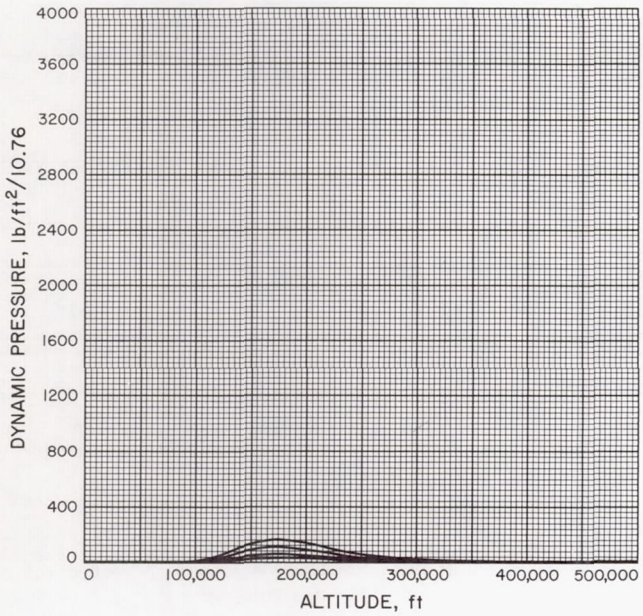

Fig. A-133

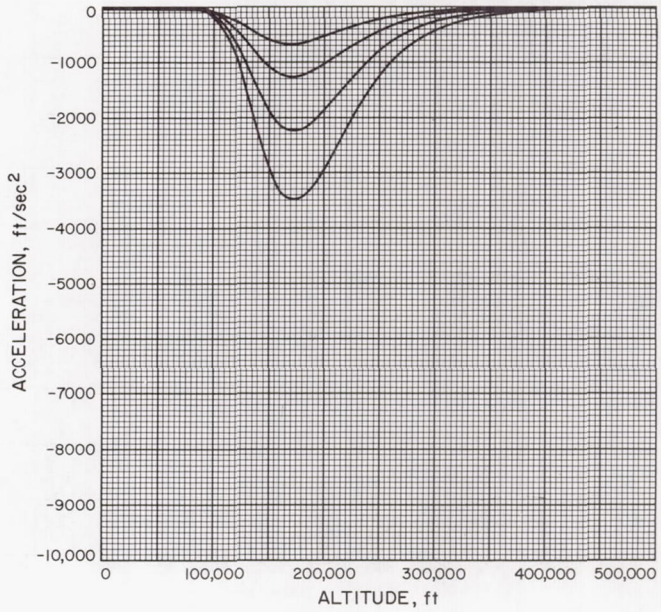

Fig. A-134

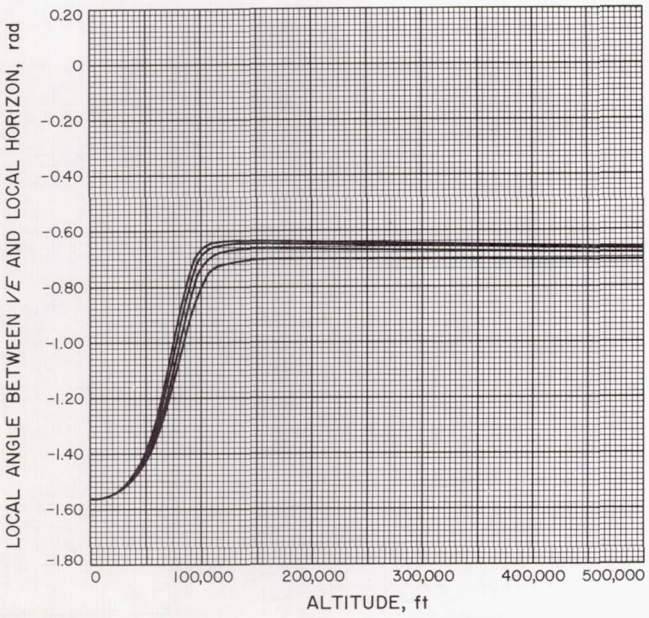

Fig. A-135

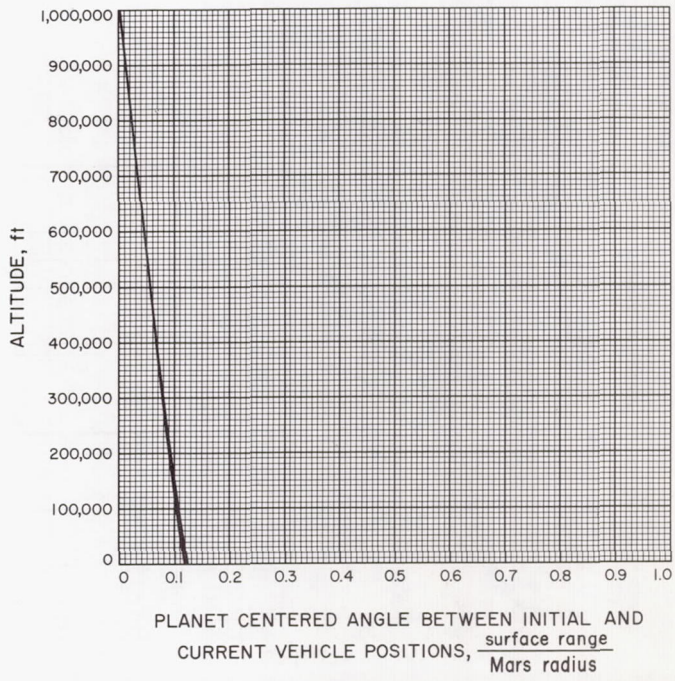

Fig. A-136

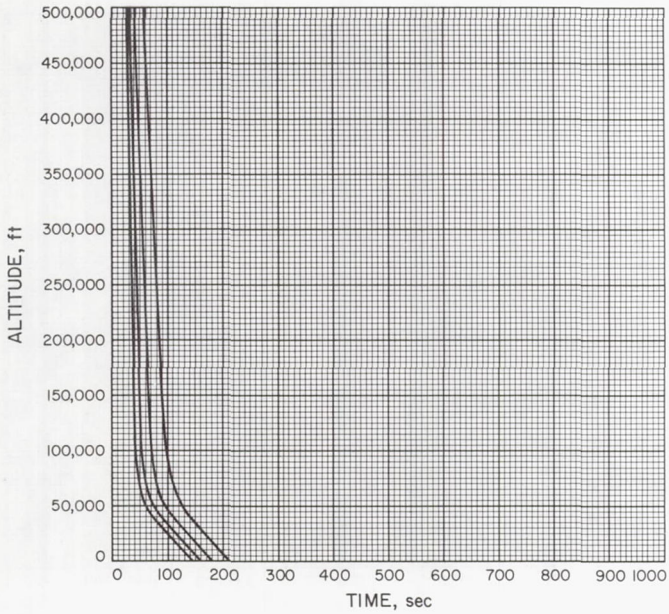

Fig. A-137

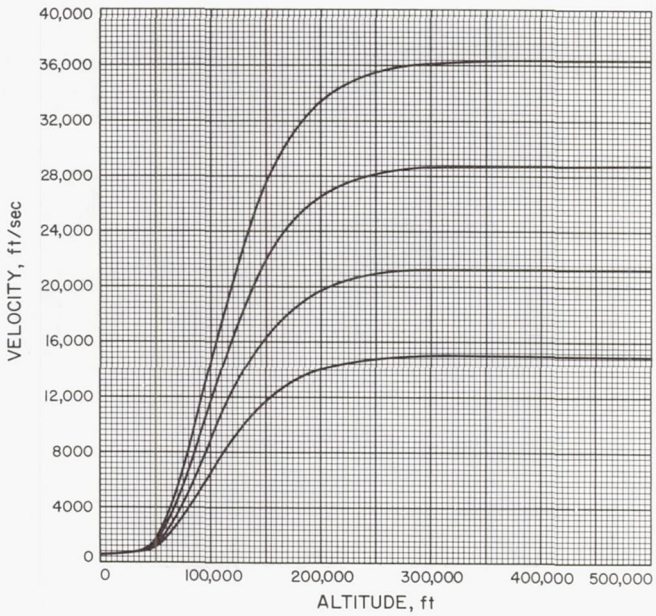

Fig. A-138

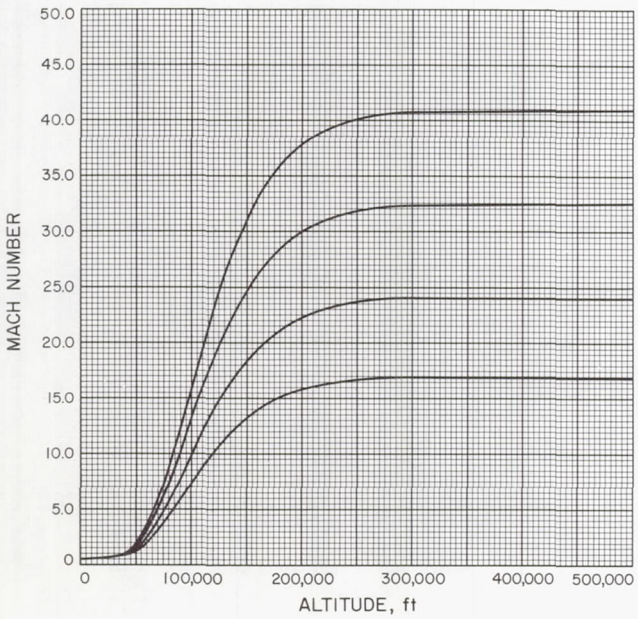

Fig. A-139

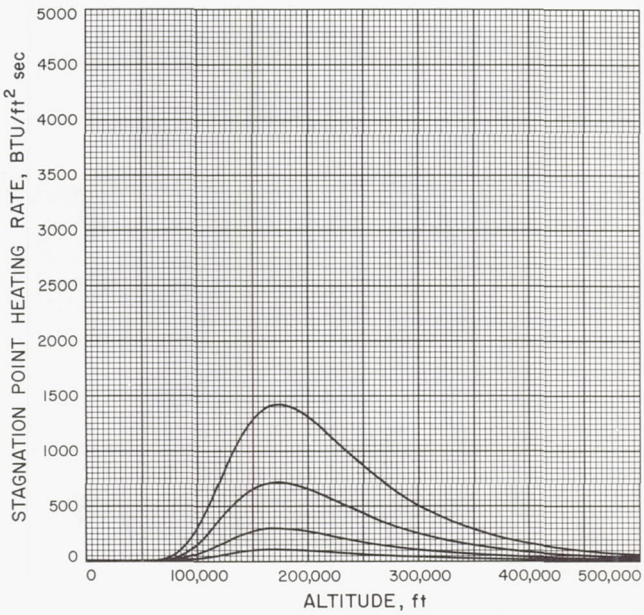

Fig. A-140

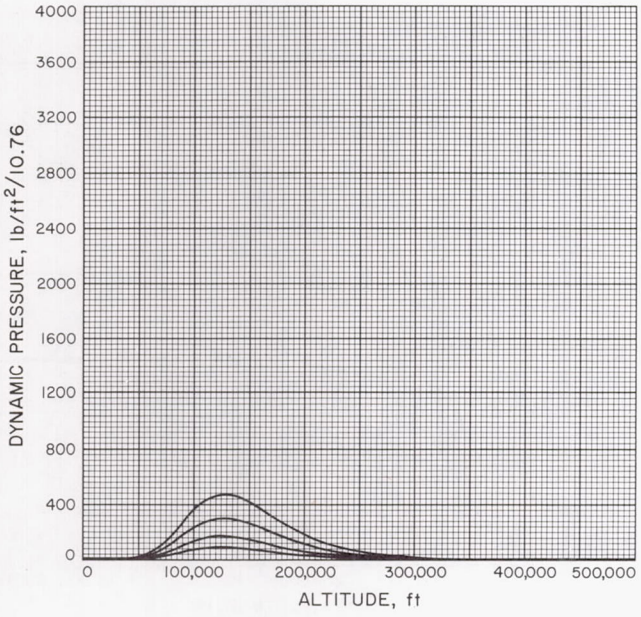

Fig. A-141

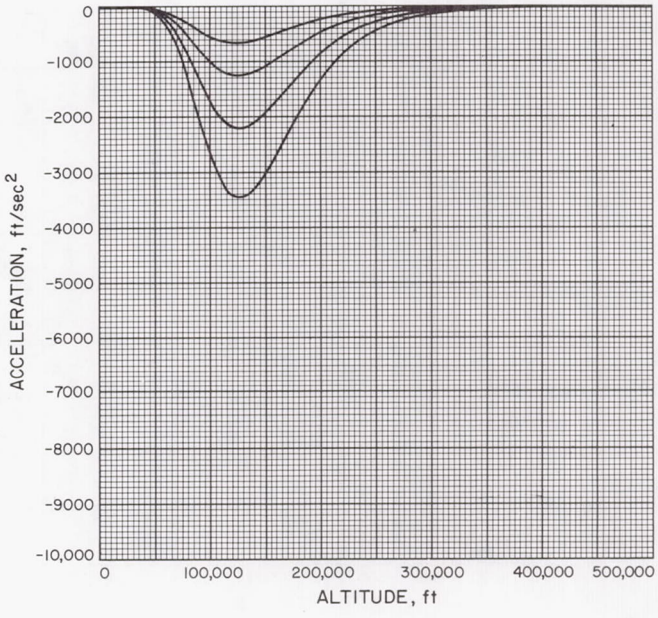

Fig. A-142

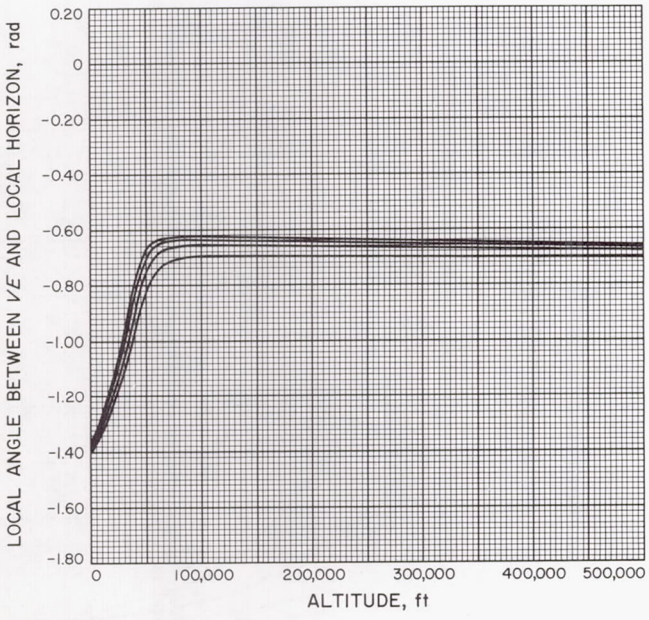

Fig. A-143

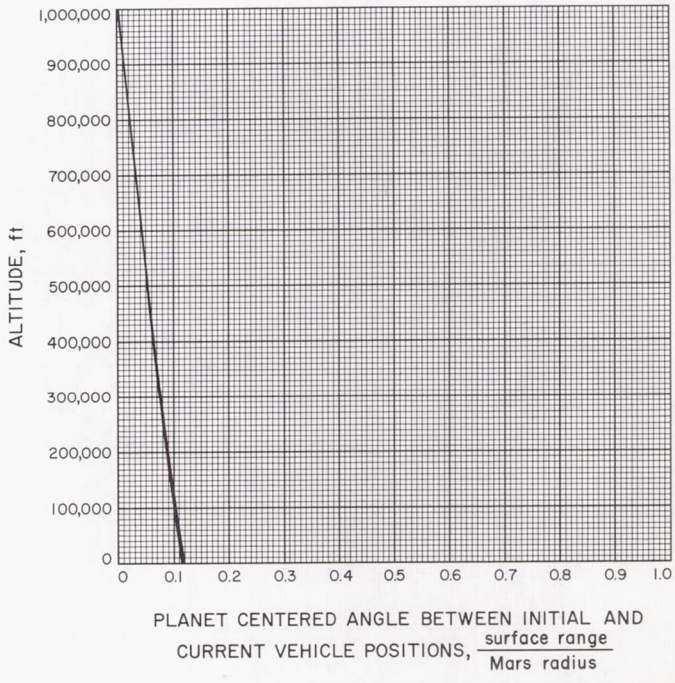

Fig. A-144

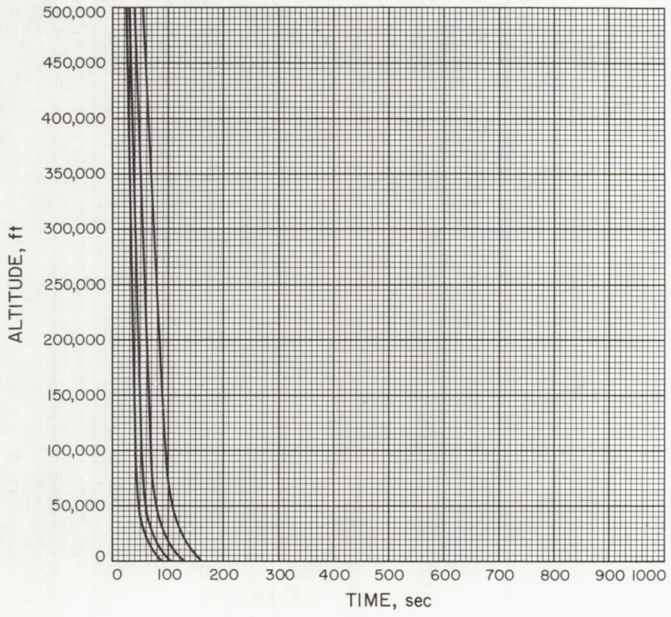

Fig. A-145

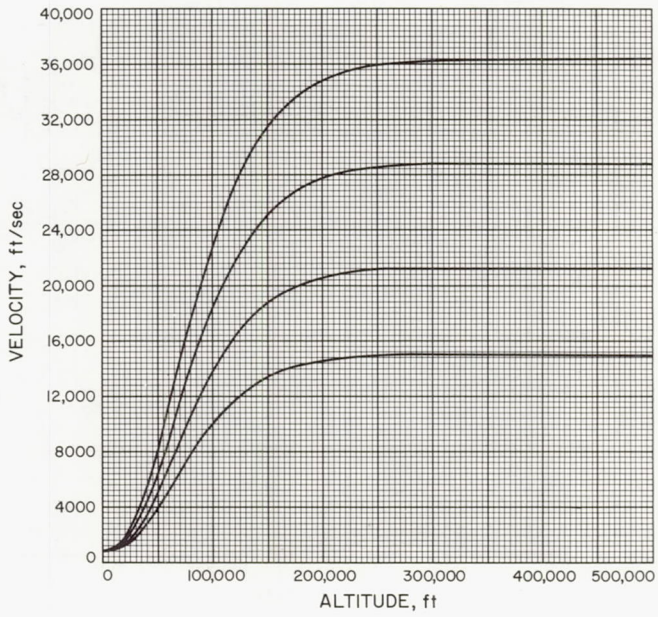

Fig. A-146

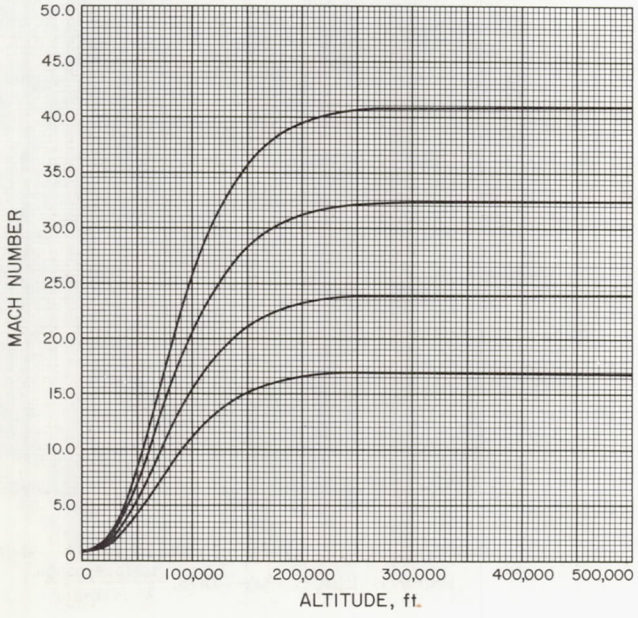

Fig. A-147

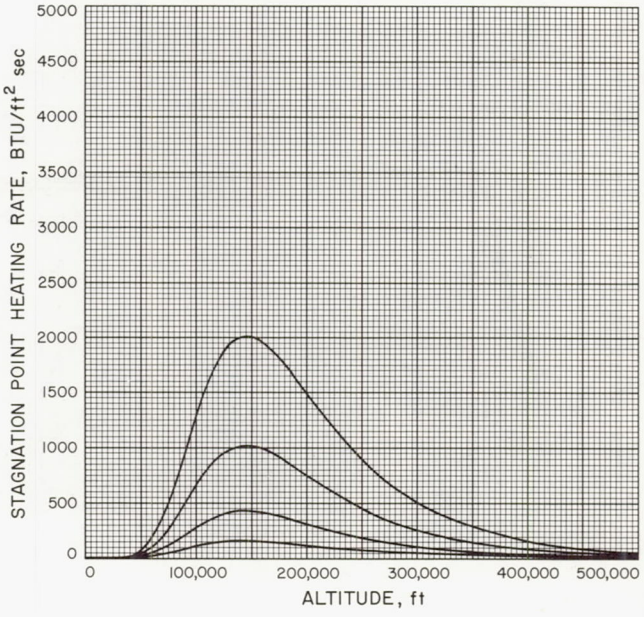

Fig. A-148

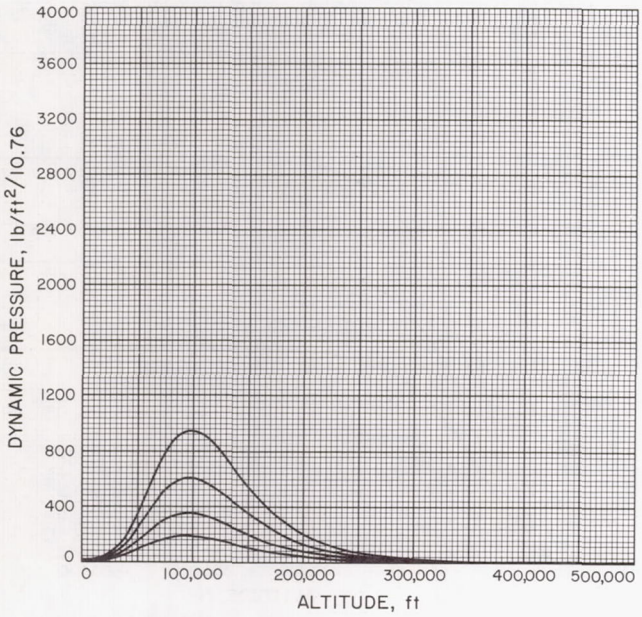

Fig. A-149

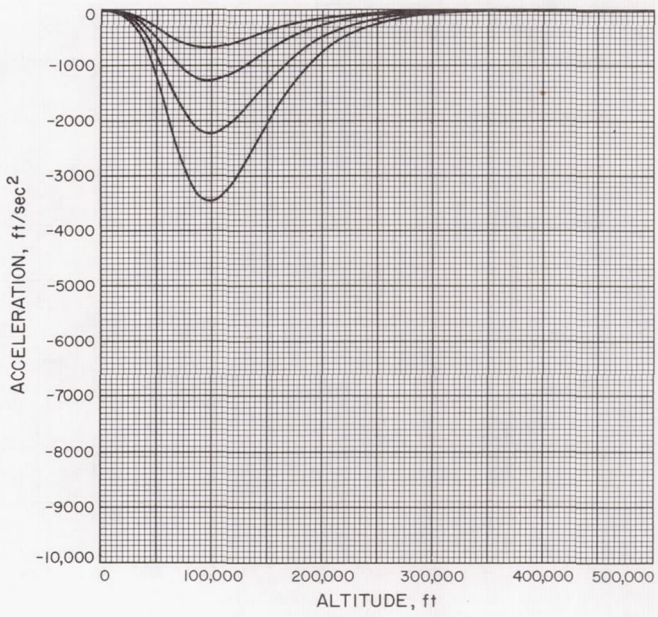

Fig. A-150

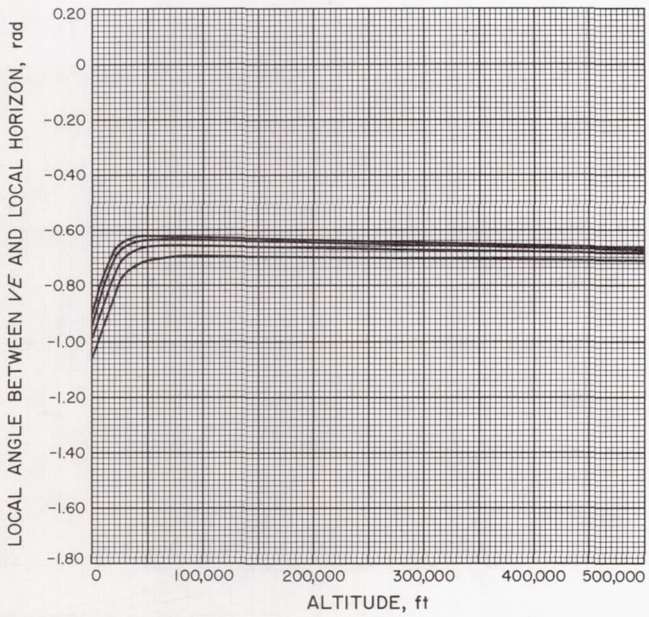

Fig. A-151

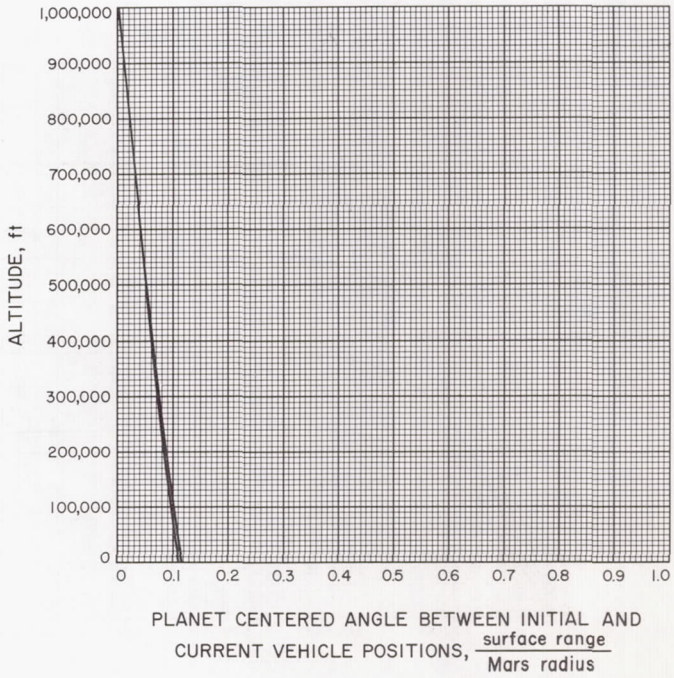

Fig. A-152

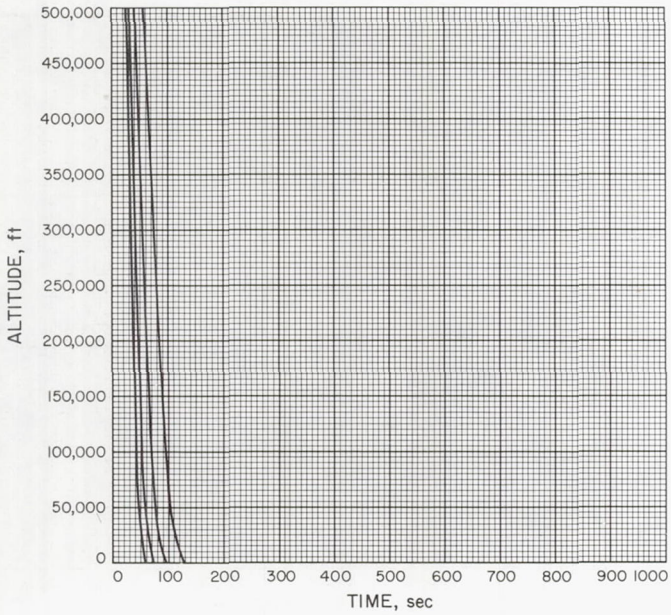

Fig. A-153

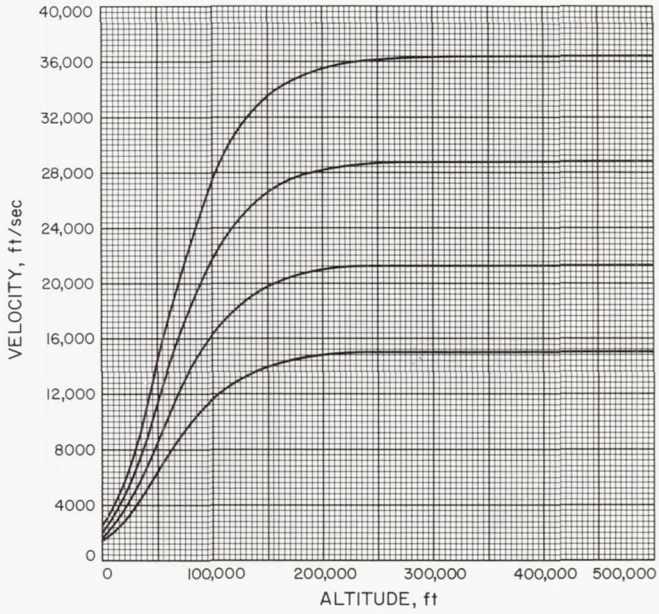

Fig. A-154

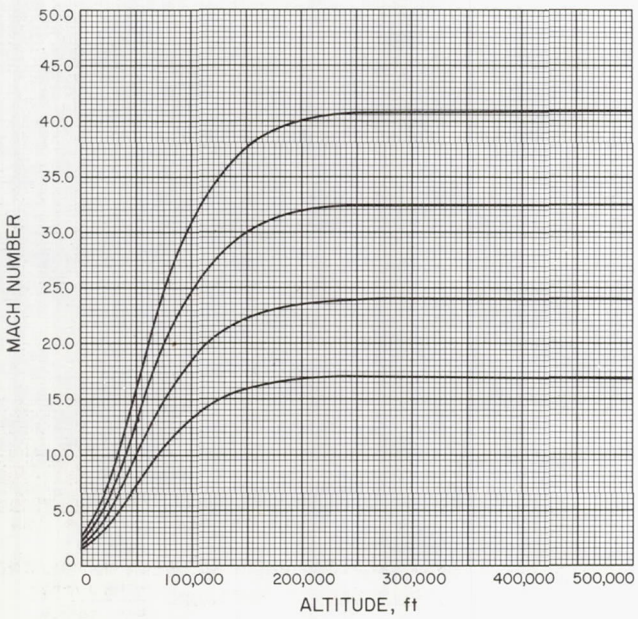

Fig. A-155

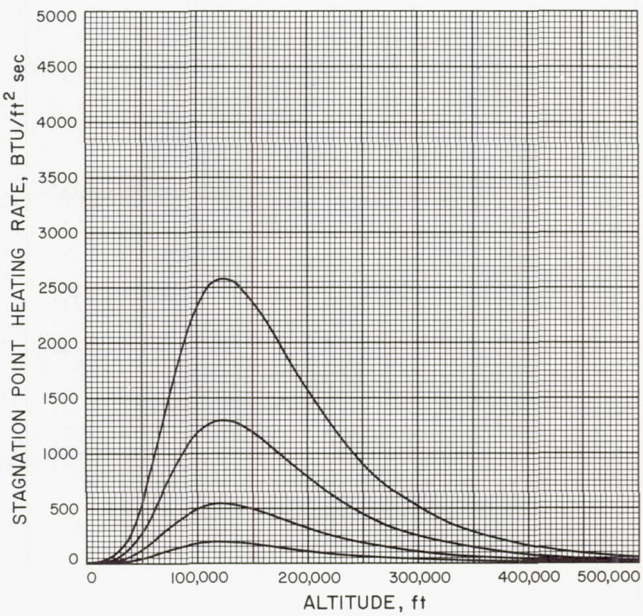

Fig. A-156

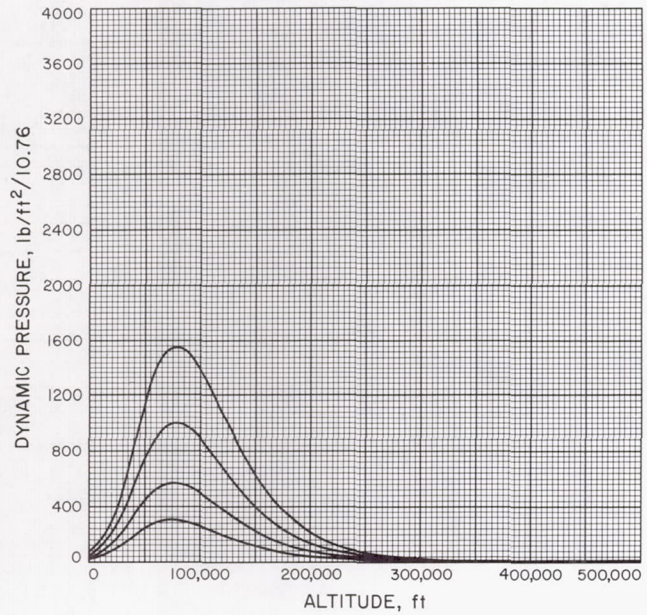

Fig. A-157

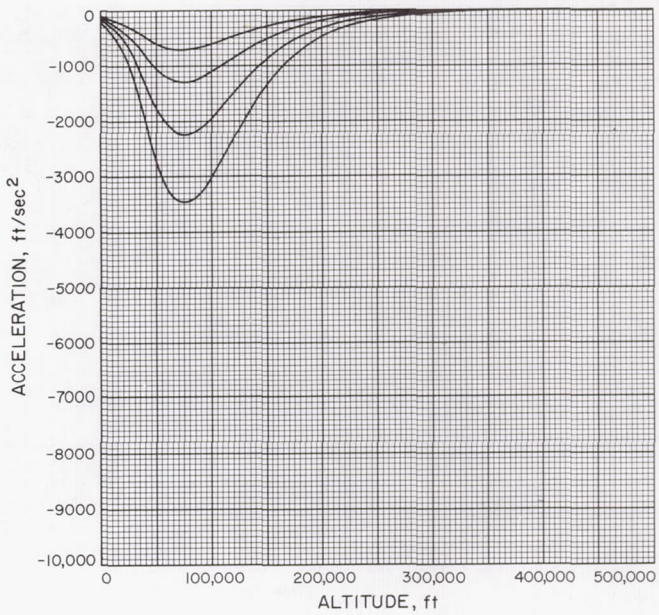

Fig. A-158

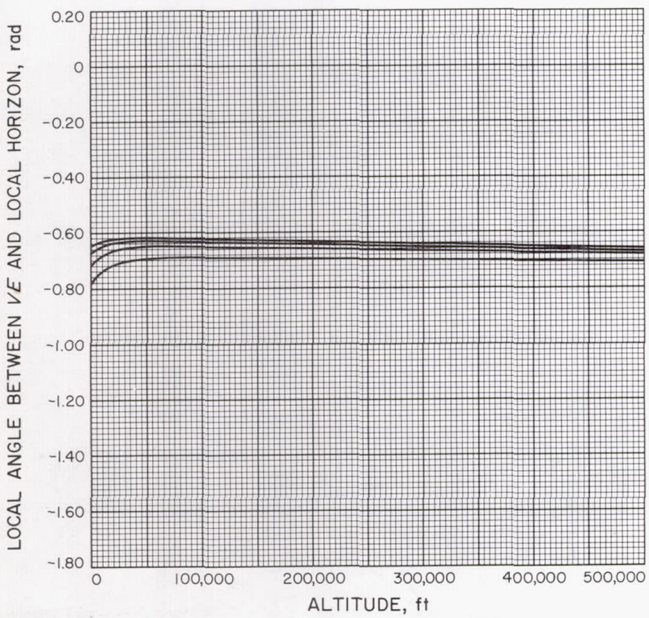

Fig. A-159

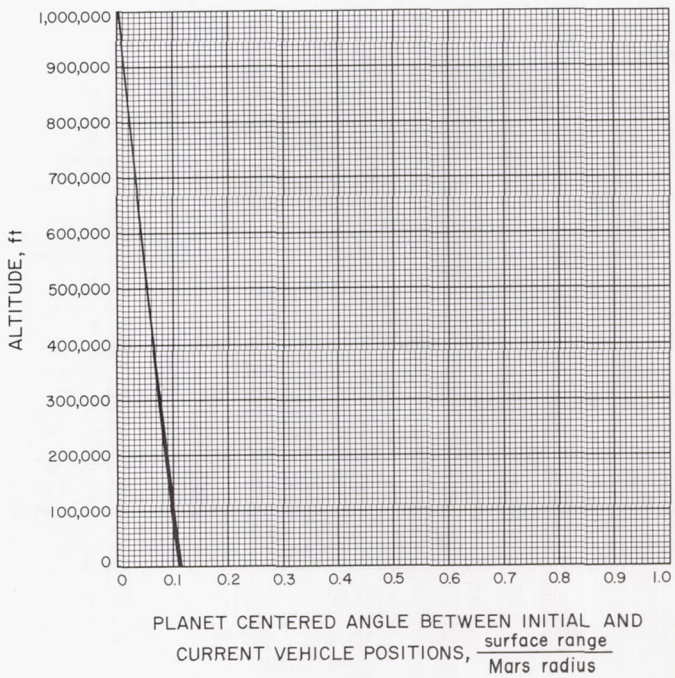

Fig. A-160

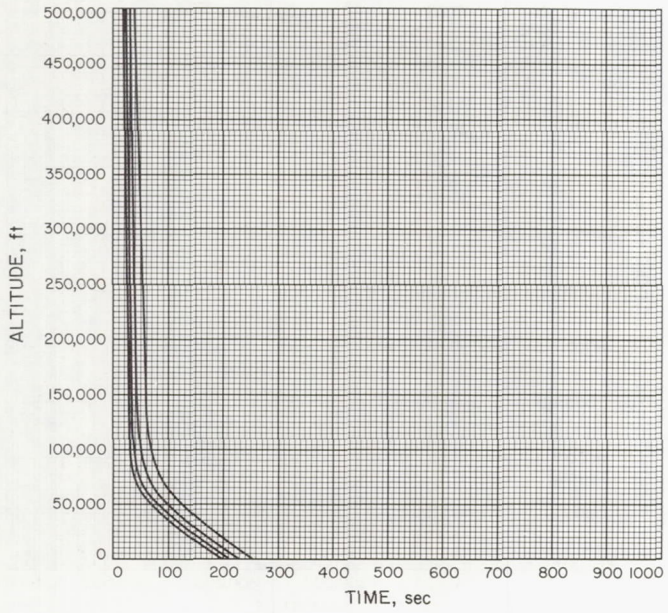

Fig. A-161

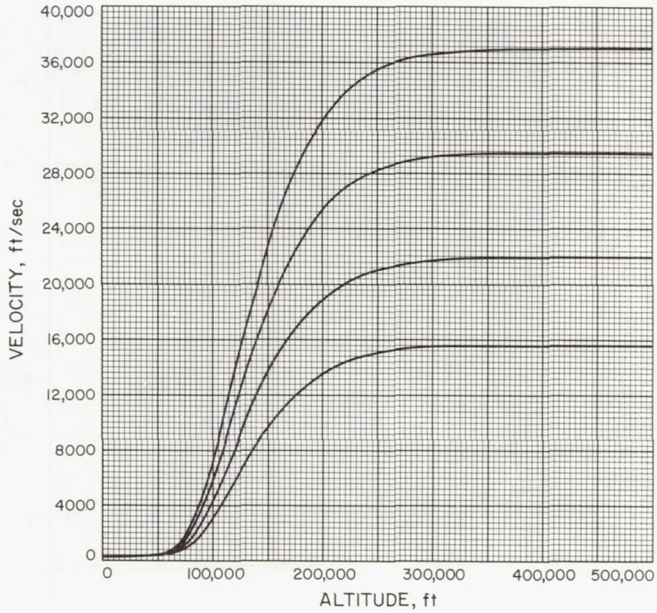

Fig. A-162

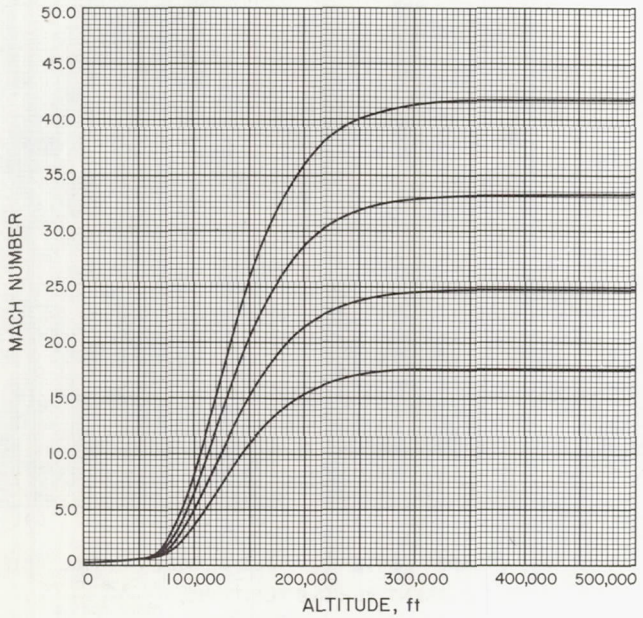

Fig. A-163

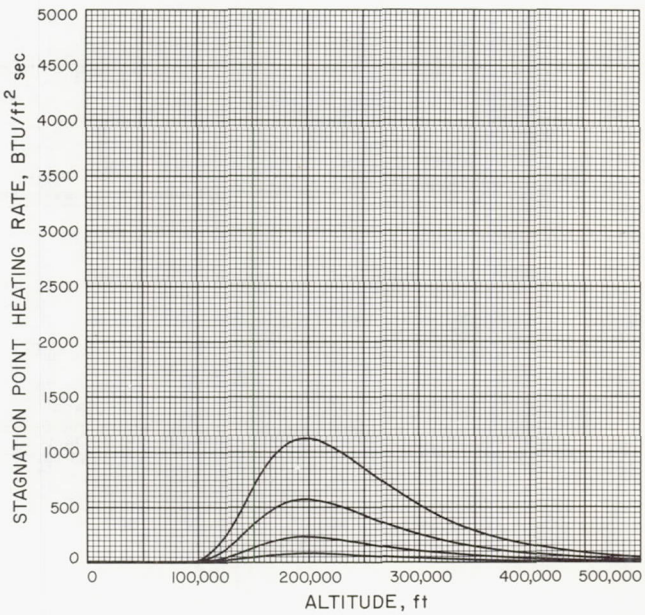

Fig. A-164

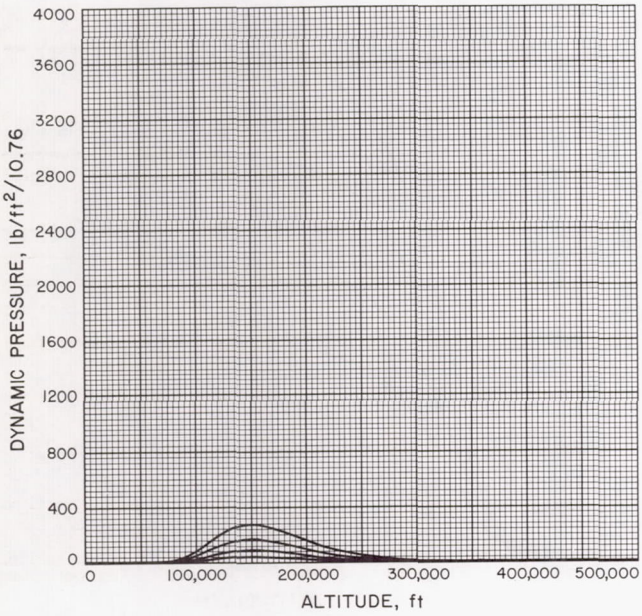

Fig. A-165

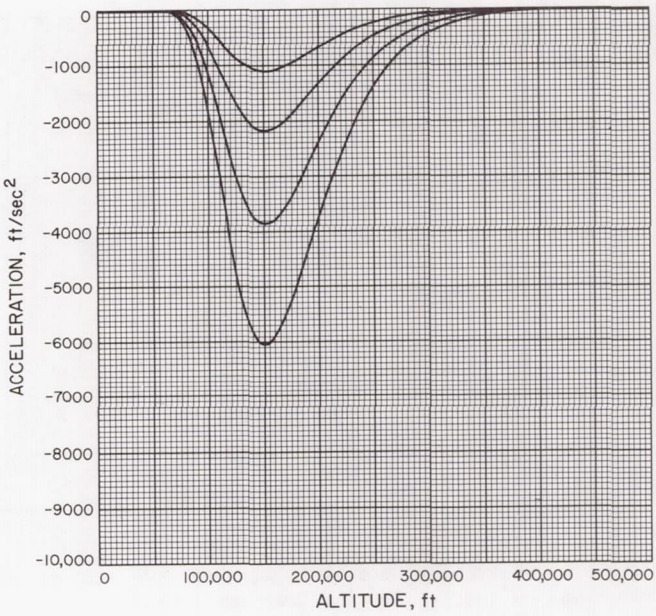

Fig. A-166

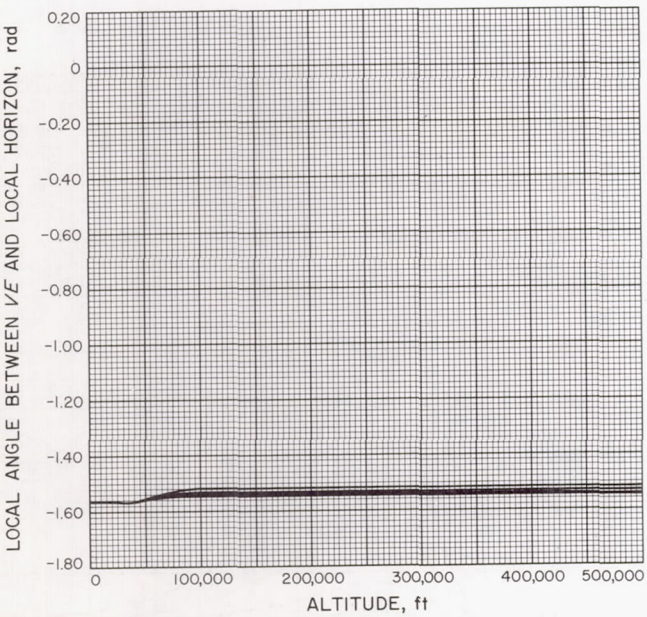

Fig. A-167

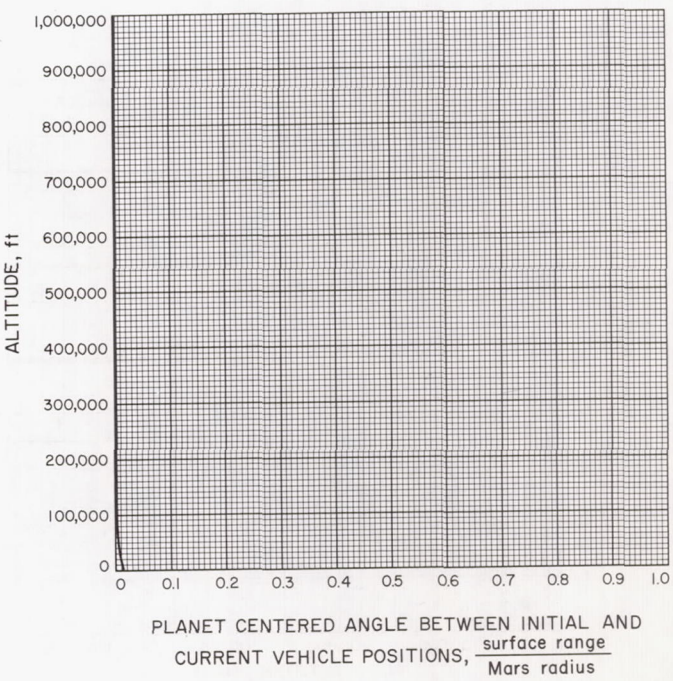

Fig. A-168

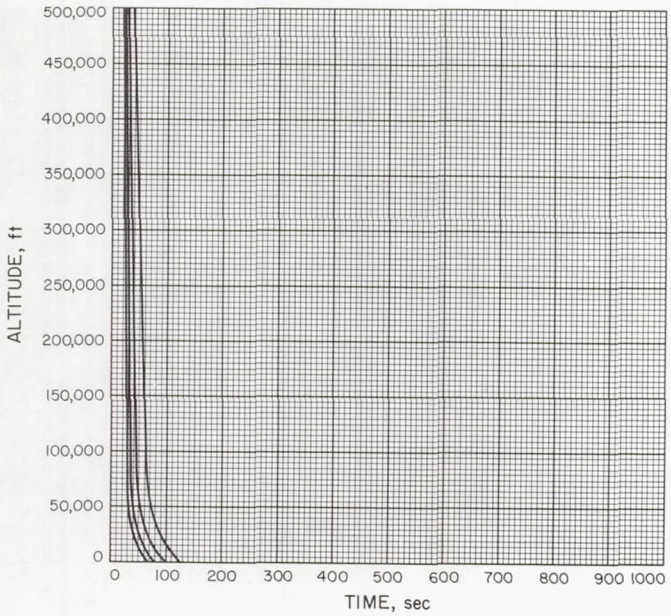

Fig. A-169

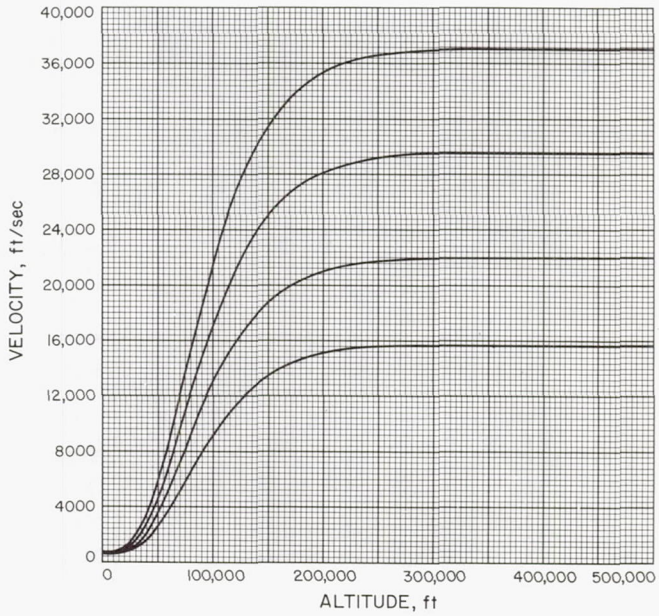

Fig. A-170

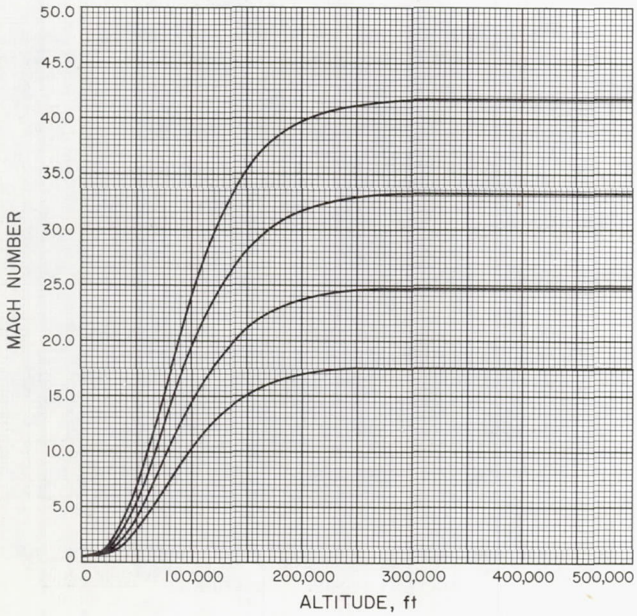

Fig. A-171

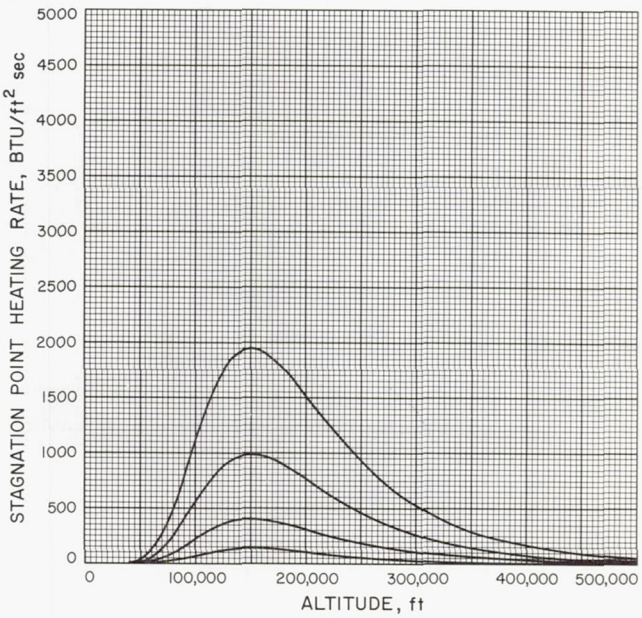

Fig. A-172

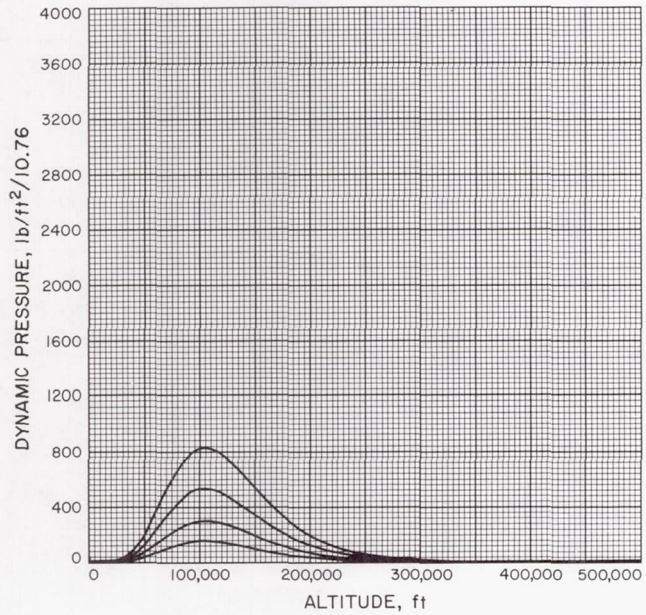

Fig. A-173

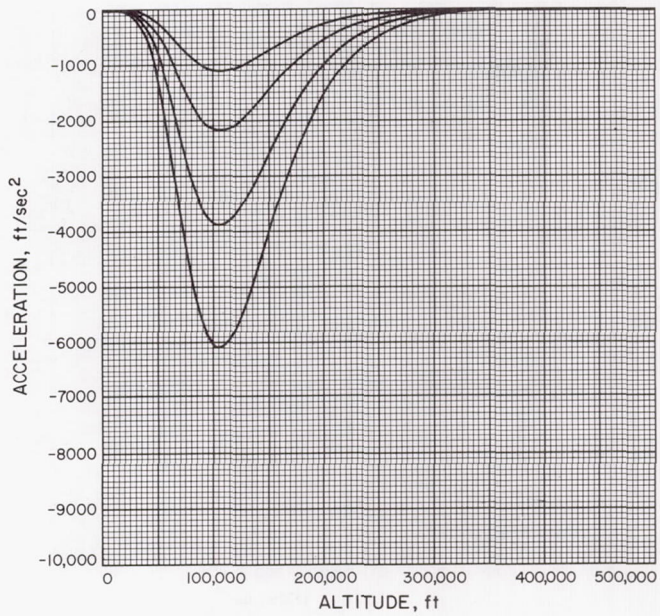

Fig. A-174

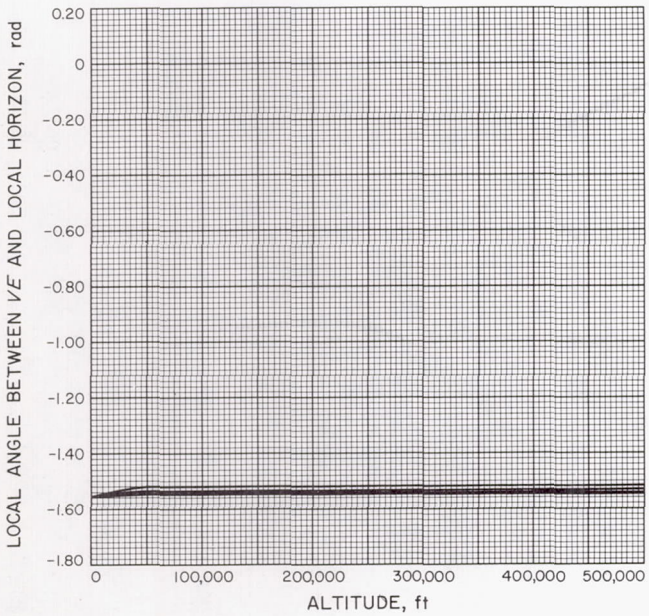

Fig. A-175

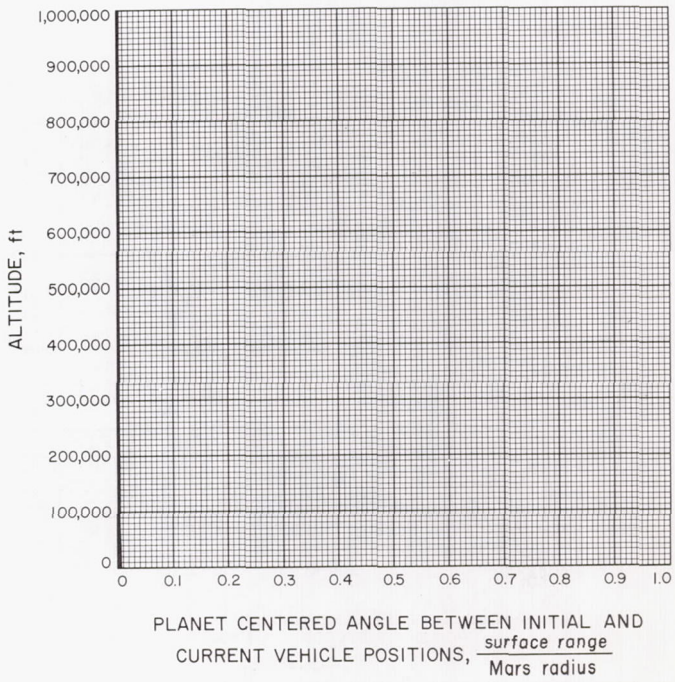

Fig. A-176

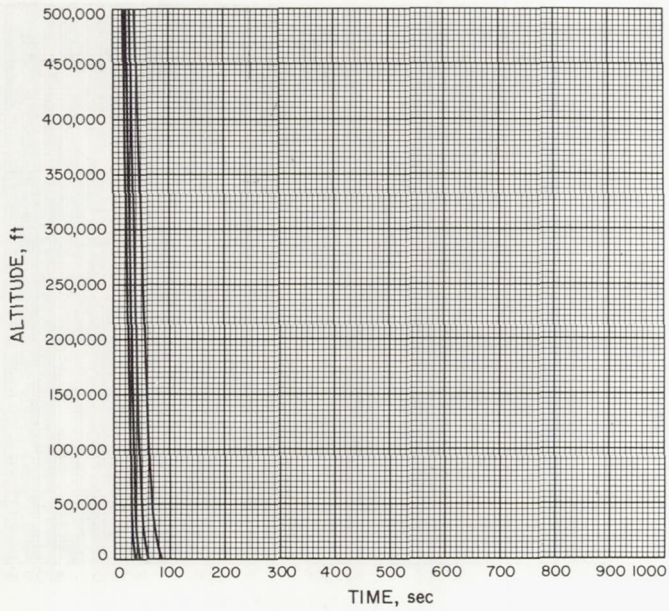

Fig. A-177

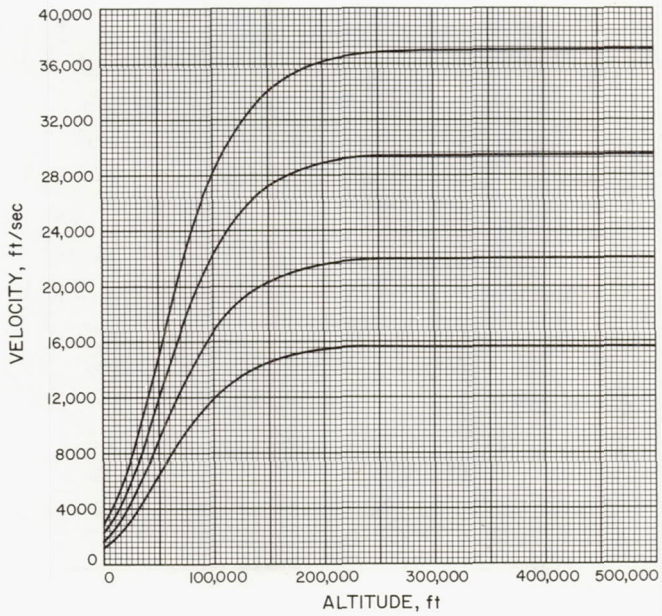

Fig. A-178

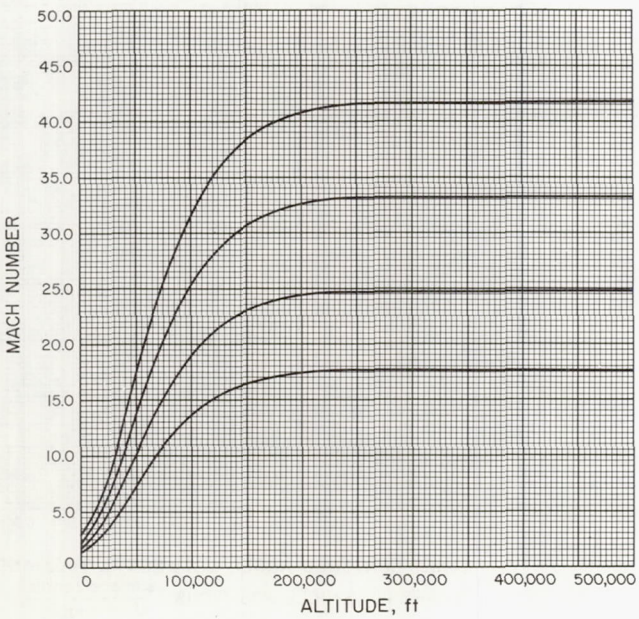

Fig. A-179

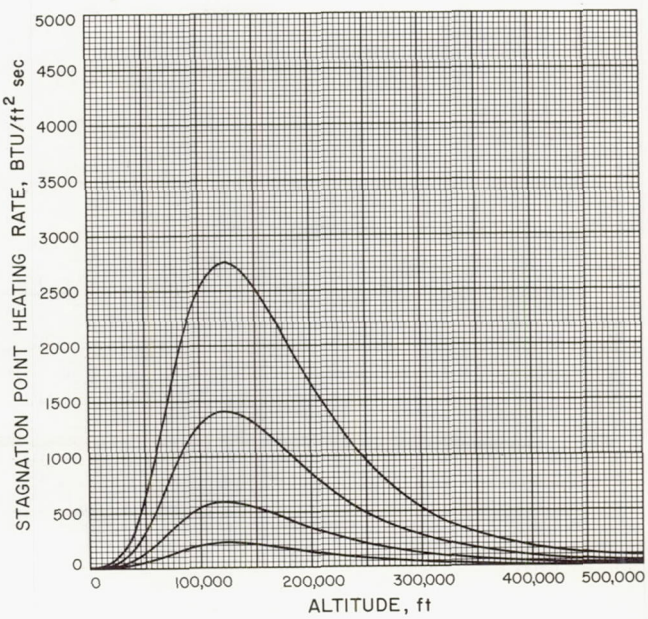

Fig. A-180

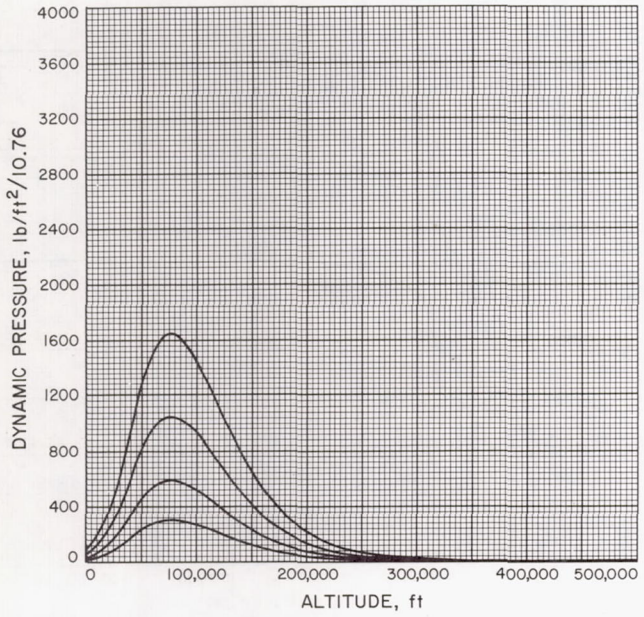

Fig. A-181

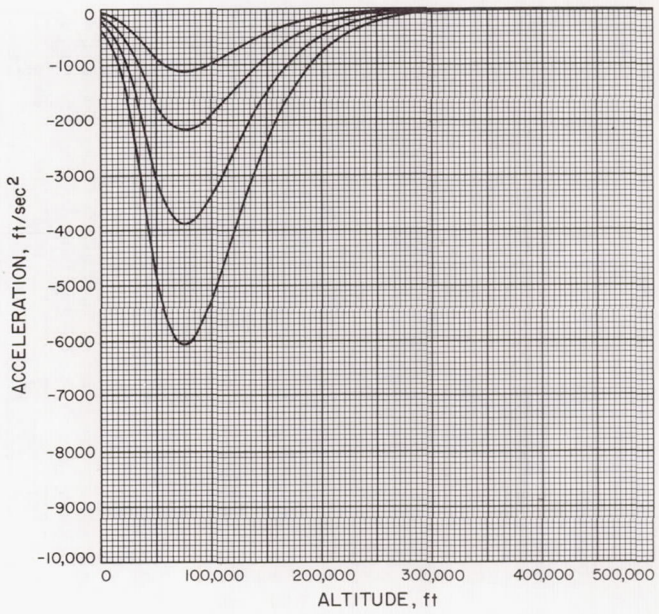

Fig. A-182

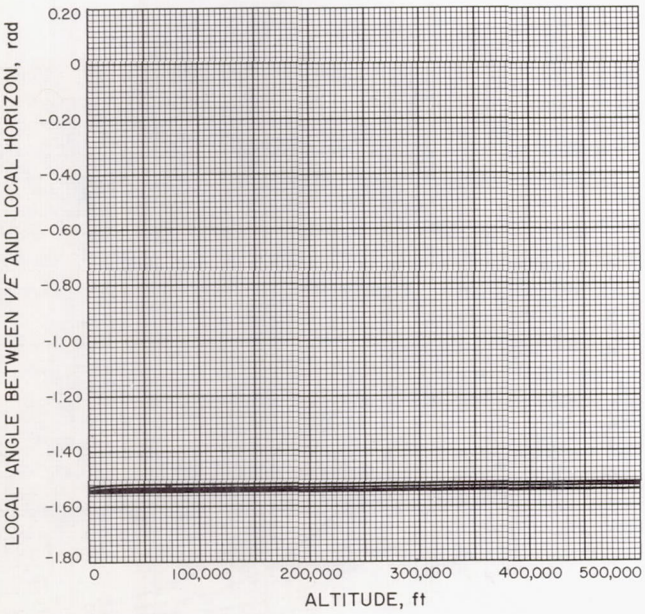

Fig. A-183

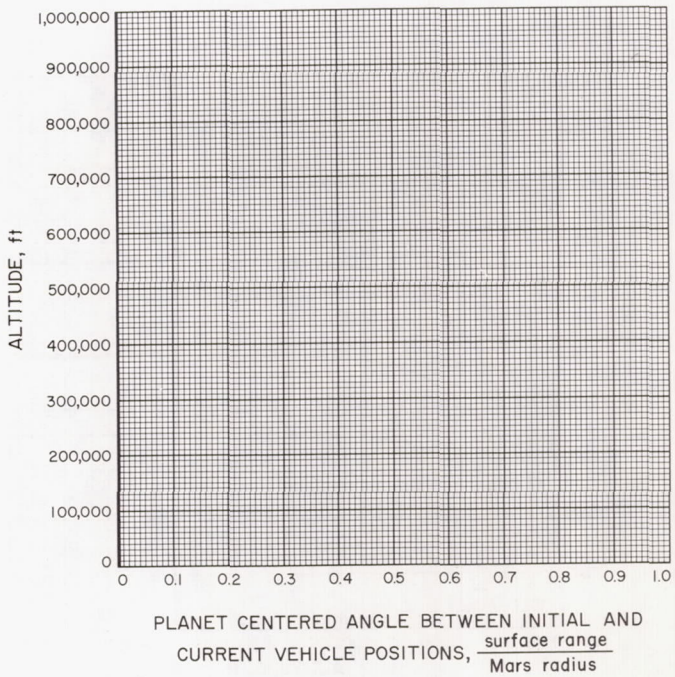

Fig. A-184

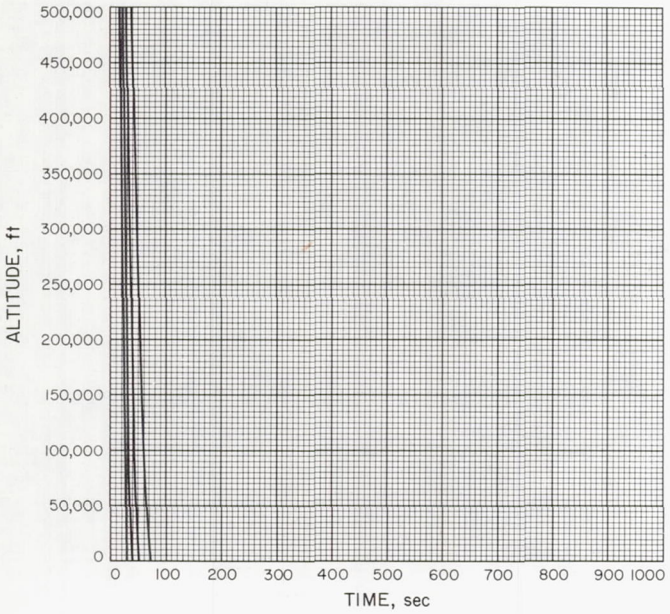

Fig. A-185

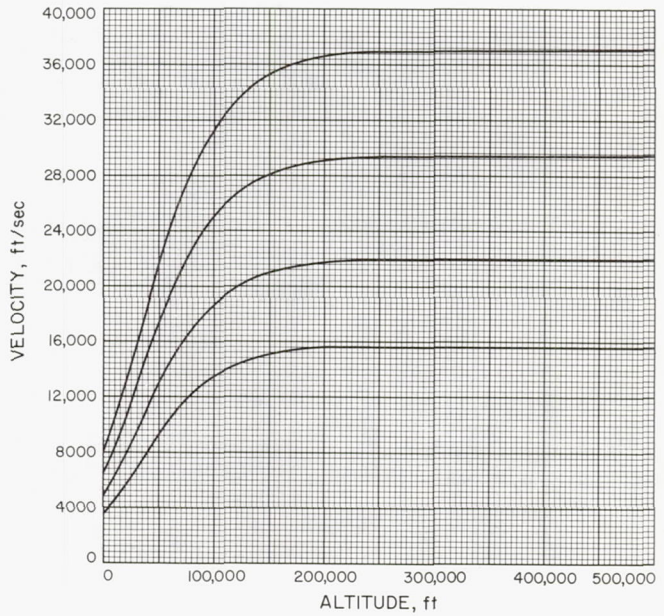

Fig. A-186

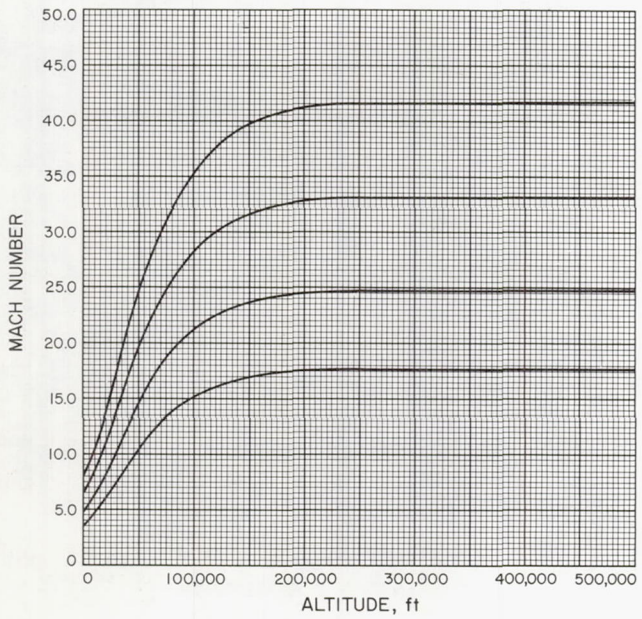

Fig. A-187

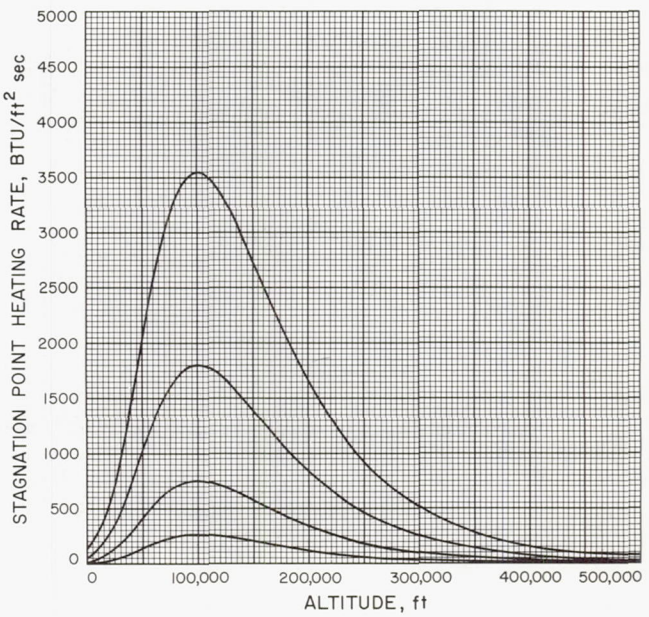

Fig. A-188

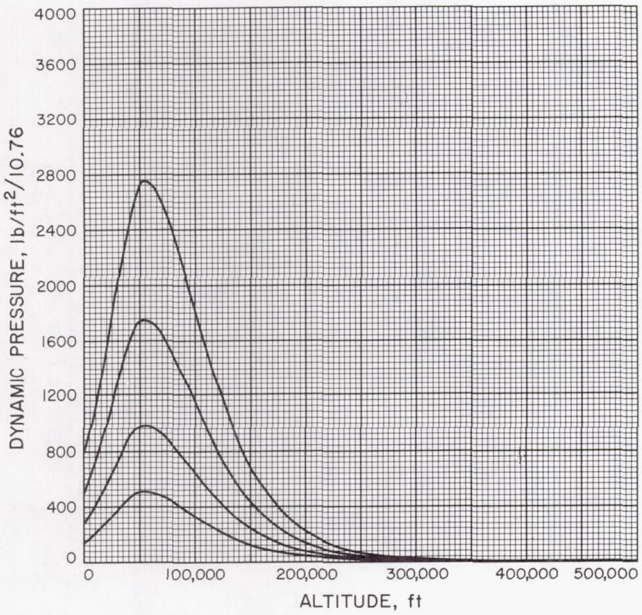

Fig. A-189

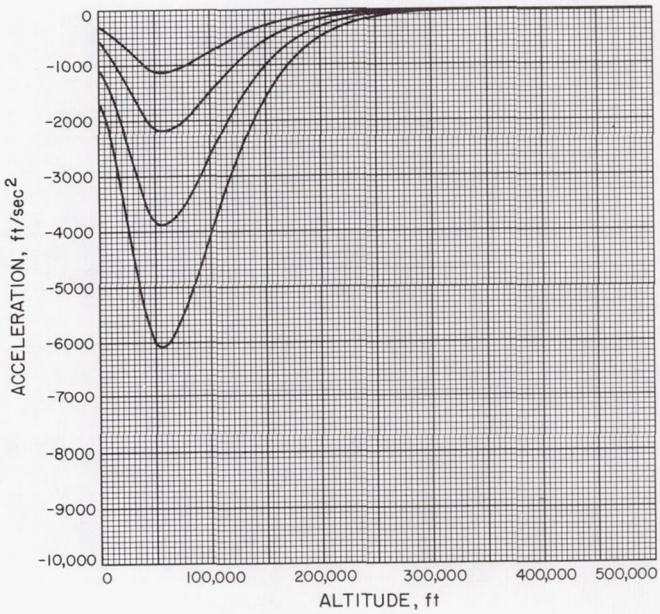

Fig. A-190

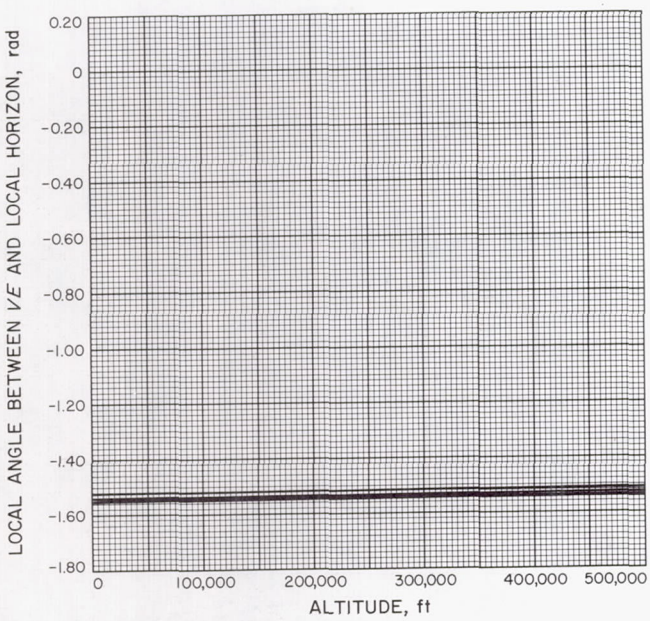

Fig. A-191

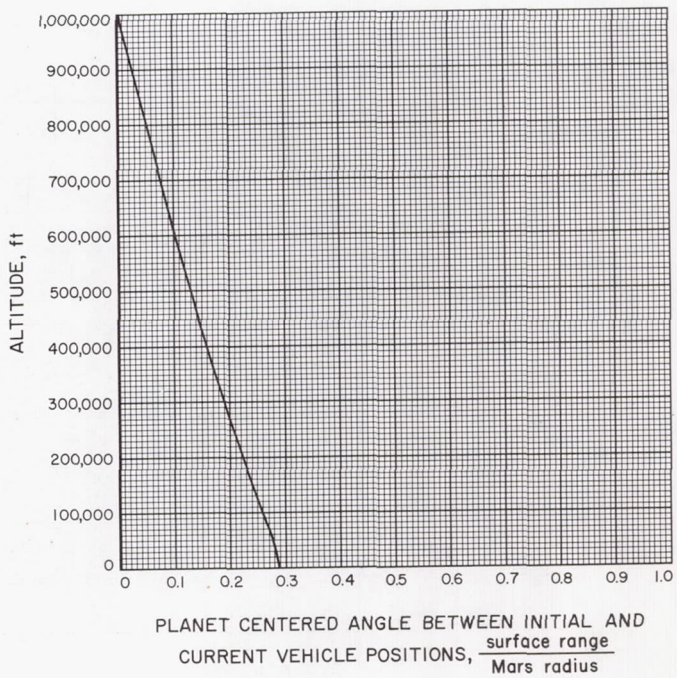

Fig. A-192

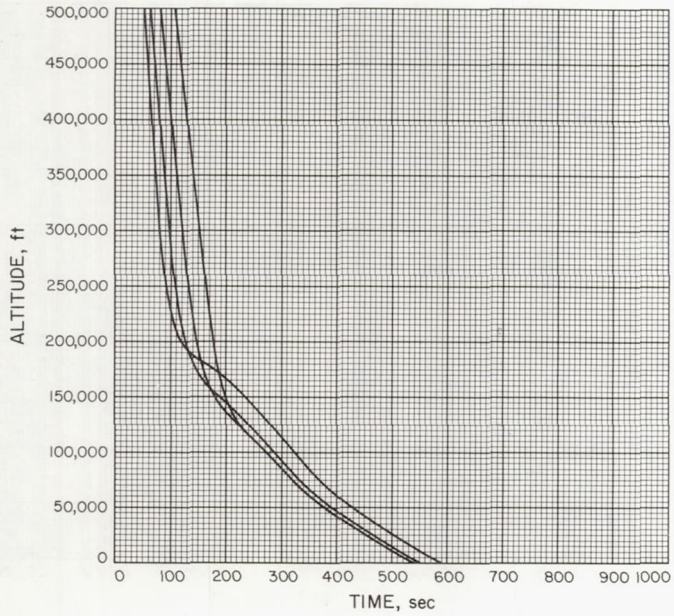

Fig. A-193

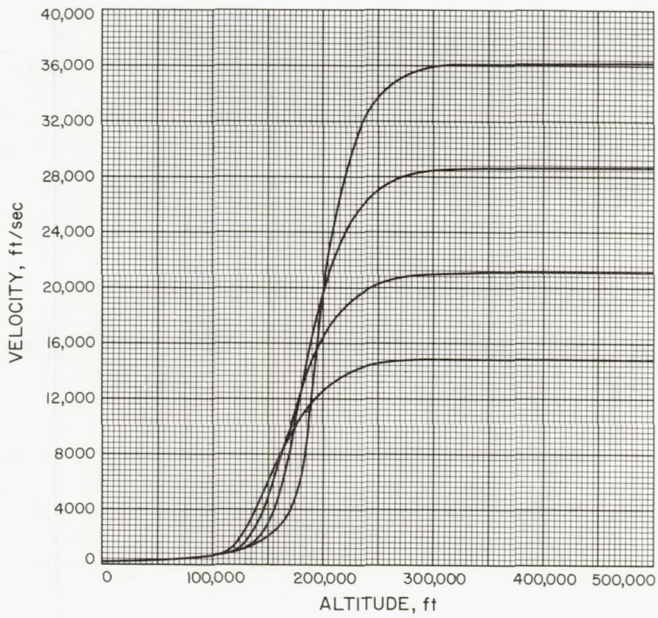

Fig. A-194

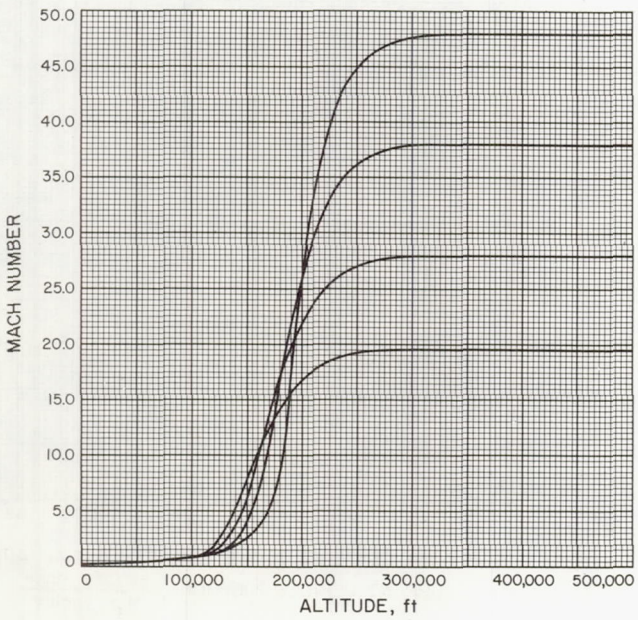

Fig. A-195

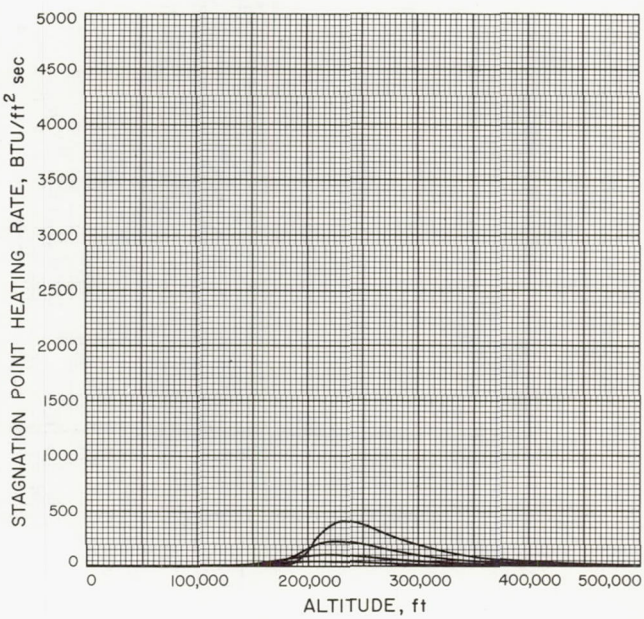

Fig. A-196

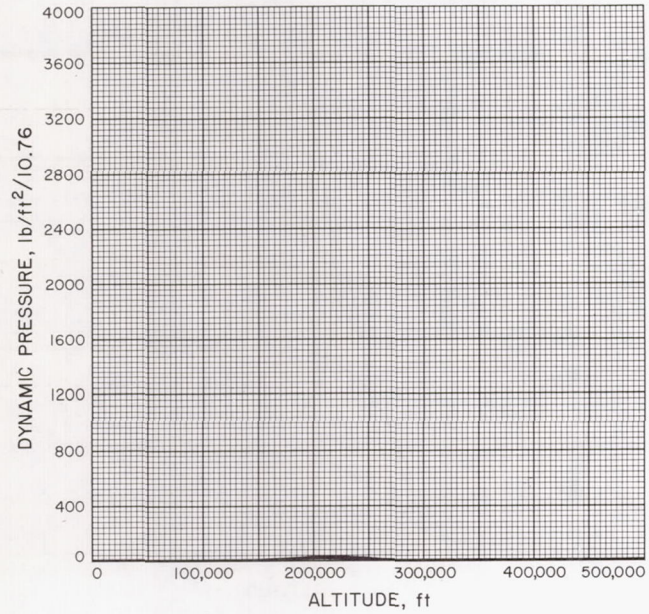

Fig. A-197

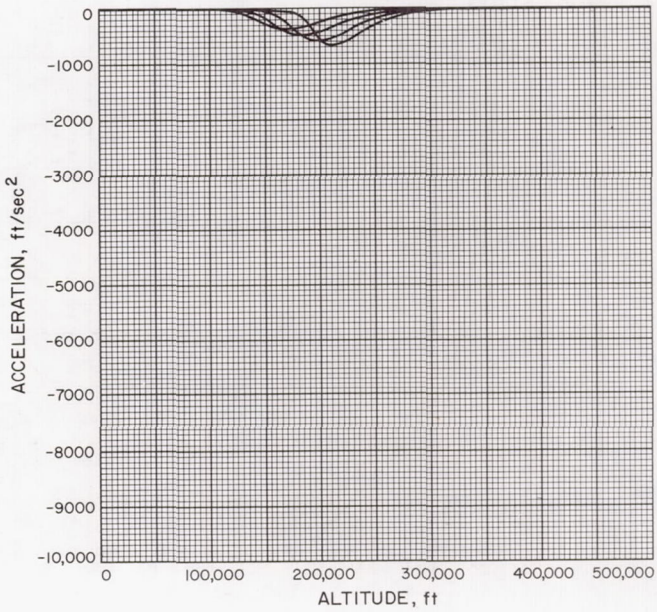

Fig. A-198

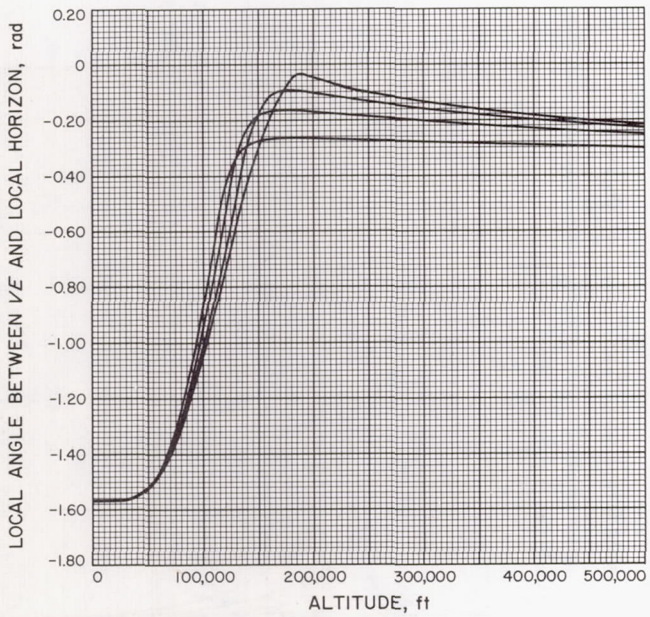

Fig. A-199

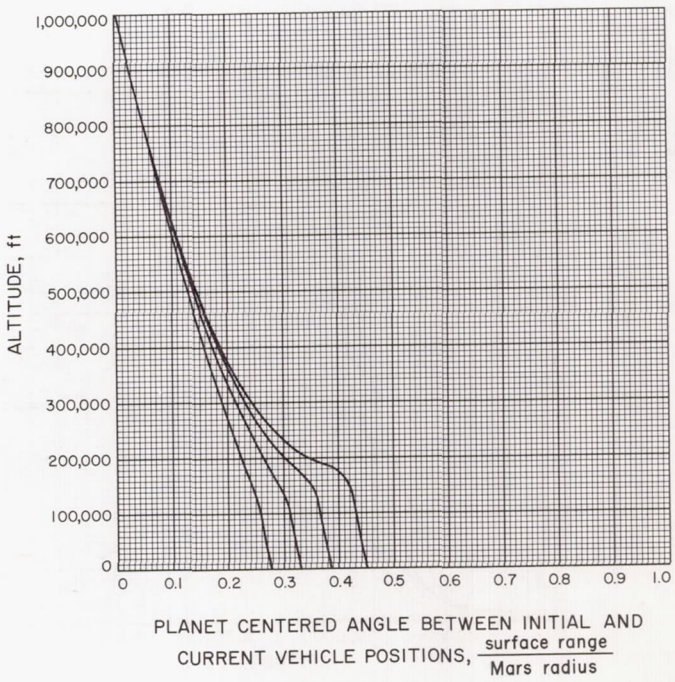

Fig. A-200

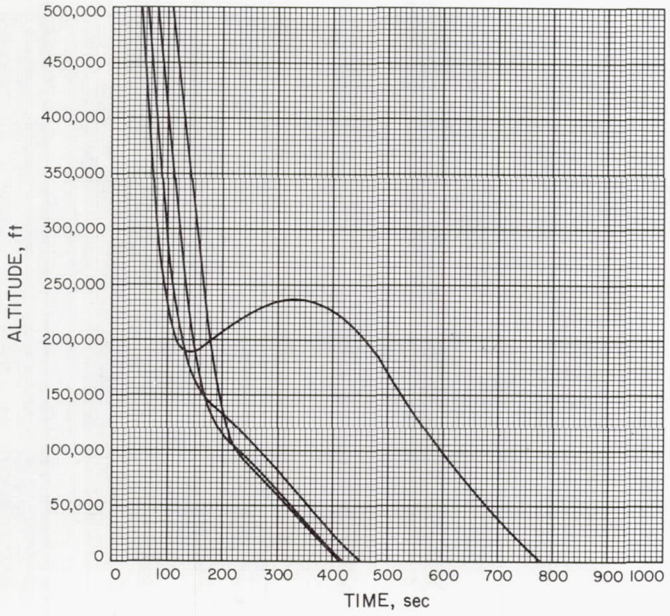

Fig. A-201

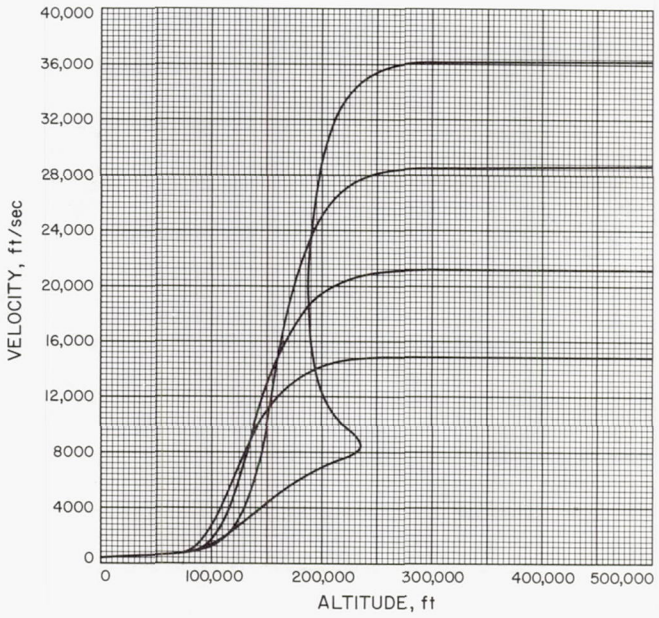

Fig. A-202

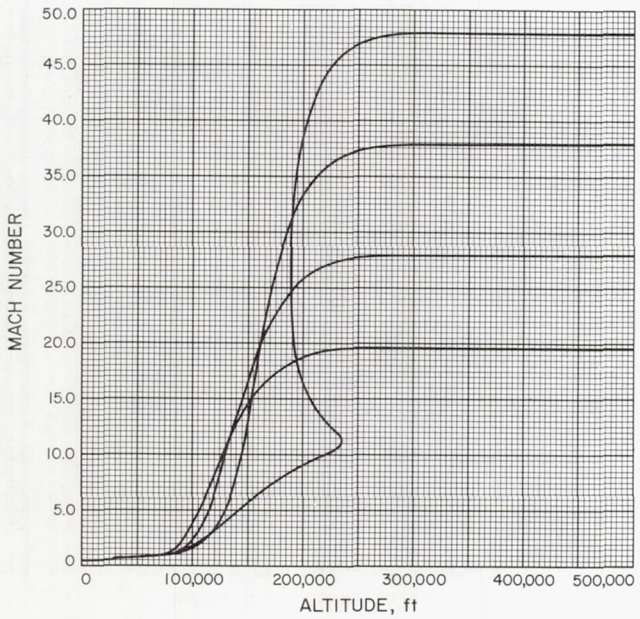

Fig. A-203

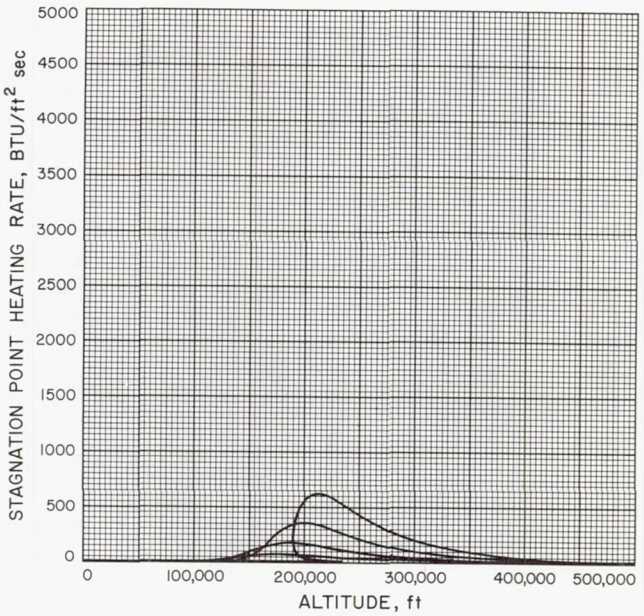

Fig. A-204

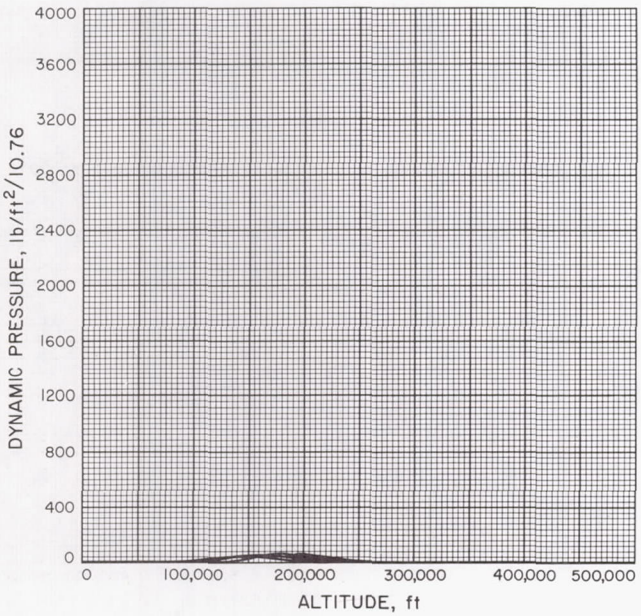

Fig. A-205

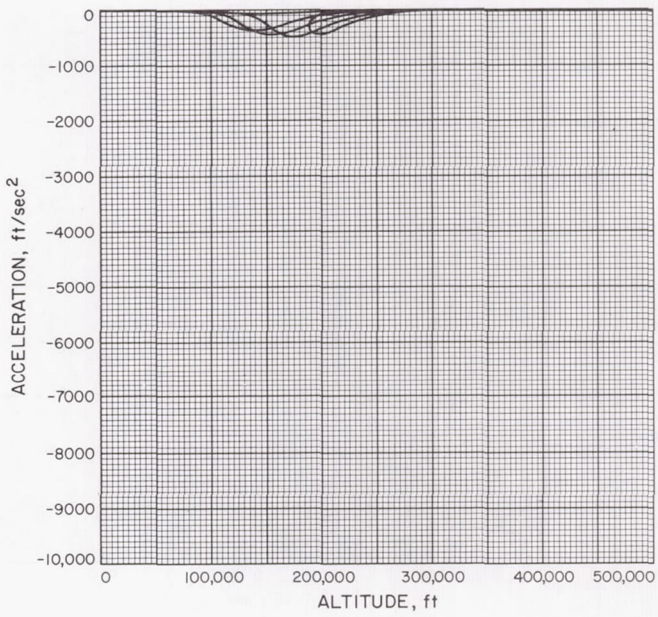

Fig. A-206

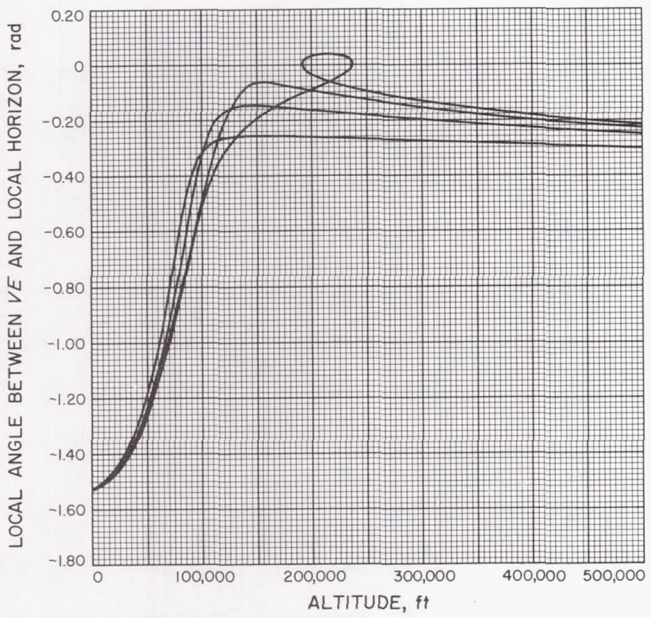

Fig. A-207

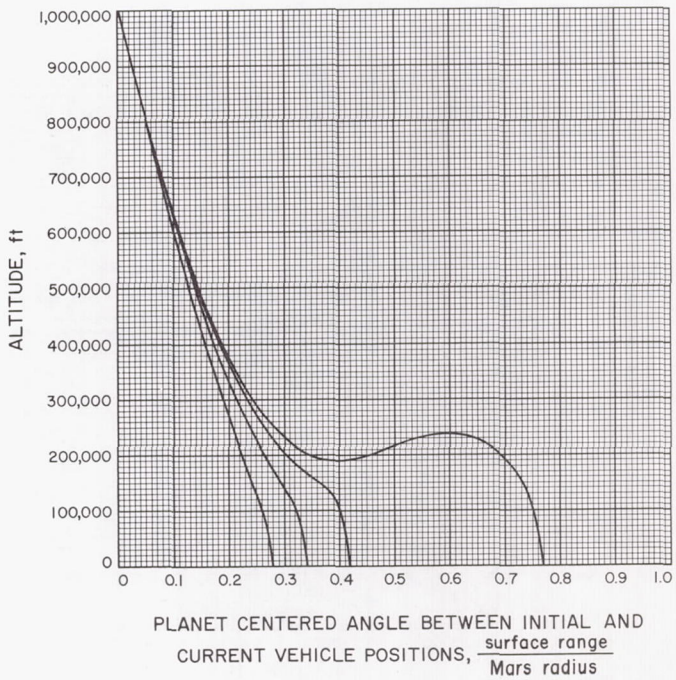

Fig. A-208

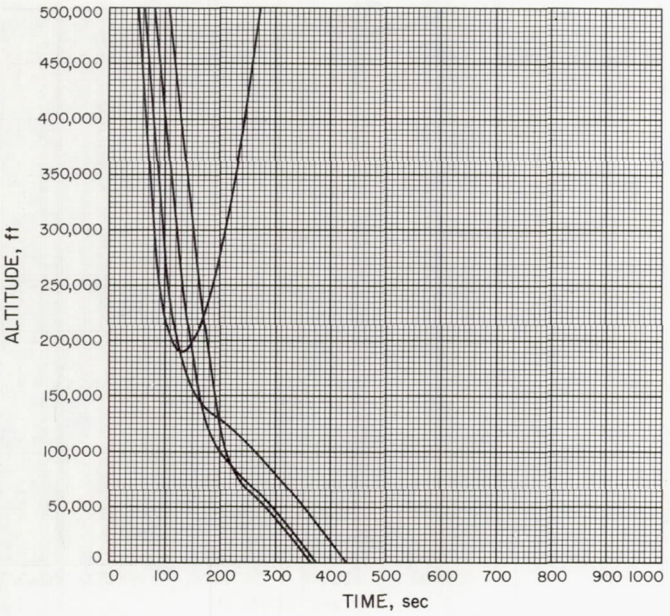

Fig. A-209

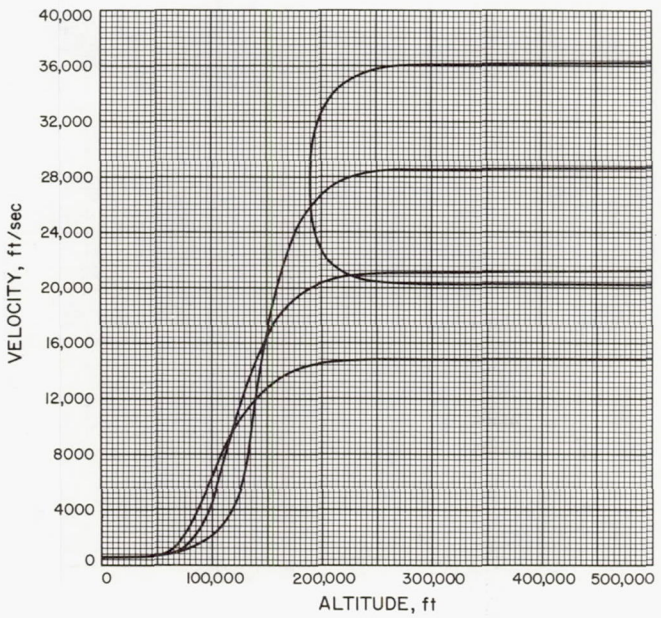

Fig. A-210

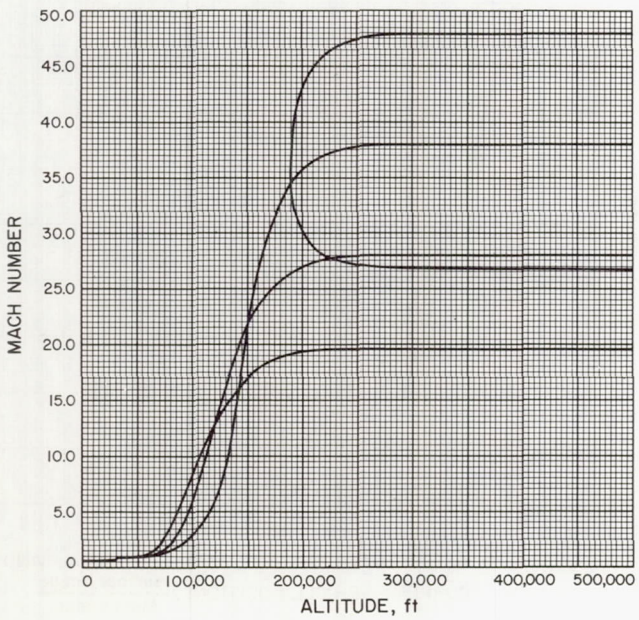

Fig. A-211

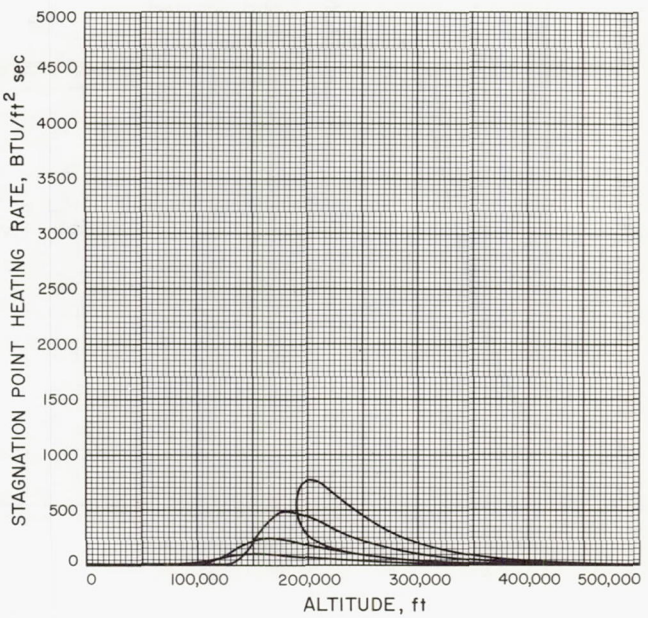

Fig. A-212

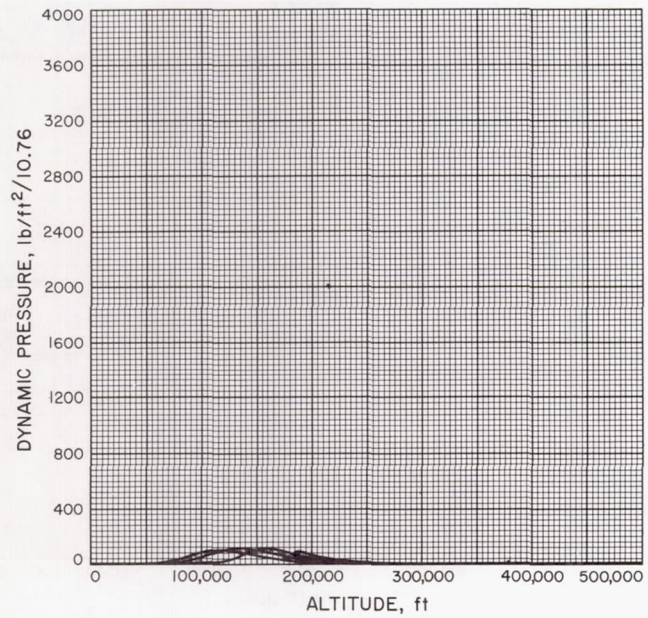

Fig. A-213

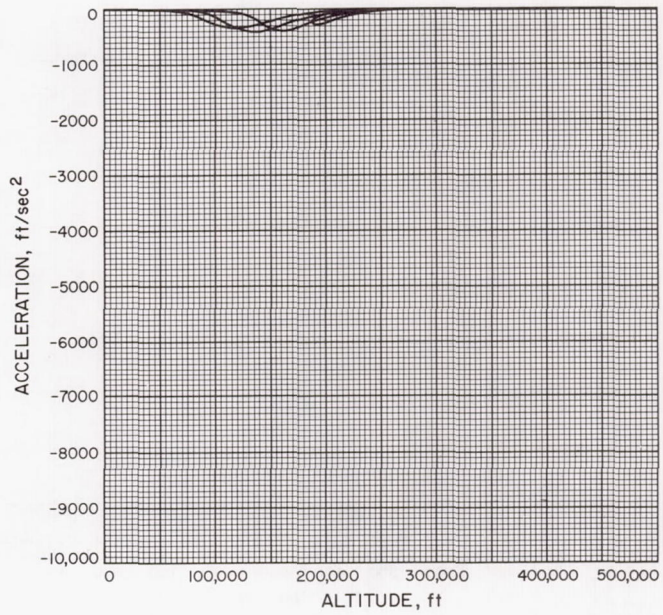

Fig. A-214

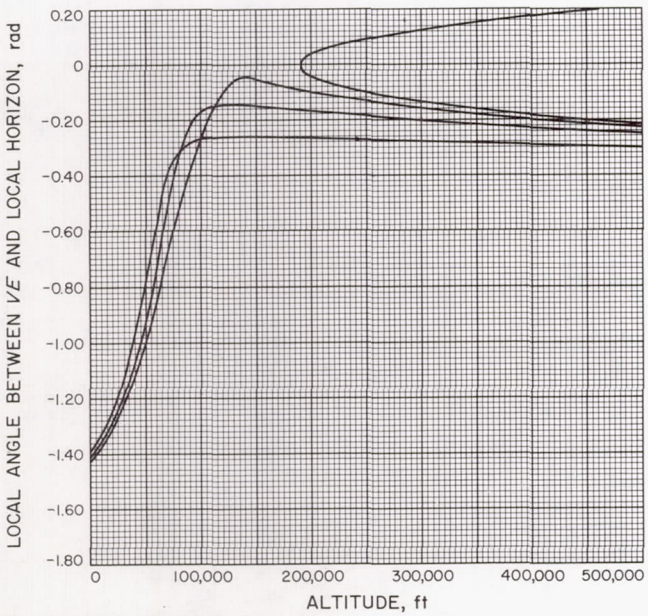

Fig. A-215

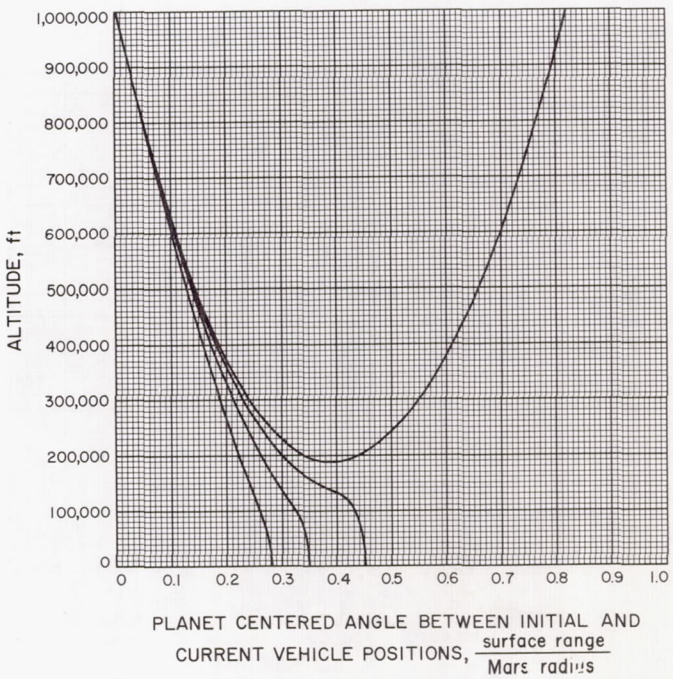

Fig. A-216

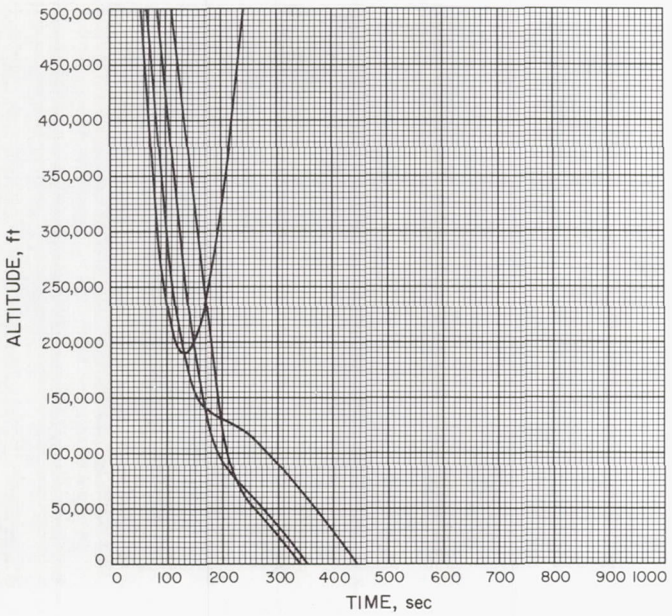

Fig. A-217

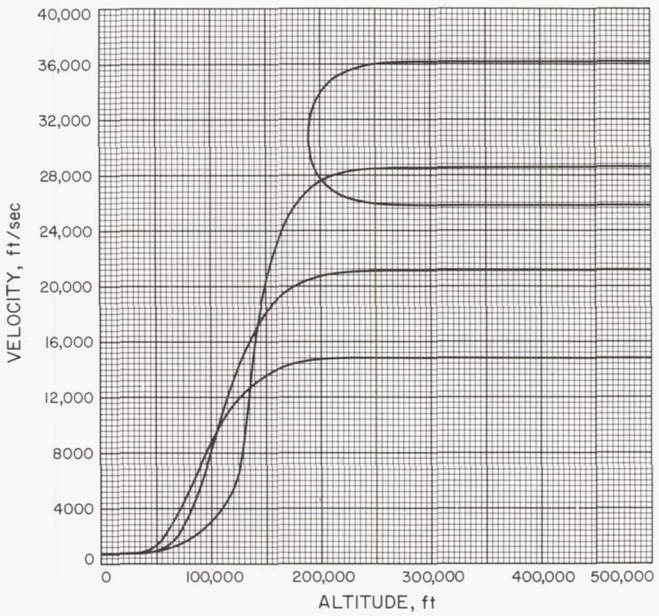

Fig. A-218

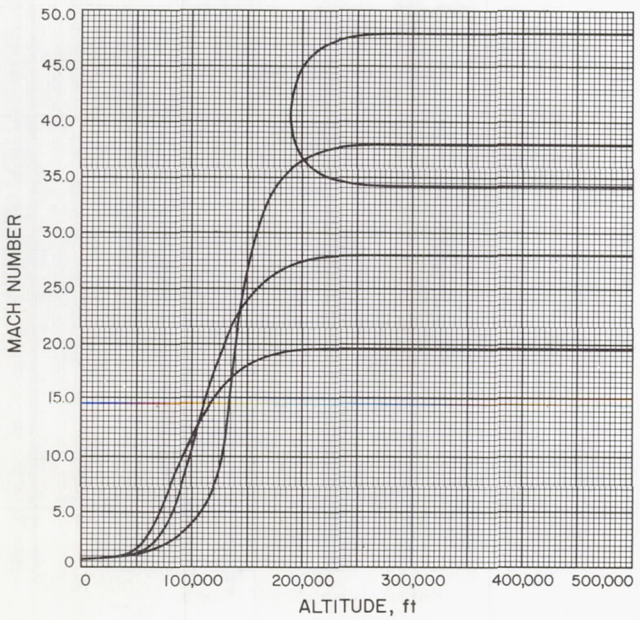

Fig. A-219

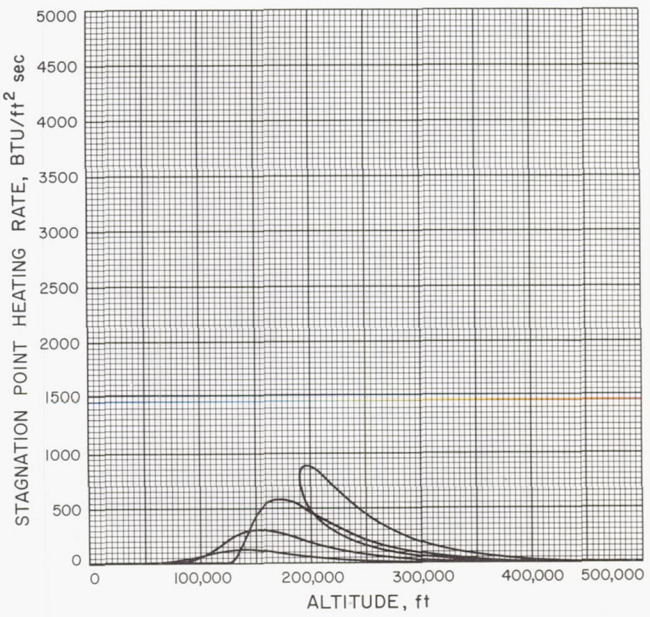

Fig. A-220

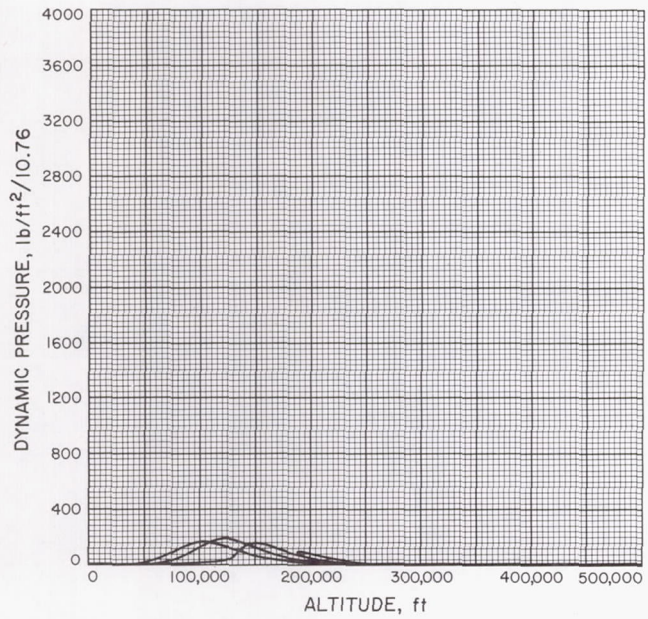

Fig. A-221

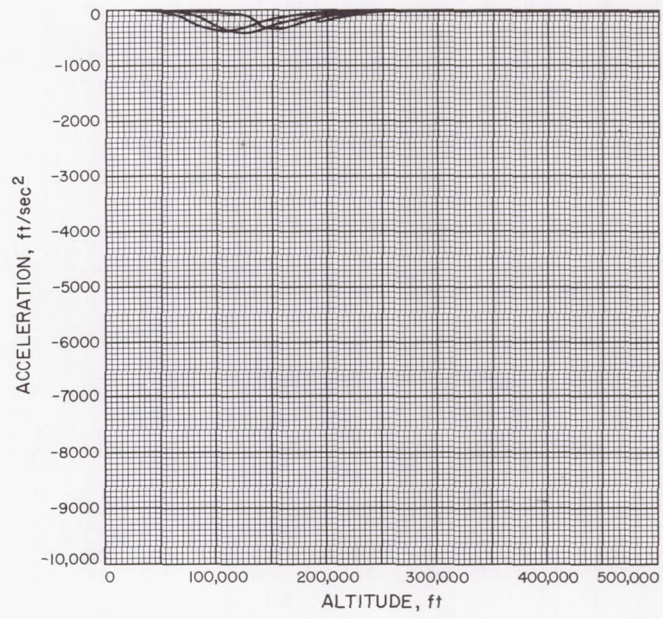

Fig. A-222

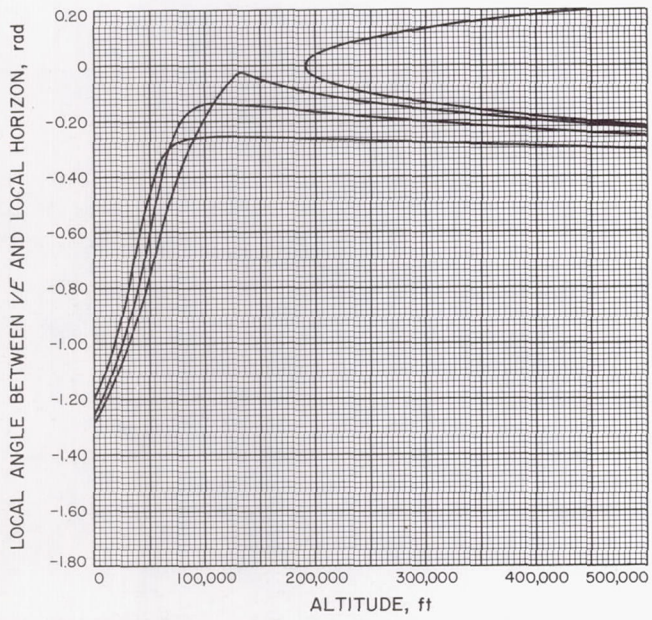

Fig. A-223

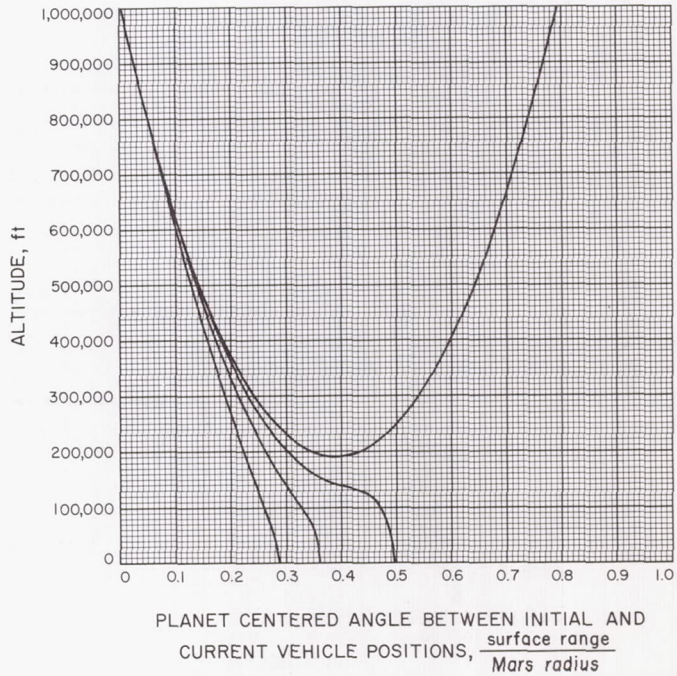

Fig. A-224

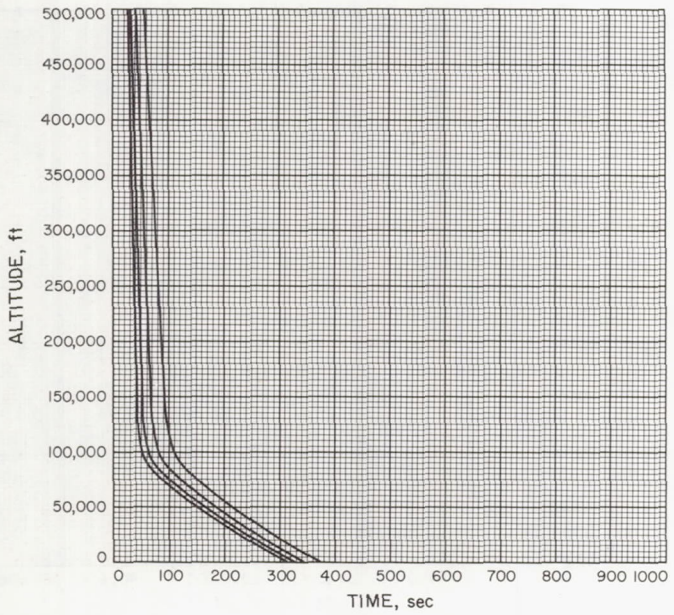

Fig. A-225

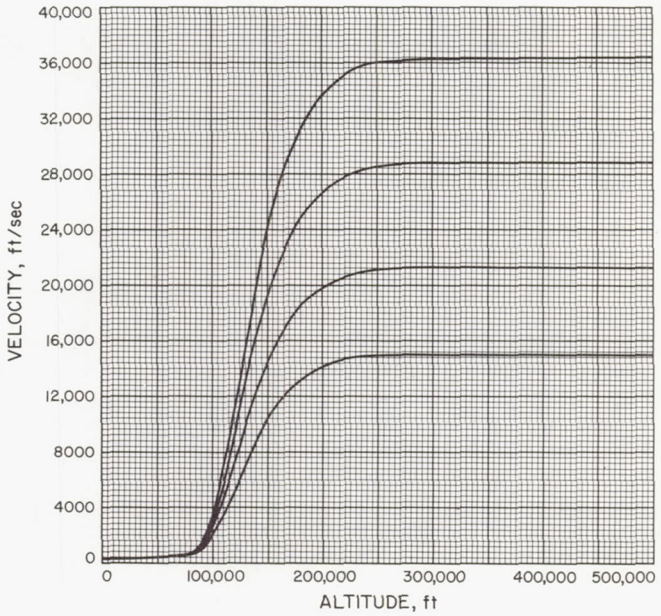

Fig. A-226

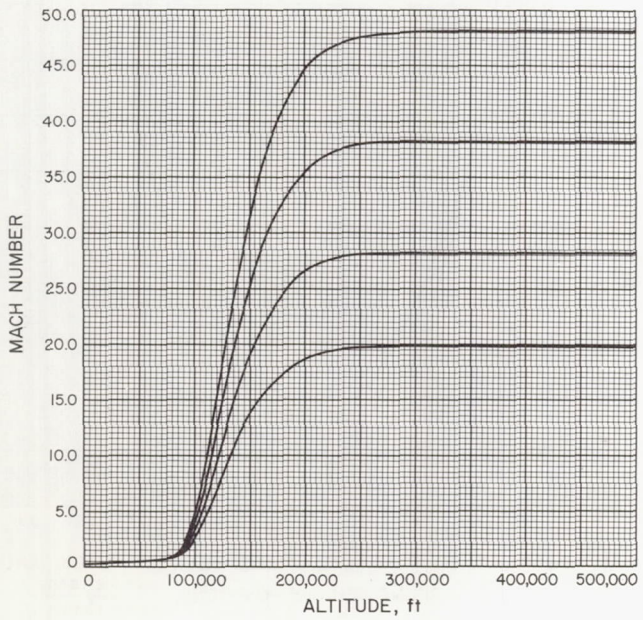

Fig. A-227

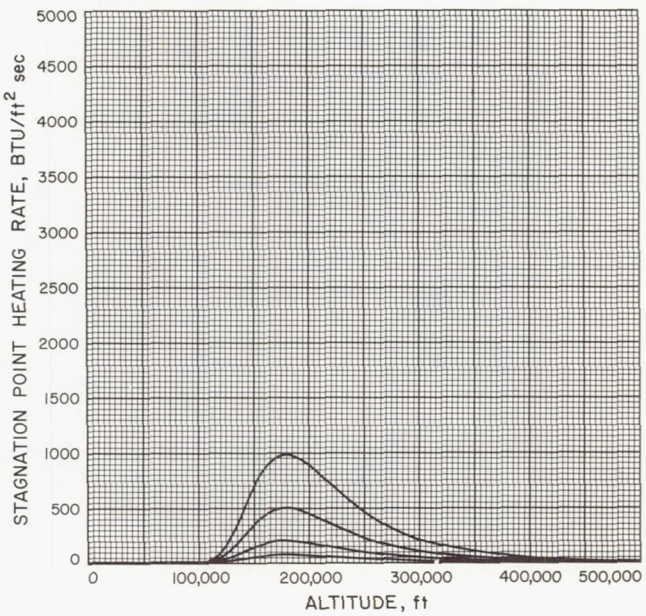

Fig. A-228

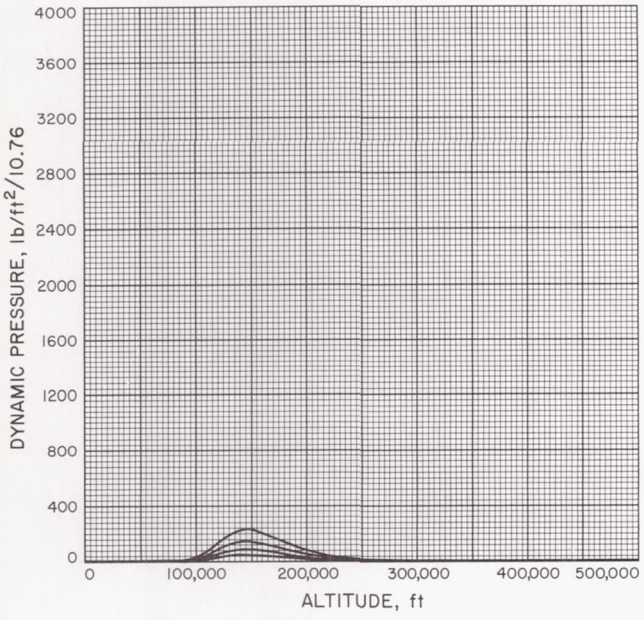

Fig. A-229

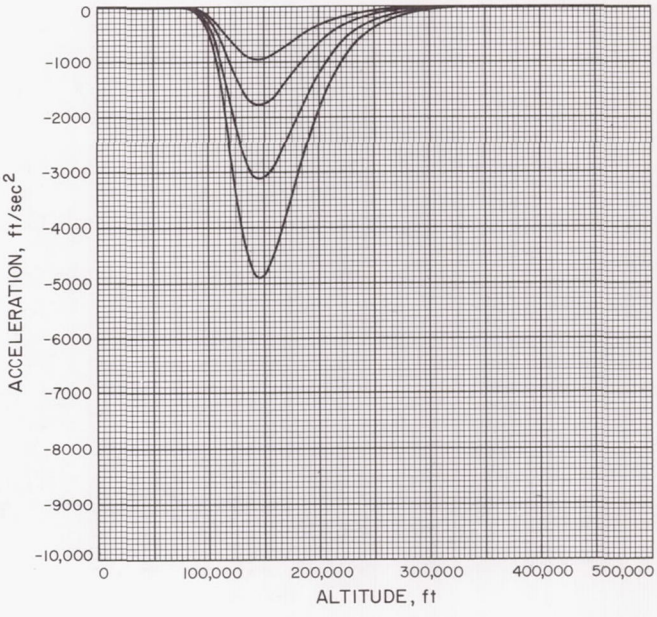

Fig. A-230

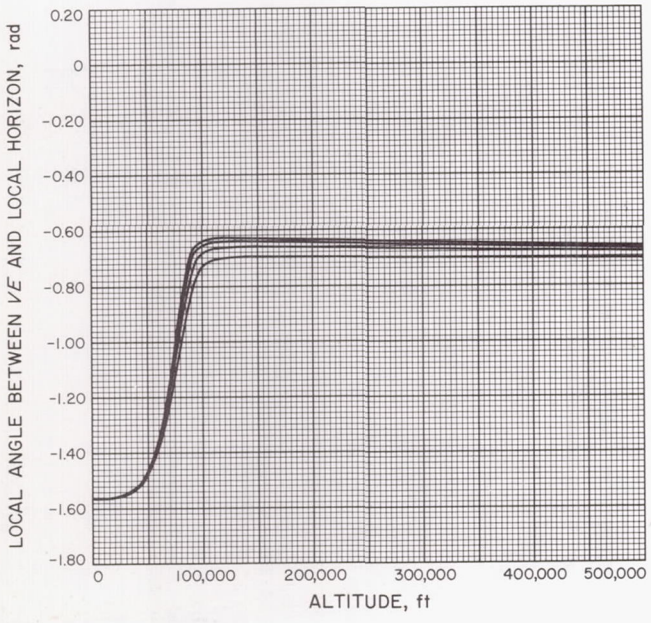

Fig. A-231

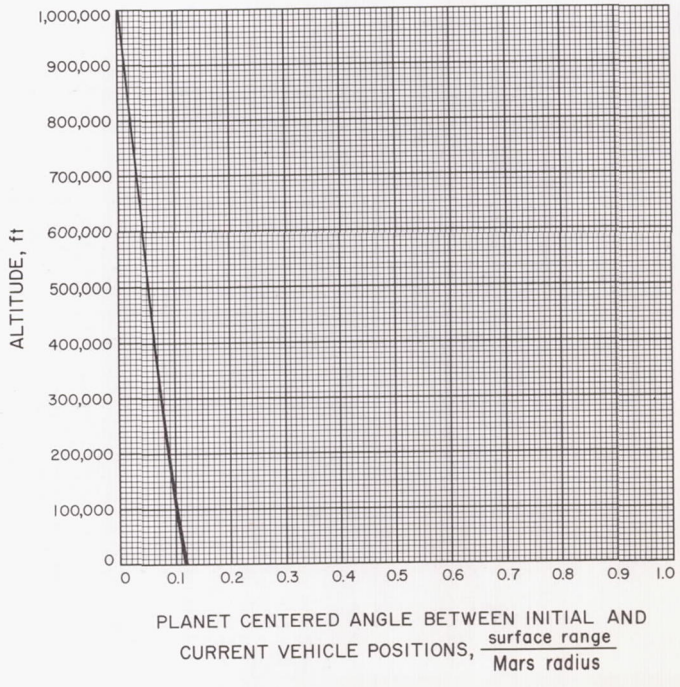

Fig. A-232

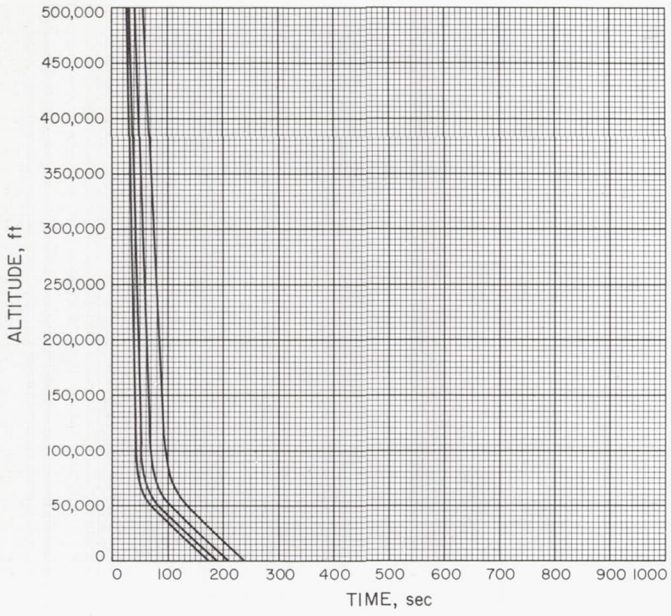

Fig. A-233

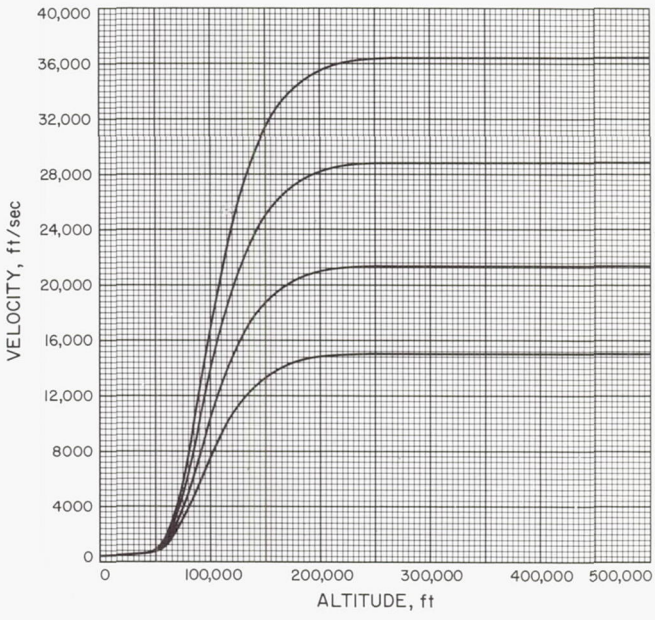

Fig. A-234

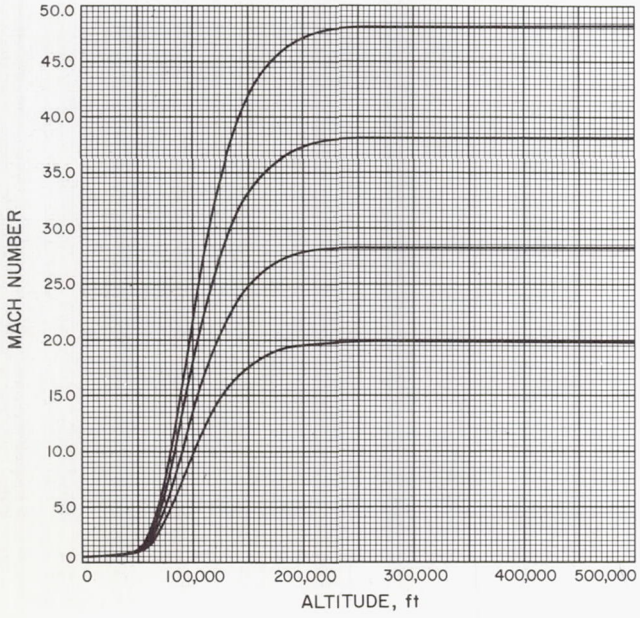

Fig. A-235

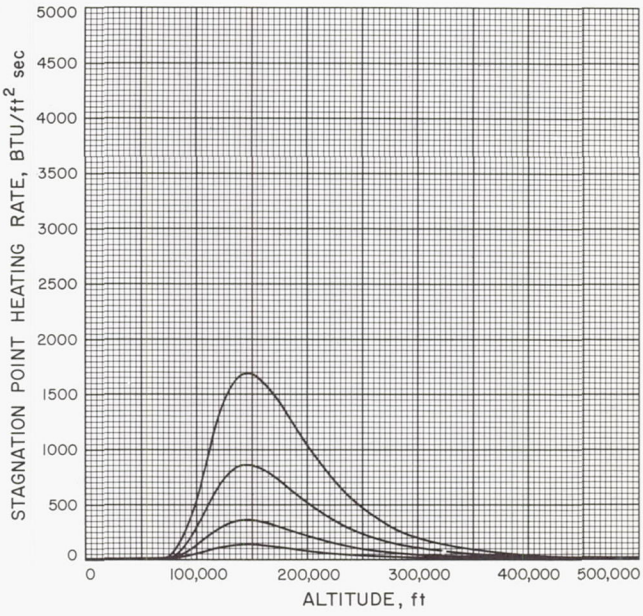

Fig. A-236

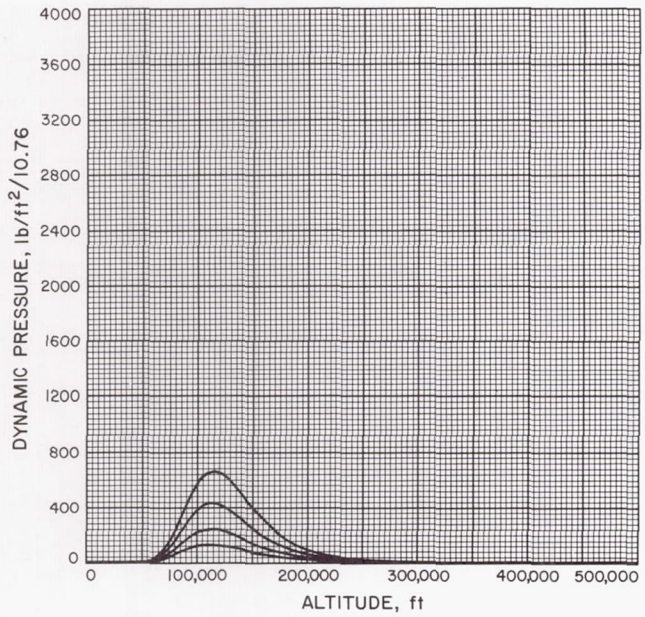

Fig. A-237

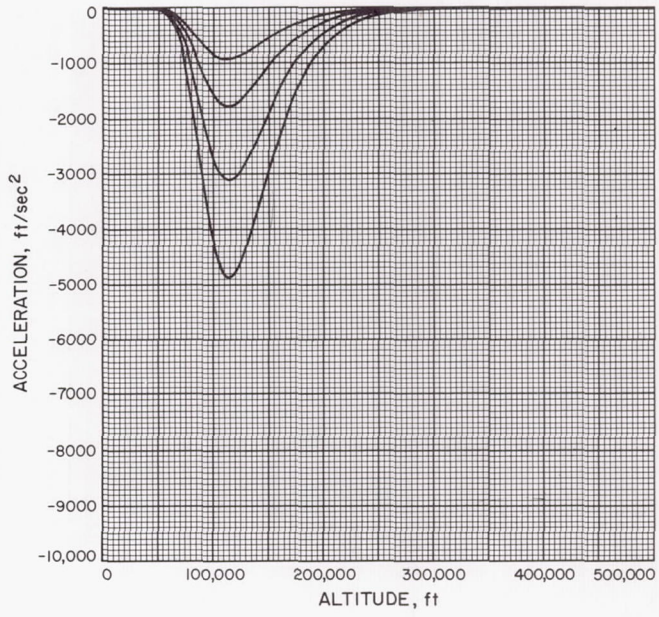

Fig. A-238

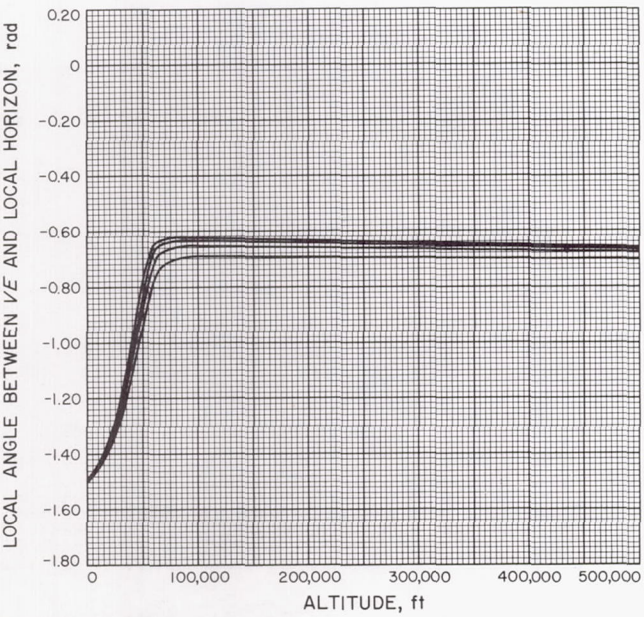

Fig. A-239

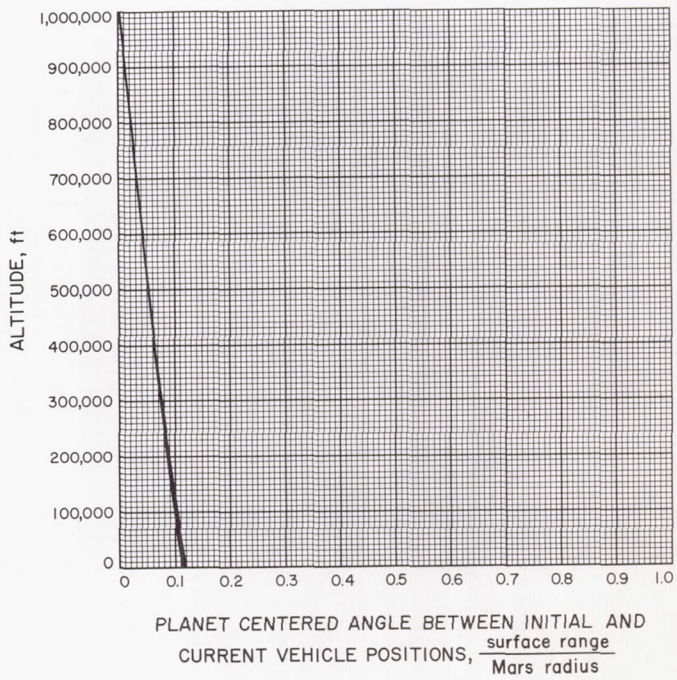

Fig. A-240

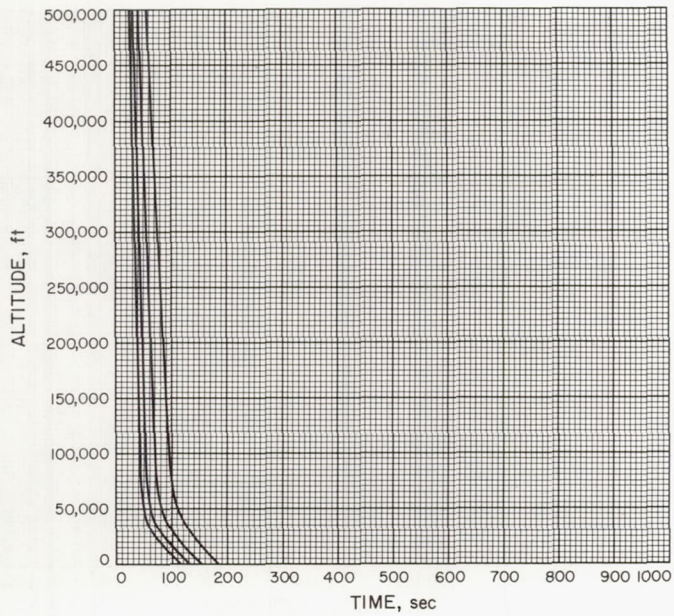

Fig. A-241

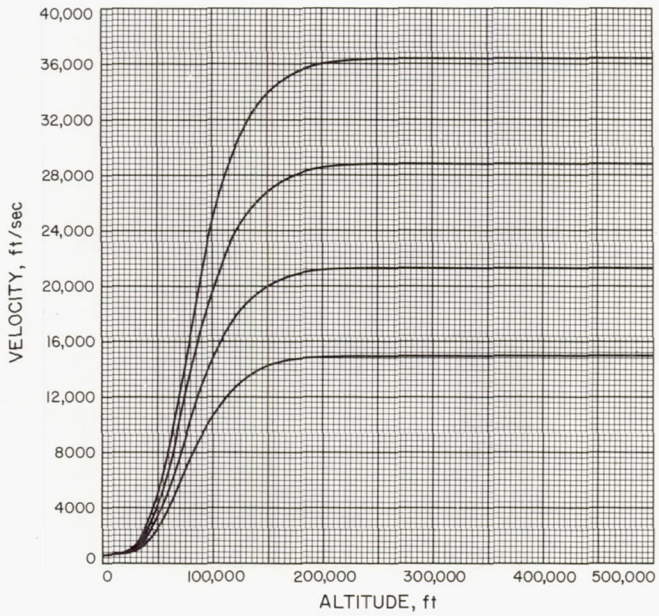

Fig. A-242

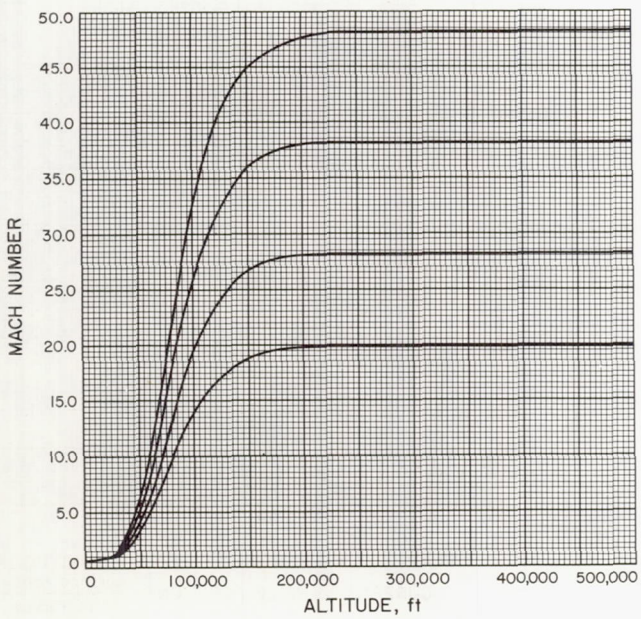

Fig. A-243

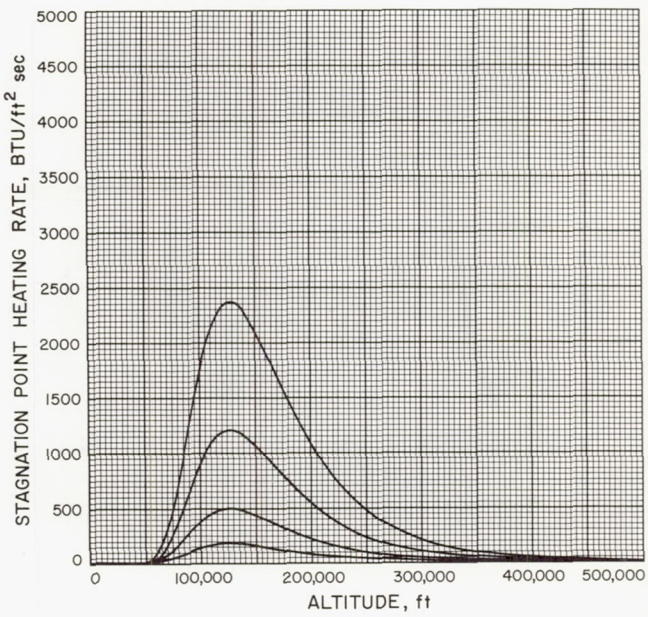

Fig. A-244

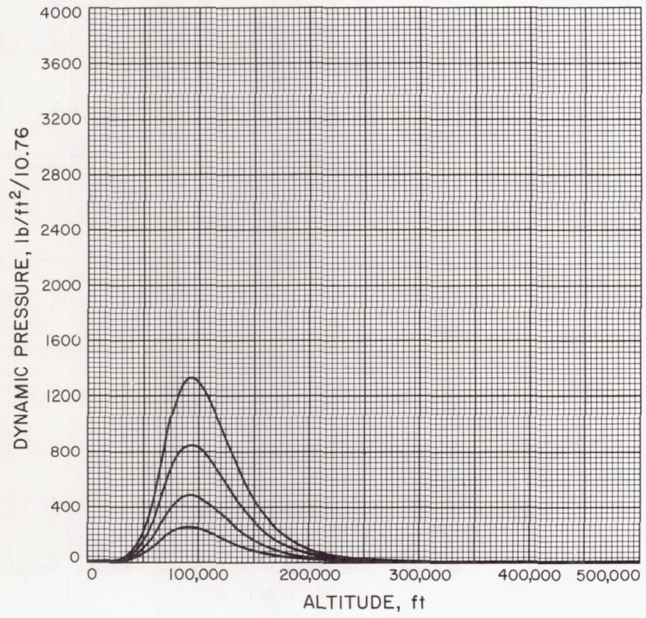

Fig. A-245

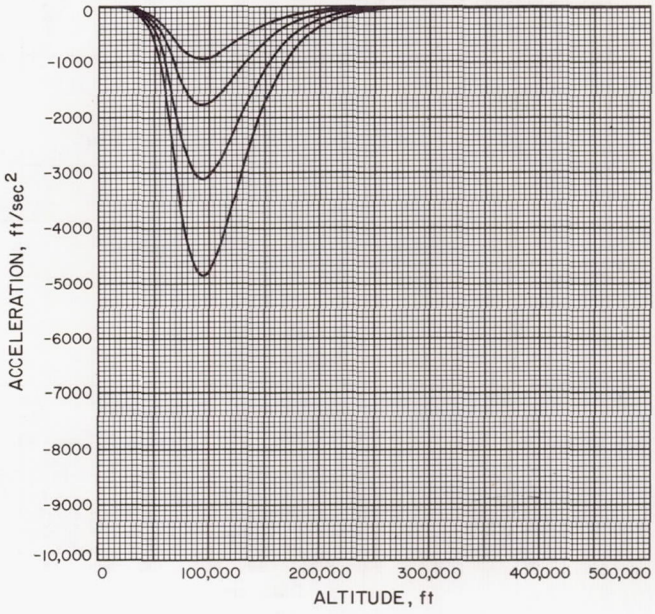

Fig. A-246

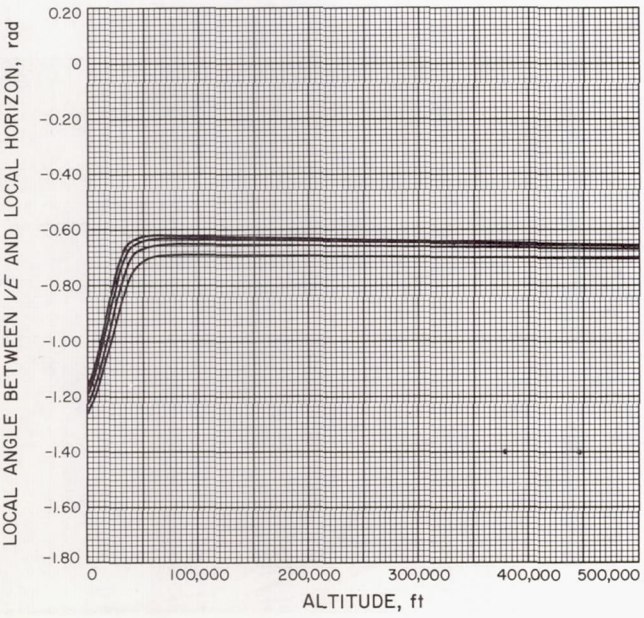

Fig. A-247

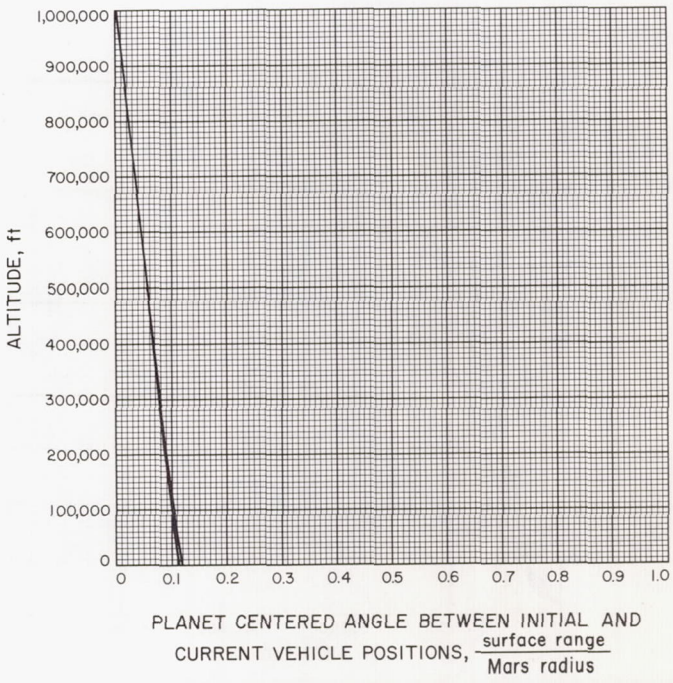

Fig. A-248

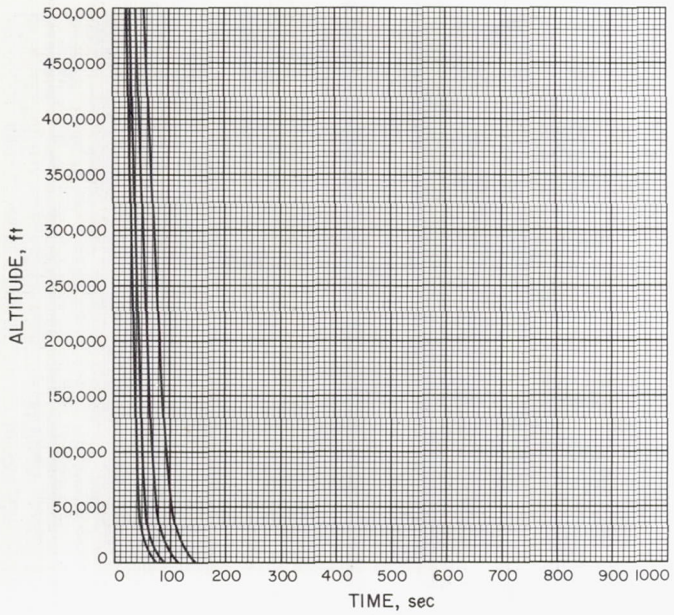

Fig. A-249

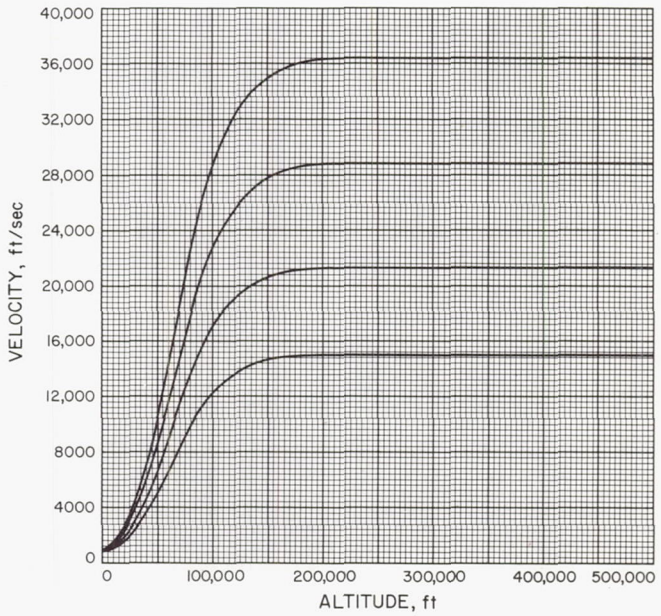

Fig. A-250

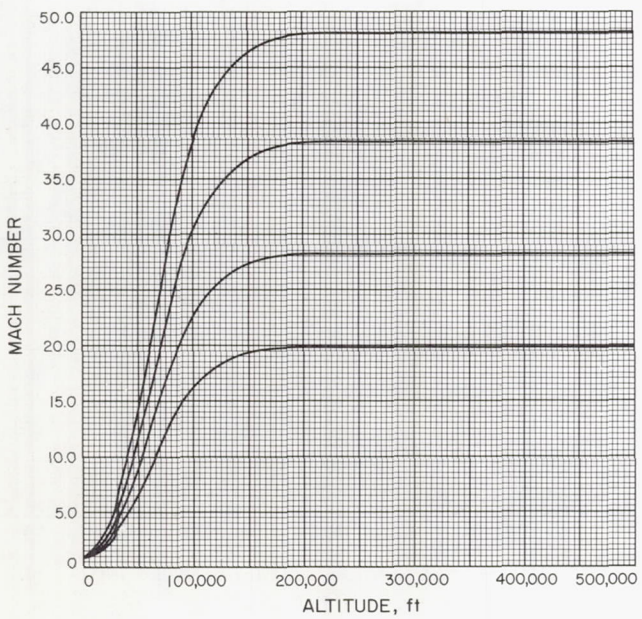

Fig. A-251

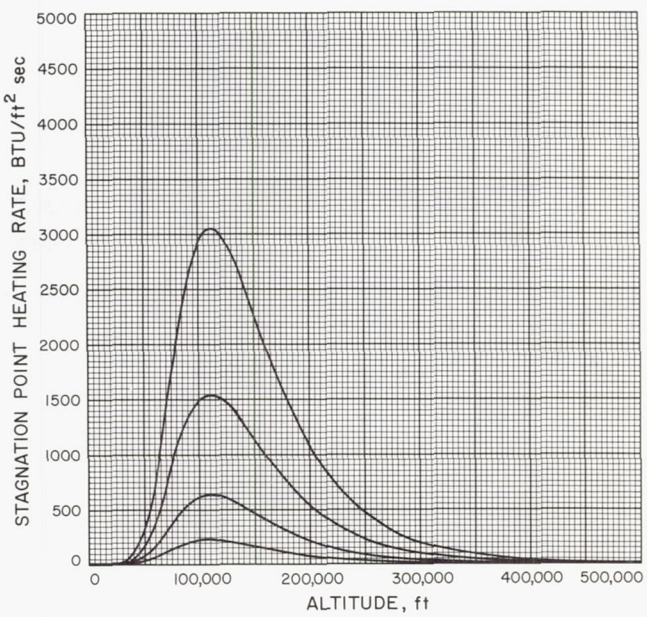

Fig. A-252

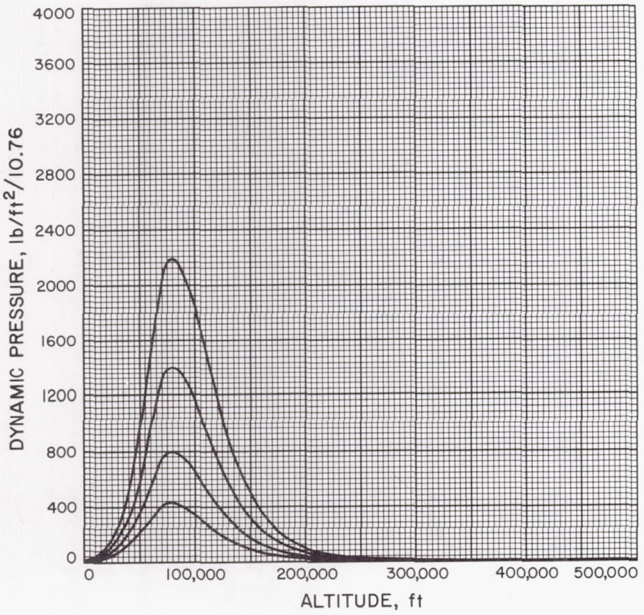

Fig. A-253

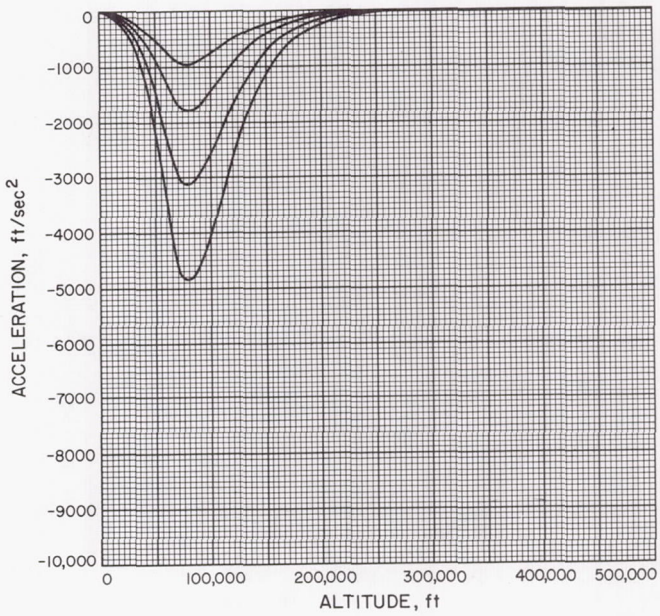

Fig. A-254

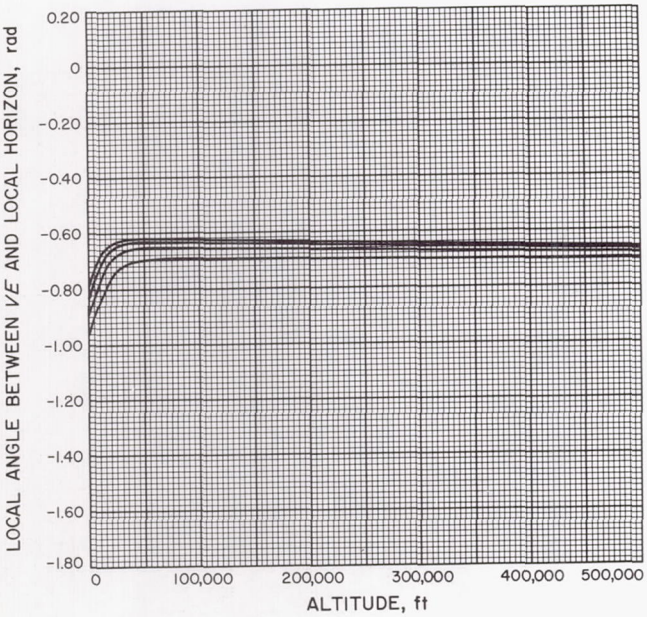

Fig. A-255

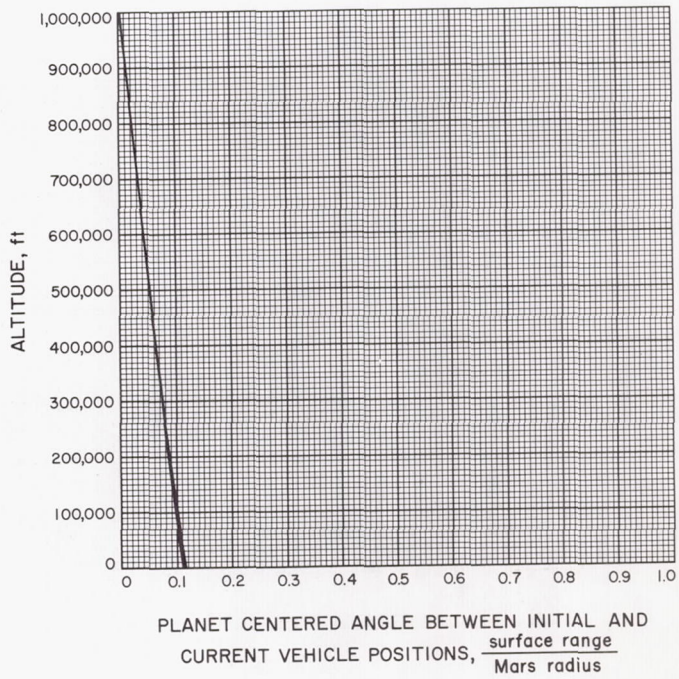

Fig. A-256

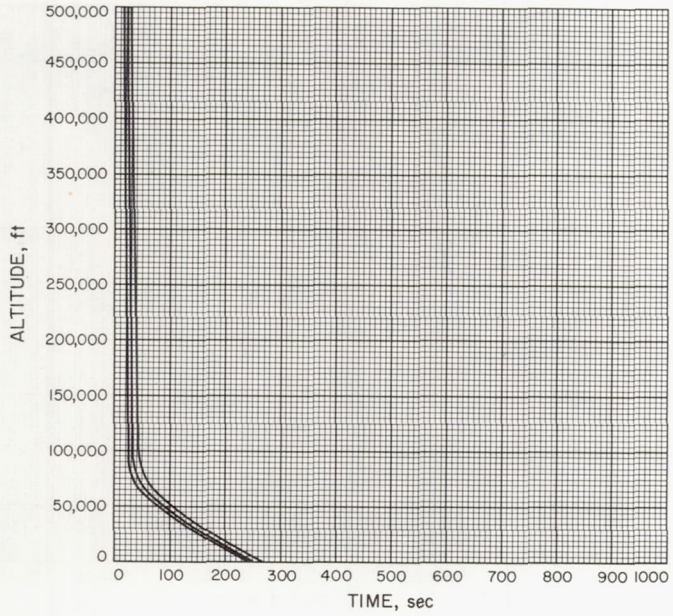

Fig. A-257

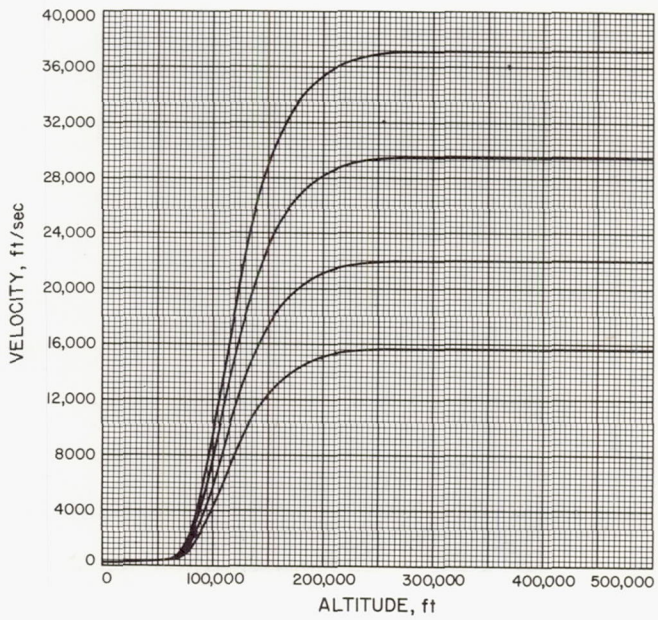

Fig. A-258

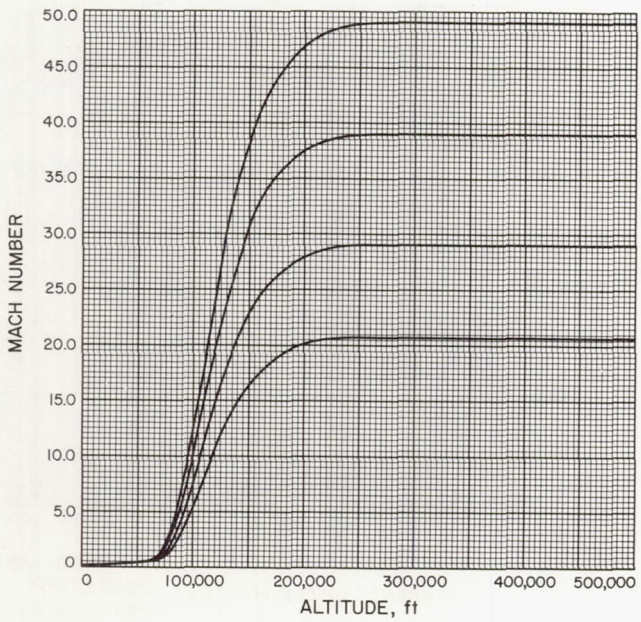

Fig. A-259

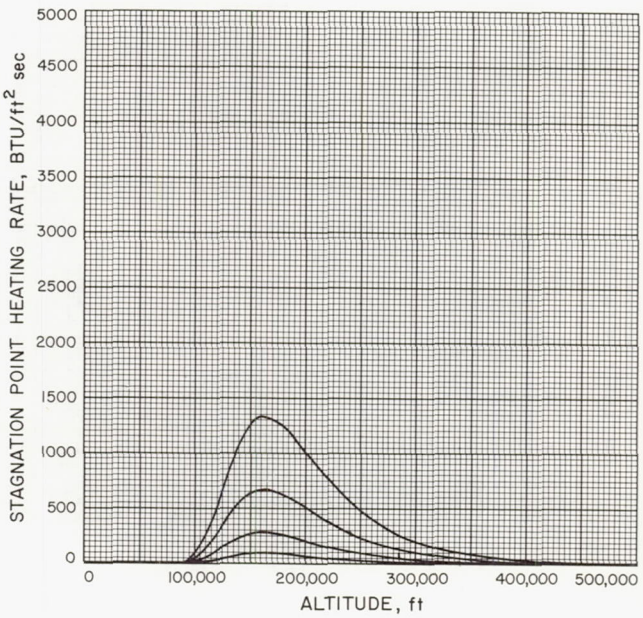

Fig. A-260

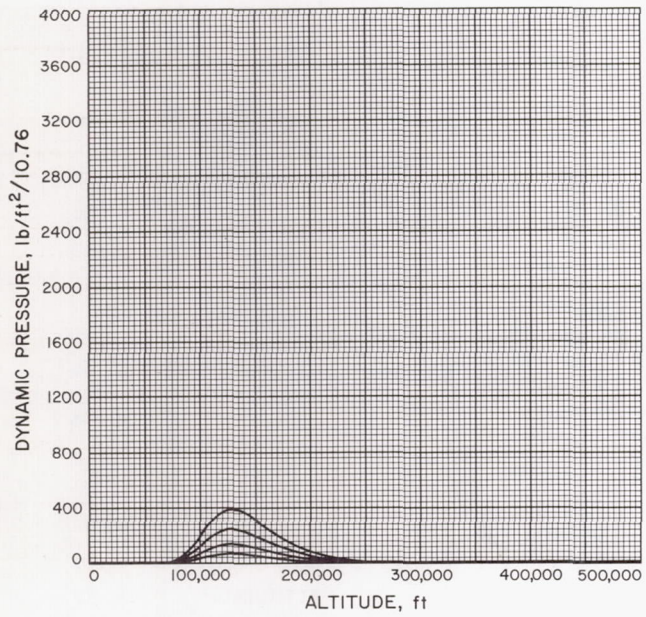

Fig. A-261

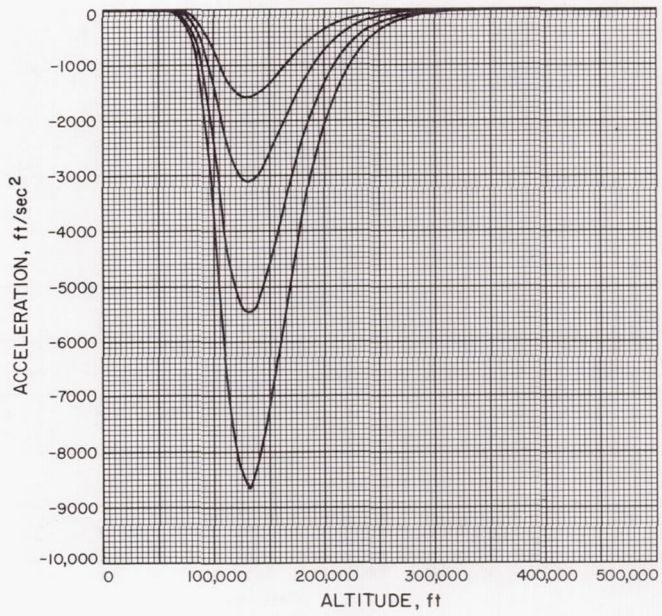

Fig. A-262

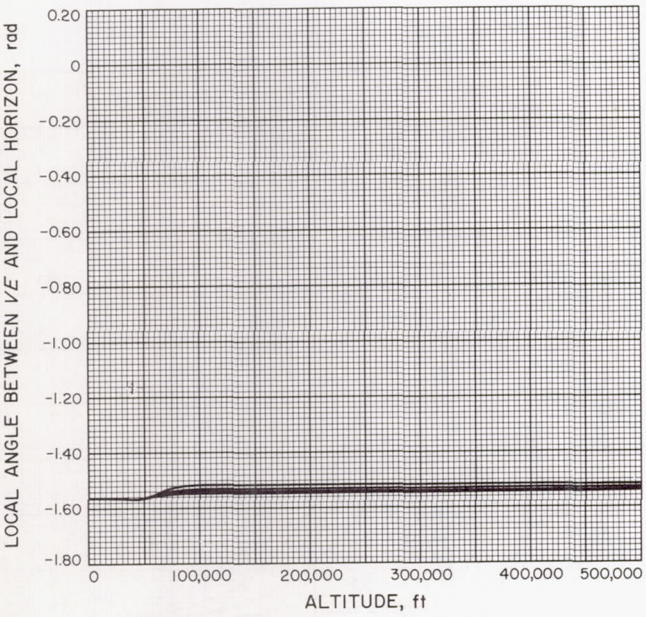

Fig. A-263

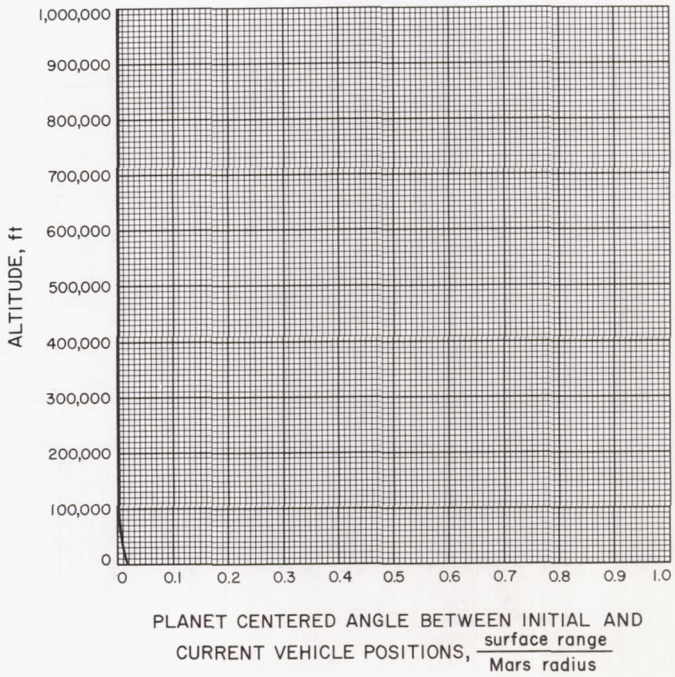

Fig. A-264

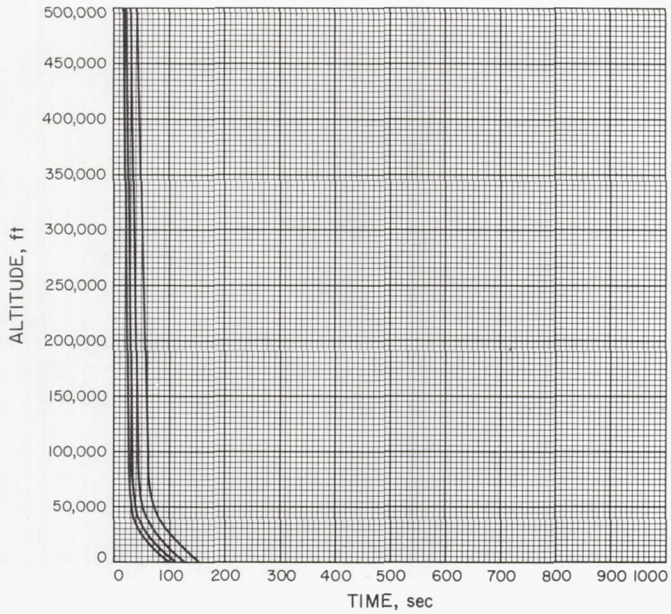

Fig. A-265

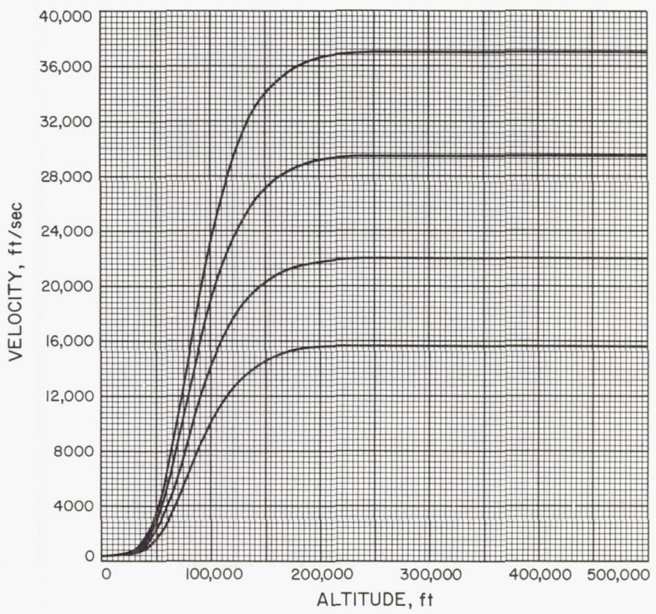

Fig. A-266

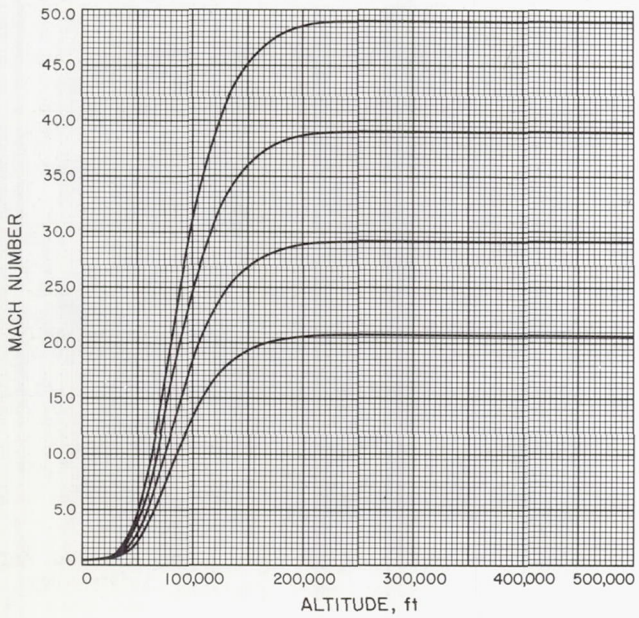

Fig. A-267

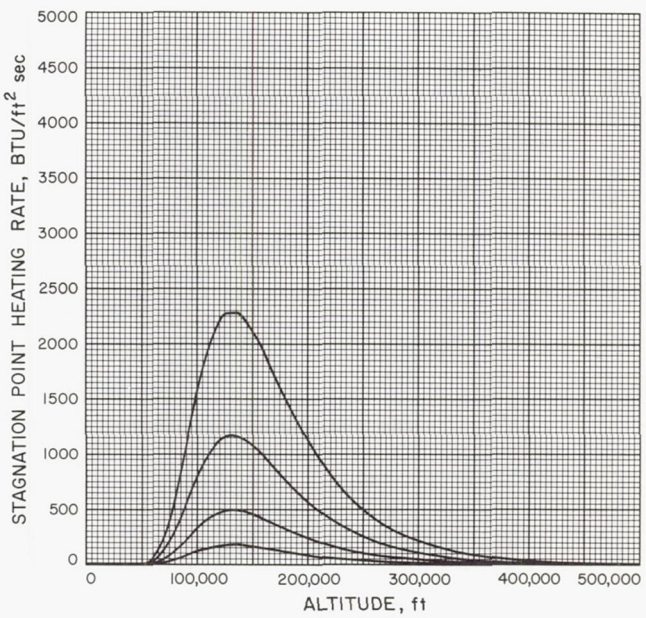

Fig. A-268

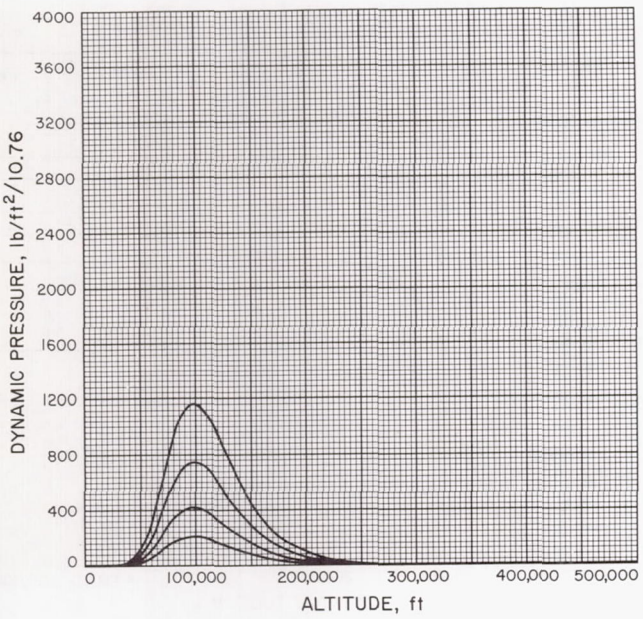

Fig. A-269

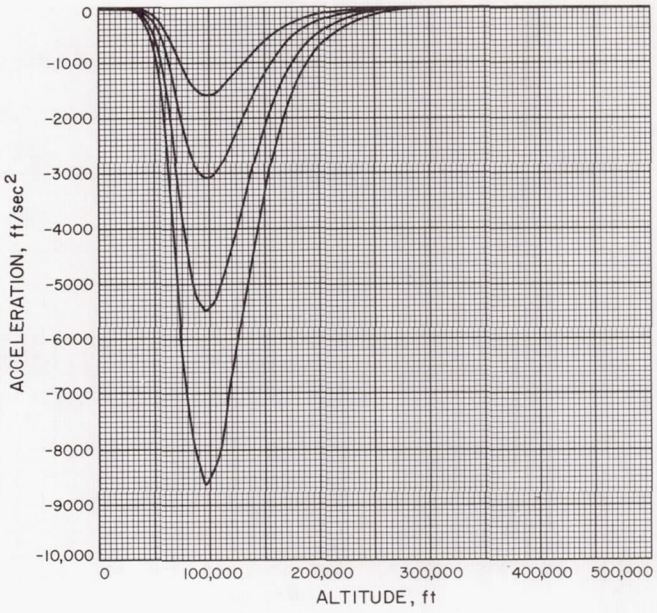

Fig. A-270

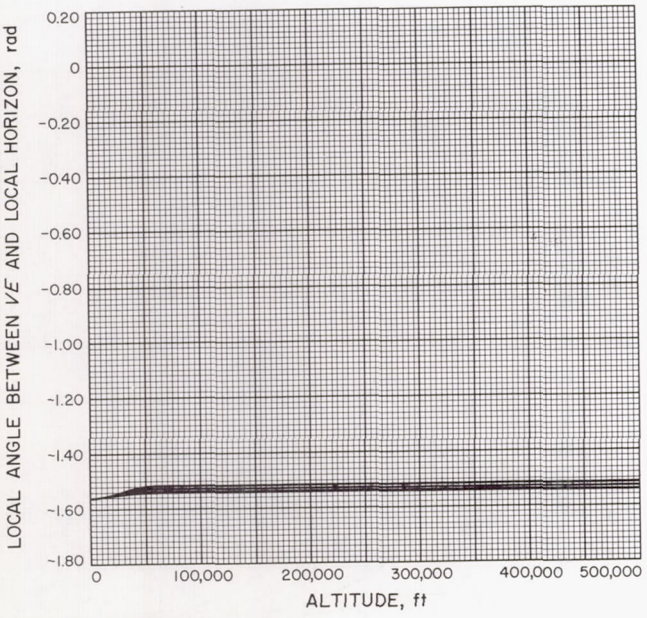

Fig. A-271

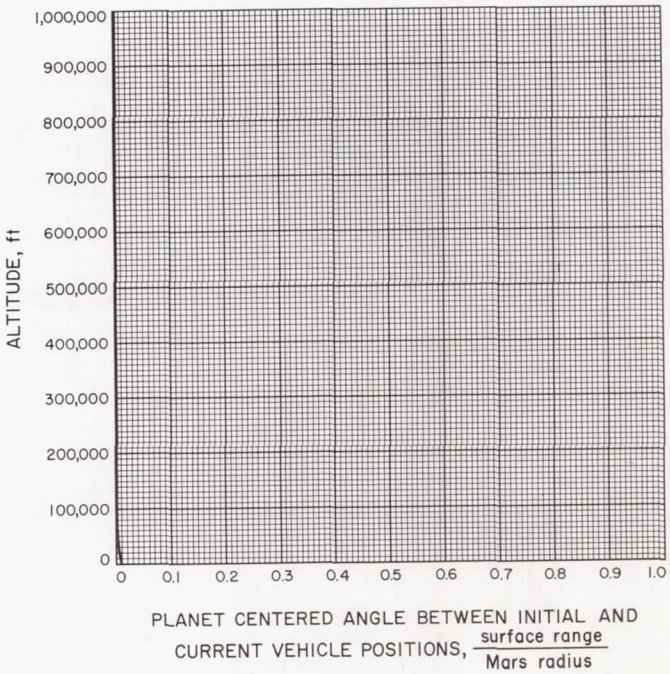

Fig. A-272

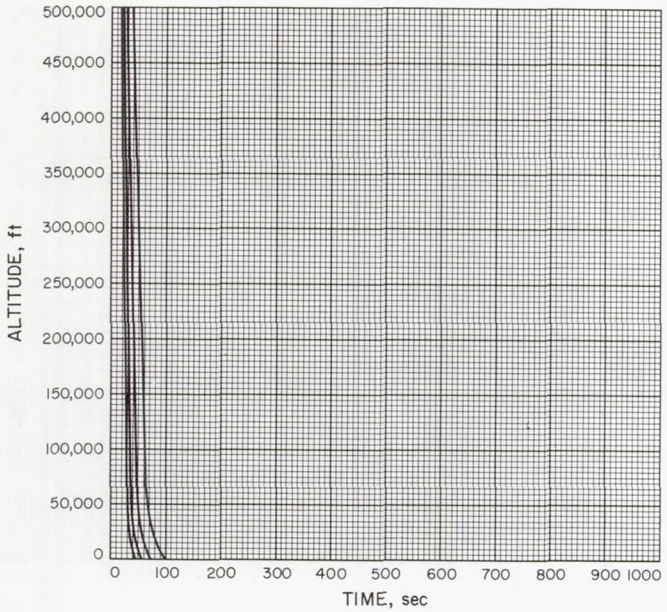

Fig. A-273

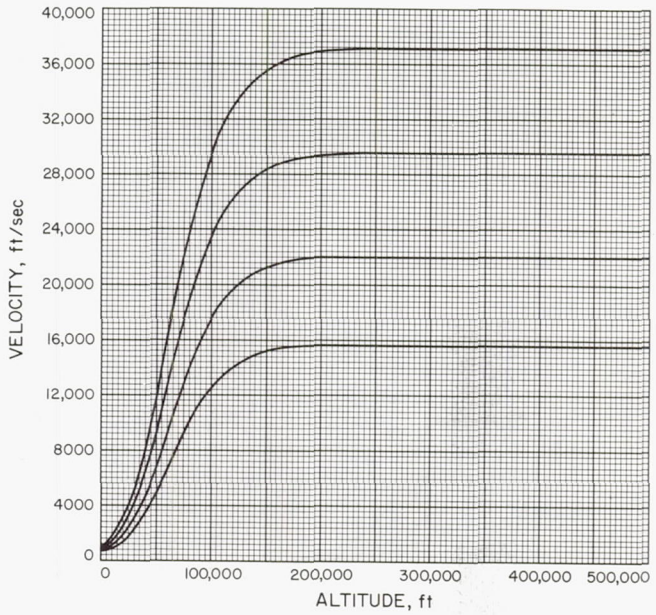

Fig. A-274

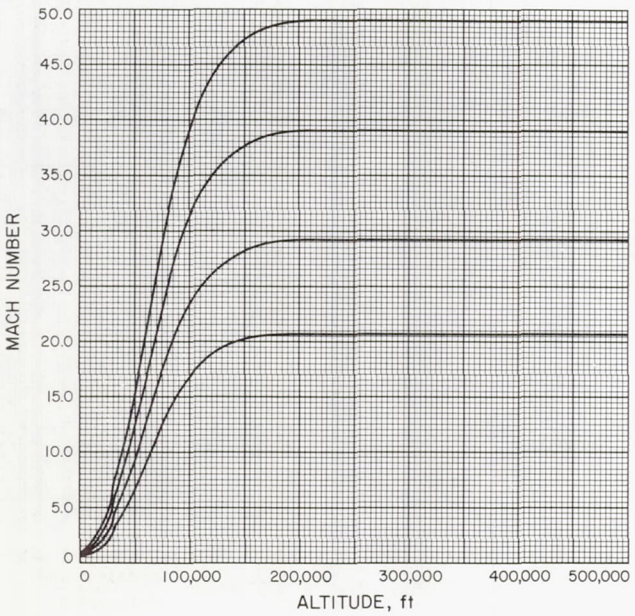

Fig. A-275

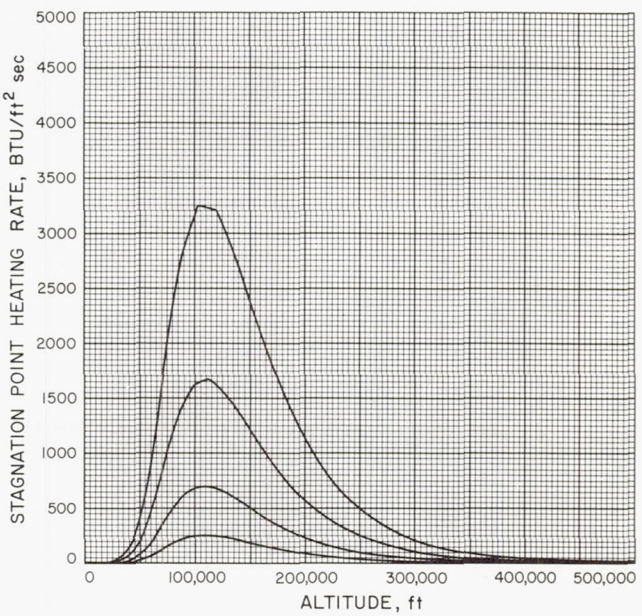

Fig. A-276

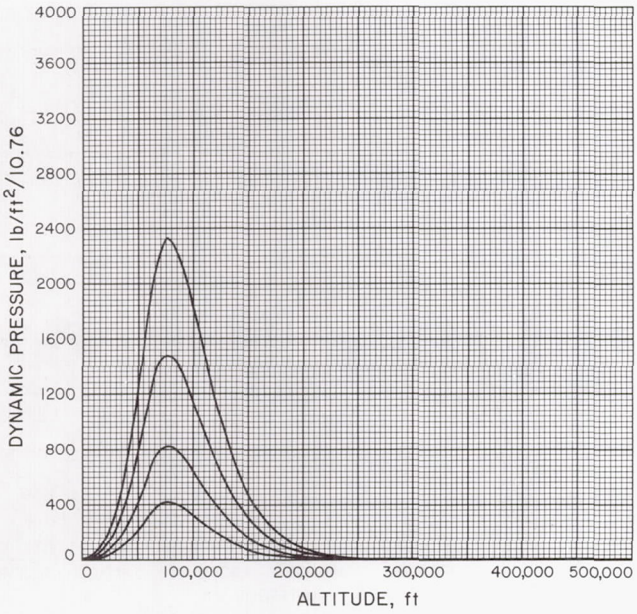

Fig. A-277

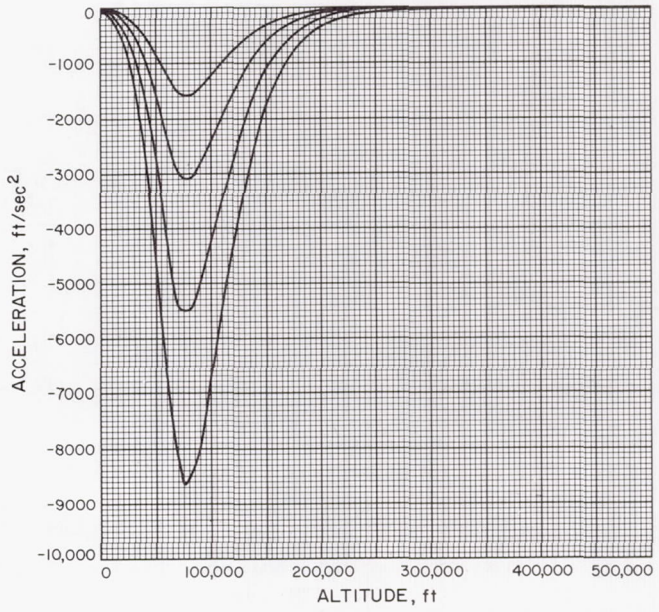

Fig. A-278

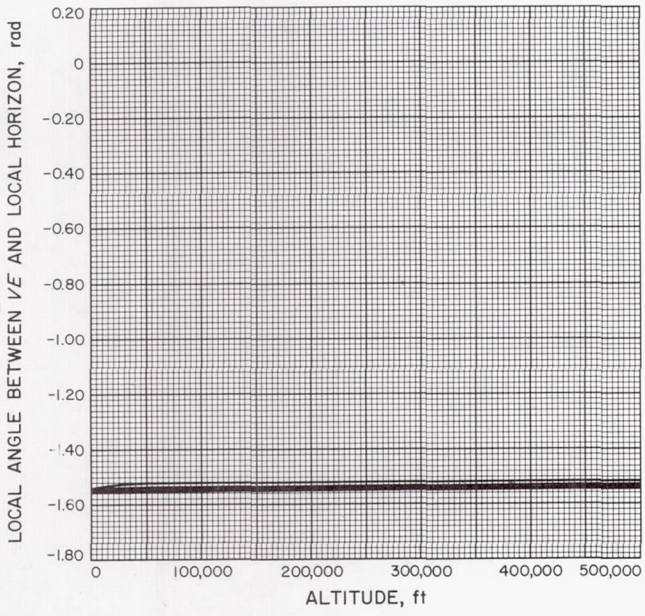

Fig. A-279

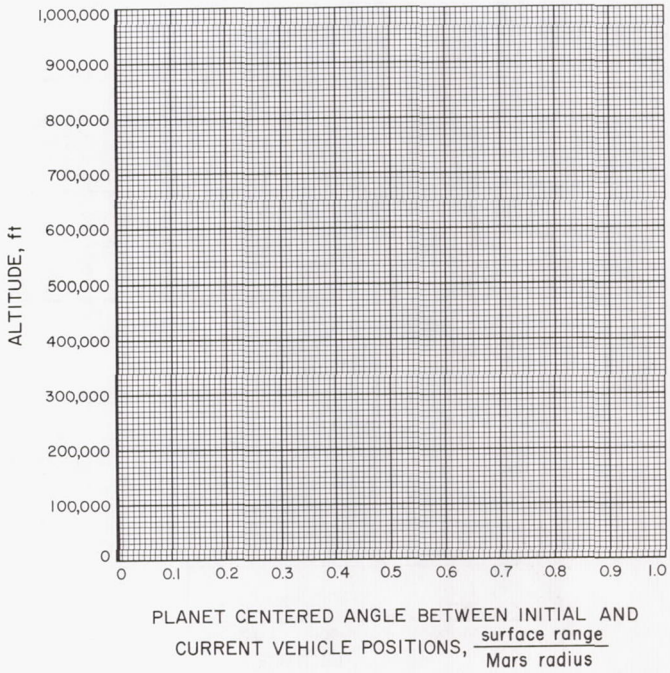

Fig. A-280

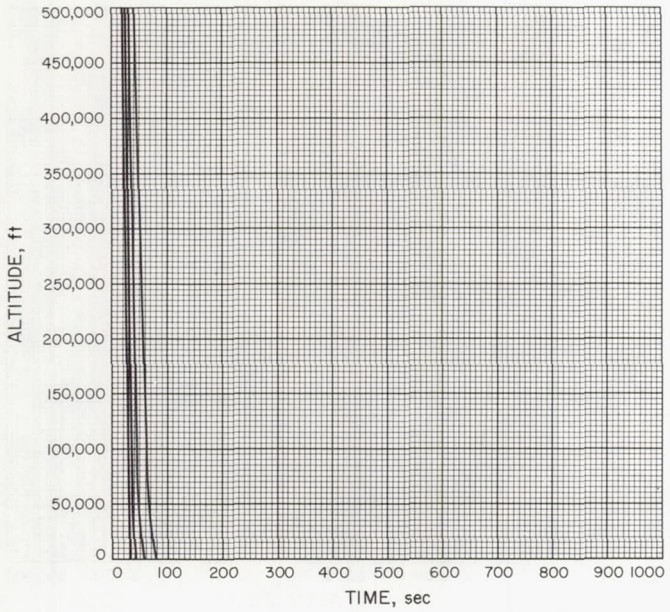

Fig. A-281

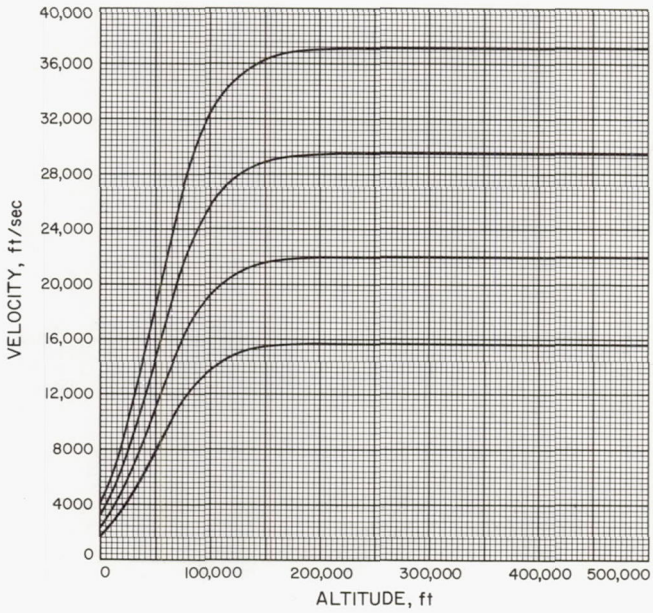

Fig. A-282

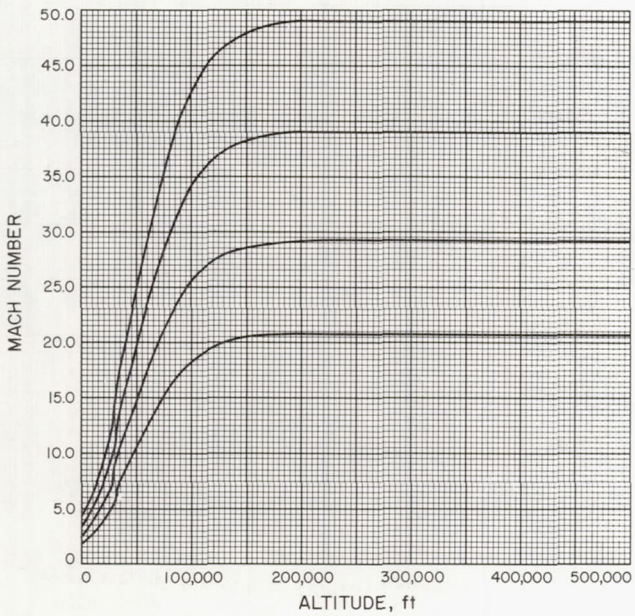

Fig. A-283

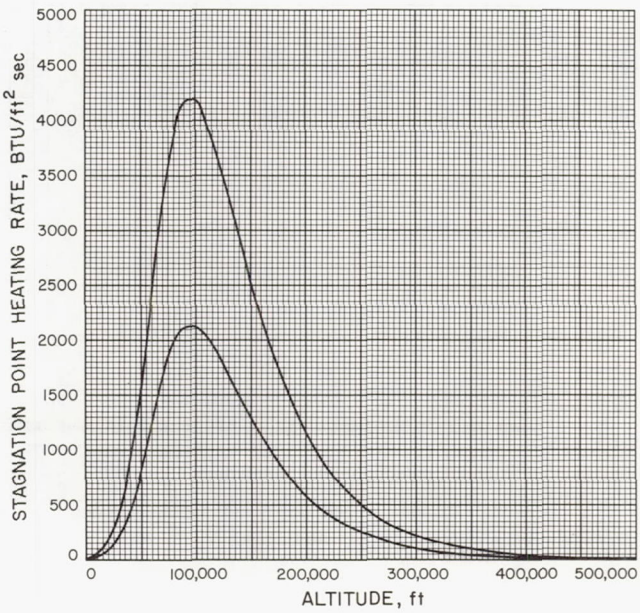

Fig. A-284

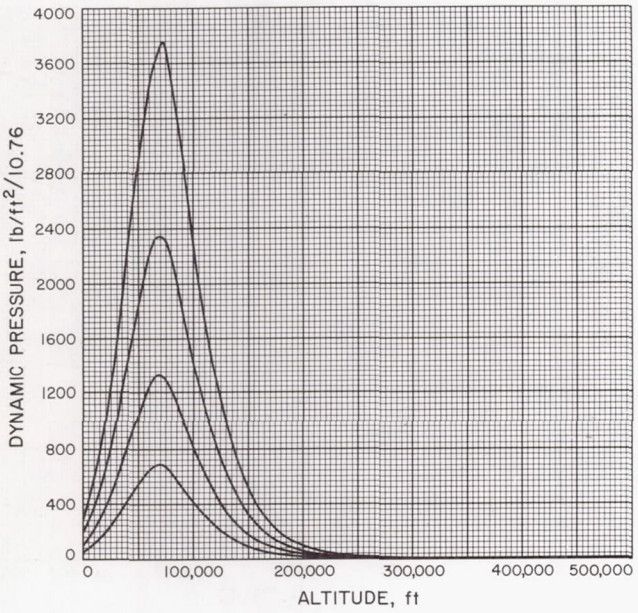

Fig. A-285

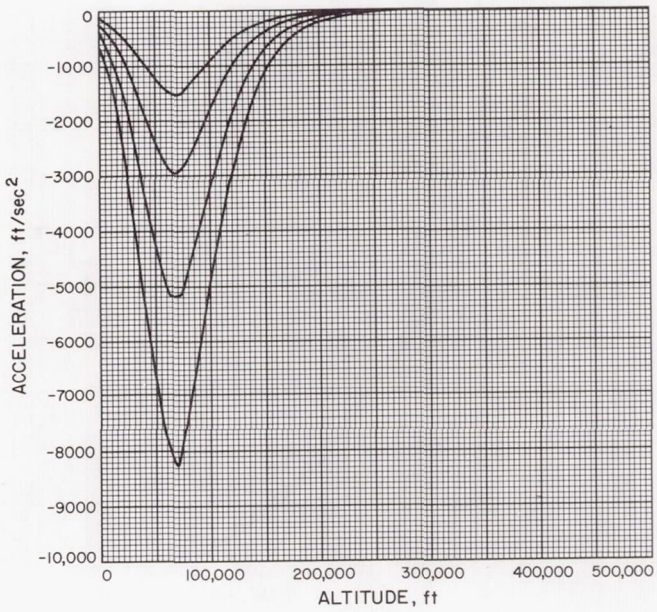

Fig. A-286

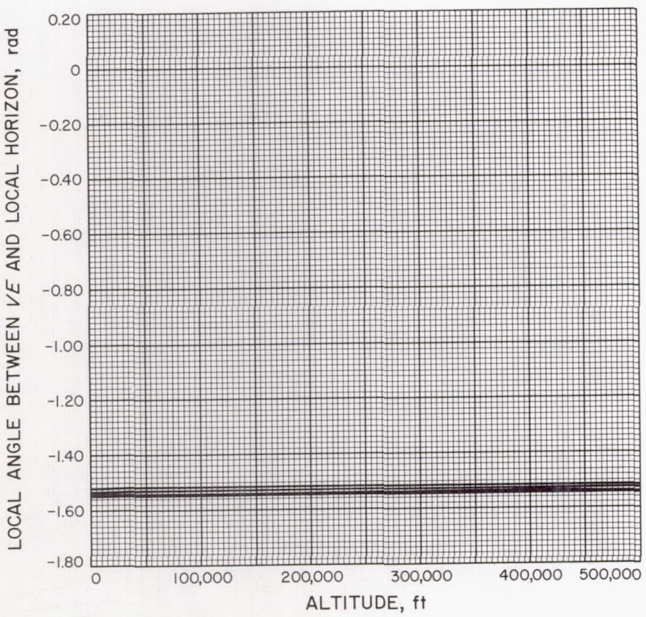

Fig. A-287

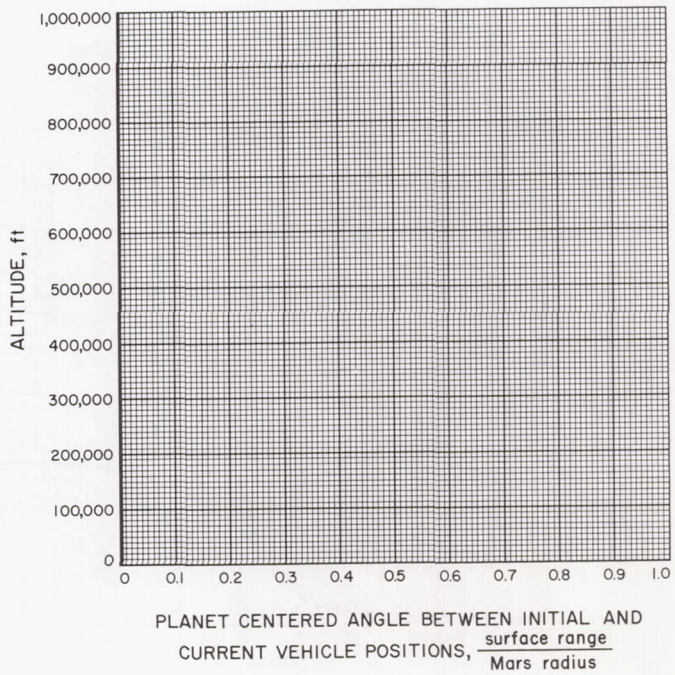

Fig. A-288

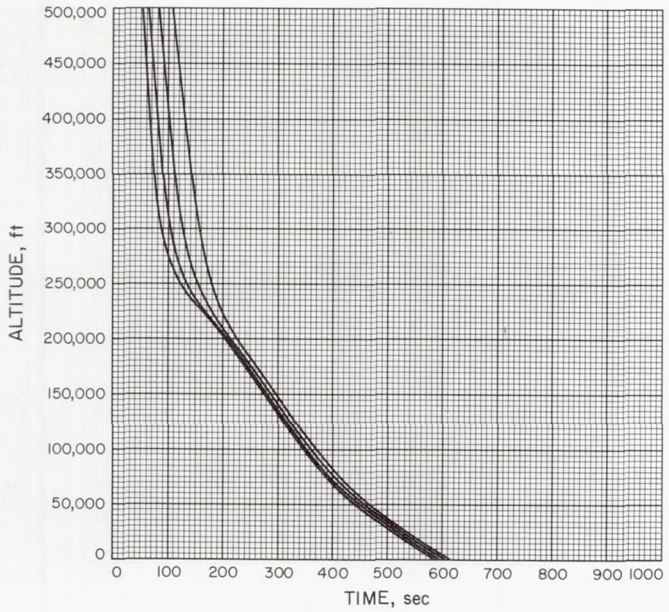

Fig. A-289

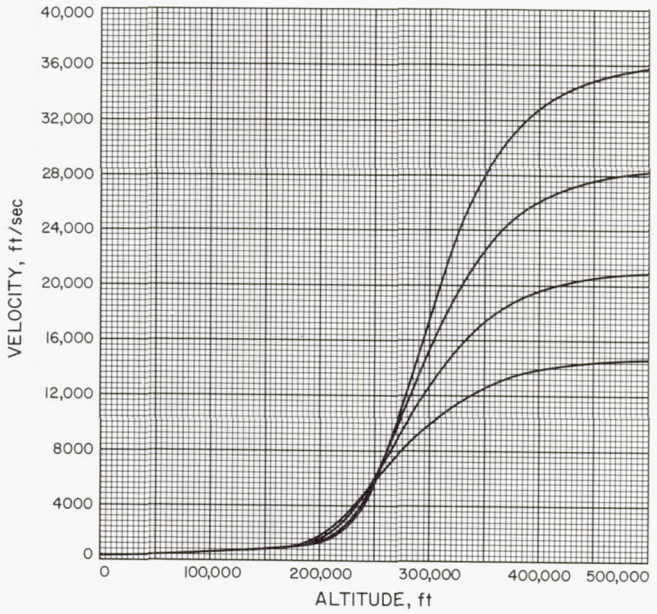

Fig. A-290

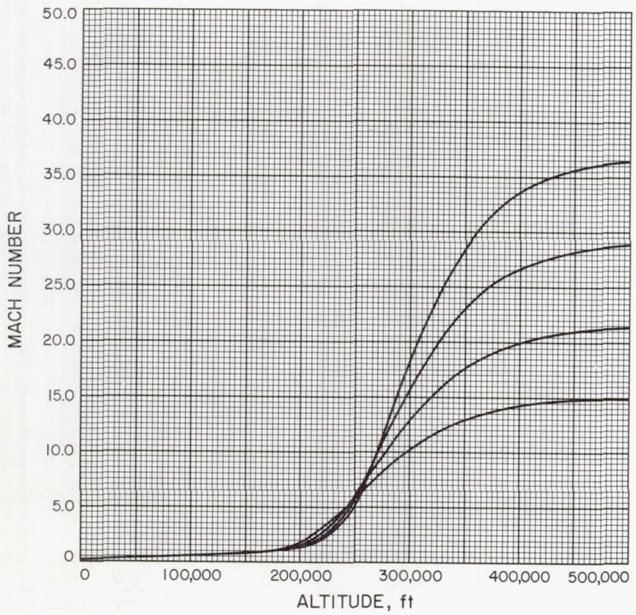

Fig. A-291

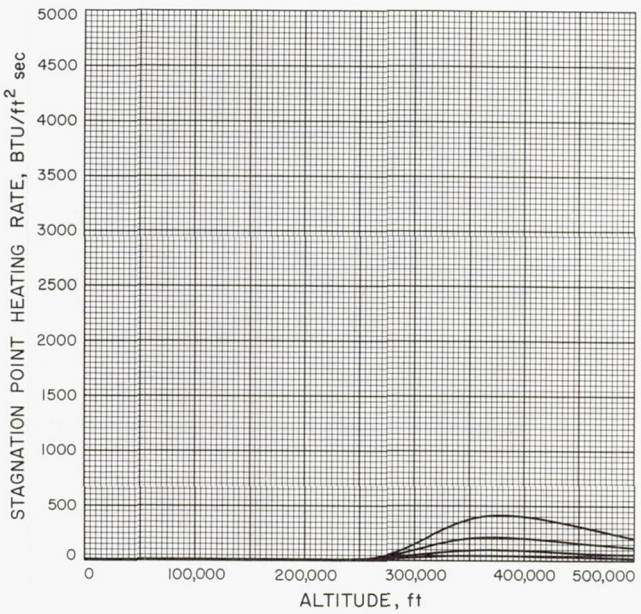

Fig. A-292

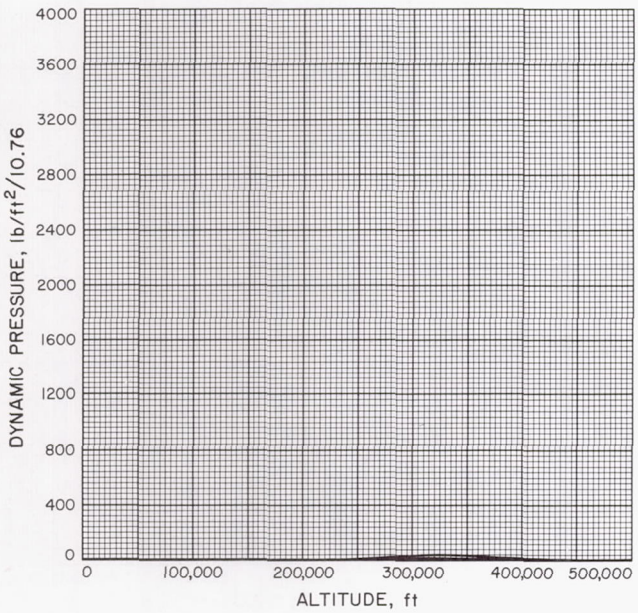

Fig. A-293

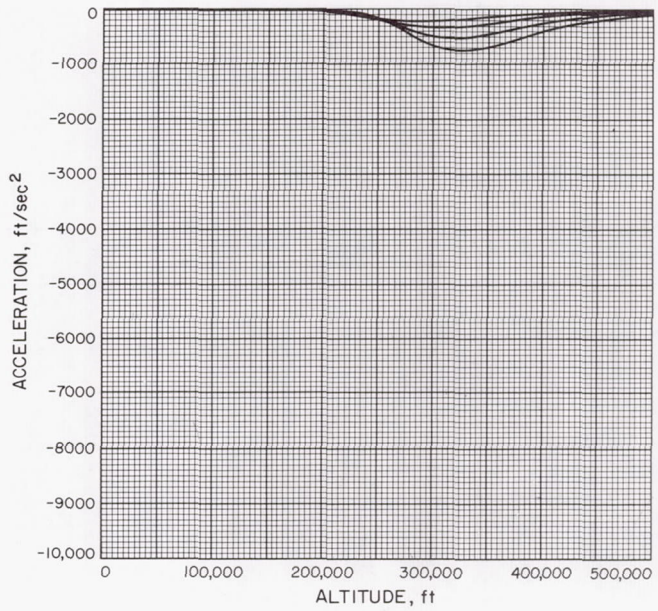

Fig. A-294

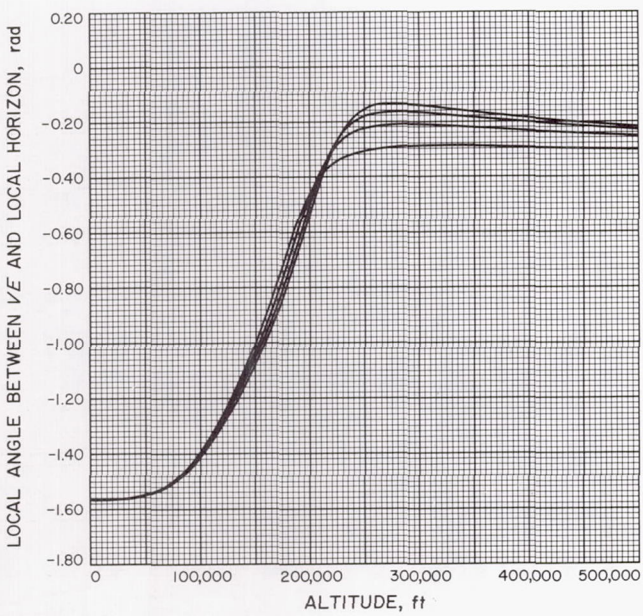

Fig. A-295

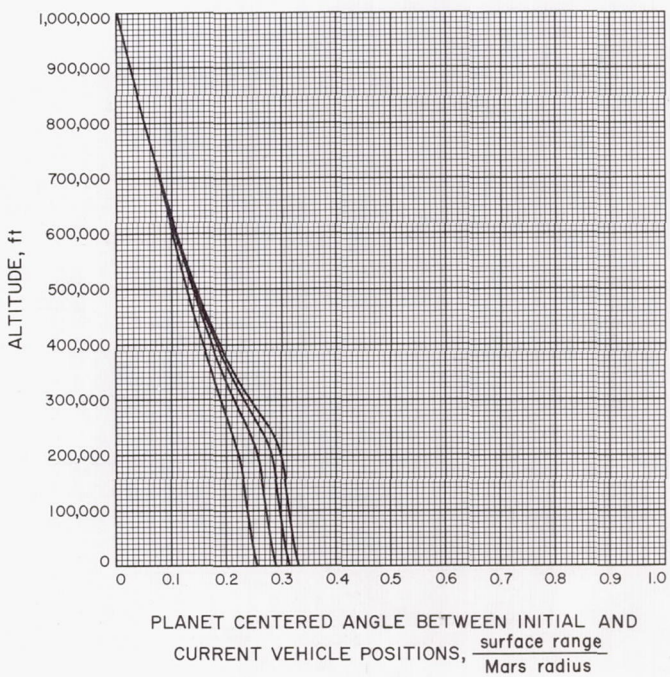

Fig. A-296

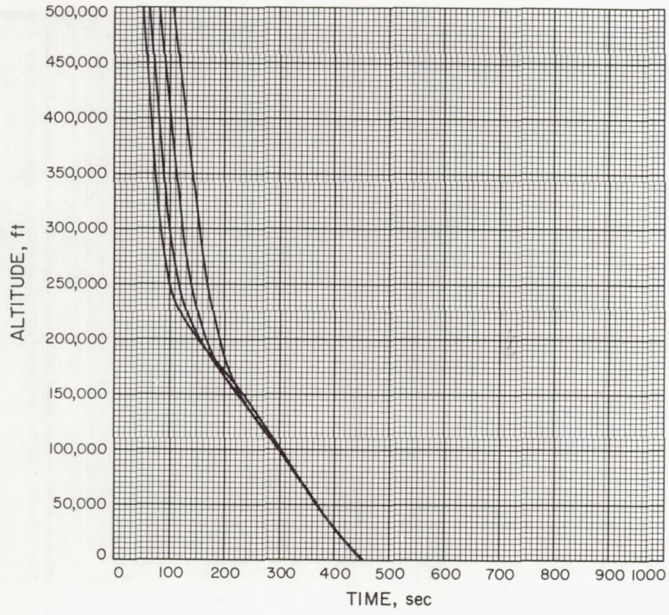

Fig. A-297

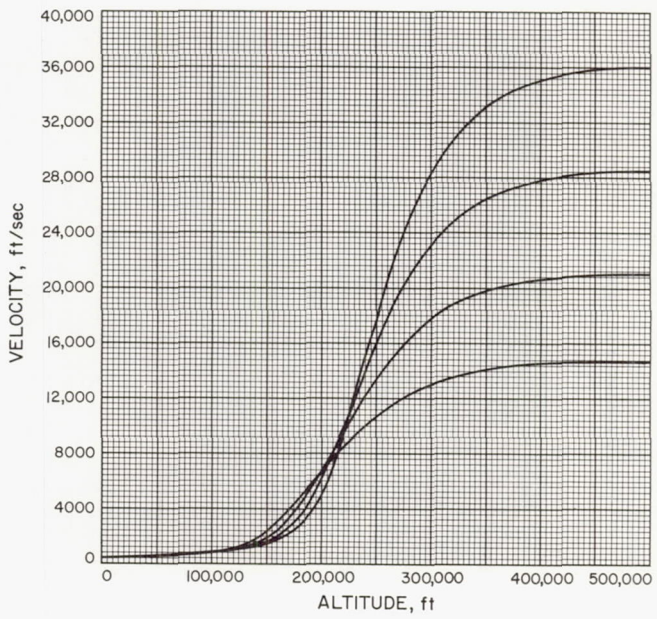

Fig. A-298

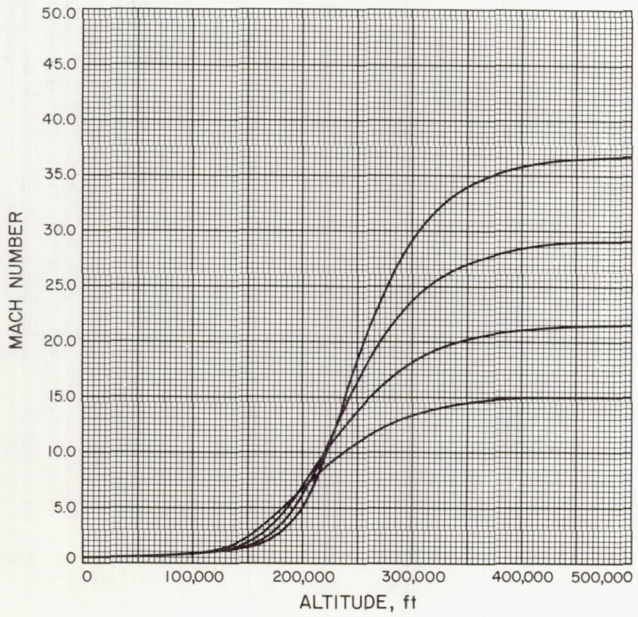

Fig. A-299

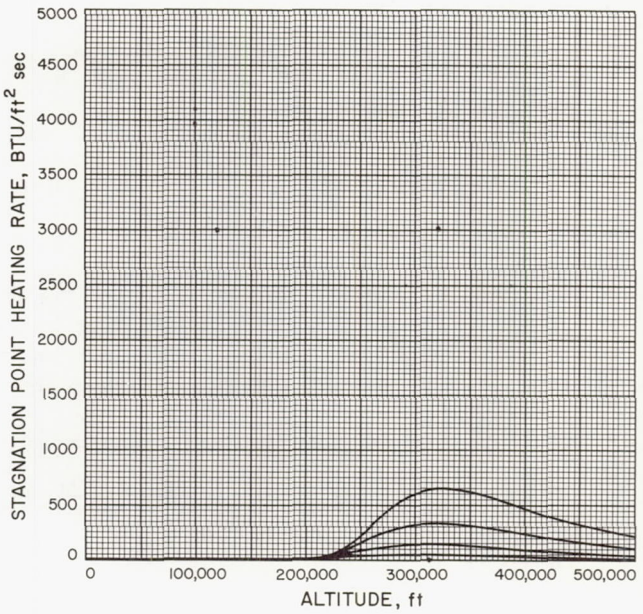

Fig. A-300

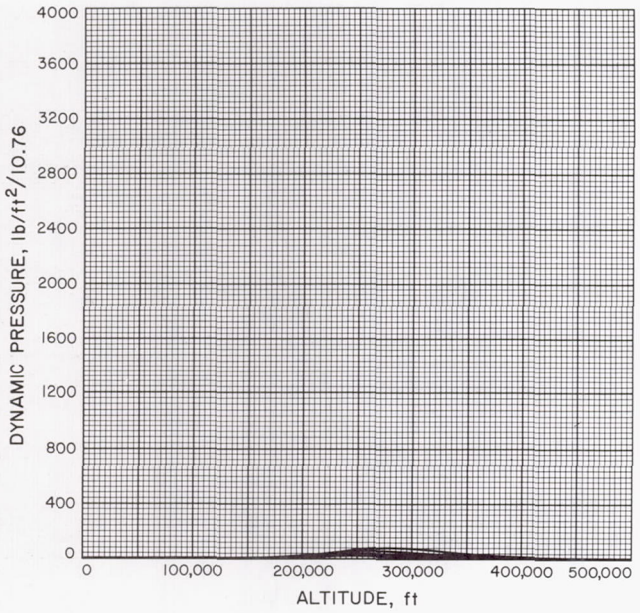

Fig. A-301

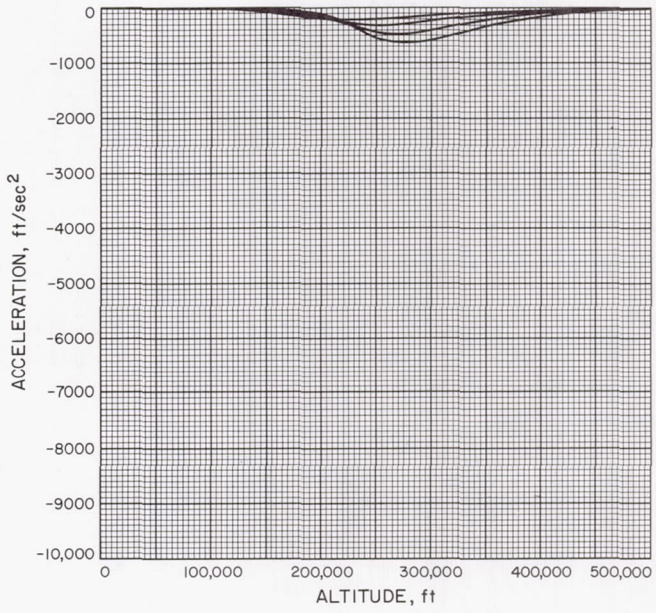

Fig. A-302

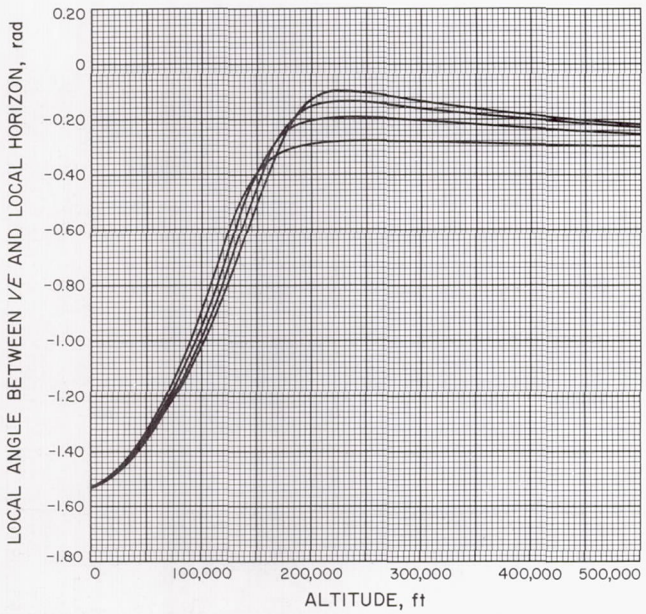

Fig. A-303

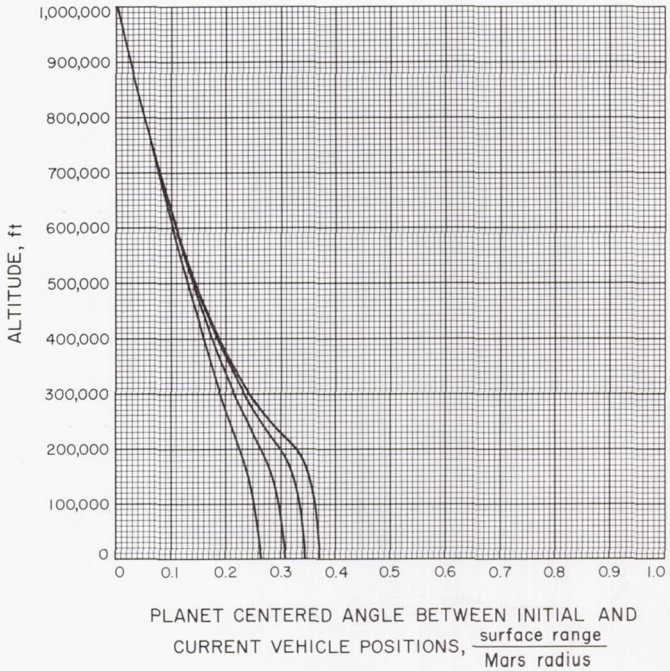

Fig. A-304

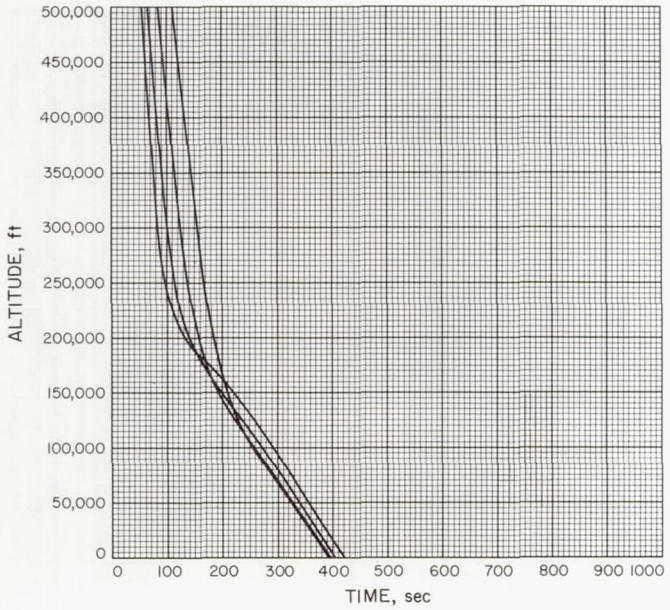

Fig. A-305

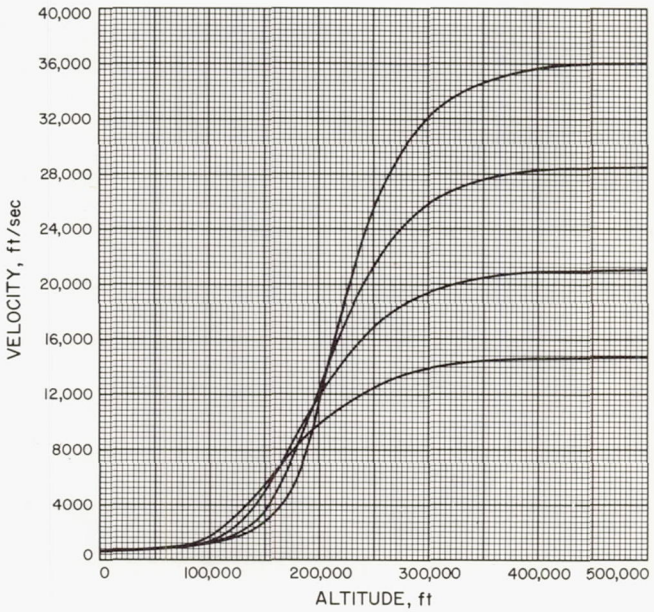

Fig. A-306

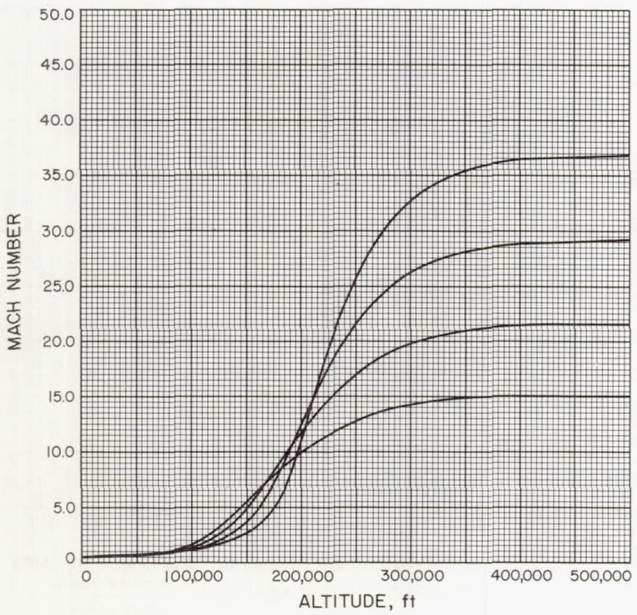

Fig. A-307

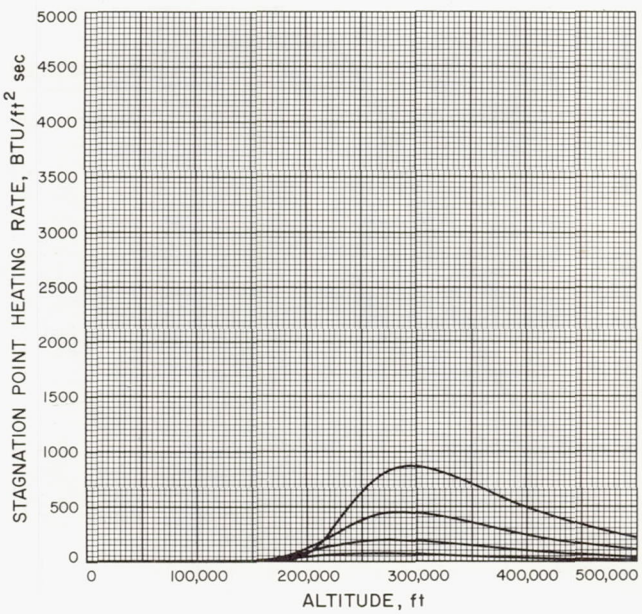

Fig. A-308

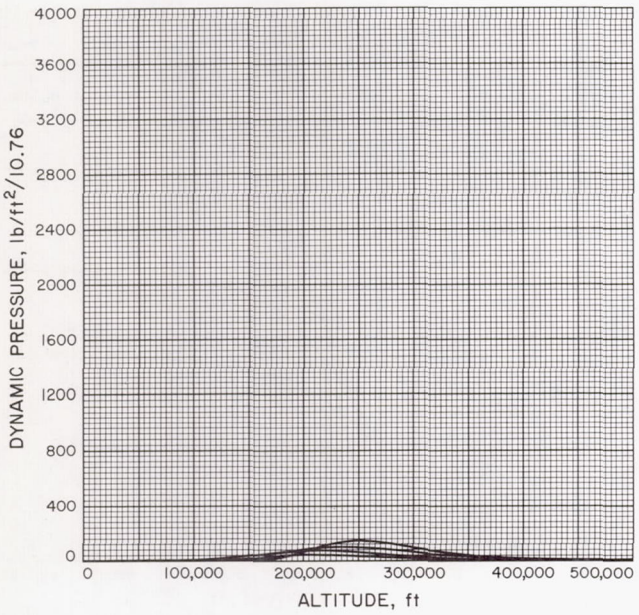

Fig. A-309

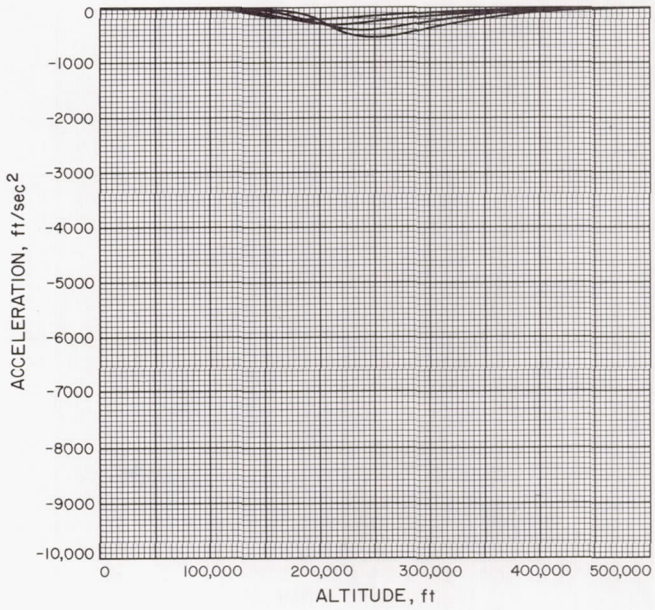

Fig. A-310

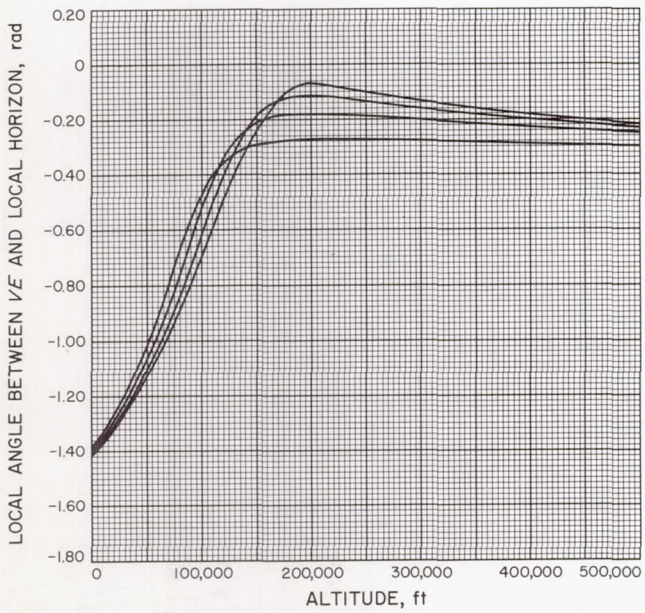

Fig. A-311

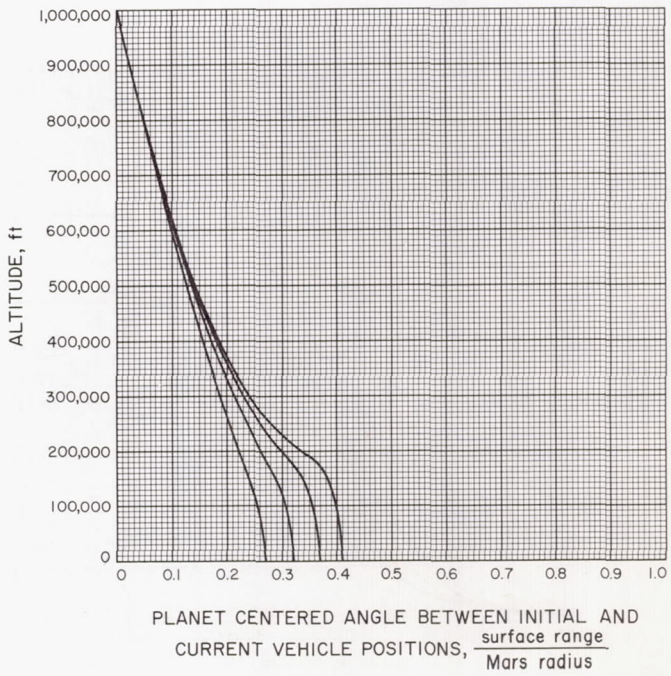

Fig. A-312

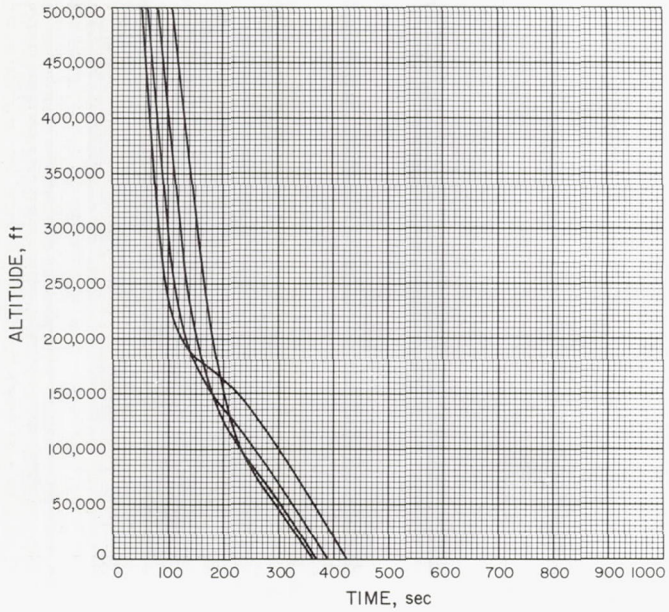

Fig. A-313

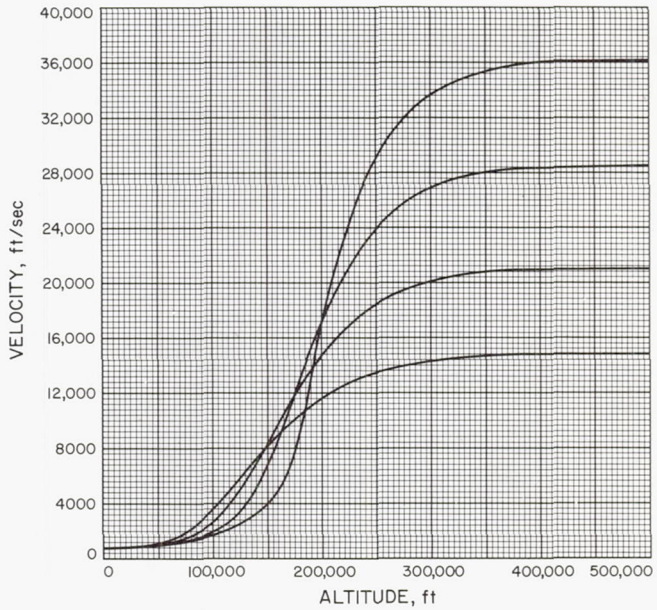

Fig. A-314

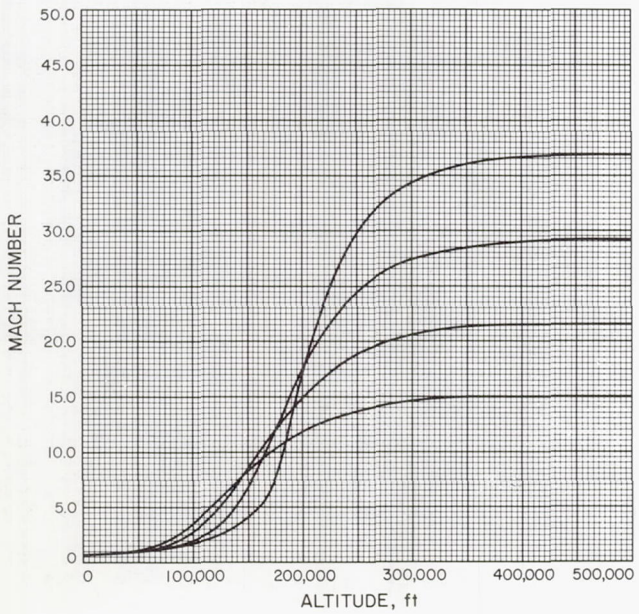

Fig. A-315

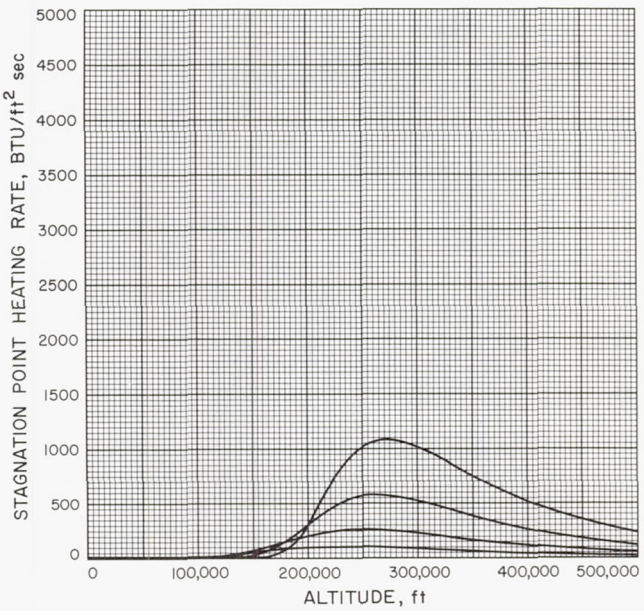

Fig. A-316

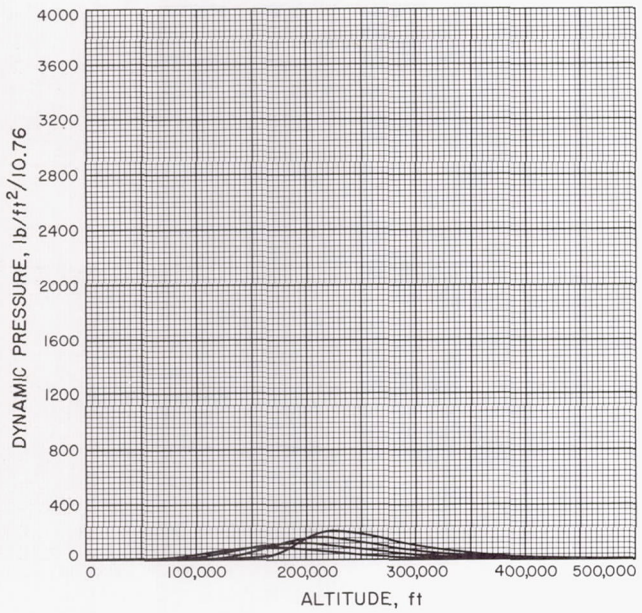

Fig. A-317

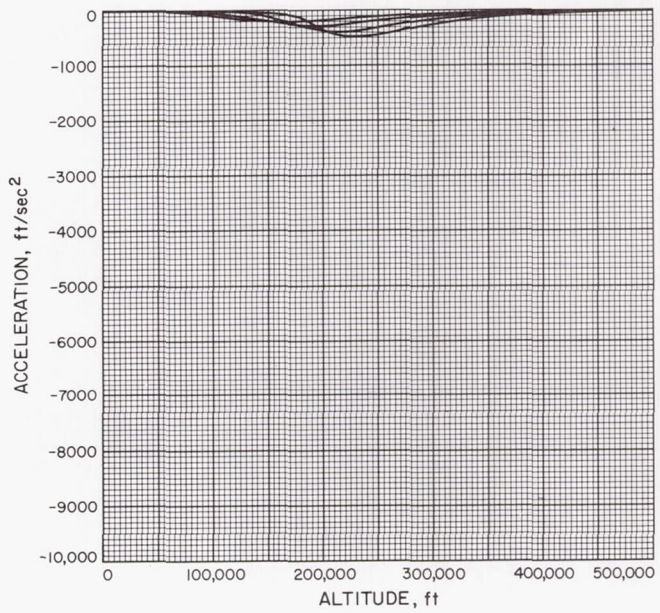

Fig. A-318

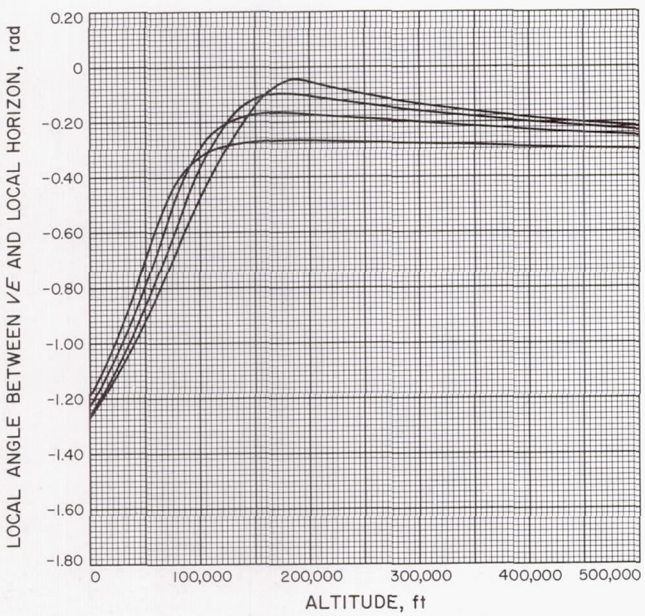

Fig. A-319

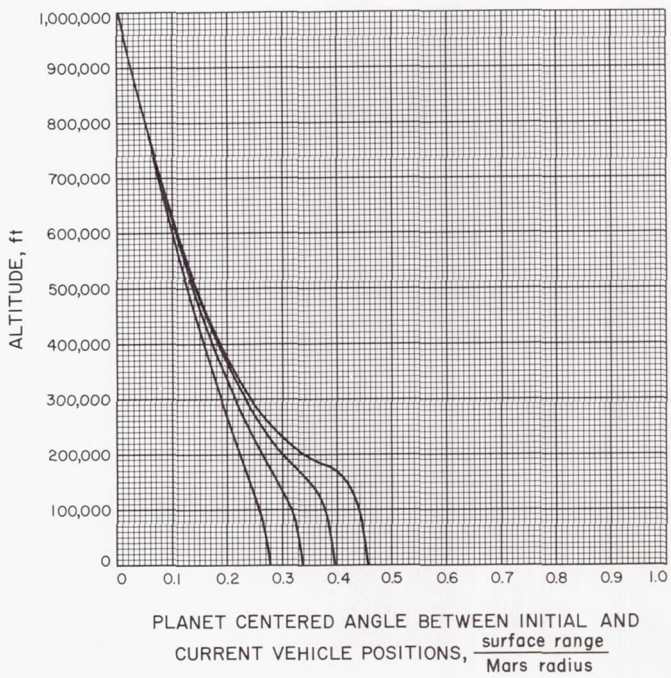

Fig. A-320

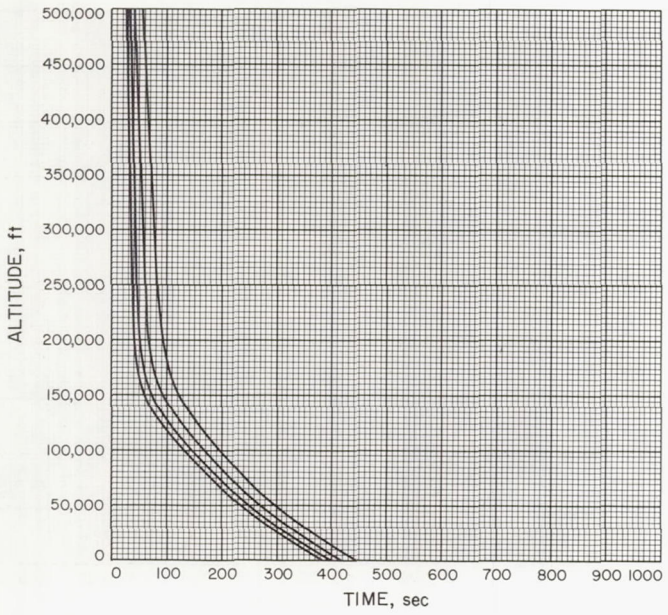

Fig. A-321

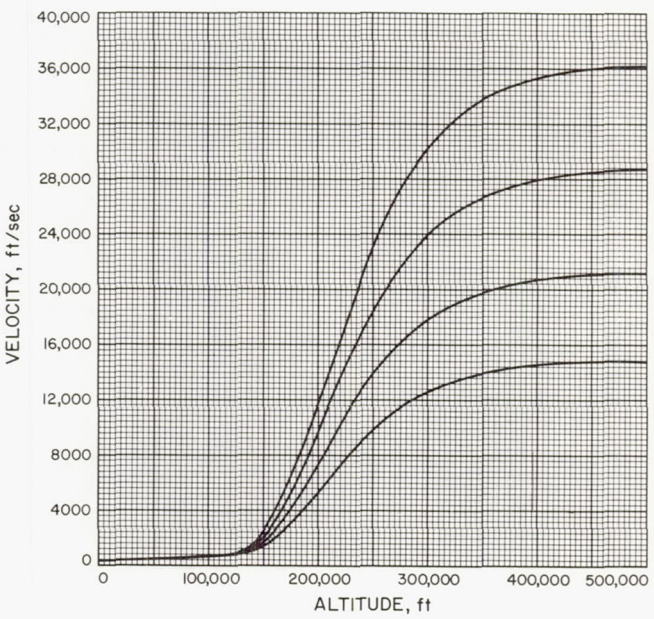

Fig. A-322

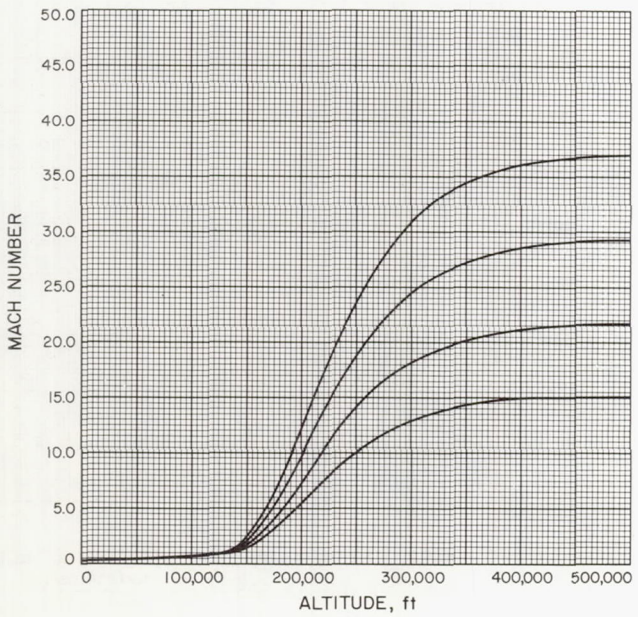

Fig. A-323

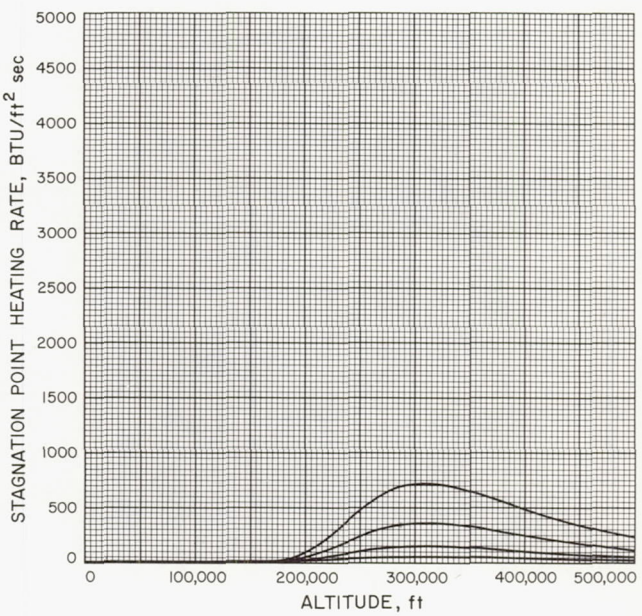

Fig. A-324

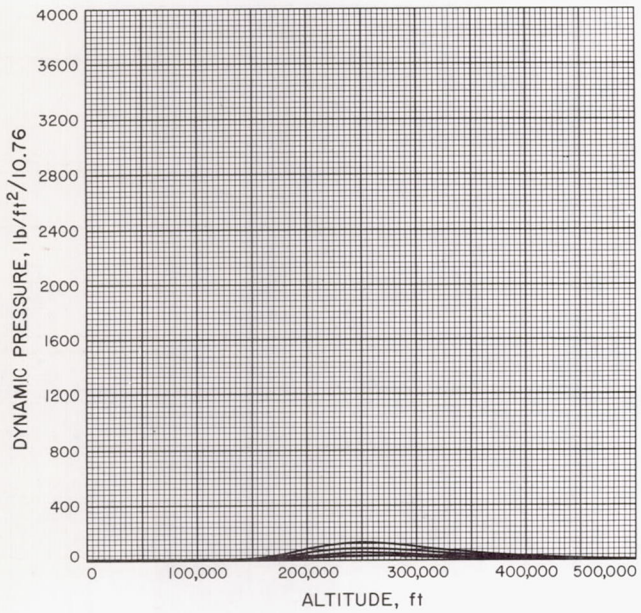

Fig. A-325

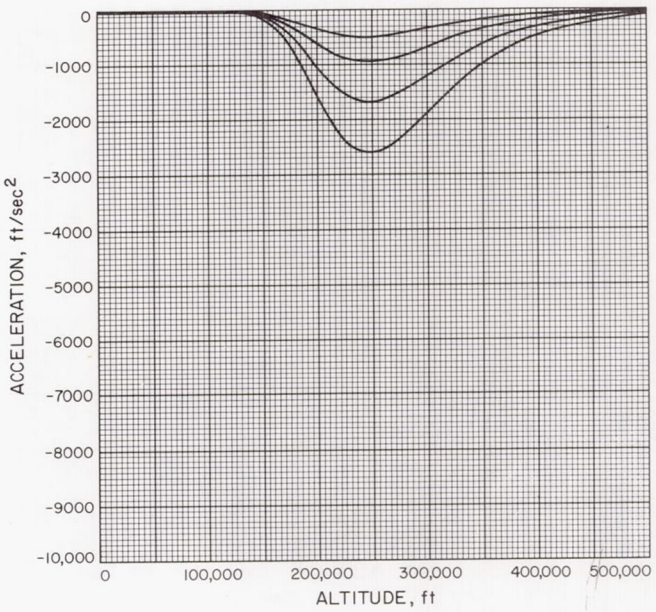

Fig. A-326

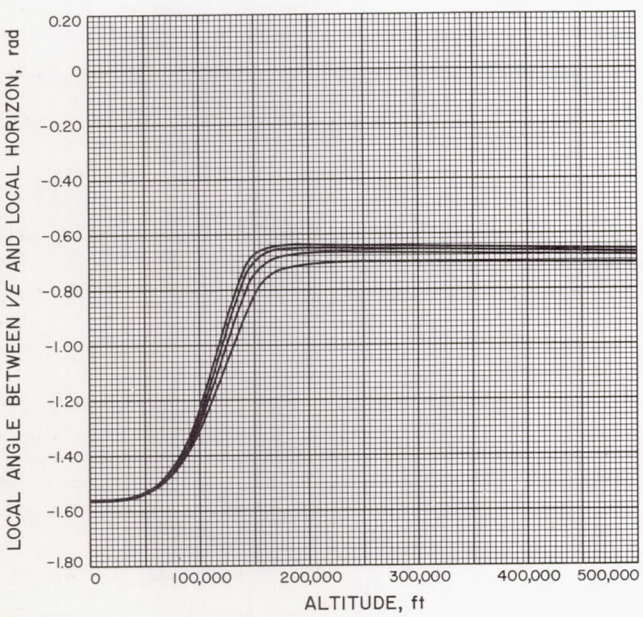

Fig. A-327

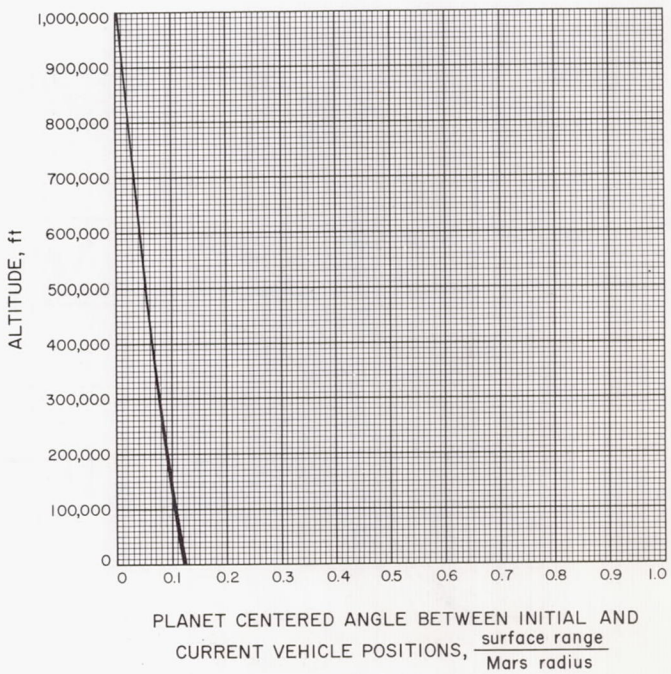

Fig. A-328

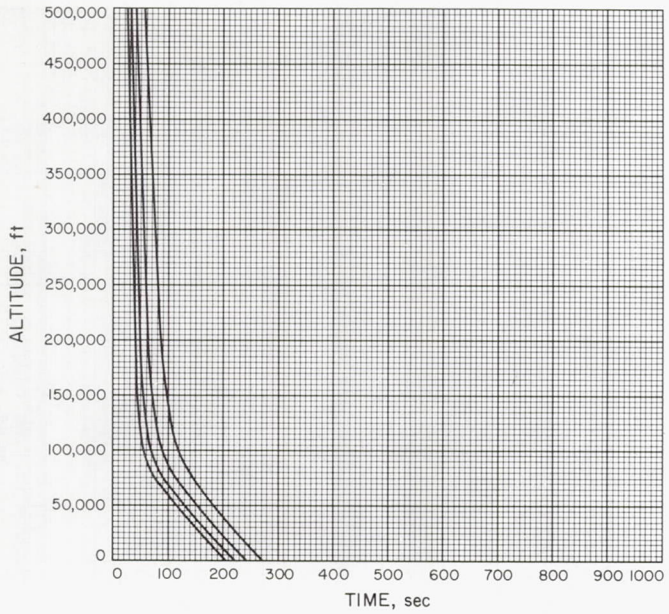

Fig. A-329

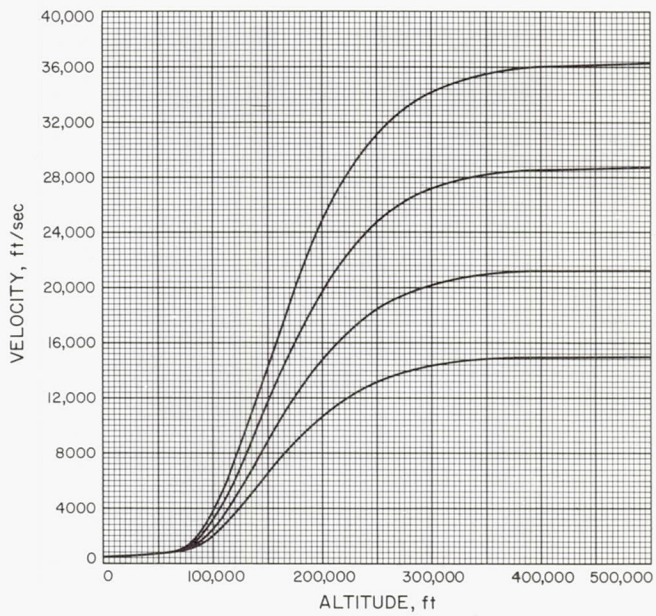

Fig. A-330

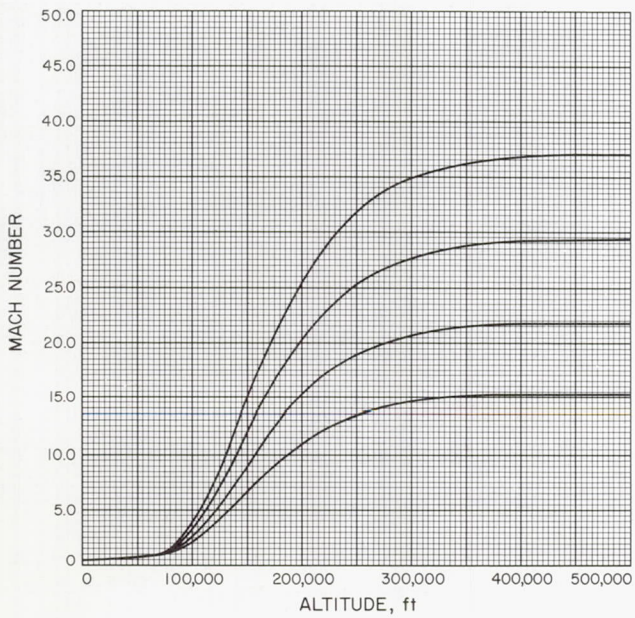

Fig. A-331

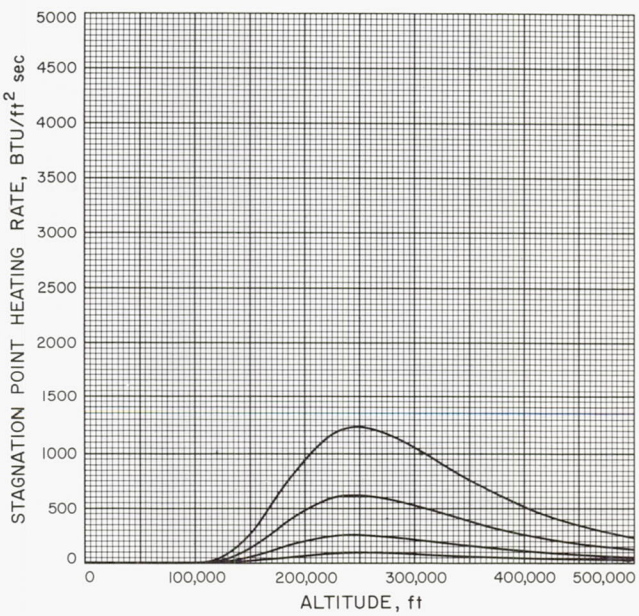

Fig. A-332

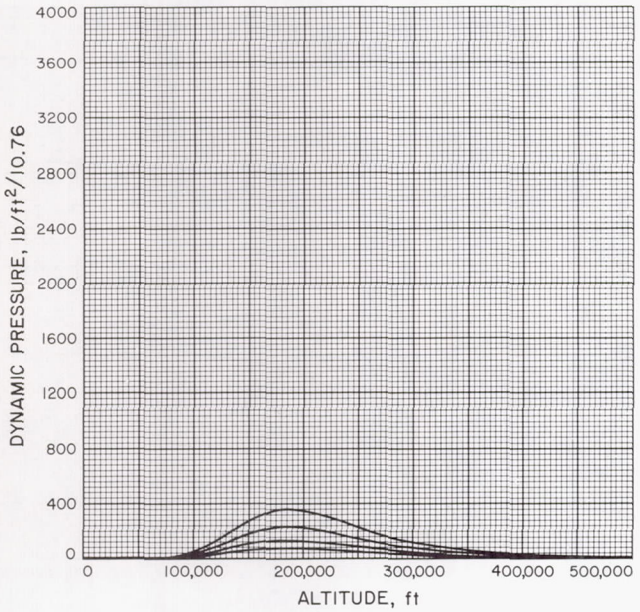

Fig. A-333

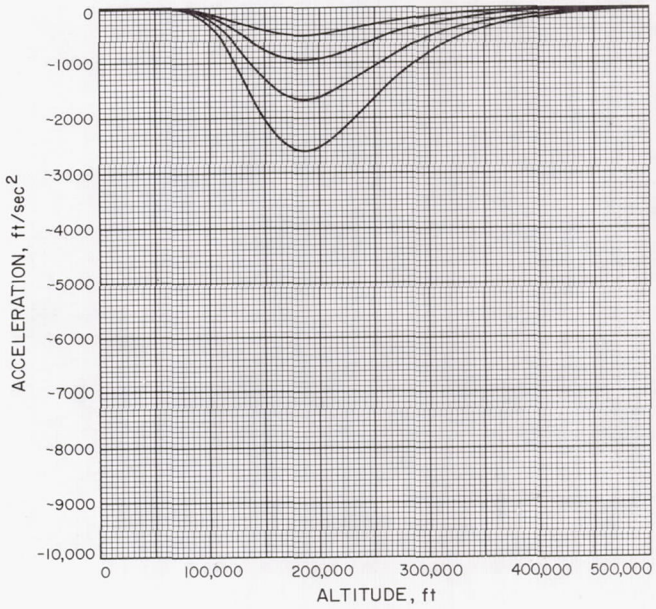

Fig. A-334

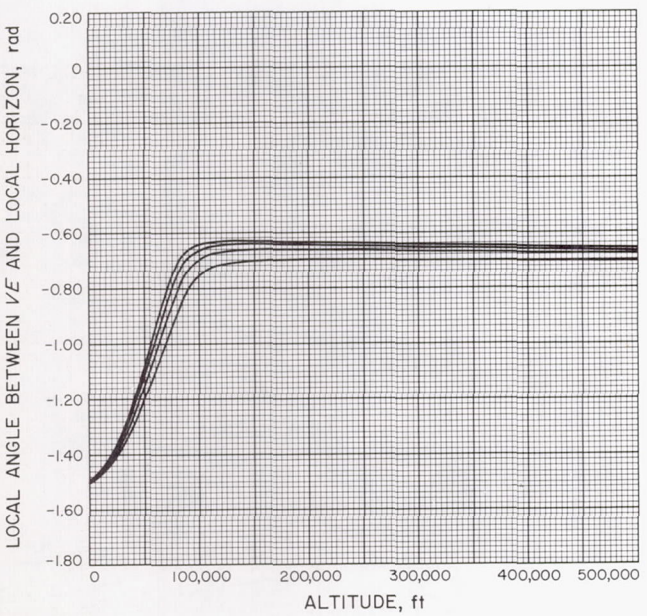

Fig. A-335

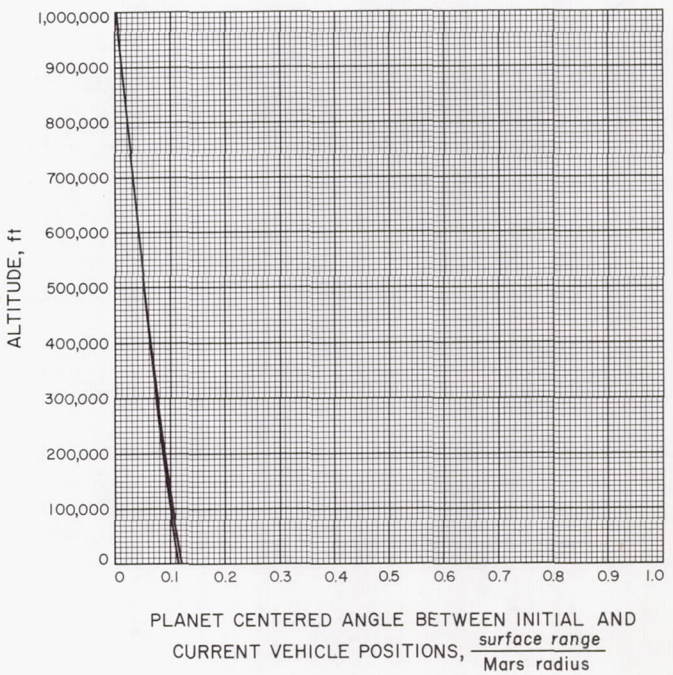

Fig. A-336

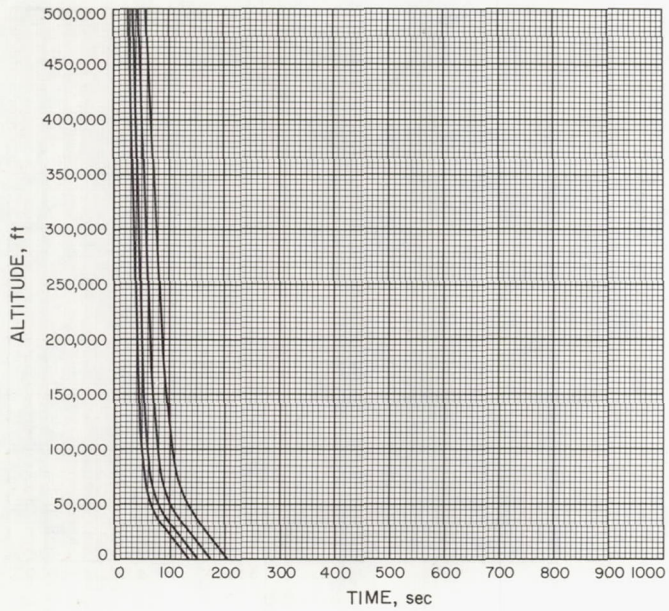

Fig. A-337

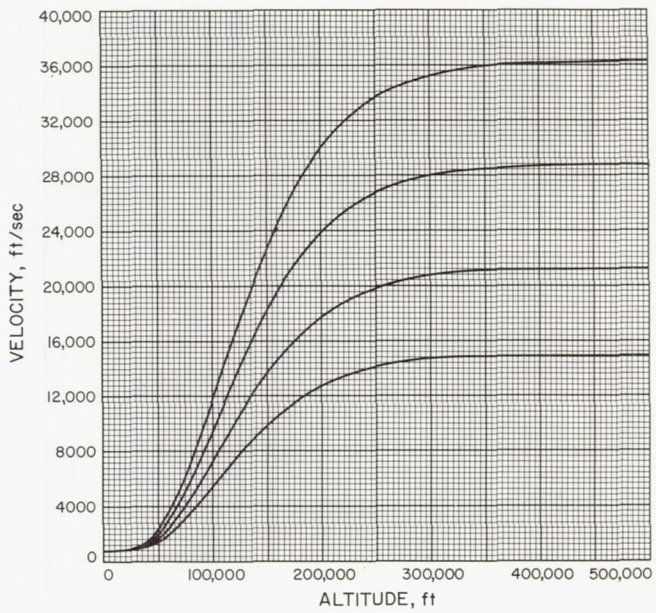

Fig. A-338

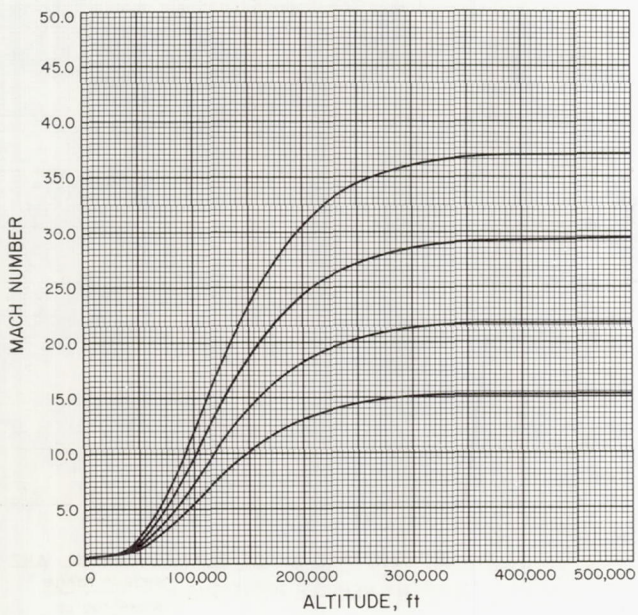

Fig. A-339

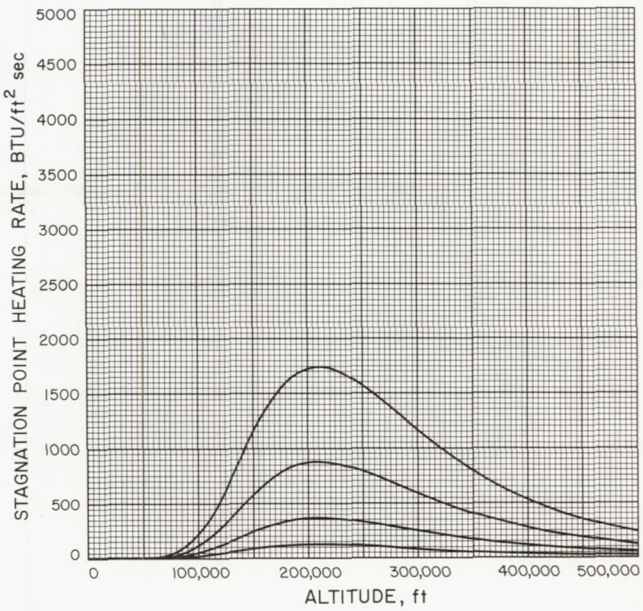

Fig. A-340

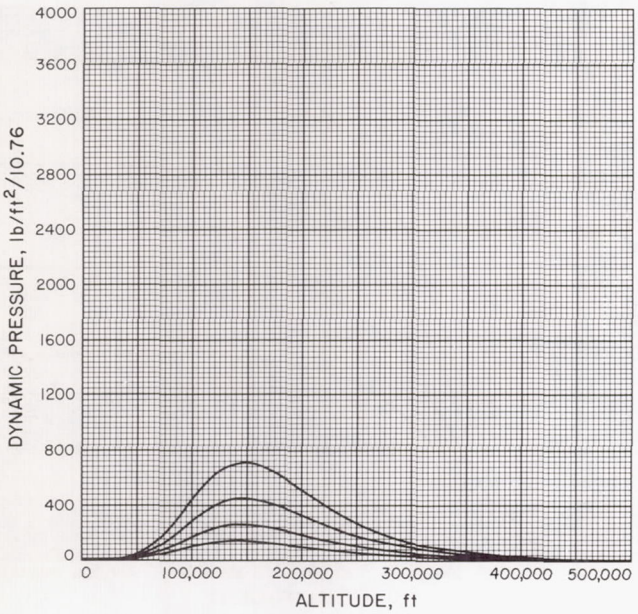

Fig. A-341

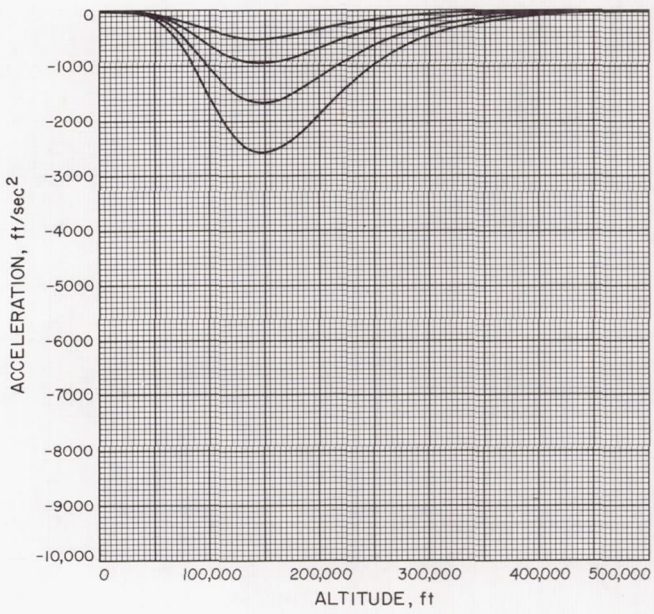

Fig. A-342

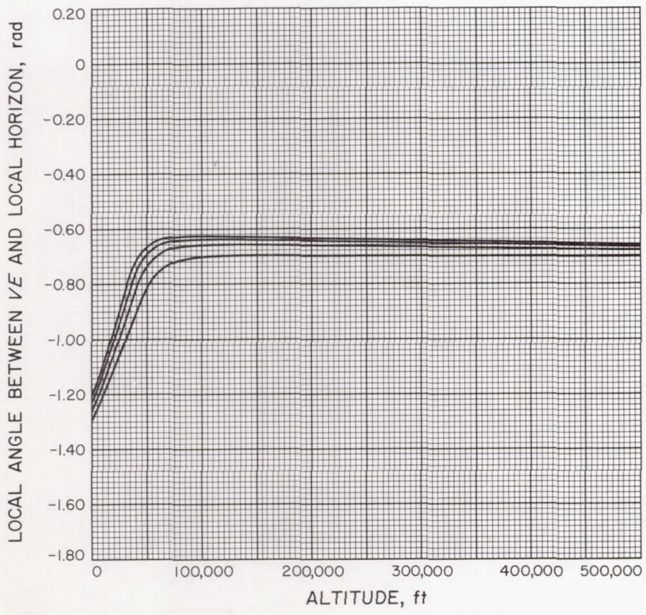

Fig. A-343

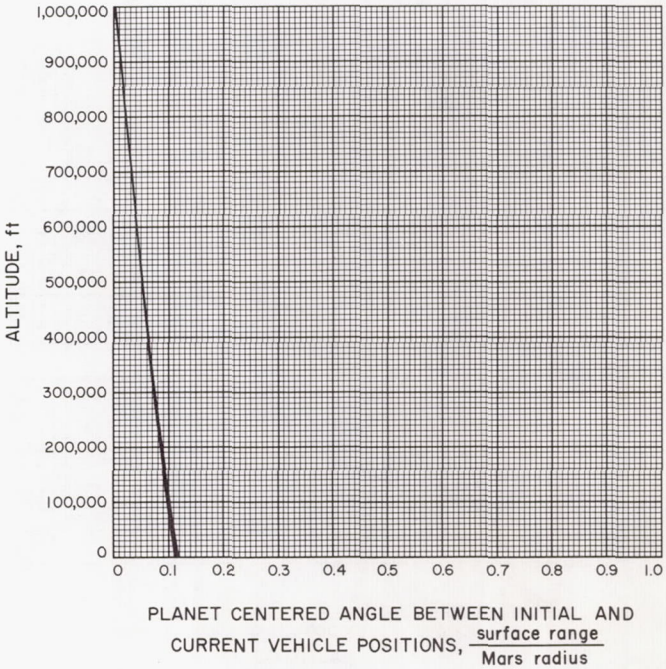

Fig. A-344

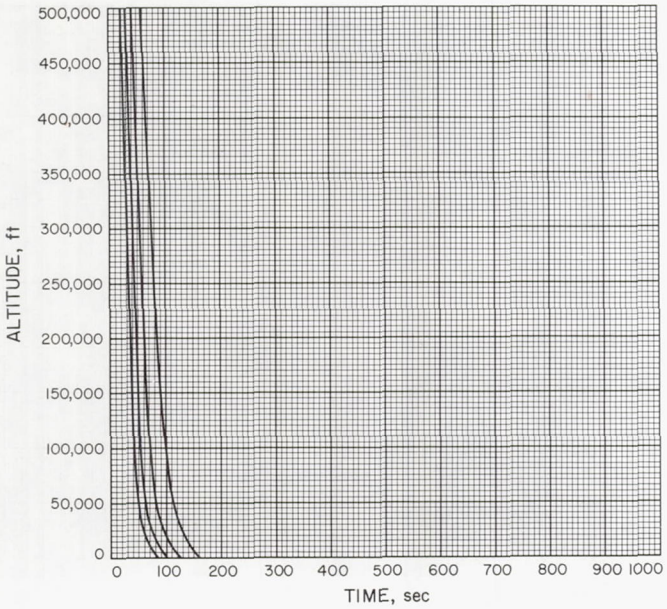

Fig. A-345

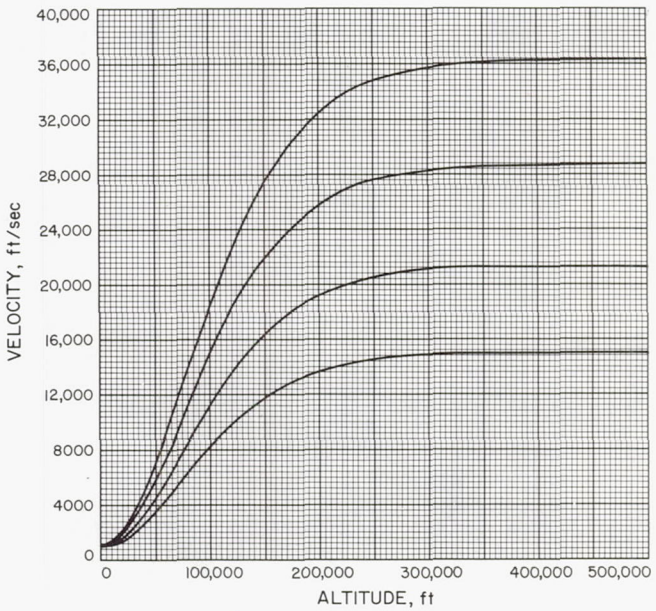

Fig. A-346

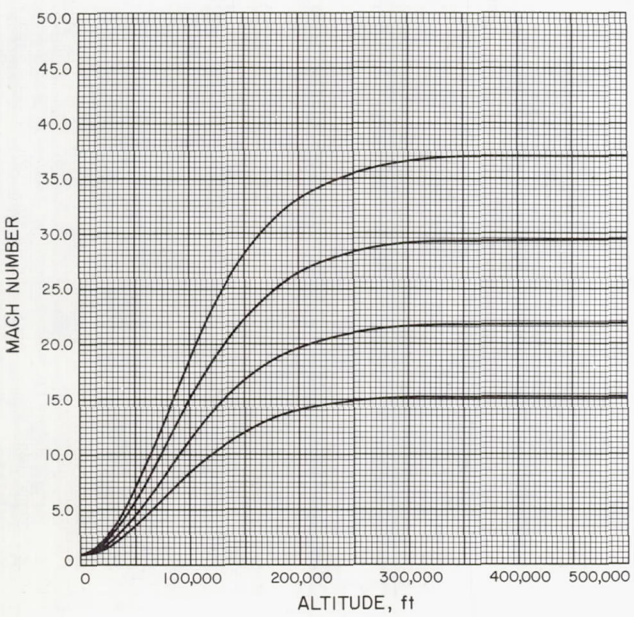

Fig. A-347

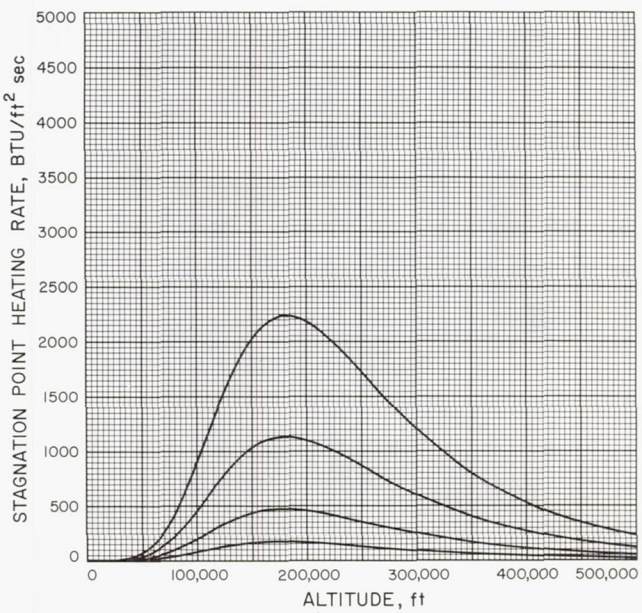

Fig. A-348

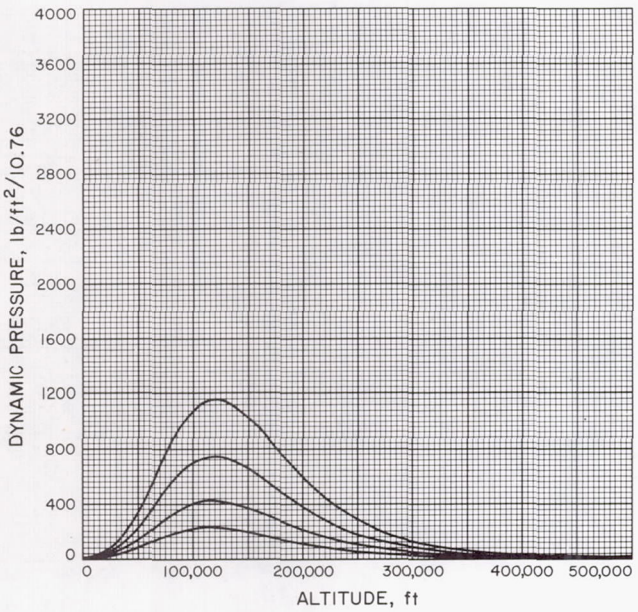

Fig. A-349

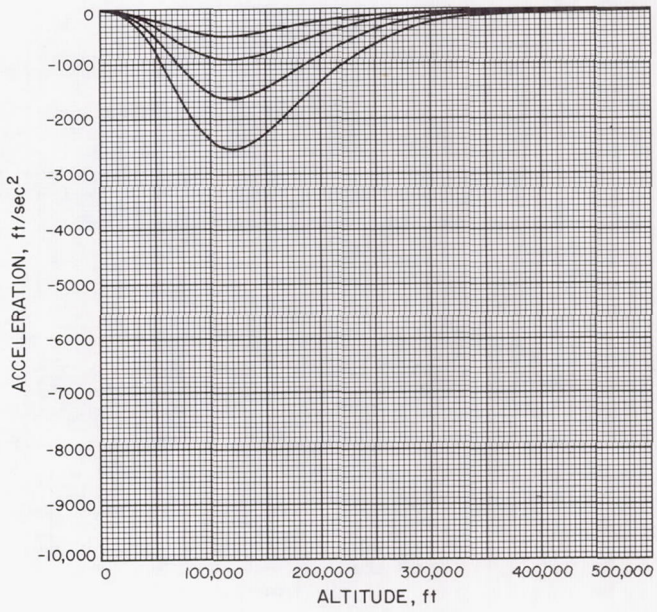

Fig. A-350

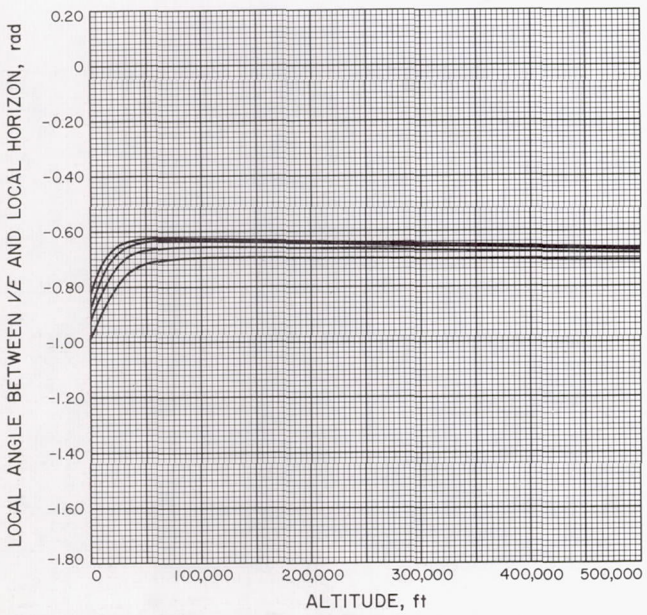

Fig. A-351

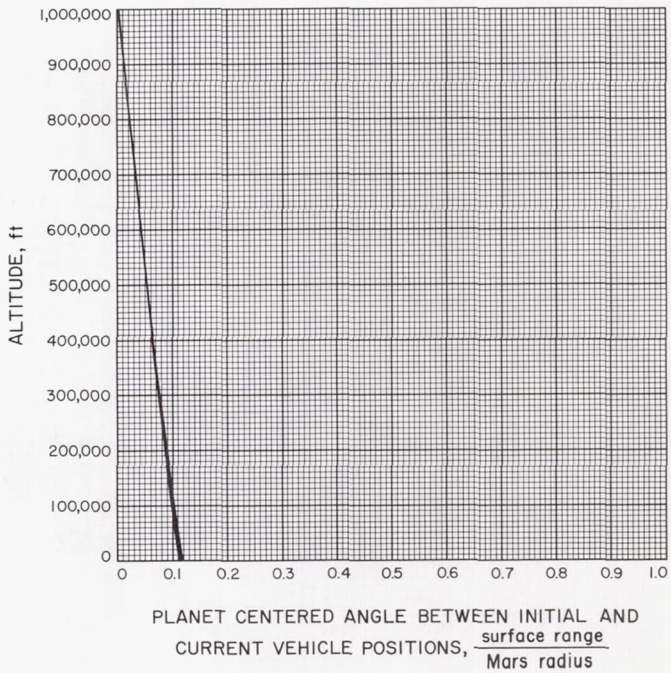

Fig. A-352

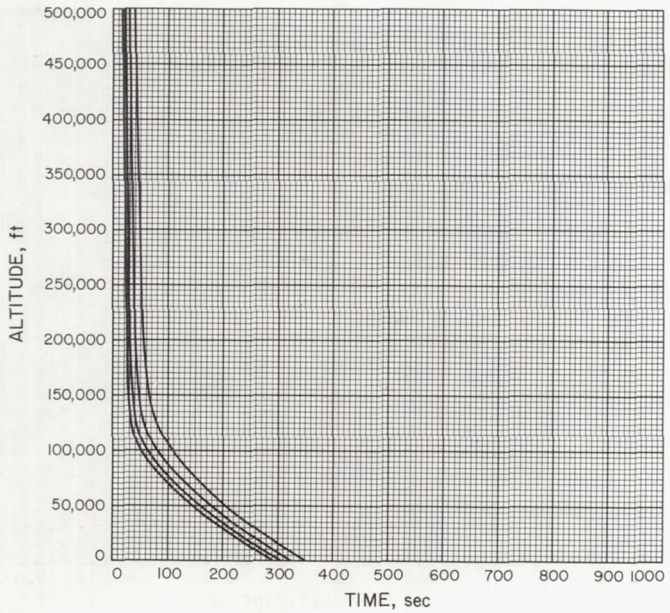

Fig. A-353

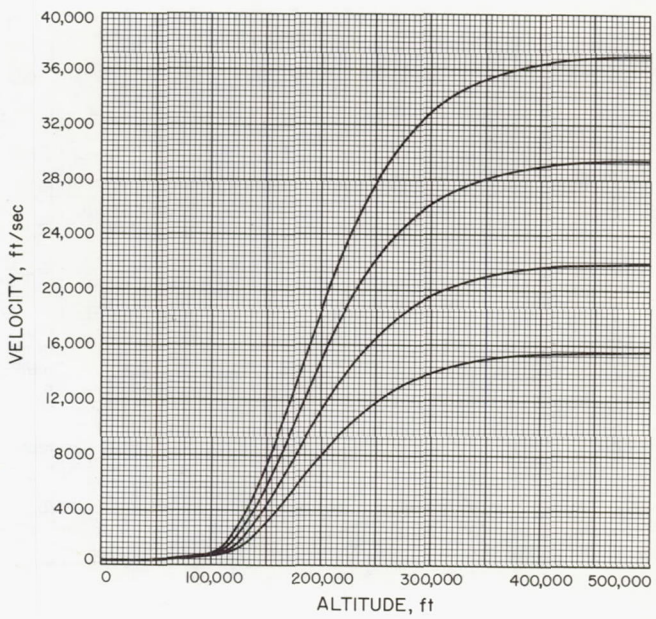

Fig. A-354

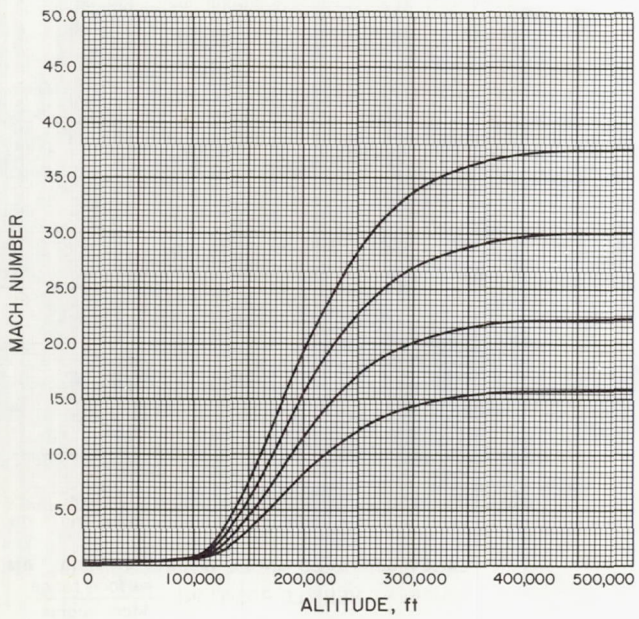

Fig. A-355

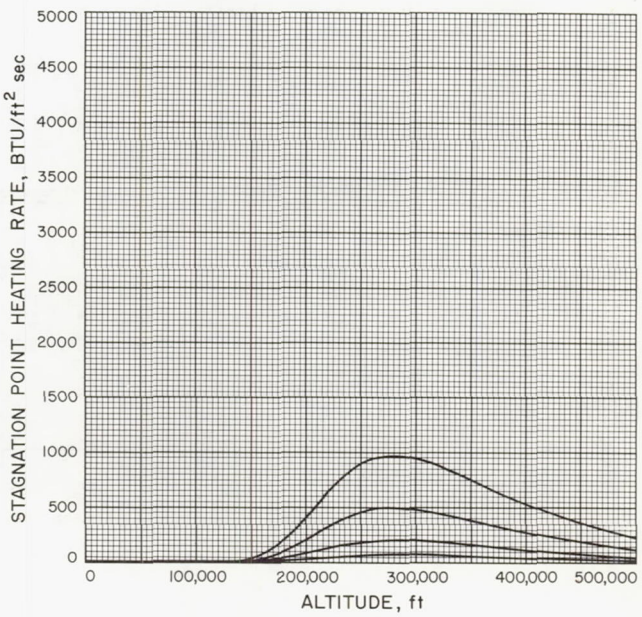

Fig. A-356

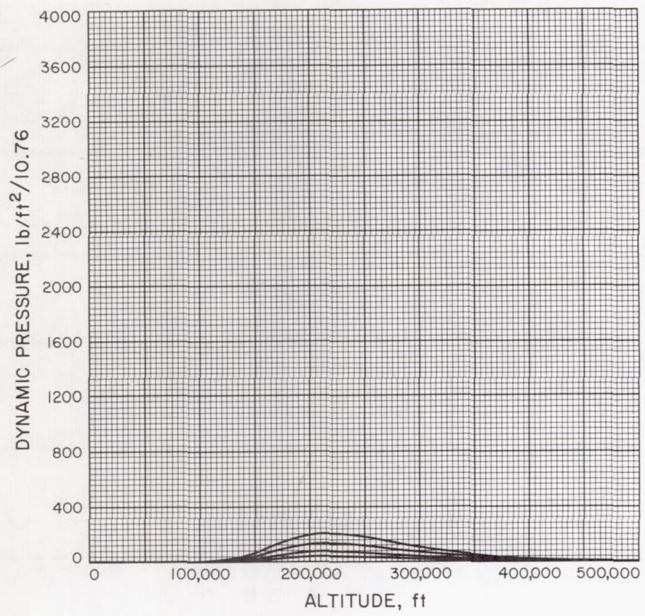

Fig. A-357

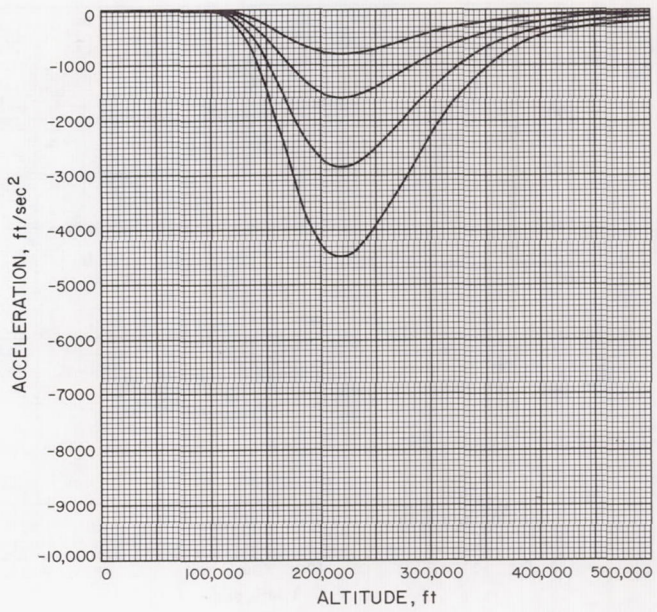

Fig. A-358

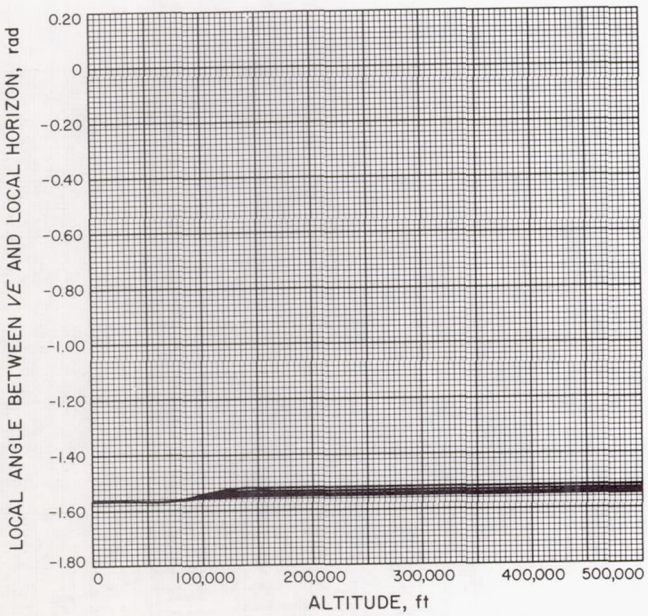

Fig. A-359

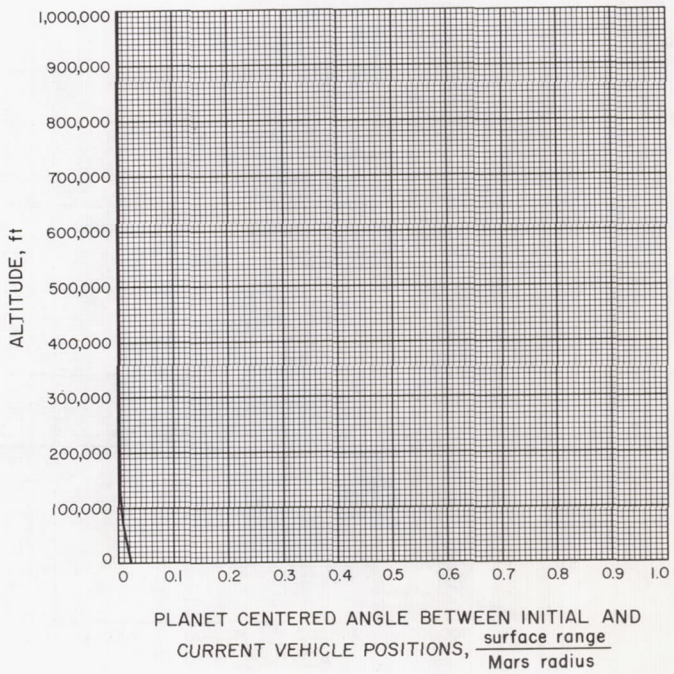

Fig. A-360

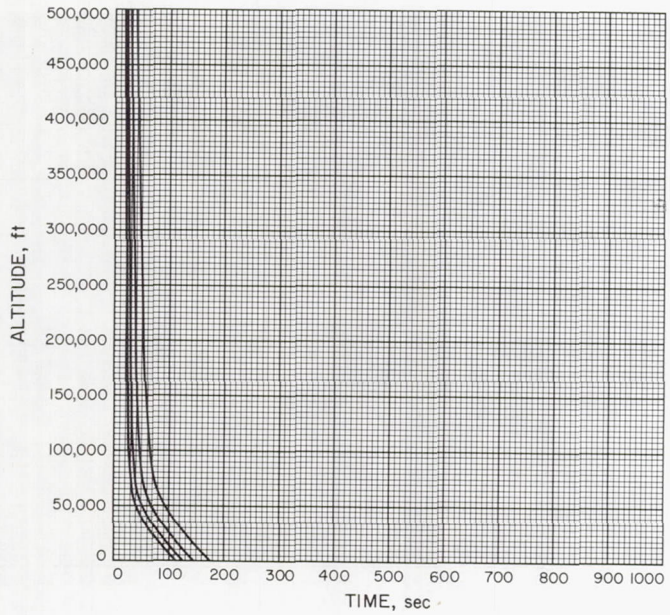

Fig. A-361

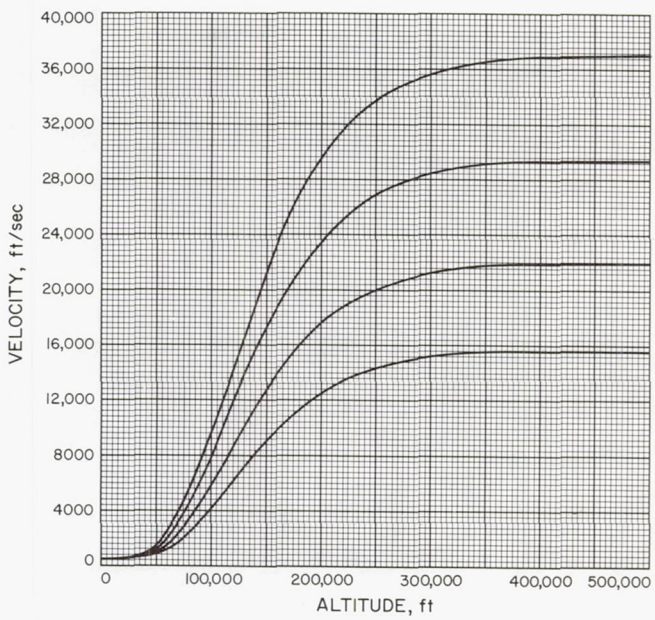

Fig. A-362

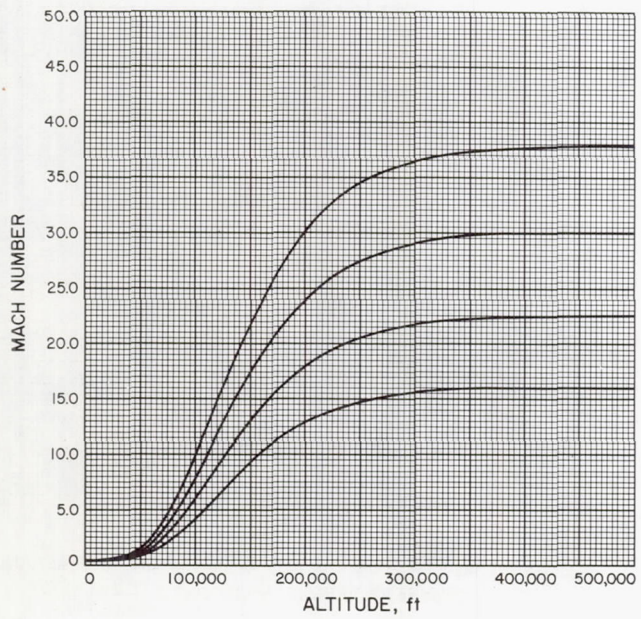

Fig. A-363

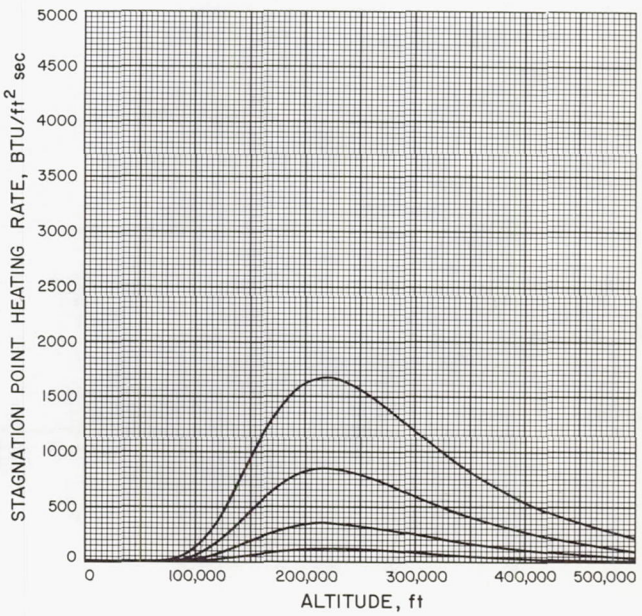

Fig. A-364

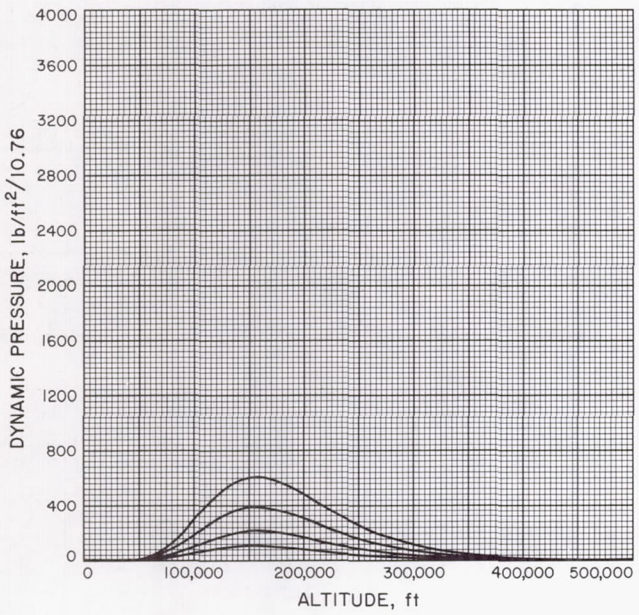

Fig. A-365

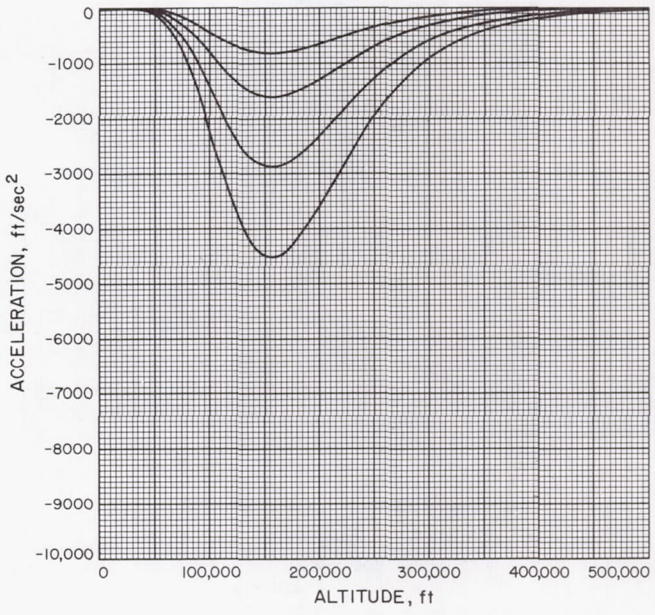

Fig. A-366

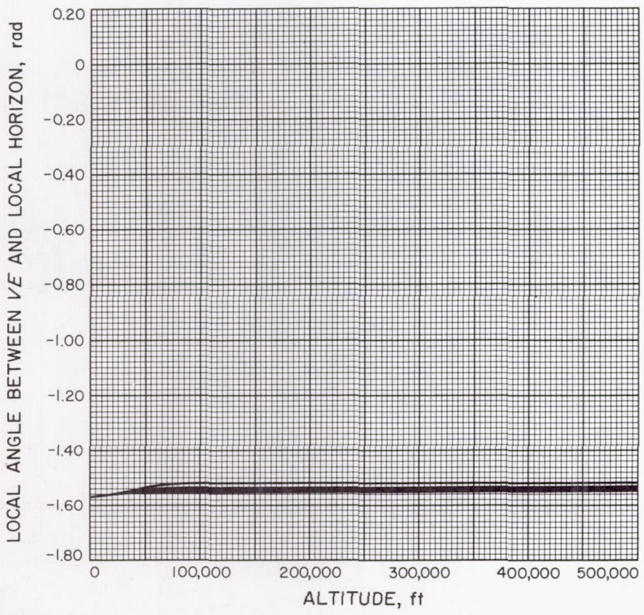

Fig. A-367

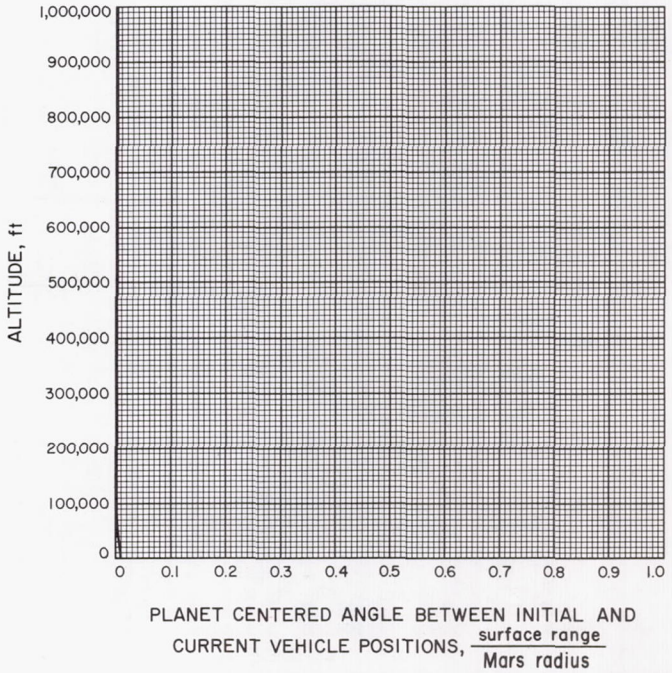

Fig. A-368

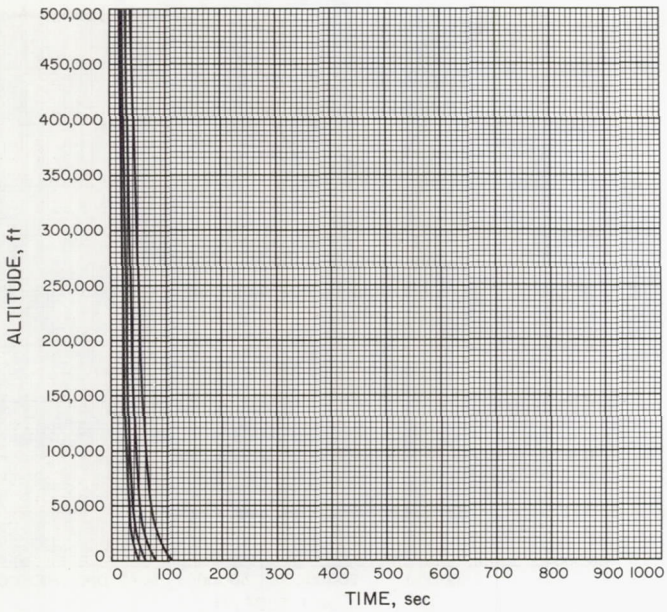

Fig. A-369

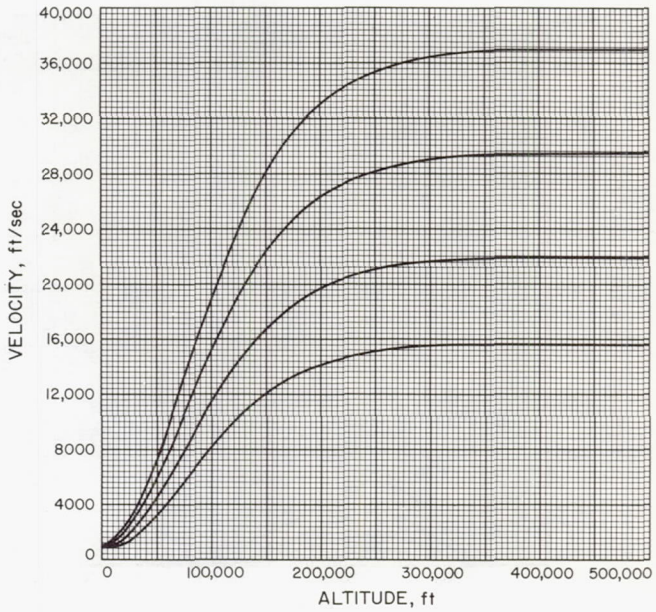

Fig. A-370

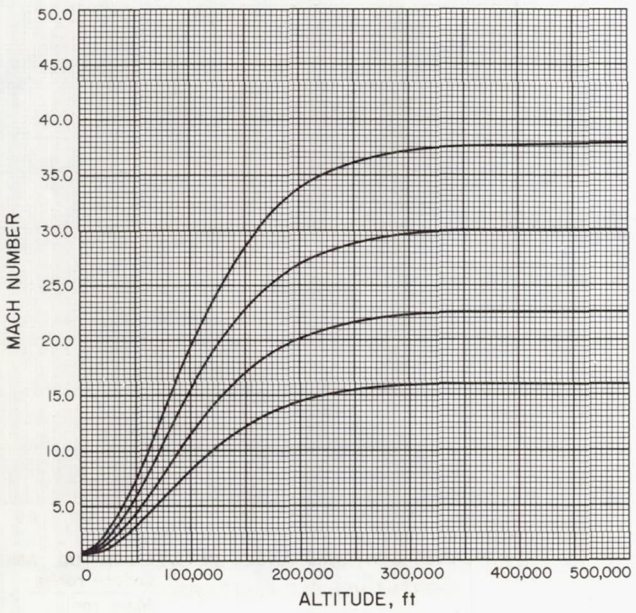

Fig. A-371

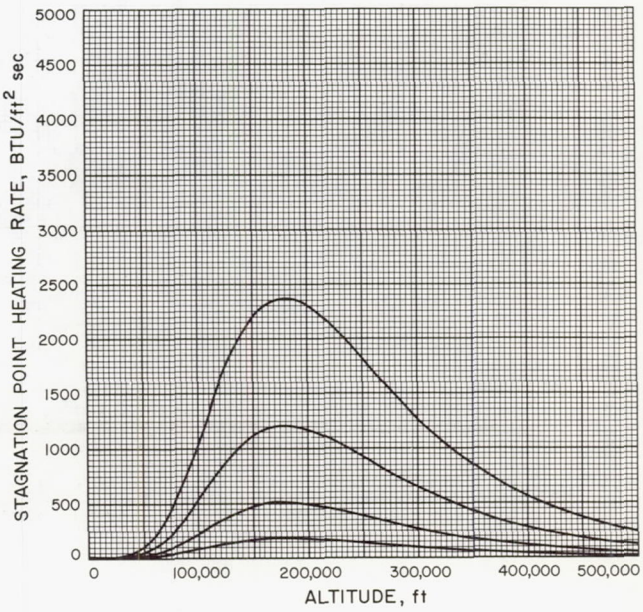

Fig. A-372

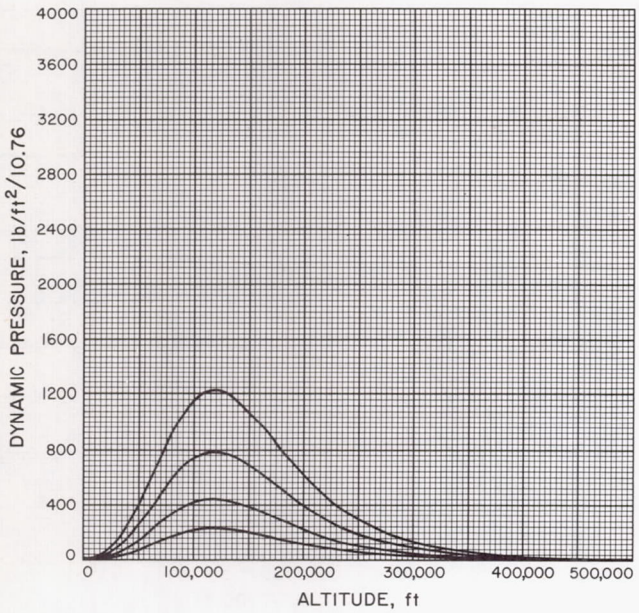

Fig. A-373

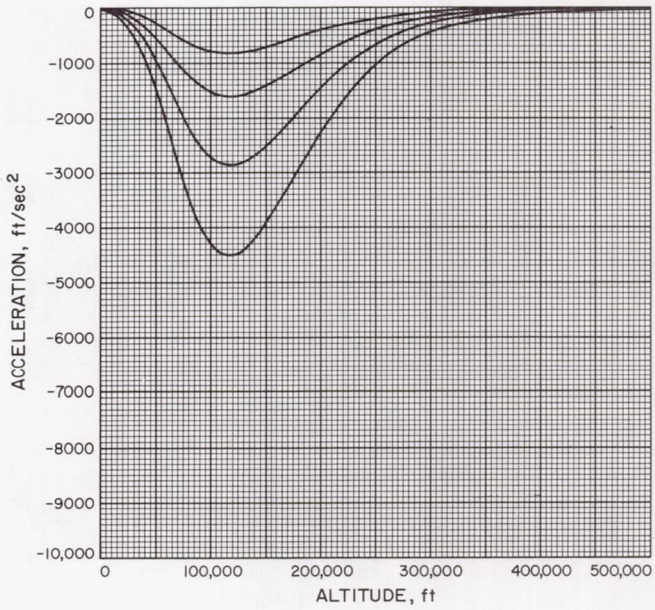

Fig. A-374

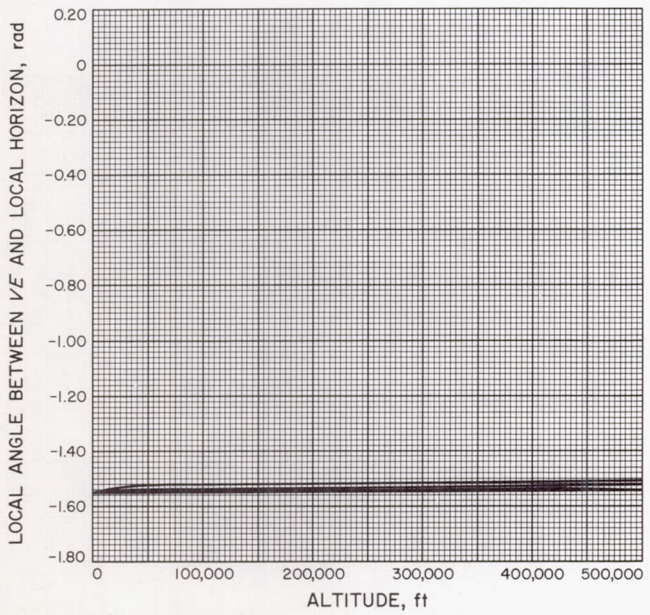

Fig. A-375

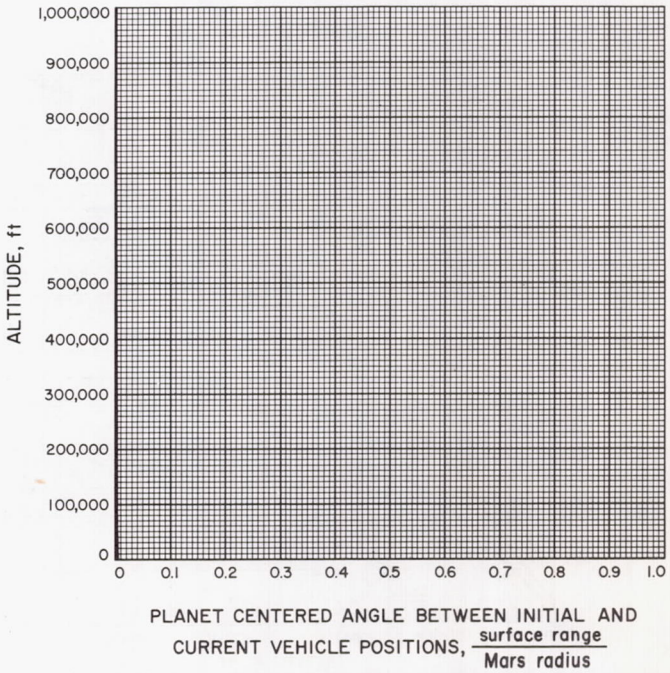

Fig. A-376

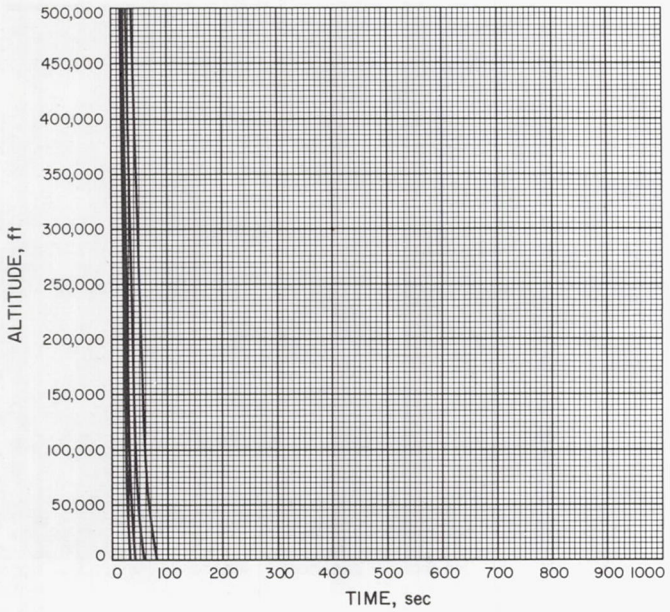

Fig. A-377

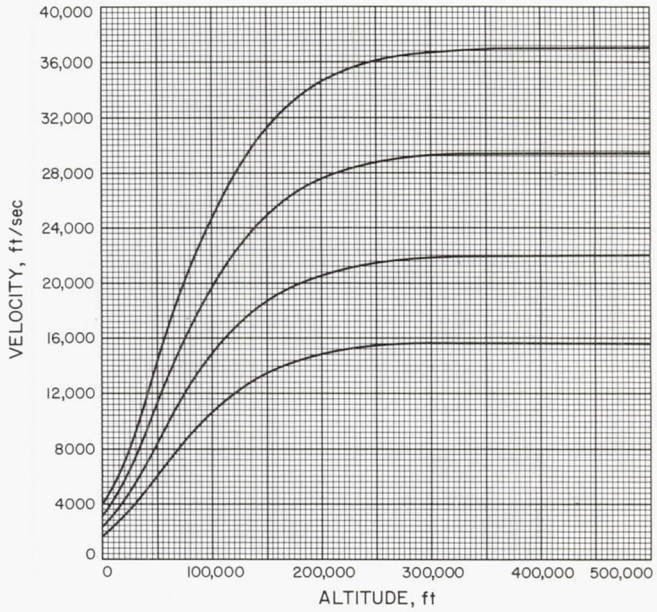

Fig. A-378

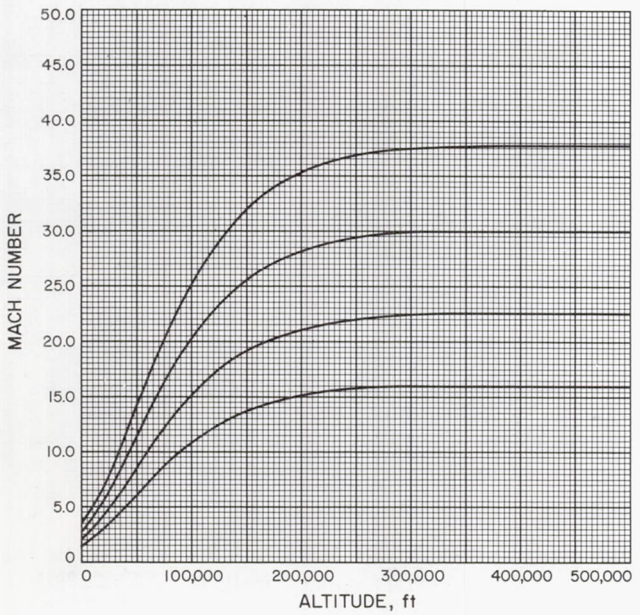

Fig. A-379

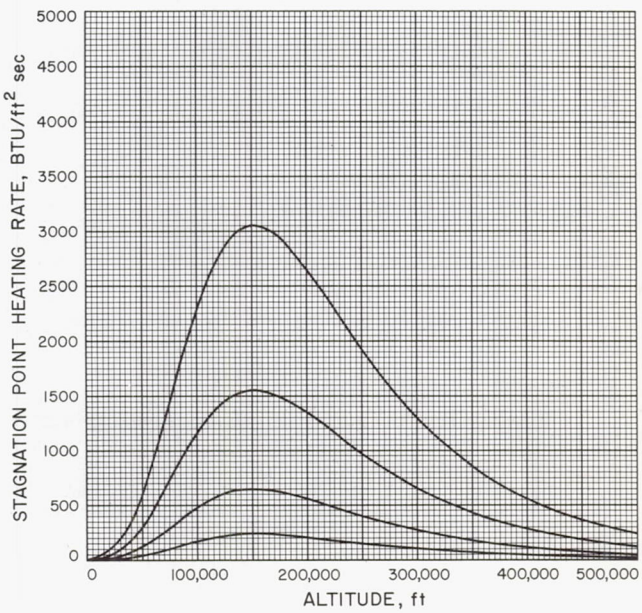

Fig. A-380

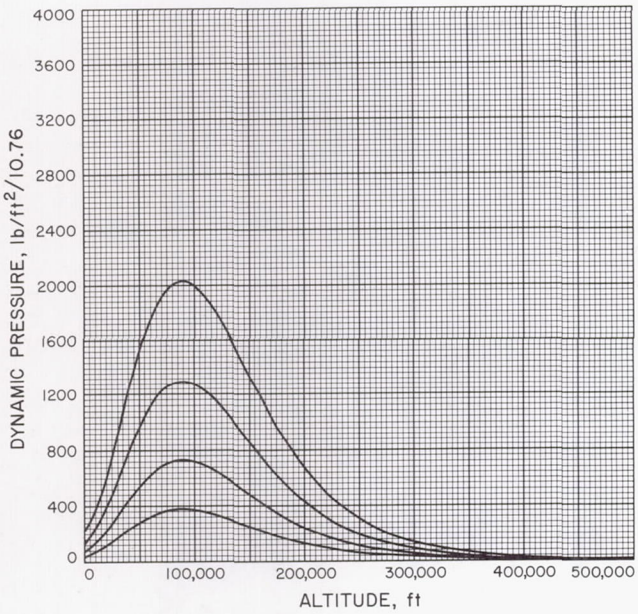

Fig. A-381

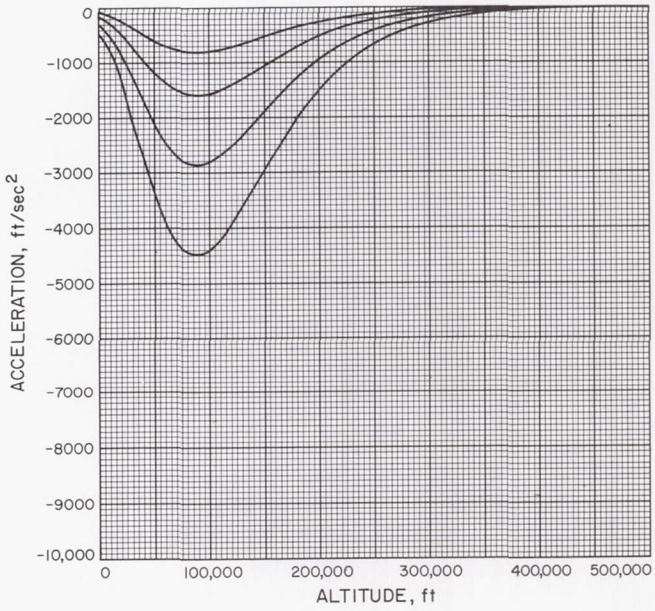

Fig. A-382

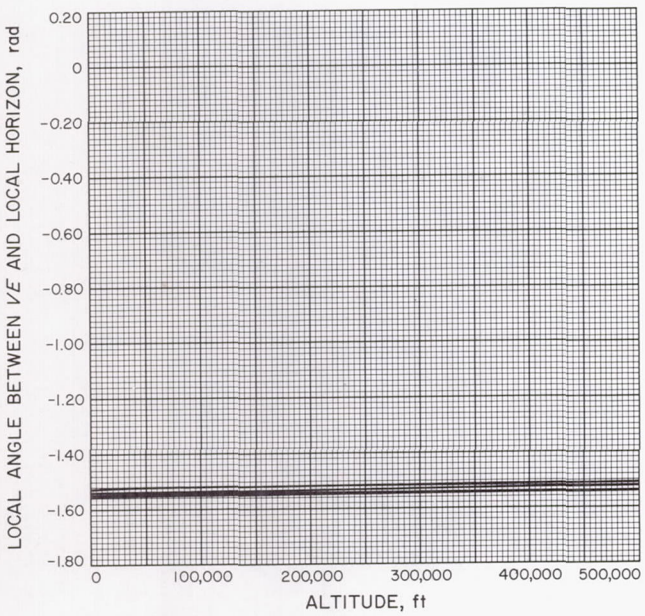

Fig. A-383

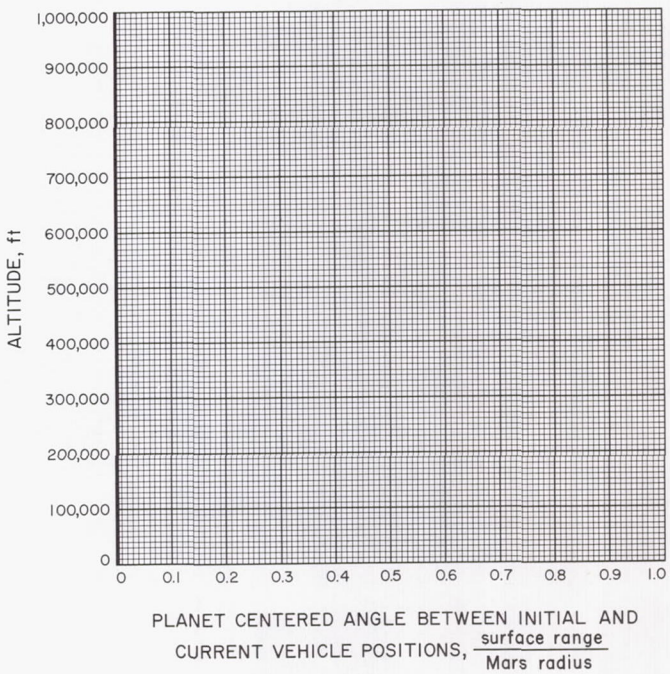

Fig. A-384